UNCLASSIFIED

MAY 21 1962

105

$11.97

COMPREHENSIVE TECHNICAL REPORT

DIRECT AIR CYCLE | AIRCRAFT NUCLEAR PROPULSION PROGRAM

~~CONFIDENTIAL~~

APEX-918

MASTER

REACTOR AND SHIELD PHYSICS

CLASSIFICATION CANCELLED
DATE 8/6/68
For The Atomic Energy Commission
Jack H. Kahn
TC
Chief, Declassification Branch

DISTRIBUTION OF THIS DOCUMENT IS UNLIMITED

FLIGHT PROPULSION LABORATORY DEPARTMENT

GENERAL ELECTRIC

~~CONFIDENTIAL~~
RESTRICTED DATA

THIS DOCUMENT CONTAINS RESTRICTED DATA AS DEFINED IN THE ATOMIC ENERGY ACT OF 1954. ITS TRANSMITTAL OR THE DISCLOSURE OF ITS CONTENTS IN ANY MANNER TO AN UNAUTHORIZED PERSON IS PROHIBITED.

L 8228

UNCLASSIFIED

UNCLASSIFIED

LEGAL NOTICE

This report was prepared as an account of Government sponsored work. Neither the United States, nor the Commission, nor the Air Force, nor any person acting on behalf of the Commission or the Air Force:

A. Makes any warranty or representation, express or implied, with respect to the accuracy, completeness, or usefulness of the information contained in this report, or that the use of any information, apparatus, method or process disclosed in this report may not infringe privately owned rights; or

B. Assumes any liabilities with respect to the use of, or for damages resulting from the use of any information, apparatus, method, or process disclosed in this report.

As used in the above "person acting on behalf of the Commission or Air Force" includes any employee or contractor of the Commission or Air Force to the extent that such employee or contractor prepares, handles, or distributes, or provides access to, any information pursuant to his employment or contract with the Commission or Air Force.

This is one of twenty-one volumes summarizing the General Electric Company's direct-air-cycle aircraft nuclear propulsion program. Additional copies are available from the United States Atomic Energy Commission, Division of Technical Information Extension, Oak Ridge, Tennessee.

The APEX number and title of each volume in the series is shown in the following list.

APEX-901 Program Summary and References
APEX-902 P-1 Nuclear Turbojet
APEX-903 Reactor Core Test Facility
APEX-904 Heat Transfer Reactor Experiment No. 1
APEX-905 Heat Transfer Reactor Experiment No. 2
APEX-906 Heat Transfer Reactor Experiment No. 3
APEX-907 XMA-1 Nuclear Turbojet
APEX-908 XNJ140E Nuclear Turbojet
APEX-909 Aircraft Nuclear Propulsion Systems Studies
APEX-910 Aircraft Nuclear Propulsion Application Studies
APEX-911 Remote Handling Equipment
APEX-912 Controls and Instrumentation
APEX-913 Metallic Fuel Element Materials
APEX-914 Ceramic Reactor Materials
APEX-915 Shield Materials
APEX-916 Moderator Materials
APEX-917 Organic, Structural and Control Materials
APEX-918 Reactor and Shield Physics
APEX-919 Aerothermodynamics
APEX-920 Applied Mechanics
APEX-921 Nuclear Safety

UNCLASSIFIED

DISCLAIMER

This report was prepared as an account of work sponsored by an agency of the United States Government. Neither the United States Government nor any agency Thereof, nor any of their employees, makes any warranty, express or implied, or assumes any legal liability or responsibility for the accuracy, completeness, or usefulness of any information, apparatus, product, or process disclosed, or represents that its use would not infringe privately owned rights. Reference herein to any specific commercial product, process, or service by trade name, trademark, manufacturer, or otherwise does not necessarily constitute or imply its endorsement, recommendation, or favoring by the United States Government or any agency thereof. The views and opinions of authors expressed herein do not necessarily state or reflect those of the United States Government or any agency thereof.

DISCLAIMER

Portions of this document may be illegible in electronic image products. Images are produced from the best available original document.

APEX-918

LEGAL NOTICE

This report was prepared as an account of Government sponsored work. Neither the United States, nor the Commission, nor any person acting on behalf of the Commission:

A. Makes any warranty or representation, expressed or implied, with respect to the accuracy, completeness, or usefulness of the information contained in this report, or that the use of any information, apparatus, method, or process disclosed in this report may not infringe privately owned rights, or

B. Assumes any liabilities with respect to the use of, or for damages resulting from the use of any information, apparatus, method, or process disclosed in this report.

As used in the above, "person acting on behalf of the Commission" includes any employee or contractor of the Commission, or employee of such contractor, to the extent that such employee or contractor of the Commission, or employee of such contractor prepares, disseminates, or provides access to, any information pursuant to his employment or contract with the Commission, or his employment with such contractor.

COMPREHENSIVE TECHNICAL REPORT GENERAL ELECTRIC DIRECT-AIR-CYCLE AIRCRAFT NUCLEAR PROPULSION PROGRAM

REACTOR AND SHIELD PHYSICS

Authors: W. E. EDWARDS, J. D. SIMPSON
Contributors: L. S. BURNS, JR., J. E. MacDONALD, J. MOTEFF, P. W. SCHREIBER
Editor: R. R. GEHRING

Facsimile Price $ 18.40
Microcard Price $ 4.25
for Access Permittees

Available from the
Division of Technical Information Extension
P. O. Box 1001
Oak Ridge, Tennessee

RESTRICTED DATA

This document contains restricted data as defined in the Atomic Energy Act of 1954. Its transmittal or the disclosure of its contents in any manner to an unauthorized person is prohibited.

This document contains Confidential-Restricted Data relating to civilian applications of atomic energy.

May 31, 1962

United States Air Force — Contract No. AF 33(600)—38062
United States Atomic Energy Commission — Contract No. AT(11-1)—171

AEC RESEARCH AND DEVELOPMENT REPORT

GENERAL ELECTRIC
NUCLEAR MATERIALS AND PROPULSION OPERATION
(Formerly Aircraft Nuclear Propulsion Department)
FLIGHT PROPULSION LABORATORY DEPARTMENT
Cincinnati 15, Ohio

DISTRIBUTION OF THIS DOCUMENT IS UNLIMITED

RECLASSIFIED 8228

DISTRIBUTION

INTERNAL

C. L. Chase
D. Cochran
E. B. Delson
M. C. Leverett
W. H. Long
H. F. Matthiesen
A. J. Rothstein (6)
D. R. Shoults
G. Thornton
Library (6)

EXTERNAL DISTRIBUTION

Col. Ola P. Thorne
Pentagon, Washington 25, D. C.

Capt. Hendricks
Andrews AFB, Md.

Lt. Col. Stanley Valcik (2)
A. S. D.
Wright-Patterson AFB, Ohio

Dr. Frank Pittman (2)
AEC
Washington 25, D. C.

DTIE (14) plus reproducible master
Oak Ridge, Tennessee

UNCLASSIFIED
CONFIDENTIAL

ABSTRACT

This is one of twenty-one volumes summarizing the Aircraft Nuclear Propulsion Program of the General Electric Company. This volume describes the experimental and theoretical work accomplished in the areas of reactor and shield physics.

The reactor physics technology for all ANP reactor types is presented in its most advanced stage; i.e., no attempt is made to present chronologically the development of the technology.

The use of automated techniques for power-mapping critical experiments in the reactor physics program are discussed, with particular attention to the use of high speed computer programs employing the IBM 704 and IBM 7090 computing systems.

In the nuclear shielding program, efforts were concentrated in two main areas: (1) the optimum placement of shield materials to reduce radiation levels, and (2) the calculation of specific nuclear data, such as nuclear heating and activation, which are important to the design of an efficient, safe power plant.

Methods were developed for determining, at any position in the reactor-shield assembly, the total flux and the angle and energy distribution of neutron and gamma rays, as well as the response of any detector used to measure radiation effects.

Important shielding computer codes described are the point kernel and single scattering codes and the more recently developed Monte Carlo codes.

CONFIDENTIAL
UNCLASSIFIED

DECLASSIFIED

DECLASSIFIED

PREFACE

In mid-1951, the General Electric Company, under contract to the United States Atomic Energy Commission and the United States Air Force, undertook the early development of a militarily useful nuclear propulsion system for aircraft of unlimited range. This research and development challenge to meet the stringent requirements of aircraft applications was unique. New reactor and power-plant designs, new materials, and new fabrication and testing techniques were required in fields of technology that were, and still are, advancing very rapidly. The scope of the program encompassed simultaneous advancement in reactor, shield, controls, turbomachinery, remote handling, and related nuclear and high-temperature technologies.

The power-plant design concept selected for development by the General Electric Company was the direct air cycle turbojet. Air is the only working fluid in this type of system. The reactor receives air from the jet engine compressor, heats it directly, and delivers it to the turbine. The high-temperature air then generates the forward thrust as it exhausts through the engine nozzle. The direct air cycle concept was selected on the basis of studies indicating that it would provide a relatively simple, dependable, and serviceable power plant with high-performance potential.

The decision to proceed with the nuclear-powered-flight program was based on the 1951 recommendations of the NEPA (Nuclear Energy for the Propulsion of Aircraft) project. Conducted by the Fairchild Engine and Airplane Corporation under contract to the USAF, the five-year NEPA project was a study and research effort culminating in the proposal for active development of nuclear propulsion for manned aircraft.

In the ensuing ten years, General Electric's Aircraft Nuclear Propulsion Department carried on the direct air cycle development until notification by the USAF and USAEC, early in 1961, of the cancellation of the national ANP program. The principal results of the ten-year effort are described in this and other volumes listed inside the front cover of the Comprehensive Technical Report of the General Electric Direct Air Cycle·Aircraft Nuclear Propulsion Program.

Although the GE-ANPD effort was devoted primarily to achieving nuclear aircraft power-plant objectives (described mainly in APEX-902 through APEX-909), substantial contributions were made to all aspects of gas-cooled reactor technology and other promising nuclear propulsion systems (described mainly in APEX-910 through APEX-921). The Program Summary (APEX-901) presents a detailed description of the historical, programmatic, and technical background of the ten years covered by the program. A graphic summary of these events is shown on the next page.

Each portion of the Comprehensive Report, through extensive annotation and referencing of a large body of technical information, now makes accessible significant technical data, analyses, and descriptions generated by GE-ANPD. The references are grouped by subject and the complete reference list is contained in the Program Summary, APEX-901. This listing should facilitate rapid access by a researcher to specific interest areas or

DECLASSIFIED

UNCLASSIFIED

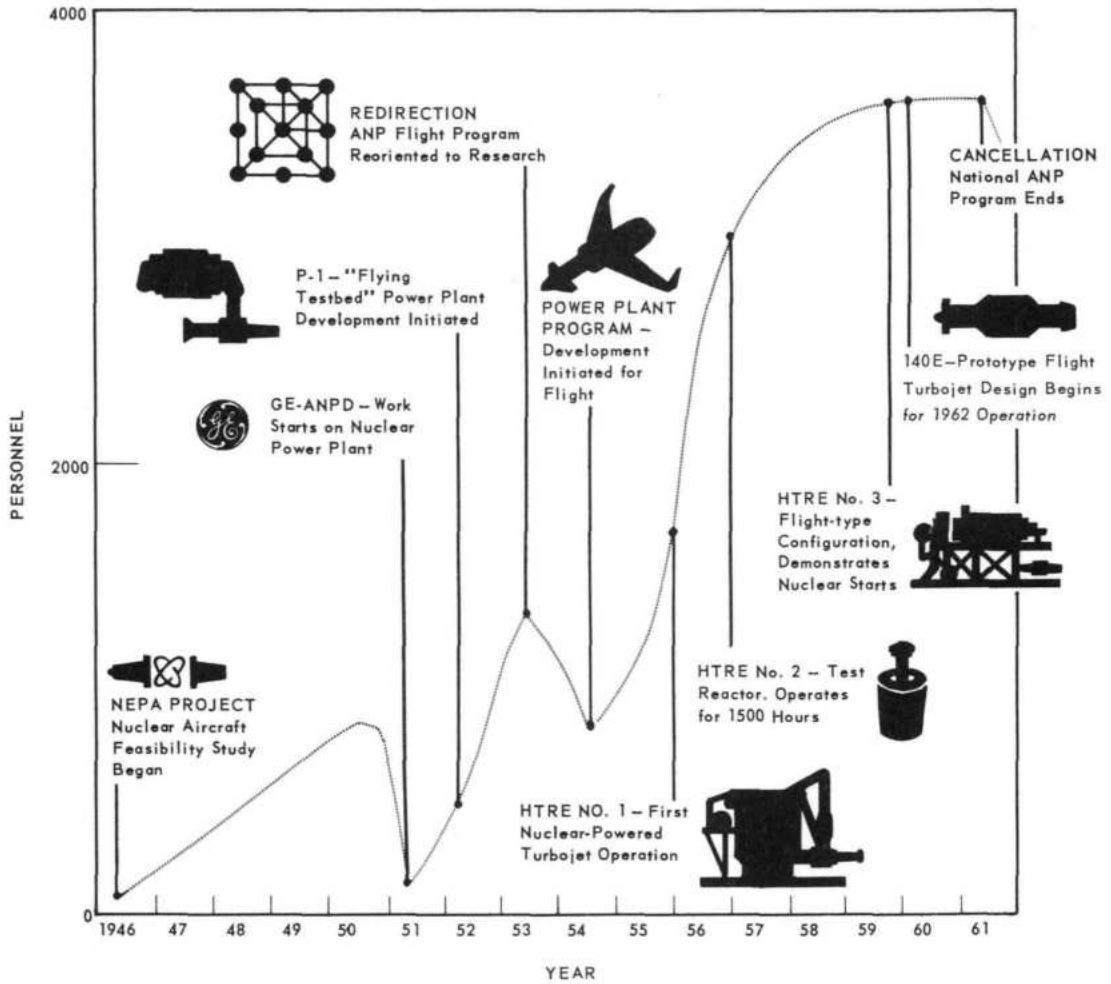

Summary of events – General Electric Aircraft Nuclear Propulsion Program*

*Detailed history and chronology is provided in Program Summary, APEX-901. Chronology information extracted from: Aircraft Nuclear Propulsion Program hearing before the Subcommittee on Research and Development of the Joint Committee on Atomic Energy, 86th Congress of The United States, First Session, July 23, 1959, United States Government Printing Office, Washington 1959.

UNCLASSIFIED

DECLASSIFIED

sources of data. Each portion of the Comprehensive Report discusses an aspect of the Program not covered in other portions. Therefore, details of power plants can be found in the power-plant volumes and details of the technologies used in the power plants can be found in the other volumes. The referenced documents and reports, as well as other GE-ANPD technical information not covered by the Comprehensive Report, are available through the United States Atomic Energy Commission, Division of Technical Information Extension, Oak Ridge, Tennessee.

The Report is directed to Engineering Management and assumes that the reader is generally familiar with basic reactor and turbojet engine principles; has a technical understanding of the related disciplines and technologies necessary for their development and design; and, particularly in APEX-910 through APEX-921, has an understanding of the related computer and computative techniques.

The achievements of General Electric's Aircraft Nuclear Propulsion Program were the result of the efforts of many officers, managers, scientists, technicians, and administrative personnel in both government and industry. Most of them must remain anonymous, but particular mention should be made of Generals Donald J. Keirn and Irving L. Branch of the Joint USAF-USAEC Aircraft Nuclear Propulsion Office (ANPO) and their staffs; Messrs. Edmund M. Velten, Harry H. Gorman, and John L. Wilson of the USAF-USAEC Operations Office and their staffs; and Messrs. D. Roy Shoults, Samuel J. Levine, and David F. Shaw, GE-ANPD Managers and their staffs.

This Comprehensive Technical Report represents the efforts of the USAEC, USAF, and GE-ANPD managers, writers, authors, reviewers, and editors working within the Nuclear Materials and Propulsion Operation (formerly the Aircraft Nuclear Propulsion Department). The local representatives of the AEC-USAF team, the Lockland Aircraft Reactors Operations Office (LAROO), gave valuable guidance during manuscript preparation, and special appreciation is accorded J. L. Wilson, Manager, LAROO, and members of his staff. In addition to the authors listed in each volume, some of those in the General Electric Company who made significant contributions were: W. H. Long, Manager, Nuclear Materials and Propulsion Operation; V. P. Calkins, E. B. Delson, J. P. Kearns, M. C. Leverett, L. Lomen, H. F. Matthiesen, J. D. Selby, and G. Thornton, managers and reviewers; and C. L. Chase, D. W. Patrick, and J. W. Stephenson and their editorial, art, and production staffs. Their time and energy are gratefully acknowledged.

THE EDITORIAL BOARD:

Paul E. Lowe
Arnold J. Rothstein
James I. Trussell

November 8, 1961

DECLASSIFIED

DECLASSIFIED

~~CONFIDENTIAL~~

CONTENTS

~~CONFIDENTIAL~~

DECLASSIFIED

DECLASSIFIED

CONFIDENTIAL

CONFIDENTIAL

DECLASSIFIED

DECLASSIFIED

DECLASSIFIED

DECLASSIFIED

CONFIDENTIAL

FIGURES

CONFIDENTIAL

DECLASSIFIED

UNCLASSIFIED

CONFIDENTIAL

CONFIDENTIAL

UNCLASSIFIED

DECLASSIFIED
CONFIDENTIAL

TABLES

CONFIDENTIAL
DECLASSIFIED

Digitized by Google

DECLASSIFIED

REACTOR AND SHIELD PHYSICS

INTRODUCTION AND SUMMARY

The technology of Reactor and Shield Physics as applied to aircraft nuclear reactors of the "direct cycle" type is discussed in this volume. The work described combined highly specialized technical analyses and versatile experimental approaches to define the basic and characteristic parameters of these unique nuclear systems.

The direct-cycle nuclear turbojet system provides for the air from a jet engine compressor to pass directly through the nuclear reactor and thence to the turbine. A reactor system, developed for this application, has a high (approximately 40 percent) void volume for coolant passages, and utilizes considerably larger passages through the shield than do reactor systems employing heat transfer media with higher density and higher heat capacity than air.

This volume is divided into two distinct but related parts, each with its own introduction. Part I deals with Reactor Physics - the basic nuclear phenomena. Methods of determining the essential nuclear constants and of optimizing the design of practical power systems are discussed. Part II treats the problems of Shield Physics and the approaches taken to evaluate the integrated effects of the nuclear radiation source, its reflector, and its shield upon the design of the flight power plant and the flight vehicle.

Also described are the analytical tools and techniques employing modern electronic computing machinery which were developed to provide a high degree of optimization in the design of nuclear power plants for flight applications.

Detailed information on each phase of the reactor and shield physics program are provided in the publications referenced at the end of each section of the report.

DECLASSIFIED

Digitized by Google

Original from UNIVERSITY OF MICHIGAN

DECLASSIFIED

PART 1 - REACTOR PHYSICS

1. INTRODUCTION

The development of a reactor physics technology for GE-ANPD was directed toward providing a fundamental basis for the nuclear design of the series of reactors required for the Aircraft Nuclear Propulsion (ANP) program. All GE-ANPD reactors were direct cycle systems; i.e., were cooled by air supplied by a turbojet which in turn was driven by the thermal energy supplied to the air by the reactor. The following four basic types of reactors were developed by the ANP Department.

1. The concentric-ring reactor with metallic fuel elements and water moderator. The only example of this type was the R-1 reactor, which was the first reactor on which major development work was done. It was proposed as a power source for six modified J-47 turbojets in order to demonstrate nuclear flight. While the R-1 reactor itself was never finished, a critical experiment mockup was built and tested, and its important nuclear characteristics were established. The R-1 reactor is discussed in APEX-902 of this Report.
2. The tube-type reactor with metallic fuel elements and water moderator. The HTRE No. 1 (Heat Transfer Reactor Experiment No. 1) was the primary example of such a system. Its nichrome, sandwich-type fuel elements were fabricated in the form of concentric rings which were located in 37 tubes. These were surrounded by the water moderator. This reactor was the first to demonstrate use of a nuclear power source to power a turbojet. The HTRE No. 2 system was a modified HTRE No. 1 with the seven central tubes removed in order that proposed reactor modules could be tested at appropriate neutron fluxes, temperatures, and air flows. Both the HTRE No. 1 and HTRE No. 2 had extensive critical experiments associated with them; in the case of the HTRE No. 2, a different critical experiment was run for each significantly different test insert. HTRE No. 1 is discussed in APEX-904, and HTRE No. 2 in APEX-905 of this Report.
3. The tube-type reactor with metallic fuel elements and hydrided metal moderator. The HTRE No. 3 and the XMA-1 reactors are the primary examples of this type of reactor. Both systems were used for extensive critical experiments in order to explore their nuclear characteristics. The HTRE No. 3 was built and run in an extensive series of power plant performance tests. The XMA-1 power plant was not built; however, its nuclear characteristics were, in the main, established through critical experiment measurements. In addition, there were measurements of a reactor with a hydrided-metallic moderator, with the fuel and moderator at varying temperatures, in the HOTCE experiment at the ITS.
4. The homogeneous ceramic reactor. The P140 reactor, the fuel elements of which were small, fueled beryllium oxide hexagonal tubes, was the primary example of this type of reactor. While this reactor was never built, its components were tested extensively in the HTRE No. 2 insert. An accurate mockup of the P140 was tested as a critical experiment, and a series of critical experiments (SMR series) to establish the characteristics of beryllium moderated reactors was performed.
5. The folded-flow reactor with hydrided metallic moderator. Preliminary designs of folded-flow reactors were explored using both metallic and ceramic fuel, but no

DECLASSIFIED

DECLASSIFIED

power reactor was built. A critical experiment (RAG-I), was made to establish pertinent nuclear characteristics. In this type of reactor the fuel and moderator are designed so that air can enter the reactor through a radial air gap, pass through the moderator, then through the fuel, and then turn and pass out of the reactor through another radial air gap.

The development of reactor physics technology was concentrated along those lines which would best serve the design of the reactor types described in the foregoing. A second trend during the ten-year ANP reactor physics program involved the gradual sophistication of the technology, primarily through the use of automated techniques for power-mapping critical experiments and through the rapidly increasing use of high speed computing machinery, progressing from the IBM-650 through the IBM-704 to the IBM-7090 computing systems.

This summary of the ANP reactor physics technology gives a description of the most pertinent technology at its most advanced stage for all ANP reactor types and makes no attempt to give a history of the order in which the technology was developed. The manner in which the reactor physics technology was applied to actual reactor designs is briefly summarized in section 2. More detailed descriptions of the actual technology are set forth in the succeeding sections.

DECLASSIFIED

DECLASSIFIED

CONFIDENTIAL

2. REACTOR ANALYSIS METHODS

2.1 OVER-ALL REACTOR ANALYSIS

2.1.1 HETEROGENEOUS CORE

The attainment of a high-performance direct-cycle nuclear power plant requires the optimization of the nuclear, mechanical, and aerothermal reactor design within the temperature limitations imposed by the possible materials to be used. To optimize the nuclear design, a very large number of configurations must be considered within each area of interest defined by the power plant size and choice of materials for the core and structure. Thus for a typical heterogeneous reactor, the nuclear design variables could include cell size and number, void and moderator volume fractions, average fuel loading, and moderator hydrogen loading. In addition, the reactor design may include several variations in geometry along each axis for both gross and fine power distribution and in multiple side- and end-reflector regions. The nuclear design of such a reactor system from feasibility study through power testing involves logically distinct areas of effort that range from entirely theoretical, through combined experimental and theoretical, to a final completely experimental fine adjustment of the reactor prior to power testing. Thus, although it is impractical to examine experimentally as many as perhaps 500 core configurations of a single type of reactor, it is virtually impossible to design and build successfully a high performance reactor with only theoretical studies. Finally, of course, manufacturing-tolerance stackups, residual design uncertainties, etc., can be compensated for only by experimental adjustment in the particular reactor.

The initial nuclear design activity in which system feasibility is investigated and a restricted range of interest for the design variables is established is of necessity largely theoretical. Even with high-speed computing equipment, however, an investigation of many possible values of many design variables is a costly and time-consuming undertaking. Both the number of systems to be investigated and the analytical detail for each chosen system must be limited if the design is to be completed within a specific time and budget. The latter restriction might imply, for example, if a one-space-dimensional few-energy-group core nuclear analysis rather than a two- or three-dimensional or a multigroup analysis were used. This approach is obviously reasonable for determining system feasibility. Investigation of the multivariable reactor core may be held within reasonable limits by employing the method of statistical experiment design, which is used, for example, in biological and agricultural research. The unique application of this technique, in which the reactor calculations performed are viewed as synthetic experiments that yield values of a dependent variable, e.g., critical mass, in terms of the independent design variables, is discussed in detail in APEX-303.[1*] A composite experiment design is used to define the calculations required, and a regression analysis employing a least-squares criterion is used to define the coefficients of a quadratic response equation giving the dependent variable in terms of linear, quadratic, and cross-product dependence on the design variables.[2] Such a procedure enables large amounts of calculated data to be

*Superscripts refer to the reference lists that appear at the end of each section.

CONFIDENTIAL

DECLASSIFIED

DECLASSIFIED

presented in a form directly usable by the nuclear design engineer, e.g., curves of critical mass versus moderator volume fraction for various moderator hydrogen loadings.

During this initial system-feasibility phase of the nuclear design process, experimental information on the major reactor core materials - i.e., moderator and fuel element clad are required in order that the adequacy of both the basic nuclear-cross-section data for these materials and the analysis methods employed can be evaluated. This information is most readily obtained from a flexible critical experiment in which effort is not generally applied to simulating the proposed reactor cell geometry, for example, but which can be utilized to determine several critical loadings, critical reflector thicknesses, structural-material danger coefficients, etc. Thus, in the hydrogenous reactor development effort, flexible critical experiments using water, acrylic plastic, and hydrided zirconium and yttrium have been performed. This experimental information along with the parametric information generated theoretically may then be combined to define a fairly restricted area of interest for further nuclear design activity. In this initial design phase the interaction with the aerothermal design is generally represented by a required heat transfer area, and power-distribution design is investigated only to insure that sufficient flexibility is retained in the proposed design area. Mechanical design interaction is largely ignored in this phase, although the nuclear effect of the core structure is usually included.

The second design phase, usually designated preliminary design, involves integration of mechanical, aerothermal, and nuclear design for a configuration chosen from the results of the initial design phase. Here the object is to demonstrate practicality for the reactor system. The strictly nuclear design activities are now centered on detailed treatment of a single or, at most, several reactor cores to establish accurate fuel-loading requirements and initial power-distribution design information. In addition, the preliminary design phase involves detailed nuclear design of a critical experiment mockup, the purpose of which is to obtain an accurate nuclear model of the proposed reactor. The information obtained from the critical experiment - including detailed power mapping of fine and gross fission power distributions, critical mass, and control rod reactivity worth - are the basic nuclear design values. Detailed theory-experiment comparisons on critical mass, for example, are used to normalize the theoretical results as the design core configuration gradually changes. The observed power distributions may dictate immediate design changes or may serve as reference data for further theoretical studies. Although the proposed reactor design usually undergoes several iterations in order to optimize the coupled thermodynamic, mechanical, and nuclear designs, these are generally not accompanied by changes in the critical experiment mockup, although proposed changes are usually evaluated for reactivity and power distribution effects.

Preliminary design also includes theoretical calculation of the various reactivity operating effects such as moderator temperature coefficients and poisoning by xenon and other fission products. Because of the relatively high fuel loading for compact heterogeneous reactors, fuel burnup during desired core life is not usually a large reactivity effect. Xenon buildup, however, because of its location is a significant though small factor in a thermal reactor. The moderator temperature coefficient is generally positive in these hydrogenous systems since the decreased moderator absorption overrides any density-reduction effects.

A very crucial part of the nuclear design of a heterogeneous reactor is the calculation and/or measurement of the secondary heating in the moderator, reflector, and structural members of the reactor since the temperatures in these components determine moderator cooling requirements, for example, and have a large affect on the over-all mechanical design. Such measurements are part of the critical experiment data for the actual core components, but much of the structural heating data must be generated theoretically. Because of the nonreproducing nature of the gamma ray diffusion problem and the need for complex geometrical representations, gamma ray heating calculations can be performed on a fairly

DECLASSIFIED

DECLASSIFIED

routine basis with Monte Carlo techniques. It is necessary to take account of the neutron capture gamma ray sources as well as the fission sources, especially in computing extra-core heating.

2.1.2 HOMOGENEOUS CORE

The basic nuclear design problem for the homogeneous high-temperature system is centered on core structure rather than on the moderator as in the heterogeneous system. The use of a high-temperature ceramic moderator avoids the problem of moderator cooling, which dominates the heterogeneous system; but it introduces mechanical design problems and coolant problems for core structure and core elements that do not produce power, such as control rods and associated guide tubes. In addition, since the ceramic moderators are not as efficient from a nuclear standpoint, resonance capture, for example, is a major design consideration. Also, the much higher operating temperatures of the changes in crystalline scattering properties that accompany the changes from room temperature to operating conditions. Since, as will be discussed in 2.2, the usual design procedure is based largely on a room-temperature critical experiment and depends almost entirely on analytical extrapolation to the operating conditions, the homogeneous-reactor design effort requires increased physical and numerical accuracy in the analytical techniques employed. These are discussed later in more detail.

The preliminary design phase concludes with the choice of a final design configuration. The chosen configuration usually allows for only minor additional design changes, and the succeeding major nuclear design activities are concerned with specifying final fuel loadings, moderator dimensions, control rod staging, etc. The nuclear mockup used in the preliminary design phase is modified to the final design configuration, or a new mockup is constructed in this configuration. This is used as the primary source of final nuclear design information, although the extrapolation from room temperature to the design operating conditions is theoretical, and care must be exercised to insure that the related uncertainties are properly considered in the final design.

After final assembly of the design core, the reactor is tested in a heated-air critical facility prior to power testing and the final adjustments of poison rods and of fine and gross power distributions are made.

2.2 DIFFUSION THEORY

Considerable effort in the general area of reactor-physics methods development has been concerned with applications of diffusion theory. The reasons for this emphasis are partly historical and partly economic. The reactors on which the principal design effort was concentrated were thermal, epithermal, or intermediate. Diffusion theory is generally adequate for analyzing neutron effects in the core and reflector regions of such reactors; and in one space dimension, calculations based on diffusion theory consume less computation time than the potentially more precise S_n transport theory and Monte Carlo methods discussed in 2.3 and 2.4. In the analysis of small fast reactors the S_n method was competitive with the standard diffusion theory methods in computation time and was therefore used because of its higher precision. In problems involving highly anisotropic vector flux, such as in deep penetration or strong local absorption of neutrons, the diffusion theory results are not reliable, and higher-order approximations such as the P_l, double P_l, S_n, or Monte Carlo methods must be employed. Nevertheless, there is a wide area of applicability for diffusion theory approximations in calculations of reactors for propulsion applications.

DECLASSIFIED

DECLASSIFIED

Virtually every reactor-analysis method has been mechanized in the form of a digital computer program. The principal reason for this general use of large-scale digital computers is the complexity of multienergy, multiregion reactor calculations. A computer program for even relatively simple calculations is justifiable, however, on grounds of speed and reliability. The objective has been to give the nuclear design engineer the means of performing nuclear calculations in the shortest time and with the least chance for error. Since the documentation of most computer programs contains the physical basis for the equations that are programmed, only the salient features of the diffusion theory applications will be mentioned herein, and references to the machine programs will indicate the sources of information on mathematical and physical details.

2.2.1 DIFFUSION APPROXIMATION

The diffusion approximation to the energy-dependent Boltzmann equation, which has been used extensively at GE-ANPD, can be classified as inconsistent B_1.[3] In this approximation, with the assumption of spatially constant, energy-independent buckling, all angular moments of the vector flux are retained while the laboratory differential scatter cross section is truncated to include only zero and first Legendre moments.[4] The inconsistency arises in neglecting energy transfers due to first-moment scatter collisions, an assumption required to obtain the diffusion equation. The error introduced by this assumption should be largest for small hydrogen-moderated reactors in which the first angular moments of scatter cross section and energy-dependent part of the vector flux are of the same order as the corresponding zeroth moments. Calculation of the multiplication constant[5] of small cylindrical critical solution experiments performed at the Oak Ridge National Laboratory[6] indicates the validity of the inconsistent B_1 approximation at sizes much smaller than the usual design cores.

The diffusion coefficient, which relates current and flux in Fick's Law, $J = -D\nabla\phi$, in this approximation is[4]

$$D = \frac{1}{3[\gamma\Sigma_t - \mu_0\Sigma_s]} \tag{1}$$

where

Σ_t = total macroscopic cross section
Σ_s = zeroth moment of the laboratory macroscopic scatter cross section
μ_0 = average value of the cosine of the laboratory scatter angle

$$\gamma = \frac{K^2\tan^{-1}(K/\Sigma_t)}{3\Sigma_t^2[K/\Sigma_t - \tan^{-1}(K/\Sigma_t)]} \text{ for positive buckling, } K^2 \tag{2}$$

2.2.2 MULTIENERGY DIFFUSION EQUATIONS

The multienergy diffusion equation, within the approximation described in 2.2.1, when written in terms of lethargy - $u = \ln E_0/E$, where E_0 is the highest source neutron energy - is

$$-\nabla \cdot D(u)\nabla\phi(u, r) + \Sigma_t(u)\phi(u, r) = \int_0^\infty \Sigma_s(u' \rightarrow u)\ \phi(u', r)du' + S(u, r) \tag{3}$$

The source term, $S(u, r)$, in the bare homogeneous critical reactor for which the diffusion coefficient was derived is given by

$$S(u, r) = X(u)\int_0^\infty \frac{\nu}{k}\Sigma_f(u)\ \phi(u, r)du \tag{4}$$

DECLASSIFIED

DECLASSIFIED

where

$\chi(u)$ = the fission spectrum for prompt plus delayed neutrons
$\nu\Sigma_f(u)$ = the fission neutron production cross section
k = the fission eigenvalue required to satisfy neutron conservation.

In practice, equation (3) is applied in multiregion reactors, taking the atomic densities to be constant for separate areas, and in fixed-source problems; however, the diffusion coefficient is then based on recipes. Generally the buckling appearing in the diffusion coefficient is, in multiplying regions, taken to be that of the fundamental oscillatory mode solution to the homogeneous Helmholtz equation

$$\nabla^2\phi + K^2\phi = 0 \tag{5}$$

in the bare equivalent reactor, defined as the bare homogeneous core with reflector savings adjusted to produce the same multiplication constant as the multiregion configuration. In nonmultiplying regions the buckling is taken to be the value for the fundamental oscillatory mode in the directions perpendicular to the normal to the core surface.

In principle the scatter-transfer source, $\int_0^\infty \Sigma_s(u'\rightarrow u)\ \phi\ (u')du'$, could be represented in digitalized form by a transfer matrix, and the multilevel calculations, which must be iterated anyhow when the source is a function of the flux, could be solved in a straightforward manner. When equation (3) is written as a group-conservation equation, this procedure is used; however an assumption must be made regarding the flux variation across the group in computing the flux-weighted group cross sections. The scatter-transfer cross sections are especially sensitive to the assumed variation of flux.

To avoid the need for transfer matrices for each element and for preweighting the transfers with an assumed flux, a slowing down model can be used. When this procedure is used, neutrons are allowed to slow down by collisions with atoms stationary in the laboratory until the average velocity of the Maxwellian distribution for the material temperature is reached. Neutrons surviving to this point are dumped discontinuously into a thermal group having cross sections weighted by the Maxwellian flux.[7,8] If the slowing down density,

$$q(u) = \int_0^u \phi\ (u')du' \int_u^\infty \Sigma_s(u'\rightarrow u'')\ du'' \tag{6}$$

can be related to the scatter-transfer source, then the differential balance equation,

$$\frac{\partial q(u, r)}{\partial u} = S(u, r) - \Sigma_a(u)\ \phi\ (u, r) + \nabla\cdot D(u)\nabla\phi(u, r) \tag{7}$$

where Σ_a = the macroscopic absorption cross section, can be used to eliminate q or ϕ in (3). The slowing-down model essentially provides the required relationship, although when it is in differential form, reference to (3) is not required.

The slowing-down model has the form

$$\gamma\ \partial q/\partial u + q = \xi\,\Sigma_s\phi \tag{8}$$

where ξ is the first moment of the transfer probability distribution in lethargy,

$$\xi(u) = \int_u^\infty P(u\rightarrow u')\,(u' - u)\,du' \tag{9}$$

DECLASSIFIED

DECLASSIFIED

Variations of the slowing-down model are obtained by the value assigned to γ. In the modified-age model[5] $\gamma = 1$. In the Coveyou-McCauley model[9] $\gamma = \xi$. In the approximate Greuling-Goertzel model[10] γ is related to the second moment of the transfer probability distribution by

$$2\xi(u)\gamma(u) = \int_u^\infty P(u \rightarrow u')\,(u' - u)^2\,du' \tag{10}$$

In the Fermi age model, $\gamma = 0$. When $\partial q/\partial u$ is large, as it is in highly absorbing or leaking regions, the value assigned to γ will be important. The Greuling-Goertzel value is recommended for all-purpose use, although in individual cases because of errors in cross sections and the inconsistent B_1 approximation, other values may happen to give better agreement with experiment.

In slowing-down calculations when the entire spatial variation is assumed to be the fundamental mode solution of (5), the leakage term $-\nabla \cdot D\nabla\phi$ in (7) is replaced by $DK^2\phi$, where K^2 is the total buckling of the bare equivalent reactor. Since the slowing-down density tends to be more slowly varying than the flux, being the difference between the integrated sources and the integrated losses at all higher energies, the flux is eliminated between equations (7) and (8) to give a first-order differential equation for q of the form

$$\frac{dq}{du} + \frac{\Sigma_a + DK^2}{\xi\Sigma_s + \gamma(\Sigma_a + DK^2)}\,q = \frac{\xi\Sigma_s}{\xi\Sigma_s + \gamma(\Sigma_a + DK^2)}\,S \tag{11}$$

Equation (11) is solved by trapezoidal integration in multilevel detail by machine programs George,[11] C_5,[12] C-Fine,[13] and ZIP.[14] The flux is evaluated by eliminating dq/du between equations (8) and (11) to give

$$\phi = \frac{q + \gamma S}{\xi\Sigma_s + \gamma(\Sigma_a + DK^2)} \tag{12}$$

In slowing-down calculations with diffusion in one spatial dimension, computed by solving the diffusion equation numerically, the spatial leakage in the directions perpendicular to the direction of calculation is replaced by $DK_\perp^2\phi$, where $K_\perp^2$ is the appropriate perpendicular buckling. Equation (3) for the multienergy, multiregion, one-dimensional reactor is written

$$-\frac{1}{r^j}\frac{d}{dr}\left(r^j D\frac{d\phi}{dr}\right) + (\Sigma_t + DK_\perp^2)\,\phi = \int_0^\infty \Sigma_s(u' \rightarrow u)\;\phi\,(u')\,du' + S \tag{13}$$

where $j = 0$ for slab, 1 for cylindrical, and 2 for spherical geometry. Again the slowing-down model can be used to replace the scatter-transfer source, but the procedure is somewhat different from that when no spatial variable is involved. Equation (8) is integrated trapezoidally between levels n and n + 1 to give

$$q_{n+1} = \frac{q_n[1 - (u_{n+1} - u_n)/2\gamma] + [(\xi\Sigma_s\phi/\gamma)_{n+1} + (\xi\Sigma_s\phi/\gamma)_n](u_{n+1} - u_n)/2}{1 + (u_{n+1} - u_n)/2\gamma} \tag{14}$$

After equation (8) is used to eliminate $\frac{\partial q}{\partial u}$ in equation (7), the balance equation at level n+1 can be written in terms of q_n from equation (14) and the fluxes at levels n and n+1. Since the values of q_n and ϕ_n are known, being taken as zero at level zero and computed successively for subsequent levels, the second-order differential equation for ϕ_{n+1} is

$$-\frac{1}{r^j}\frac{d}{dr}\left(r^j D\frac{d\phi}{dr}\right) + \left[\Sigma_a + DK_\perp^2 + \frac{\xi\Sigma_s}{\gamma + (u_{n+1} - u_n)/2}\right]\phi_{n+1} =$$

$$\frac{q_n[1 - (u_{n+1} - u_n)/2\gamma]}{\gamma + (u_{n+1} - u_n)/2} + \frac{(u_{n+1} - u_n)\,(\xi\Sigma_s\phi)_n}{2\gamma + u_{n+1} - u_n} + S_{n+1} \tag{15}$$

DECLASSIFIED

DECLASSIFIED

Equation (15) is of the form

$$- D\nabla^2 \phi + A\phi = S \qquad (16)$$

which is solved subject to Dirichlet-type boundary conditions as a second-order differential equation for computer applications. The resulting three-point flux equations when written in tridiagonal matrix form are readily solved by the forward-elimination backward-substitution method.[15] The left and right boundary conditions are specified as albedos, defined as the ratio of the inward-directed current to the outward-directed current. Both the multilevel slowing-down diffusion program G-2[16] and the multigroup diffusion program F-N[15] solve the one-dimensional diffusion equation (16) in identical fashion, although the quantities A and S are of different form.

2.2.3 HOMOGENIZATION

Before diffusion theory can be applied to multiregion reactors, it is usually necessary to homogenize fine-detail inhomogeneities existing in some regions. The core region may be made up of multiregion cells containing fuel, moderator, cladding, and other structure. In addition there may be coolant passages that are virtually void in gas-cooled reactors. When structural members and control elements are located symmetrically, a two-dimensional r-θ diffusion calculation[17] may be used in determining rod worth and in power mapping; but for most purposes one-dimensional calculations are relied upon.

Generally these inhomogeneities do not lend themselves to treatment by the diffusion approximation. The material regions are generally too small, or the variations in the vector flux too rapid for the asymptotic diffusion theory flux to become established in the regions of interest. The streaming of neutrons in the void channels in low-density materials tends to increase the leakage rate beyond the value predicted by diffusion theory for the homogenized medium, and in cylindrical geometry it produces in effect an anisotropic diffusion coefficient.[18]

In principle it is possible to use the S_n transport methods or the Monte Carlo methods to define effective-region cross sections and diffusion coefficients, and work along these lines was carried out as a development effort.[19,20,21] Other methods were used in most design calculations, however, partly because they were developed earlier in the program and had been correlated with experiment to some extent, and partly because they were relatively simple, short, and easy to use. A notable exception is the use of one-dimensional S_n calculation to compute the worth of a bank of control rods, discussed in section 3.

The general method for computing homogenized cross sections in design calculations is to define a one-dimensional cell in either slab or cylindrical geometry, whichever more closely describes the actual configuration. The cell boundary should be a line of zero current (mirror boundary). The cell correction for each cell region is defined as the ratio of the average flux in that region to the average flux in the moderator region. The reason for this normalization is that the density of the homogenized moderator primarily determines the diffusion coefficient. The cross sections of each cell region when multiplied by the cell correction and volume fraction of the region are the regional contributions to the homogenized cross sections. This homogenization procedure preserves the cell regional reaction rates relative to the moderator.

If the cell consists of a moderator containing a single optically thin absorber region as either a slab, cylinder, or annular cylinder with central void, the albedo of the absorber can be derived by the method of successive collisions in a monoenergetic transport approximation by assuming spatially flat collided flux distribution, isotropic scattering, and cosine current entrance distribution.[22,23] A cell correction can then be computed assuming diffusion theory and a constant source spatially in the moderator. A machine program for

DECLASSIFIED

DECLASSIFIED

CONFIDENTIAL

the slab configuration is available,[24] and results compare favorably with more sophisticated methods when the absorber is thin. This program was especially useful in analyzing critical experiments containing fuel foils sandwiched between moderator slabs.

For more-complex slab cells containing as many as 50 regions and variable source distributions the monoenergetic P_1 and double P_1 methods are available in program SHAG.[25,26] The double P_3 results compare favorably with S_{12} transport calculations (12 angular increments) and consume about 1/4 the machine time, since the double P_3 calculation is carried out as an equivalent 4-group diffusion calculation.[27]

For multiregion concentric-ring cylindrical fuel cells to be analyzed, a monoenergetic P_3 calculation with piecewise constant-value sources was mechanized as program I_2.[28]

The S_n transport codes were used for cell-correction calculations primarily to verify the validity of the other methods. Special treatment of the mirror outer-boundary condition is required for cell calculations using the various S_n programs because only the zeroth and first moments of the vector flux are reflected with nonzero albedo. The use of a very thin, very dense, nonabsorbing scatterer to provide a mirror material gives satisfactory results.

The correction to the diffusion coefficient as obtained from homogenized cross sections that has been used in design calculations is a recipe based on the early work of Behrens[18] for computing the increase in diffusion area in an infinite medium caused by closely spaced holes. As applied in ANPD programs,[29] where the holes may actually contain absorber materials, the Behrens correction is reduced by the transmission of the hole. The Behrens correction has yielded good correlation with experiments in graphite[30] containing 25 percent void, but in small acryllic-plastic systems[31] containing 50 percent void the leakage is overestimated in proportion to the size of the void.

Although not handled as a problem in homogenization, the streaming of particles from cylindrical tubes has been computed analytically[32] and the average albedo determined. The treatment of a central shaft hole in a reactor has been handled by applying the albedo as a boundary condition to the diffusion-theory calculations.

2.2.4 CROSS SECTIONS

The processing of experimental cross section data to a form usable by machine programs has been a continuing effort based upon the principle that the best available microscopic cross section data should be used in any analysis method in order to assess the reliability of the method. Virtually all machine programs using diffusion theory and requiring cross section data have been written to make use of nuclear data stored on magnetic tape. The principal nuclear data tape that has been used in design calculations contains the cross sections σ_s, $\xi\sigma_s$, σ_{tr}, σ_a, and $\nu\sigma_f$ in either microscopic or macroscopic form at 19 energy levels between 10^7 and 0.0322 electron-volts, plus Maxwellian-averaged thermal-group cross sections for temperatures of 68°, 500°, 1000°, 1500°, 2000°, 2500°, and 3000°F. The data on this tape have been published[33] along with a brief description of the method of processing and will not be discussed further here.

Digitalized cross sections in 19-energy-level detail, even though preserving infinite-dilution cross section integrals and containing cell corrections using the 19-level cross sections, are not adequate to treat resonance absorption effects when the absorber is appreciably self-shielded in resonances. In a brute-force solution to this problem a nuclear data tape in fine energy detail was prepared,[34,35] and a fundamental-mode slowing-down program, C-Fine,[13] was written to make use of these data. The principal features of this C-Fine tape follow.

1. The use of single-level Breit-Wigner formulae[36] to generate resonance cross sections.

CONFIDENTIAL

DECLASSIFIED

DECLASSIFIED

2. The use of a transfer matrix to handle the (n, 2n) reaction in beryllium.
3. The use of high-energy inelastic and anisotropic elastic cross section data to define an effective slowing-down cross section, $\xi\sigma_s$.

The beryllium (n, 2n) reaction in 19-level slowing-down calculations is treated as if one neutron is inelastically scattered and the second neutron arises from fission with no absorption.[37] This procedure has yielded good correlation with experimental multiplication constants,[37] but the spatial distribution of fissions computed from group constants containing beryllium should not be interpreted as a power profile until the effect of beryllium "fissions" is removed. This problem can be avoided in C-Fine, where the Be(n, 2n) transfer cross sections from the statistical-continuum model[38] are used. A more refined treatment of the beryllium cross sections[39,40] shows somewhat different transfer cross sections, but the effect will not become appreciable except in fast reactors.

Program C-Fine provides a direct method of handling Doppler broadening of resonances for which resonance parameters are available. An auxiliary Doppler-broadening program, ANP No. 508, computes Doppler-broadened cross sections from the unbroadened values on the C-Fine tape and makes these broadened cross sections available to the C-Fine calculation.[41]

Although Program C-Fine calculates slowing-down density, flux, multiplication constant, and multigroup constants in a bare, homogenized reactor, its principal application has been to generate cross sections for the 19-level tape by appropriately averaging the fine-detail cross sections. The recently developed 25-group nuclear data tape[42,43] for use with the one-dimensional multigroup diffusion program ODD[44] also contains epithermal cross sections prepared in large measure from data contained on the C-Fine nuclear data tape.

Consistent trends in correlation of multiplication constant with clean, bare critical experiments have been obtained with the C-Fine program and data.[45] Some excellent correlation of danger-coefficient measurements[46] was obtained using 19-level cell-corrected cross sections from program C-Fine in the slowing-down diffusion program G_2,[16] indicating that good results can be obtained for self-shielded resonance absorbers by performing the self-shielding corrections in fine-energy detail before reducing the cross sections to fewer-level detail. An alternative method for handling resonance absorption[47] has been incorporated in program ODD.[44]

2.2.5 KINETICS

Two methods have been incorporated in diffusion codes to determine the period-reactivity relationship; both methods assume six delayed-neutron groups. The first approach is to insert a time dependence, $e^{\omega t}$, for the neutron density in the time-dependent balance equation and solve the resulting diffusion equation as a steady-state problem by reinterpreting the removal and source terms.[48] This procedure has been incorporated in Programs George[11] and G-2.[16] In order to determine a period-reactivity relation, however, it is necessary to run separate calculations for each inverse period, ω, to determine the corresponding multiplication constant. A more efficient method is coded in Program C-5,[12] where the kinetic "constants" in the inhour equation,

$$\rho = l\omega_o + \sum_{j=1}^{6} \bar{\beta}_j \frac{\omega_o}{\omega_o + \lambda_j} \qquad (17)$$

are computed by first-order perturbation theory.[49]

This latter procedure is adequate for reactor periods of interest in critical experiments and normal reactor operation unless a bare-core analysis itself is inadequate. The multiplication of the Be(n, 2n) reaction in beryllium reflectors may require a one-dimensional analysis to obtain correct kinetic effects.

DECLASSIFIED

DECLASSIFIED

2.2.6 POWER HISTORY AND THERMALIZATION EFFECTS

The problems on one hand of fuel burnup, fission product buildup, and other isotopic production dependent on power history and the problems on the other hand of neutron thermalization are interrelated and complicated effects to compute. The former require at least two-space-dimensional calculations to compute adequately the effects of neutrons on the isotopic content of the reactor and vice versa, whereas the latter require reasonably correct treatment of neutron interactions with solid materials to predict the correct neutron spectrum. These calculations have not been as thoroughly mechanized as the less complex calculations discussed in the preceding sections. A semimechanized procedure that combines the two-dimensional, three-group diffusion Program CURE[17] with a 20-group F-N[15] calculation and isotopic concentration subroutine has been written,[50] but has not been used in design calculations. An independent isotopic history trace program is also available.[51]

Since the cross section of fission products, particularly xenon-135 and samarium-149, show resonance structure at energies at which the thermal motions of the scattering nuclei are not negligible compared with the neutron velocity, the adequate prediction of reactivity effects associated with isotopic changes and temperature changes might be expected to require a reasonably correct treatment of neutron interactions with solids. Multi-thermal-group methods using Program F-N[15] have been applied to spectral calculations in hydrided zirconium[52] and beryllium oxide.[53] The square-matrix transfer cross sections were generated by a monatomic gas model[54] (ANP Program 396), a bound oscillator model[55] (ANP Program 419), and a multiphonon model[56] (ANP Program 671) calculations. This procedure has been mechanized in Program ODD,[44] which contains a five-group thermal transfer matrix; however, the adequacy of few-group transfer cross sections preweighted by an assumed (generally nonequilibrium) flux has not been evaluated. More information is retained in slowing-down and thermalization calculations using the transfer kernel, $\Sigma(u' \rightarrow u)$, directly in a multilevel calculation. The integration of the $\Sigma(u' \rightarrow u)\ \phi\ (u')$ product using the computed equilibrium flux to obtain the scatter transfer source seems more desirable.

2.3 TRANSPORT THEORY

To improve the nuclear analysis of heterogeneous epithermal reactors, the machine analysis of multienergy transport theory was extended to a variational- optimum formulation having a broad range of applicability to both neutron and photon aspects of aircraft power reactors.[57,60]

GE-ANPD digital computer Program S constructs neutron and photon transport fields having plane, cylindrical, or spherical symmetry. Lattice detail in geometry, energy, and momentum angles is flexible. Nuclear analysis capabilities not previously available include: (1) simultaneous calculation of both adjoint and flux, combined with first-order-perturbation-theory convergence acceleration applied to eigenvalue, isotropic adjoint field or source, isotropic flux field or source, adjoint current field or source, and current field or source, with eigenvalue acceleration chain-compounded continually to any specified order; (2) isotropic and anisotropic scatter transfer, both exoergic and endoergic, through an unlimited energy range; (3) flexible array of measurable eigenvalues, including critical fuel loading, critical moderator loading, critical poison loading, and reactor period with inclusion of any number of delayed-production groups; (4) neutron-moderation heating, photon-energy production, photon-energy deposition, and biological-dose deposition; (5) performance trends, provided as differential perturbation ratios spanning coupled variation of all eigenvalues and reactor material loadings; (6) material action traverses,

DECLASSIFIED

DECLASSIFIED

giving the perturbation worth of materials as functions of location; (7) eigenvalue statistical perturbation accruing from uncorrelated cross-section uncertainties; (8) variational-optimum space-energy cell homogenization, weighted with the product of adjoint and flux, providing complete quasi-constant input for gross diffusion analyses; (9) variational-optimum gross reactor kinetics, with inclusion of reflector effects and method-of-control effects; (10) manifestly firm assurance of unbiased convergence, for any physical problem, provided by use of a mathematical iteration loop constructed in precise correspondence with the physics of successive free flights.

The analysis method is a logical extension of ideas originated by B. G. Carlson in the Los Alamos S_n neutron codes.[58] The program uses Carlson's composite discrete-point and piecewise-linear digital representation, as well as selected portions of his integration method. The calculation has been coded for the IBM 7090 electronic data processing system, using a parallel-logic symbolic-binary reformulation of Carlson's FLOCO compiler to provide construction of the dual four-dimensional transport field on a basis sufficiently flexible to span the range of interest in reactor design.[59]

References 61 through 74 provide a complete summary of the physics and mathematical techniques adapted to engineering problems. These applications include the analysis of fast reactors and the extension of the theory to photon behavior.

2.4 MONTE CARLO APPLICATIONS TO HETEROGENEOUS CORE ANALYSIS

The Monte Carlo approach to solving numerical-analysis problems is particularly useful when the problem is probabilistic in nature. Clearly the electron, photon, and neutron transport problems that arise in analyzing a reactor core can be expressed in terms of a set of probability functions. By utilizing the voluminous compilations of experimental and theoretical cross section data, it is possible to isolate the important particle interactions and characterize them in terms of the probability functions as required for a particle life-history Monte Carlo analysis. As a particle life history is traced from the source point to eventual escape or absorption, the transport characteristics are tallied with the fine detail limited only by computer storage or running-time considerations. It follows that an approximation of the particle distribution in space and energy can be obtained by a superposition of many individual life histories. It also follows that the accuracy of the approximation is dependent on the number of life histories included in the final result.

One of the most important assets of the Monte Carlo method as a reactor-analysis technique is the versatility available for specifying the reactor geometry with three space dimensions and for treating the rapidly varying material compositions of a heterogeneous system. The use of the Monte Carlo method for shield analysis, which is discussed in a later section, was recognized fairly early as a useful and valid analysis technique. However, the use of Monte Carlo for reactor analysis has not received such clear-cut acceptance. The objection to Monte Carlo as a reactor-analysis technique arises primarily from the fact that the characteristic reactor parameters are determined by the thermal neutron distribution and this is the most difficult property to compute from a probable-life-history program. Specifically, a source distribution of neutrons must be followed down in energy via some slowing-down model until a sufficiently large number of particles reach thermal energy. First, the slowing-down process requires a relatively long time, even with high-speed computers, before an individual-particle life history can be terminated by a thermal-energy cutoff. Second, the results from a statistical slowing-down technique may tend to be unstable in the thermal-energy range because of the slow convergence of the method.

DECLASSIFIED

DECLASSIFIED

The work done to develop Monte Carlo as an effective neutron-analysis technique started with two definite types of neutron transport problems. The first effort centered around the development of digital-computer slowing-down programs. Five slowing-down programs were written. Three of them were development experiments from which two production programs evolved. The first production code, "Slowing Down Probability in a Lattice Generated by a Three-Region Cell of Finite Length"[75] follows neutrons down in energy from a monoenergetic point source to a specified energy cutoff. The second production code, "Slowing Down in a Finite Heterogeneous Cylinder with Fuel Tubes"[76] follows neutrons down in energy from an energy distribution at an arbitrary point source. Both programs were written for a very specific geometry since the programming time required to write a specialized program is shorter than that required to write a general-purpose program. Furthermore, the amount of computer time consumed in running a given production case using a specialized program is less than the time consumed using a general-purpose program.

The second effort centered around the development of digital-computer diffusion tensor programs. The diffusion coefficients computed by the Monte Carlo technique are directly applicable to multigroup computations. Three programs evolved for the computation of diffusion coefficients in heterogeneous systems. The first program, "Diffusion Tensor for Slab Geometry,"[77] is limited to a lattice of alternate solid-slab and void-gap regions. The second program was a development experiment designed to compute the diffusion length in a heterogeneous slab system of up to 300 distinct slab regions. The third program computes the diffusion length in a lattice generated by a three-region hexagonal cell identical with that used in the slowing-down program.

One further step is required in the analysis if the diffusion coefficients are to be used for a multigroup calculation. That is an investigation of the "Validity of the Homogenization Approximation for End-Leakage Calculations."[78]

The most recent work with Monte Carlo in neutron analysis involves the modification and application of a generalized Monte Carlo neutron program[79] to the advanced reactor configurations wherein a three-space-dimension analysis was required to represent accurately the material-composition variations. The "Flexible Monte Carlo," FMC, analysis was quite successful in computing neutron leakage parameters and fine power distributions. The correlation was attained by a farily definite experiment-theory correlation with the results of the critical experiment measurements.

The problems mentioned earlier regarding the difficulty in treating the thermal neutron characteristics of a reactor by a Monte Carlo technique have been largely resolved by work at various other installations. The work of Drawbaugh of Combustion Engineering, Spanier and Amster at Westinghouse, Penny and Zerby at Oak Ridge, and Rief at Brookhaven has provided the basis for the calculation of conditional, adjoint, and self-refining Monte Carlo analysis procedures for computing the response at a given receiver point due to either neutrons or photons.

The use of Monte Carlo as a technique for computing the secondary heating from gamma radiation has proved quite successful. Consequently, a gamma-heating program written for 400 cylindrical annular regions has become an invaluable production program.[80]

DECLASSIFIED

DECLASSIFIED

2.5 REFERENCES

1. Krase, J. M., and Cyl-Champlin, C., "Synthetic Experiment Design Techniques in Reactor Analysis," GE-ANPD, APEX-303, November 30, 1956.
2. Wenstrup, F. D., "SEDP - Synthetic Experiment Design Program," GE-ANPD, APEX-521, November 1958.
3. Hurwitz, Jr., H., and Zweifel, P. F., "Slowing Down of Neutrons by Hydrogenous Moderators," Journal of Applied Physics 26, 923, 1955.
4. Selengut, D. S., "Critical Mass Calculations for Bare Hydrogen Moderated Reactors by Means of Transport Theory," GE-ANPD, APEX-121, September 1952.
5. Selengut, D. S., "Criticality Calculations on the 701 Computer (Program A)," GE-ANPD, XDC 55-3-18, February 17, 1955.
6. Beck, C. K.; Callihan, Dixon; Morfitt, J. W.; Murray, Raymond L., "Critical Mass Studies. Part III," Carbide and Carbon Chemical Corp., K-343, April 19, 1949.
7. Terrall, J. R., and Barnett, A. H. "The Calculation of Thermal Average Cross Sections," GE-ANPD, XDC 59-6-627, June 1, 1959.
8. Cooper, J. R., and Henderson, W. B., "A Program for the Calculation of Average Thermal Cross Sections on the IBM 704," GE-ANPD, XDC 60-5-51, March 15, 1960.
9. Coveyou, R. R., and McCauley, B. T., "Suggested Correction to the Age-Diffusion Equation as Used by the ANP Physics Group," Oak Ridge National Laboratory, AECD-4043, November 6, 1951.
10. Goertzel, Gerald, and Greuling, Eugene, "An Approximate Method of Treating Neutron Slowing Down," Nuclear Science and Engineering 7, 69, 1960.
11. Hoffman, T. A., and Henderson, W. B., "General Reactor Analysis Computer Program for the IBM 704, Program George," GE-ANPD, APEX-543, October 1959.
12. Fischer, P. G.; Wenstrup, F. D.; Pastore, R. A.; "Program C_5 - Direct and Adjoint Bare Reactor Program - Multigroup Constant Generator," GE-ANPD, XDC 59-6-220, May 13, 1959.
13. Klingenberg, E. W., and Henderson, W. B., "Program C-Fine, A Bare Reactor Slowing Down Calculation With Fine Energy Detail," GE-ANPD, XDC 59-12-230, December 22, 1959.
14. Orr, W. L., "Program ZIP, A Generalized Reactor (Nuclear Analysis) Sequence (IBM 7090)," GE-ANPD, APEX-601, May 26, 1961.
15. Fischer, P. G., "Multigroup, Multiregion, One Space Dimension Neutron Diffusion Theory Calculation - Program F-N (ANP No. 308)," GE-ANPD, XDC 60-3-68, January 15, 1960.
16. Haffner, J. W., "Use of Program G-2 for Shielding Calculations," GE-ANPD, DC 59-7-170, July 20, 1959.
17. Trantham, Jr., F. M., "CURE, A Two-Space-Dimension, Multigroup Code for the IBM 704," GE-ANPD, APEX-452, August 12, 1958.
18. Behrens, D. J., "The Effect of Holes in a Reacting Material on the Passage of Neutrons, With Special Reference to the Critical Dimensions of a Reactor," United Kingdom Atomic Energy Authority, AERE-T/R 103, February 21, 1949.
19. Beeler, J. R., and Popp, J. D., "Monte Carlo Research Series: Directional Diffusion Coefficients for a Lattice Generated by a Three-Region Hexagonal Cell," GE-ANPD, XDC 59-8-56, October 1, 1958.
20. Duane, B. H., and Stanley, M. J., "Space-Energy Cell Homogenization," GE-ANPD, APEX-489, August 1, 1958.
21. Duane, B. H., "Neutron and Photon Transport Plane-Cylinder-Sphere GE-ANPD Program S Variational Optimum Formulation," GE-ANPD, XDC 59-9-118, January 9, 1959.
22. McLennan, J. A., "Reactor Cell Calculations," GE-ANPD, APEX-197, August 15, 1955.

DECLASSIFIED

DECLASSIFIED

23. Mezger, F. W., "Analysis of Thermal Flux Distribution in the Direct Cycle Aircraft Reactor," GE-ANPD, APEX-120, December 8, 1952.
24. Henderson, W. B., "Modifications to Analytic, Two-Zone, Slab Cell Correction Program (Program No. 209)," GE-ANPD, DC 59-4-45, April 1, 1959.
25. Wenstrup, F. D., "Program SHAG - A Monoenergetic Multiregion Slab Cell Correction Calculation," GE-ANPD, XDC 60-8-22, June 8, 1960.
26. Wenstrup, F. D., "Conversion of Program SHAG to the IBM 7090 (ANP Program No. 518)," GE-ANPD, APEX-607, April 28, 1961.
27. Anderson, B. L.; Dawis, J. A.; Gelbard, E. M.; Jarvis, P. H.; "FLIP - An IBM 704 Code to Solve the P_1 and Double P_1 Equations in Slab Geometry," Westinghouse Electric Corporation, WAPD-TM-134, March 1959.
28. McCready, R. R., and Vollenweider, D. B., "IBM 704 Program for the Solution of the Neutron Transport Equation in Fifty Concentric Annuli by the Weil Method (Program I_2)," GE-ANPD, APEX-468, September 1959.
29. Henderson, W. B., "Behrens' Correction in ANPD Computer Programs," GE-ANPD, XDCL 59-7-176, July 20, 1959.
30. Seren, L., Transactions of the American Nuclear Society 1, 1958
31. Check, P. S., "Pulsed Neutron Determination of the Diffusion Coefficient of Void-Containing Plexiglas," GE-ANPD, DC 59-10-117, October 16, 1959.
32. Terrall, J. R., "Particle Escape From the Ends of Cylindrical Tubes," GE-ANPD, APEX-525, March 1958.
33. Henderson, W. B., and Stanley, M. J., "Cross Sections for Reactor Analysis," GE-ANPD, APEX-515, May 1957. Stanley, M. J., "Supplement I to APEX-515," XDC 59-11-72, October 26, 1959. Ferry, M. S., "Supplement II to APEX-515," XDC 60-6-148, April 21, 1960. Ferry, M. S., "Supplement III to APEX-515," XDC 61-4-34, April 1961.
34. Cooper, J. R., and Henderson, W. B., "Nuclear Data Tape Program with Fine-Energy Detail," GE-ANPD, XDC 60-8-69, May 13, 1960.
35. Sullivan, R. E., and Henderson, W. B., "Reactor Neutron Cross Sections in Fine-Energy Detail," GE-ANPD, APEX-704, November 1961.
36. Sullivan, R. E.; Cooper, J. R.; Henderson, W. B.; "Breit-Wigner Program (ANP No. 181)," GE-ANPD, APEX-641, August 1961.
37. Dawson, F. G., "Evaluation of Beryllium and Uranium Cross Sections for Neutron Diffusion Theory Calculations," GE-ANPD, APEX-633, August 1961.
38. Feld, B. T.; Feshbach, H.; Goldberger, M. L.; Goldstein, H.; Weisskopf, V. F.; "Final Report of the Fast Neutron Data Project," Nuclear Development Associates, NYO-636, January 31, 1951.
39. Kostigen, T. J., "Beryllium Neutron Cross Sections," GE-ANPD, DC 60-12-98, December 13, 1960.
40. Kostigen, T. J., "Nineteen-Group Beryllium Cross Sections," GE-ANPD, DC 60-8-108, August 15, 1960.
41. Henderson, W. B., "The Effect of Doppler Broadening on Multiplication Constant in an Intermediate Reactor (D141-A-1)," GE-ANPD, DC 60-4-143, April 18, 1960.
42. Wenstrup, F. D.; Hoffman, T. A.; Wilcox, A.; Herrmann, R.; "IBM 7090 Programs to Complete and Modify a Nuclear Data Tape," GE-ANPD, APEX-708, August 1961.
43. Zwick, J. W., and Kostigen, T. J., "Twenty-Five Group Reactor Nuclear Data Tape Cross Sections," GE-ANPD, APEX-709, July 1961.
44. Fischer, P. G.; Wenstrup, F. D.; Hoffman, T. A.; "Program ODD - A One-Dimensional Multigroup Reactor Analysis Program for the IBM 704," GE-ANPD, DC 61-2-97, February 10, 1961.

DECLASSIFIED

DECLASSIFIED

45. Henderson, W. B., and Klingenberg, F. W., "Correlation of Many-Energy Bare-Reactor Analysis (Program C-Fine) With Clean Critical Experiments Including Beryllium-Oralloy and Beryllia-Oralloy Systems," GE-ANPD, XDC 60-1-211, January 25, 1960.
46. Cooper, K. V., and Henderson, W. B., "Reactivity Effects of Structural Materials in the BEM-IIB," GE-ANPD, APEX-705, August 1961.
47. Fischer, P. G., "An Alternate Method of Computing Resonance Absorption and Resonance Escape Probability in Intermediate Reactors," GE-ANPD, DC 60-2-295, February 1960.
48. Duane, B. H.; Reid, R. E.; Selengut, D. S.; "Off-Critical Reactor Theory," GE-ANPD, APEX-458, October 1956.
49. Fischer, P. G., "Reactor Kinetic Theory," GE-ANPD, XDC 58-10-105, August 18, 1958.
50. Breslauer, S. K., "HADES - A Two-Dimensional Burnup Analysis, Program 623," GE-ANPD, DC 61-1-132, January 20, 1961.
51. Karriker, F. P., "Extension of Isotopic History Trace (Program 431), GE-ANPD, XDC 60-5-144, May 3, 1960.
52. Wetzel, D. E., "Multigroup Calculation of Thermal Spectra in Hydrogen Bound to Zirconium," GE-ANPD, XDC 60-6-134, June 8, 1960.
53. Henderson, W. B.; Klingenberg, F. W.; Sullivan, R. E.; Cooper, K. V.; "Application of Multi-thermal Group Calculations to Ceramic Reactors," GE-ANPD, DC 61-3-160, March 30, 1961.
54. Bareiss, E. H.; Denes, J. E.; Jankus, V. Z.; "Calculation of Group Cross Sections for Hot Monatomic Moderator with Variable Flux Weighting Within Groups, 704 Code 521/RE 145," Argonne National Laboratory, ANL-5984, May 1959.
55. Cohen, E. R., and Vaughan, E. U., "Thermal Neutron Spectrum in Harmonically Bound Hydrogen Moderators," Atomic International, NAA-SR-3377, January 15, 1959.
56. Schofield, P., and Hassitt, A., "The Calculation of Thermal Spectra," Second United Nations International Conference on the Peaceful Uses of Atomic Energy, Vol. 16, 1958, p 18.
57. Duane, B. H., "Neutron and Photon Transport Theory, Plane-Cylinder-Sphere, GE-ANPD Program S, Variational Optimum Formulation," GE-ANPD, XDC 59-9-118, September 1959.
58. Carlson, B. G., "Solution of the Transport Equation by S_n Approximations," Los Alamos Scientific Laboratory, LA-1891 1955.
59. Duane, B. H., "Symbolic Matrix Translator, GE-ANPD Program FLOCO-V, Field-Test Formulation," GE-ANPD, APEX-618, March 2, 1961.
60. Duane, B. H., "Transport Perturbation Theory of Convergence Acceleration," Transactions of the American Nuclear Society, Vol. 2, No. 2, 1959 Winter Meeting, Session 13-3, November 1959.
61. Duane, B. H., "Neutron and Photon Transport: Plane, Cylinder, Sphere," GE-ANPD, APEX-394, July 31, 1957.
62. Carlson, B. G., "The S_n Method and SNG Codes," Los Alamos Scientific Laboratory, LAMS 2201, January 26, 1956.
63. Duane, B. H., and Stanley, M. J., "Space-Energy Cell Homogenization," GE-ANPD, APEX-489, August 1, 1958.
64. Duane, B. H., "Cross Sections for Reactor Analysis," GE-ANPD, XDC 58-8-146, August 6, 1958.
65. Stanley, M. J., "Digital Computer Program S_3," GE-ANPD, XDC 58-12-73, August 15, 1958.
66. Stanley, M. J., "Klein-Nishina Photon Cross Sections," GE-ANPD, APEX-487, May 1959.

DECLASSIFIED

DECLASSIFIED

CONFIDENTIAL

67. Stanley, M. J., "Klein-Nishina Photon Cross Sections," Transactions of the American Nuclear Society, Vol. 2, No. 1, June 1959.
68. Reid, R. E., "Development and Correlation of Analysis Methods for Fast Reactors," GE-ANPD, XDC 59-12-94, November 1959.
69. Ferry, M. S., "Pair-Production Cross Sections for Gamma Rays (gamma-2, ANP Program 397)," GE-ANPD, XDC 60-3-67, January 12, 1960.
70. Reid, R. E., and Breslauer, S. K., "Correlation of ZPR-III Spherical Fast Critical Assemblies," GE-ANPD, XDC 60-12-156, December 1960.
71. Reid, R. E., "A First-Order Perturbation Theory Approach to the Calculation of Parametric Information for Fast Reactors," Transactions of the American Nuclear Society, Vol. 3, No. 2, 1960 Winter Meeting, Session 15-6. December 1960.
72. Ferry, M. S., "Reactor Photon Data Tape," GE-ANPD, XDC 61-5-36, March 15, 1961.
73. Ferry, M. S., "Photon Cross Sections," GE-ANPD, APEX-613, August 1961.
74. Zwick, J. W., and Kostigen, T. J., "Twenty-Five Group Reactor Nuclear Data Tape Neutron Cross Sections," GE-ANPD, APEX-709, June 13, 1961.
75. Beeler, J. R., and Lutz, J. M., "Slowing-Down Probability in a Lattice Generated by a Three-Region Cell of Finite Length," GE-ANPD, XDC 59-7-57, January 1, 1959
76. Beeler, J. R., and Martin, D. R., "Interim Report on Heterogeneous Cylinder Slowing-Down Program 0159," GE-ANPD, XDC 60-5-52, March 18, 1960.
77. Beeler, J. R., "SLAB Geometry, Diffusion Tensor," GE-ANPD, XDC 59-1-254, December 1, 1958.
78. Beeler, J. R., "Validity of the Homogenization Approximation for End-Leakage Calculations," Nuclear Science and Engineering, Vol. 9. No. 1, January 1961, pp. 35-40.
79. MacDonald, J. E., and Loechler, J. J., "Flexible Monte Carlo Program, FMC-N and FMC-G," GE-ANPD, APEX-706, April 28, 1961.
80. Beeler, J. R.; McGurn, J. L.; et al.; "Interim Report on Gamma Heating Program 0307 for a Finite Heterogeneous Cylinder," GE-ANPD, XDC 59-11-12, September 1959. Smith, M. R., "Modification to the Heterogeneous Cylinder Gamma Heating Program 0307," GE-ANPD, XDC 60-9-19, July 15, 1960.

CONFIDENTIAL

DECLASSIFIED

DECLASSIFIED
CONFIDENTIAL

3. CONTROL ROD EXPERIMENTS AND ANALYSIS METHODS

Control of a nuclear chain reaction and the related problem of predictability of the nuclear effectiveness of a reactor control system are of great practical concern in establishing the design of reactors in general and of highly optimized reactors such as those for aircraft propulsion in particular. Although available methods and procedures of analysis were satisfactory for nuclear calculations of ANP reactors with no control elements inserted, evaluating control element effects was very difficult. The difficulties depend upon the type of reactor and such factors of the control elements as the shape, size, and complexity, number, radial location, and degree of insertion. Mathematical models that treat control elements as transparent to fast neutrons or black to thermal neutrons are not adequate for control elements in epithermal or intermediate reactors.

To test ANP Department methods for evaluating control rod effects, systematic calculations were made for solid-moderator-reactor configurations, for which a series of control rod experiments was performed. The reactor assemblies were hydrogen-moderator, beryllium-reflector, epithermal reactors that were under development by the GE-ANP Department.

3.1 SM-1 REACTOR ASSEMBLY

Each SM-1 reactors[1, 2] consisted of a hydrogen-moderator cylindrical core and a beryllium side reflector. The core had an effective radius of 12.981 inches and a height of 30 inches. The effective reflector thickness varied with each configuration. The moderator in each fuel-moderator cell was a hydrided zirconium rod within a mild-steel support tube. The fuel was in the form of Oralloy tube sheets wrapped around the support tube and held in place by type 302 stainless steel filler sheets. These cells were inserted into aluminum hexagonal tubes of the reactor matrix.

Hexagonal beryllium blocks 1.66 inches across flats placed in the aluminum matrix made up the side reflector. There were no end reflectors.

The assembly was separable into halves along a vertical plane. One half was mounted on a fixed table, and the other half on a movable table.

3.1.1 CONTROL ELEMENTS

Measurements were made and analytical calculations were performed of effects of three categories of circular cylindrical rod assemblies:

1. B_4C rods.
2. B_4C rods in acrylic plastic hexagons.
3. Mild-steel jackets in acrylic plastic hexagons.

CONFIDENTIAL
DECLASSIFIED

DECLASSIFIED

In addition, the worths of noncircular boral rods that replaced, one at a time, a central fuel-moderator cell of the fixed half of the reactor matrix were determined both experimentally and theoretically.

Rod-cell specifications are listed in Table 3.1. Their cross-sectional views are shown in Figures 3.1, 3.2, and 3.3.

3.2 GENERAL ANALYSIS PROCEDURE

Calculations of control element effects can be reduced to the following major steps:

1. Calculation of effects of fully inserted central rods.
2. Correction for partial rod insertion, if applicable.
3. Determination of worths of noncentral rods as a function of radial location.
4. Computation of the worths of rings of rods.

The control rod effects were calculated on a two-group basis employing flux-weighted fast-group constants from a multienergy, normal-mode, slowing-down diffusion treatment. Thermal-flux depression factors calculated with P_3 approximation to transport theory were used.

Three combinations of models were employed in the computation of the core and reflector two-group constants in the case of central circular rods. These combinations were:

1. Modified-age theory with no Behrens* correction for both the core and beryllium reflector.
2. Modified-age theory with no Behrens correction for the core, Coveyou-Macauley theory for the reflector.
3. Modified-age theory with Behrens correction for the core, Coveyou-Macauley theory with no Behrens correction for the reflector.

Modified-age theory with no Behrens correction was used in getting the core and reflector two-group constants in the case of single noncentral rods or rings of rods.

The multiplication constant, k, of a reactor with no control elements inserted was obtained by employing Program George[3] multiplication-constant matching procedure. The associated core and reflector two-group constants were used in calculations of the multiplication constant, k_{in}, of the reactor with control elements inserted.

Reactivity worth of a control element is defined as percent $\Delta k/k = \frac{k_{in} - k}{k} \times 100$. Group-averaged albedos express the insertion of control elements for which the available rod-transmission programs are applicable. The rod-transmission subroutine in Program George using McLennan's treatment,[5] and Multienergy Transport Theory 704 Program S[6] were employed to compute rod albedos. When a poison rod or a mild-steel jacket in an acrylic plastic hexagon replaces a central fuel-moderator cell, the rod or the steel jacket is represented by albedos and the acrylic plastic is treated as a separate region. When a single-rod assembly of this type is noncentrally located, both the rod and acrylic plastic or the jacket and acrylic plastic must be represented by albedos.

*The application of Behrens correction accounts for the change in the diffusion coefficients caused by the presence of voids in the reactor.[4]

DECLASSIFIED

DECLASSIFIED

CONFIDENTIAL

TABLE 3.1

CONTROL ROD SPECIFICATIONS

Boron Carbide Poison Rods

Rod No.	Diameter, in.	Length, in.	Weight, g
B1	0.500	14.879	91
B3	1.000	14.974	351
B5	0.750	14.938	198
B32	1.11 (ID) 1.41 (OD)	15.250	269

Mild-Steel Jackets

Nominal Diameter, in.	Inner Diameter, in.	Outer Diameter, in.	Weight, g
1/2	0.518	0.563	76
3/4	0.768	0.813	107
1	1.018	1.063	142
1-1/2	1.555	1.625	369

Noncircular Boral Rods

Rod Cross Section Shape	Dimensions, in.	Weight, g
Slab	1 strip 1/8 x 7/8 x 16	72.3
Cruciform	2 strips 1/8 x 3/8 x 16 each	147
Square	7 strips 1/8 x 7/8 x 16 each	506
Truncated triangle (Actually an isoscelle trapezoid)	Base: 7/8; top flat: 1/8; Altitude: 5/8; length: 16	210

Acrylic Plastic Moderator

Hexagonal Tube

Cross Section: Regular hexagon 1.600 in. across flats.
A full-length axial hole through each hexagon

Length: 15.00 ± 0.04 in.

Nominal Hole Size, in.	Hole Diameter, in.	Weight, g
1/2	0.594	565
3/4	0.844	485
1	1.094	372

Rod P41

Length: 15.000 in.
Diameter: 0.993 in.
Weight: 225 g

CONFIDENTIAL

DECLASSIFIED

DECLASSIFIED

CONFIDENTIAL

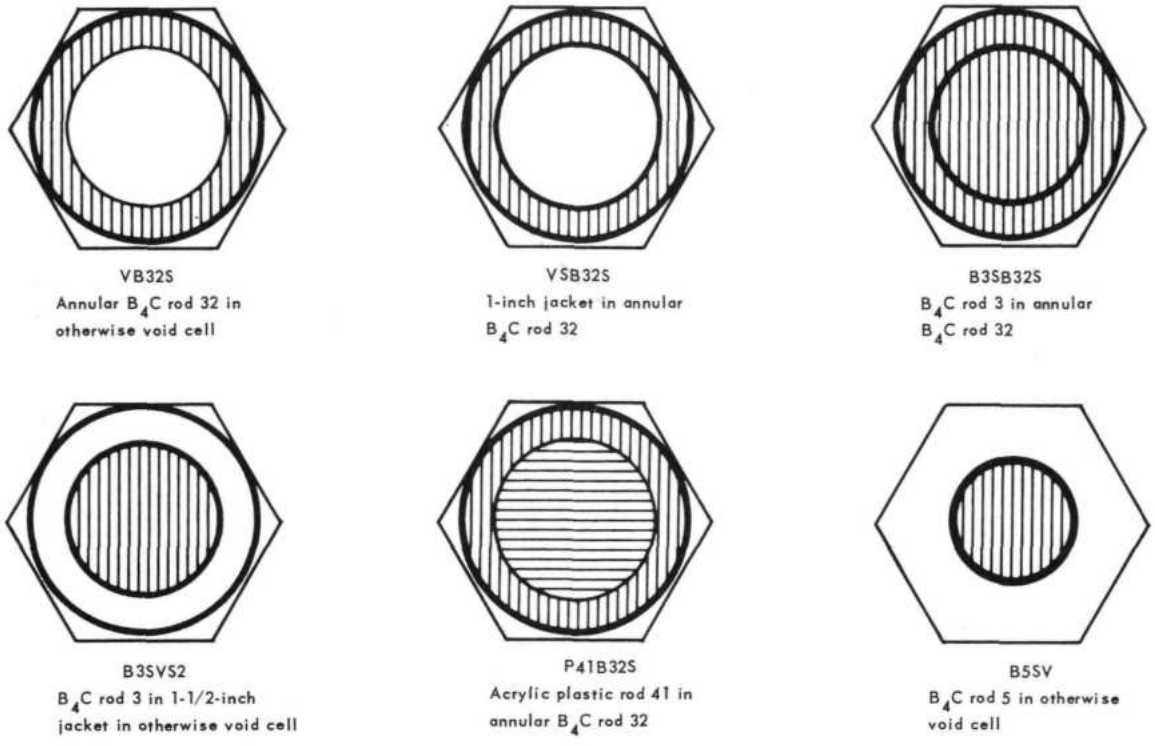

Fig. 3.1 – Cross-section views of various B_4C rods

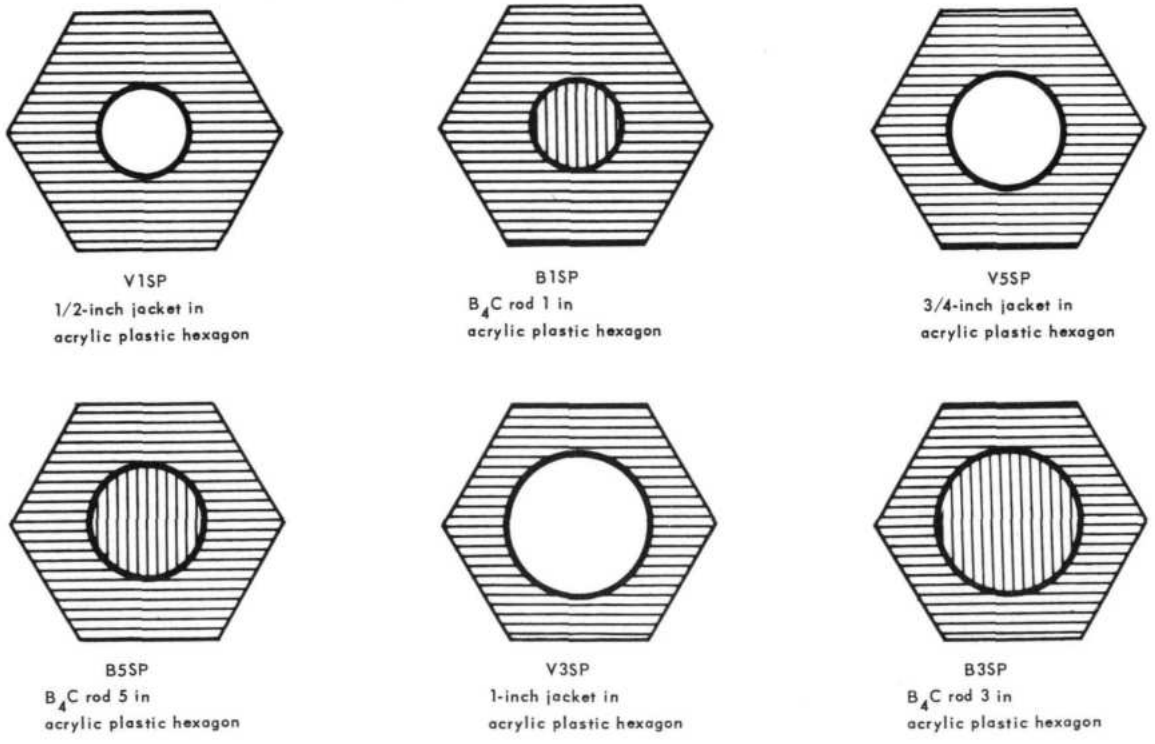

Fig. 3.2 – Cross-section views of various B_4C rods and steel jackets in acrylic plastic hexagons

CONFIDENTIAL

DECLASSIFIED

DECLASSIFIED

CONFIDENTIAL

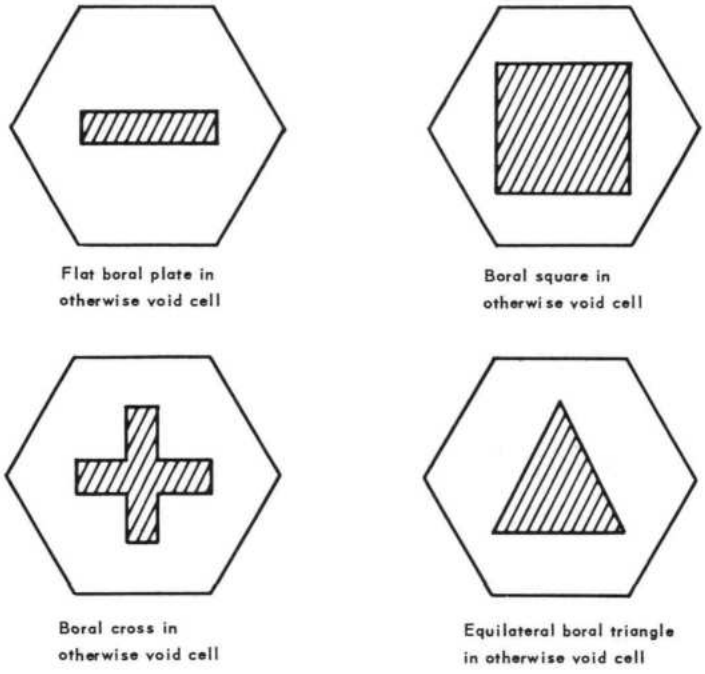

Fig. 3.3 – Cross-section views of boral rods with non-circular cross sections

3.3 RESULTS OF THEORY-EXPERIMENT COMPARISON

3.3.1 CIRCULAR CYLINDRICAL CENTRAL RODS

The effect of a fully inserted central control rod assembly was calculated with one-dimensional, multiregion, multienergy, two-group diffusion theory Program F-2.[7] The halfway insertion of the rods was accounted for by cosine-squared longitudinal weighting.* The effect of either a B_4C rod 5 (solid absorber rod) in a void or an identical B_4C rod 5 is an acrylic plastic hexagon (solid absorber rod in a moderating hexagonal tube) replacing a fuel-moderator cell was determined by running two-dimensional, diffusion-theory Program CURE[8] in R, Z geometry. A comparison of experimental and calculated worths (percent $\Delta k/k$) of various central, circular rods halfway inserted in SM-I-2-C reactor is shown in Table 3.2.

When the insertion of a rod is represented in terms of albedos computed by McLennan's treatment, theory-experiment discrepancies† range from about plus or minus 5 percent for B_4C absorber rods to about 20 percent (overprediction) for B_4C rods in acrylic plastic hexagons. When albedos computed with Program S are used, theory-experiment discrepancies amount to about 40 percent.

It should be noted that the worth computed by Program CURE of a B_4C absorber rod halfway inserted into a channel of a considerably larger radius than that of the rod is about 61 percent of that of a fully inserted identical rod; the longitudinal cosine-squared weight-

*This is equivalent to flux-squared longitudinal weighting, since in the absence of end reflectors a cosine distribution can be assumed for the longitudinal flux.

†$$\text{Percent discrepancy} = \frac{\text{calculated \% } \Delta k/k - \text{experimental \% } \Delta k/k}{\text{experimental \% } \Delta k/k} \times 100$$

CONFIDENTIAL

DECLASSIFIED

UNCLASSIFIED

CONFIDENTIAL

TABLE 3.2

COMPARISON OF EXPERIMENTAL AND CALCULATED WORTHS OF CIRCULAR CENTRAL RODS

Circular Cylindrical Rod Assembly	Experimental Worth, %Δk/k	Calculated Worth, Cosine-Squared Longitudinal Weighting[a] Core: MA,[a] NB[a] Reflector: MA,[a] NB[a] %Δk/k	% Discrepancy	Core: MA,[a] NB[a] Reflector: CM,[a] NB[a] %Δk/k	% Discrepancy	Core: MA,[a] B1[a] Reflector: CM,[a] NB[a] %Δk/k	% Discrepancy	
B5SV	-0.893 ± 0.013	-0.688	-23.0	-0.667	-25.3	-0.637	-28.7	↑
B3SVS2	-1.086 ± 0.021	-0.997	- 8.2					
B3SB32S	-1.488 ± 0.030	-1.552	+ 4.3	-1.534	+ 3.1	-1.451	- 2.5	
VB32S	-1.303 ± 0.026	-1.245	- 4.5					
VSB32S	-1.299 ± 0.026	-1.245	- 4.2	-1.229	- 5.4	-1.162	- 6.7	B_4C rods
P41B32S	-1.443 ± 0.029	-1.262	-12.5	-1.239	-14.1	-1.183	-18.0	
S-B5SV[b]	-0.893 ± 0.013	-0.482	-46.0	-0.495	-44.6	-0.453	-49.3	
S-B3SVS[b]	-1.086 ± 0.021	-0.632	-41.8			-0.581	-46.5	↓
S-B3SB32S[b]	-1.488 ± 0.030	-1.014	-31.9					
B1SP2	-0.394 ± 0.008	-0.464	+17.8	-0.506	+28.4	-0.435	+10.4	↑
B5SP2	-0.675 ± 0.013	-0.782	+15.9	-0.805	+19.3	-0.717	+ 6.2	B_4C rods in acrylic plastic hexagons
B3SP2	-0.939 ± 0.019	-1.082	+15.2	-1.086	+15.7	-0.988	+ 5.2	
S-B5SP2[b]	-0.675 ± 0.013	-0.494	-27.0					↓
V1SP2	+0.206 ± 0.004	+0.154	-25.2	+0.128	-37.9	+0.147	-28.6	SS jackets in
V5SP2	+0.163 ± 0.003	+0.122	-25.2	+0.103	-36.8	+0.123	-24.6	acrylic plastic
V3SP2	+0.086 ± 0.002	+0.082	- 4.7	+0.076	-11.6	+0.081	- 5.8	hexagons
		Longitudinal Worth Computed with CURE						
B5SV	-0.893 ± 0.013	-0.844	- 5.5	-0.816	- 9.4	-0.780	-12.7	
B5SP2	-0.675 ± 0.013	-0.811	+20.1	-0.835	+23.7	-0.744	+10.2	
S-B5SV[b]	-0.893 ± 0.013	-0.590	-33.9	-0.605	-32.2	-0.554	-38.0	

[a]Explanation of abbreviations:
MA Modified-age slowing-down model
CM Coveyou-Macauley slowing-down model
NB No Behrens Correction
B1 Original (701) Behrens Correction
[b]Albedos computed with Program S

ing result is 50 percent. The rod worth computed by means of CURE is in good agreement with its measured value; the rod worth computed by the cosine-squared method is not. However, when the same B_4C rod in a tightly fitting acrylic plastic hexagon replaces a fuel-moderator cell in one-half of the reactor matrix, both CURE and cosine-squared longitudinal weighting overpredict the rod effect. In the case of the B_4C poison rod in a void, Program CURE apparently accounts for the "lightning-rod" effect, i.e., for the increase in absorption at the rod tip.[9, 10]

Figure 3.4 shows radial fluxes calculated by Program F-2 in the SM-I-2-C reactor with a central B_4C rod-5 inserted. Figure 3.5 shows CURE-computed longitudinal flux distributions in the core 2.251 centimeters from the reactor axis with the central rod halfway inserted. Figures 3.6 and 3.7 illustrate the respective flux distributions with the same B_4C rod 5 in an acrylic plastic hexagon replacing a central fuel-moderator cell.

3.3.2 NONCIRCULAR CENTRAL RODS

Since GE-ANPD machine programs employed in albedo calculations for control elements inserted into circular channels require circular cylindrical geometry, it was necessary for computational purposes to replace a noncircular rod by an equivalent circular one. Hurwitz and Roe's[11] scheme was followed in determining the effective radii, r_{eff}, for the "circularized" flat plate, the square, and the cross-shaped rods. An intuitive method of letting r_{eff} be equal to the mean of the radii of inscribed and circumscribed cylinders was employed for the triangular and cross-shaped rods.

The circularized control rods were represented in terms of albedos based upon effective radii and either upon conservation of boral density or conservation of boral weight in the rods. The rod worths were determined by the procedure outlined in section 3.2. It was found[12] that albedos based upon the conservation of boral density yield closer theory-

CONFIDENTIAL

UNCLASSIFIED

DECLASSIFIED

CONFIDENTIAL

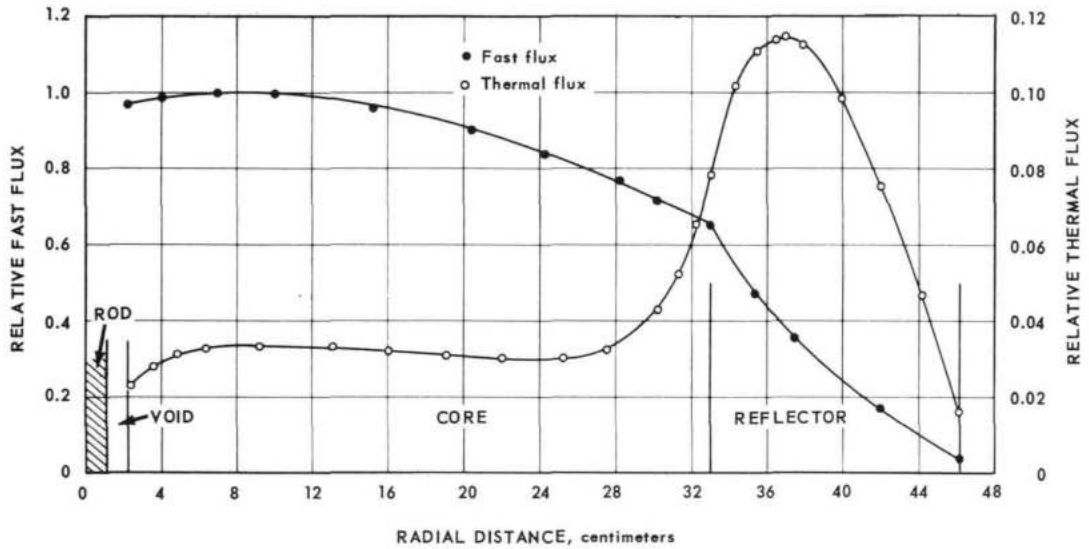

Fig. 3.4 – Radial flux distribution in SM-I-2-C reactor configuration – B_4C rod 5 in void replaces a central fuel-moderator cell

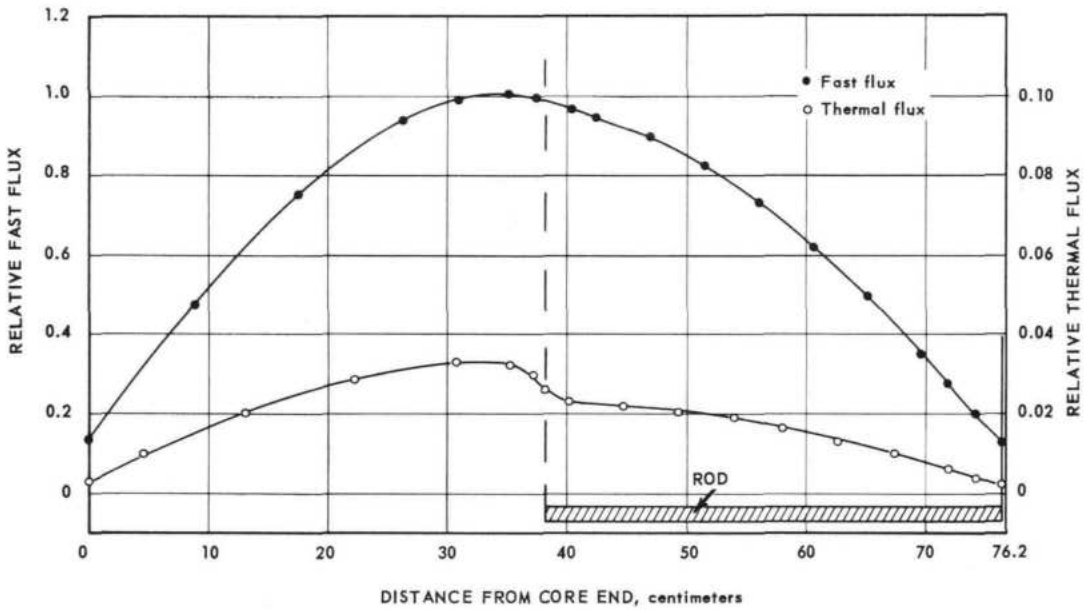

Fig. 3.5 – Longitudinal flux distribution 2.2511 centimeters from core axis in SM-I-2-C reactor configurations – B_4C rod 5 in void replaces a central fuel-moderator cell in the movable half of the reactor

CONFIDENTIAL

DECLASSIFIED

DECLASSIFIED

CONFIDENTIAL

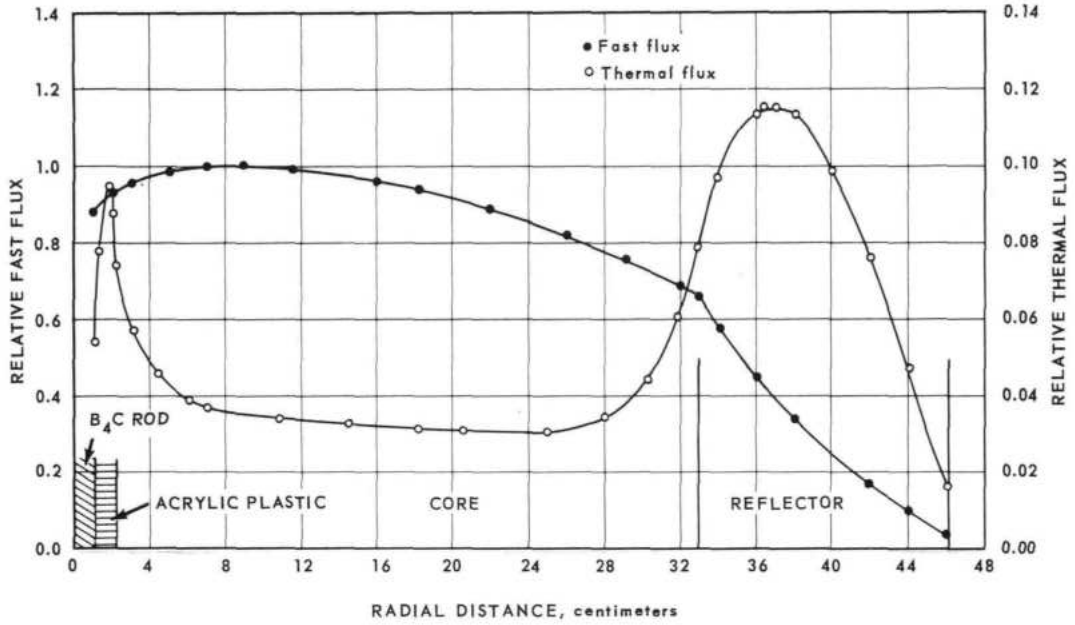

Fig. 3.6 – Radial flux distribution in SM-I-2-C reactor configuration – B_4C rod 5 in acrylic plastic hexagon replaces a central fuel-moderator cell

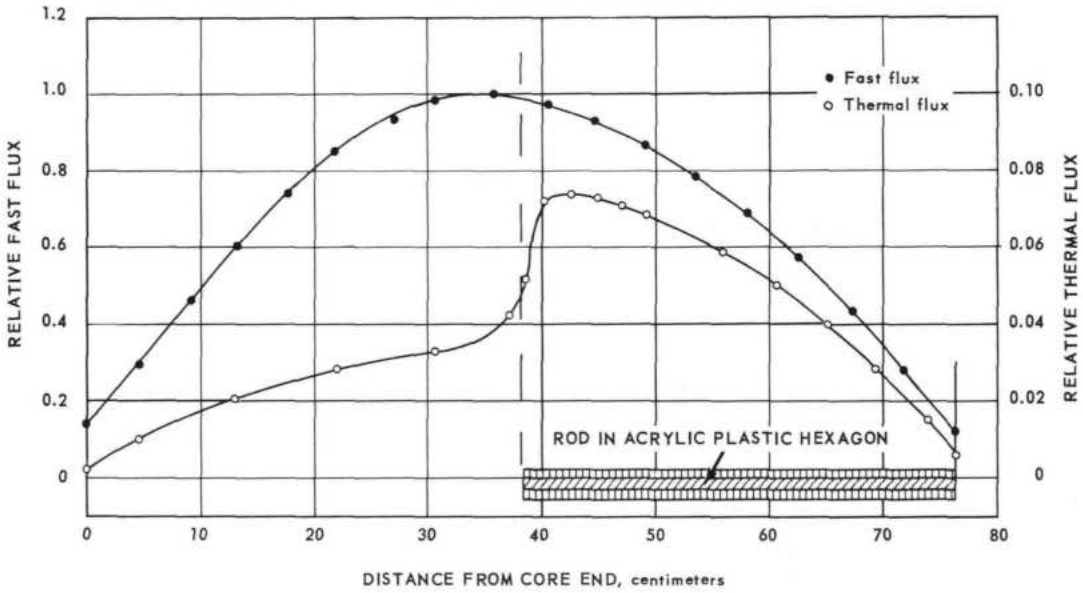

Fig. 3.7 – Longitudinal flux distribution in SM-I-2-C reactor configuration 2.2511 centimeters from core axis – B_4C rod in acrylic plastic hexagon replaces a central fuel-moderator cell in the fixed half of the reactor

CONFIDENTIAL

DECLASSIFIED

DECLASSIFIED

experiment correlation than those based upon conservation of boral weight. Theory-experiment correlation is satisfactory for control elements of square and triangular cross sections, but it is not satisfactory for the plate and cross. Furthermore, the intuitive method for the circularization of the cross, yields lower theory-experiment discrepancies than the scheme of Hurwitz and Roe.

For control slabs or plates inserted into noncircular channels[13] the group-averaged albedos were determined by the slab-transmission subroutine in Program George. Program CURE was then employed to calculate the effects of the control slabs. Since experimental data on the effects of control slabs inserted into noncircular channels were not available, the accuracy of prediction by the latter method was not evaluated.

3.3.3 SINGLE NONCENTRAL RODS

The method of applying radial weighting to central control rod worths and Program K[14] were used in determining the effects of single noncentral rods.

The following were used as radial weighting functions:

$$J_0\left(\frac{2.405\ r}{R}\right),\ \phi_1\ \phi_1 + \phi_2\ \phi_2^*,\ P\ P^*,$$

and the sum

$$J_0^2\left(\frac{2.405\ r}{R}\right) + \frac{1}{4} J_1^2\left(\frac{3.832\ r}{R}\right),$$

where R is the bare equivalent radius plus the radial extrapolation distance; r is the core center to rod center distance; ϕ_1, ϕ_2, ϕ_1^*, ϕ_2^*, P, and P* are calculated fast and thermal fluxes, adjoint fluxes, fission density and adjoint fission density; and J_0 and J_1 are Bessel functions of the first kind of order, zero and one, respectively.

Program K calculates the multiplication constant k of a system consisting of a reactor core and a central or single noncentral rod; it computes fast flux, thermal flux, and power distributions in rod-centered and core-centered cylindrical coordinates.

A detailed comparison of results[12] indicates that the radial weight function,

$$J_0^2\left(\frac{2.405\ r}{R}\right) + \frac{1}{4} J_1^2\left(\frac{3.832\ r}{R}\right)$$

yields the smallest theory-experiment discrepancies. It introduces no deviation on account of the noncentral rod location for rod-to-reflector distances larger than about 10 centimeters, and only about 10 percent deviation in the remaining core region.

The discrepancies between measured effects of noncentral rods and those computed by Program K stay well within the discrepancies for central rod worths. Hence, no deviation between computed and experimental rod worths was introduced by Program K on account of the noncentral rod location within the maximum distance from core center to rod center imposed by Program K limitations.

3.3.4 RINGS OF RODS

If more than one control rod is inserted into a reactor, the effectiveness of each rod depends upon the position and worth of every other rod. This interdependence is a complex function of geometry, reactor parameters, rod parameters, and rod location.

A theory-experiment comparison was made of the worth of identical rod assemblies consisting of B_4C rods 5 in acrylic plastic hexagons, each replacing a fuel-moderator cell in one-half of the reactor matrix and arranged in symmetrical patterns of 2, 3, 4, 6, and 7 rods.

DECLASSIFIED

UNCLASSIFIED

The following two methods were employed in computing rod worths.

Procedure 1

1. Center-rod worth was determined.
2. Cosine-squared longitudinal weighting accounted for insertion of the rod halfway.
3. Off-center importance weighting accounted for the noncentral location of the rod.
4. Rod worths were corrected for shadowing-rod interactions.[12]

Procedure 2

1. Few-group, two-dimensional, multiregion, diffusion-theory Program CURE was employed to compute the worth of a symmetrical ring of fully inserted rods.
2. Cosine-squared longitudinal weighting accounted for the insertion of the rod halfway.

Both methods overpredict rod worths.[12] This also occurred with both single central and noncentral B_4C rods in acrylic plastic hexagons - the thicker the acrylic plastic annular wall, the larger the discrepancy.

The consistently high rod worths suggest that the albedos used to express a rod insertion do not accurately represent the rod when it is embedded in an acrylic plastic annulus. When the rod is embedded in an acrylic plastic annulus, the core flux spectrum is changed. Neutrons are also reflected into the core. Thus only a portion of the core flux spectrum used in the rod albedo calculations is incident upon the absorbing rod, and therefore fewer neutrons than predicted are actually absorbed by the rod. This leads to an overprediction in rod worth when acrylic plastic or, for that matter, any moderating and reflecting material, fills the void between the rod and the core.

A different method was used with an intermediate-spectrum reactor with a ring of control rods inserted into the reflector.[15] For analysis rod poison was homogenized over a gross annular region. Multienergy, one-dimensional transport theory Program S-V[6] was employed in computing the effects of the control system.

The calculations consisted of the following major steps.

1. Preliminary gross radial analysis of the reactor with all control rods withdrawn.
2. Fine radial analysis of the control rod cell.
3. Gross radial analysis of the reactor with the control rods, represented as an annulus, inserted into the reflector.
4. Gross radial calculations of the reactor with all control rods withdrawn.

The preliminary gross radial analysis serves the purpose of supplying flux and current spectra to be used as surface sources at the edge of a control rod cell in the fine analysis.

The purpose of the fine rod-cell calculation is:

1. To obtain neutron-absorption rates in the rod.
2. To get radial flux and current distributions in the control rod cell.
3. To compute isotropic (flux) and anisotropic (current) rod-cell homogenization factors. They are used to weigh poison rod cross sections in the gross analysis to account for the self-shielding in representing the rods as an absorber homogenized over a gross annular region.

3.4 CONCLUSIONS

The rod-analysis methods discussed yield relatively satisfactory theory-experiment correlation for circular cylindrical pure poison rods. The worths of B_4C rods in acrylic

UNCLASSIFIED

DECLASSIFIED

plastic moderator hexagons are overpredicted by about 15 percent, and those of steel jackets in acrylic plastic hexagons underpredicted by about 20 percent.

Thus, the accuracy of the results obtained by the same method depends upon the kind and complexity of an analyzed rod regardless of its location. This seems to indicate that the discrepancies are due to inaccurate rod-albedo values.

In the case of insertion of the rod halfway, cosine-squared longitudinal weighting is unsatisfactory for B_4C rods in voids, but relative rod worths determined by Program CURE are in good agreement with experiment.

Results obtained indicate that either Program K or off-center weighting of control rod worths by

$$[\phi_1 \ \phi_1^* + \phi_2 \ \phi_2^*] \text{ , P P*, or } \ J_0^2\left(\frac{2.405\ r}{R}\right) + \frac{1}{4} J_1^2\left(\frac{3.832\ r}{R}\right)$$

can be used to compute worths of single noncentral rods without introducing any appreciable deviation on account of the noncentral location.

Both Program CURE and the application of shadowing coefficients to worths of single noncentral rods yield overpredicted effects of rings of rods.

DECLASSIFIED

DECLASSIFIED

CONFIDENTIAL

3.5 REFERENCES

1. Fraembs, D. H., "Reflector and Control Studies in Small, Thermal, Highly Enriched Systems," GE-ANPD, APEX-526, October 1959.
2. Simpson, J. D., "Summary Hazards Evaluation of the SMR Facility," GE-ANPD, APEX-536, December 1959.
3. Hoffman, T. A., and Henderson, W. B., "General Reactor Analysis Computer Program for the IBM 704, Program George," GE-ANPD, APEX-543, February 1960.
4. Behrens, D. J., "The Effect of Holes in a Reacting Material on the Passage of Neutrons, with Special Reference to the Critical Dimensions of a Reactor," United Kingdom Atomic Energy Authority, AERE T/R 103.
5. McLennan, J. A., "Reactor Cell Calculations," GE-ANPD, APEX-197, August 15, 1955.
6. Duane, B. H., "Neutron and Photon Transport, Plane-Cylinder-Sphere, GE-ANPD Program S, Variational Optimum Formulation," GE-ANPD, XDC 59-9-118, January 1959.
7. Smith, F. B., "F2 Two-Group Neutron Diffusion Program," GE-ANPD, APEX-539, January 1960.
8. Trantham, F. M., Jr., "CURE - A Two-Space-Dimension, Multigroup Code for the IBM-704," GE-ANPD, APEX-452 (rev), August 12, 1958.
9. Goertzel, G., "Reactor Dynamics," The Reactor Handbook, Volume 1, Chapter 1.6, March 1955.
10. Weinberg, A. M., and Wigner, E. P., "The Physical Theory of Neutron Chain Reactors," University of Chicago Press, 1958, page 768.
11. Hurwitz, H., Jr., and Roe, G. M., "Absorption of Neutrons by Black Control Rods," Journal of Nuclear Engineering, Vol. 2, 1955.
12. Zwick, J. W., "Control Rod Theories Evaluation Based Upon Measurements of Control Rod Worths in SM-I-2 Reactor Assemblies," GE-ANPD, APEX-578, April 21, 1959.
13. Zwick, J. W., "P126A Polygon Reactor Nuclear Analysis," GE-ANPD, XDC 59-4-47, March 1959.
14. Moore, C. L., "Off-Center Control Rod Program (Digital Computer Program K)," APEX-461, February 1959.
15. Zwick, J. W., "Reflector Control Rod Analysis P140-B1 Ceramic Reactor," GE-ANPD, XDC 60-11-61, August 1960.

CONFIDENTIAL

DECLASSIFIED

DECLASSIFIED
CONFIDENTIAL

4. REACTOR RUNAWAY ANALYSIS

As in all reactor operations the evaluation of the safety of the reactor is extremely important. The hazards normally associated with reactor operation were compounded in Evendale by the presence of off-site personnel living within 270 meters of the test cell. Consequently, the hazards associated with this reactor operation were evaluated rather extensively. The analytical procedures outlined apply primarily to critical experiments fueled with metallic uranium. However, the same analytical procedures are useful for other reactors that differ only in a modification or a change in the shutdown procedure or mechanism. Calculational methods and receptor dosages are evaluated in "HTRE Hazards Report"[1] and in APEX-921.

4.1 CAUSES OF NUCLEAR INCIDENTS

Various causes for the initiation of reactor runaways have been considered. These fall into two broad classes, accident and sabotage. Accidents are defined as incidents due to human error or equipment failure. Sabotage involves tampering with intent to cause damage, either physical or psychological.

Careful examination of accident conditions reveals that multiple failures and in most cases some degree of negligence must be assumed for an accidental reactor runaway.

A reactor could be sabotaged in a number of ways, provided that a saboteur could successfully circumvent all security measures that should prevent his access to the cell. Since the psychological and political effects of a minor accident resulting from sabotage might be as serious as the effects of a major accident, no attempt is made to identify a most-probable or worst-possible sabotage.

For an accident to occur, at least two things must happen. First, the reactor must be critical or near critical; then a fast-acting initiating mechanism must operate to make the reactor supercritical. Analysis of the various means of initiating reactor runaways in the flexible critical experiment facility has shown that the most probable and the maximum accidents are due to a potentially critical reactor being made supercritical by the joining of the table halves.

The following sequence is postulated to be the maximum credible accident. The reactor would have operated with a particular core for some time. Sequence of operations would have indicated a change in the core configuration to be necessary. An analytical evaluation indicates the configuration change will increase the worth of the reactivity by a little less than 1 dollar. To compensate for the added reactivity, an amount of poison equal in worth to this increase will be added to keep the reactivity within the control system bounds. A member of the operating crew makes a mistake in the sign of the worth of the change he is to make, and he adds a positive contributor to the reactivity of the system. The net increase in system reactivity will be approximately 2 dollars. During sub-

CONFIDENTIAL
DECLASSIFIED

DECLASSIFIED

sequent operation the speed-limiting system of the table fails, and all other mechanical safety systems fail allowing table closure at constant maximum rate. As the separation distance lessens, the reactor rapidly becomes supercritical, and a runaway occurs.

4.2 DESCRIPTION OF THE MAXIMUM CREDIBLE ACCIDENT AND METHODS OF CALCULATING IT

The maximum credible accident may be considered to occur in three distinct stages.

The first stage starts when the reactor reaches delayed critical during table closure. Reactivity is continuously added at a decreasing rate with table closure at constant maximum speed. The reactor reaches and exceeds prompt critical, and power rises through many decades. This stage is terminated when the fuel in the region of highest power density reaches vaporization temperature.

During the second stage a portion of the fuel in the reactor is vaporized and is ejected after sufficient fuel vapor pressure is built up in the core. The reactivity at any instant during the second stage is the sum of the reactivity produced by table closure minus the worth of the ejected fuel vapor. The duration of this stage is a fraction of a second and is over before table closure is completed. The second stage ends when the neutron flux is reduced to a level corresponding to that of the delayed neutrons produced in the runaway.

The delayed neutrons produced in the power excursion contribute to the now-subcritical reaction as it gradually dies out. More energy is released, and fuel vaporization continues in the third stage because of the thermal inertia of the system. This final stage of the runaway is assumed to be terminated when any further energy contribution becomes a negligible fraction of the total energy hitherto released during the runaway.

The analysis of the second stage is based on the following basic model.

1. The vaporized fuel flows according to equations describing the steady-state flow of compressible fluid. The fuel vapor is at any time distributed uniformly throughout the free-flow volume of the reactor. To compensate for this assumed uniformity, the calculated flow out is not allowed to occur until after an imposed delay time, which is the time required for a pressure wave to travel from the center of the reactor to the opening through which the vapor escapes.
2. The flow of fuel out of the reactor is described as occurring from one steady-state flow to another. Thus, the fuel can be in one of three stages:
   a. Unvaporized fuel that is motionless inside the reactor and hence possesses only internal energy.
   b. Gaseous fuel inside the reactor that has, in addition to internal energy, kinetic energy resulting from the motion of the gas as it flows out of the reactor. At any time, a unit mass of gaseous fuel inside the reactor is at a pressure, P, and has a density, ρ ; thus, neglecting the volume of a unit mass of unvaporized fuel because it is small in comparison with the volume of the gas, the flow work done by a unit mass in expanding after it has vaporized is equal to P/ρ.
   c. Gaseous fuel ejected from the reactor that has, in addition to internal energy, kinetic energy due to a net motion in the outward direction and that in escaping does flow work on whatever gas is already outside the reactor.

   States a and b are true states in the sense that at any time all the material in each state has exactly the same internal and kinetic energy, and has done the same amount of work in expanding. State c is really a sum of states since the characteristics of the ejected gas vary and depend upon when it was ejected.

DECLASSIFIED

DECLASSIFIED

3. It is assumed the reactor contains 1 atmosphere of fuel vapor at the start of the accident; i.e., vaporization does not take place until the temperature of the fuel is high enough to maintain vaporization with 1 atmosphere of fuel vapor pressure present. The fuel taking part in the vaporization process has the same temperature as the vaporized fuel. This common temperature is determined by a Clapeyron-type equation appropriate to the change of phase in question.
4. The runaway is stopped as fuel vapor leaves the reactor. It is assumed that the effect on reactivity is linear with the total flow out and that it does not take place until the vapor has actually left the reactor. In addition, the flow out is not counted as having any effect on reactivity until after an amount of fuel having the same weight as the air originally in the reactor has been ejected.
5. The duration of the second stage is of the order of 10 milliseconds. Because of this short duration and the decreasing slope of the reactivity-addition function with table closure, the continued addition of reactivity during this period is quite negligible in comparison with the large negative-reactivity effect of the fuel-mass removal.
6. The reactivity effect of the homogeneous fuel vapor inside the reactor free-flow volume is essentially the same as that of an equal weight of fuel in the original solid-state distribution.
7. The temperature-reactivity coefficient is neglected.
8. Heat transfer to the metal sheet surrounding the uranium in metallic fuel elements is not included in the analysis of the runaways. This omission is based on the consideration of the temperature distribution through a laminar array of 0.0005-inch uranium, 0.001-inch Teflon, 0.001-inch air, and 0.003-inch stainless steel. The heat-propagation time constants for this array are calculated with the standard time-dependent heat diffusion equation in which a temperature perturbation in the uranium is represented by an additional delta function source term, $\delta(x)\ \delta(t)$. The time constants so developed are 7 microseconds for uranium, 330 microseconds for common metals, 300 microseconds for air, and 75×10^3 microseconds for Teflon. Therefore, the propagation rate is essentially controlled by the Teflon alone. The outer surface of Teflon reaches a maximum temperature 75 milliseconds after insertion of a temperature pulse. The uranium reaches vaporization temperature within 80 milliseconds, and stage 2 of the runaway is terminated 10 milliseconds later. The heat drainage into the Teflon is calculated to be less than 10 percent of the total fission energy release in the runaway. An increase in the calculated energy release during the runaway due to the exclusion of the heat transfer to the metal and heat drainage through the Teflon is thus within the bounds of accuracy that can be claimed for this type of analysis. The Teflon coating of the uranium foil is thus a considerable safety feature.
9. Vapor loss through the transverse gap between table halves is neglected, although stage 2 of the runaway is completed well before the table is closed. This is an obviously pessimistic assumption because the area available to the escaping vapor is considerable.
10. The total energy released during the runaway is the sum of the total fission energy plus the energy of combustion of the expelled uranium fuel vapor. All of the expelled vapor is assumed to oxidize and the reaction is assumed to proceed directly to U_3O_8 exclusively.

Program 0129

Program 0129[2] divides the history of the runaway into three successive regions. In each region the reactivity at any time, t, is said to contain an external component, k_{ext}, which may be defined as the addition of reactivity with table closure, and an internal component, k_{in}, which in this case is defined as the worth of the ejected fuel vapor. The ex-

DECLASSIFIED

DECLASSIFIED

CONFIDENTIAL

ternal reactivity input is described by a second-order polynomial time function and can therefore be used to introduce reactivity as a step function, a linear function, or an ac-

DECLASSIFIED

CONFIDENTIAL

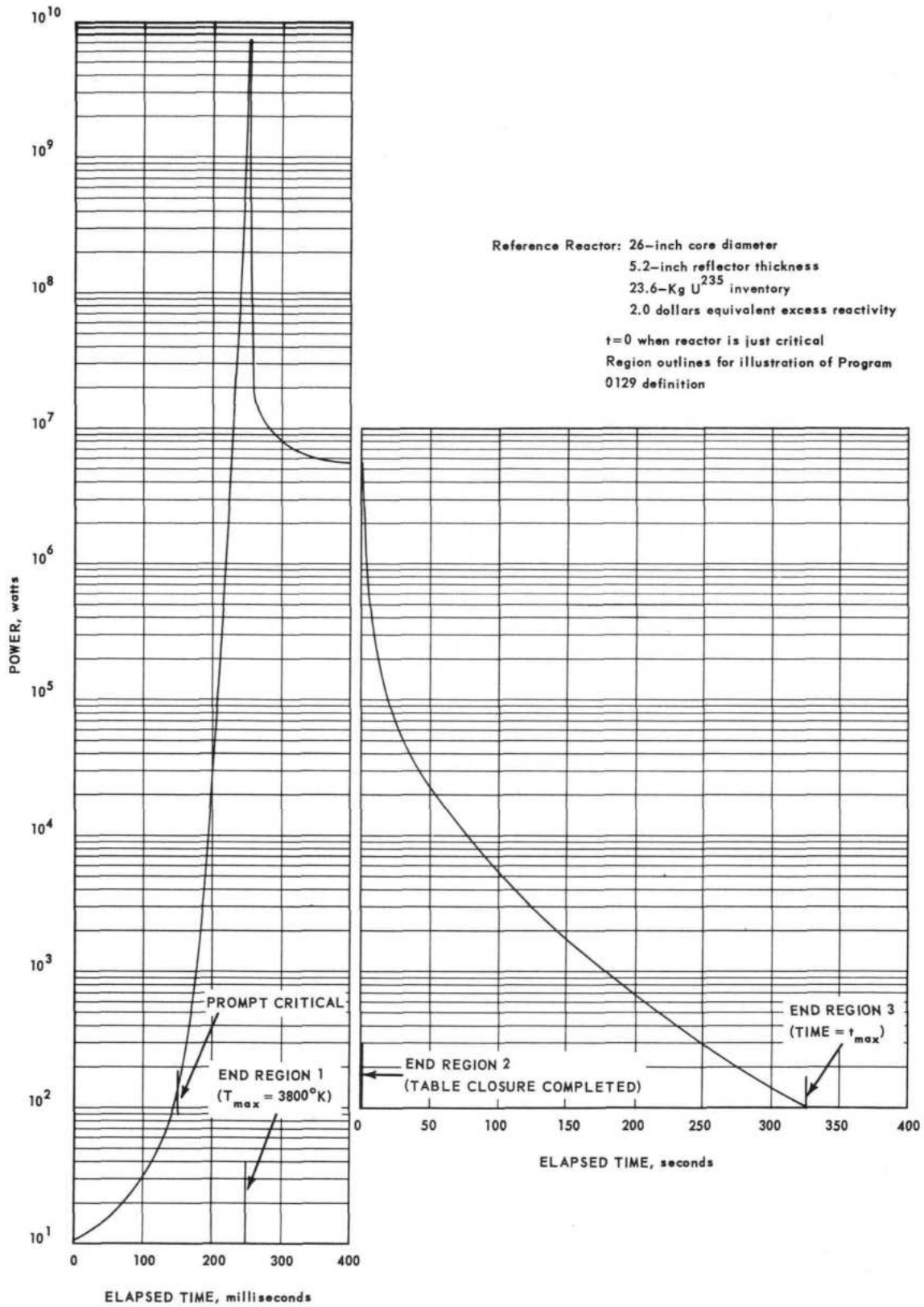

Fig. 4.1 – Power profile of an SMR maximum credible accident, including both prompt and delayed neutrons, per Program 0129

CONFIDENTIAL

DECLASSIFIED

DECLASSIFIED

CONFIDENTIAL

an accelerated reactivity increase if both cause the reactor to be on the same period at that instant when the fuel in the highest-power-density region reaches vaporization temperature.

This program is designed to analyze only above-prompt-critical runaways. Delayed neutron reactions can, therefore, be disregarded in the first and second stages of the runaway. It can be further shown that the fission energy content will be essentially the same for a runaway in which delayed neutron reactions are included as the fission energy content for a runaway in which delayed neutrons are neglected, provided that in the latter case the prompt-neutron flux level is extended to a factor of 10^6 below its peak value. The equivalent fission energy of the delayed-neutron-sustained after-reactions is thus calculated in Program 0031 by continuing time iterations until the prompt neutron flux has decreased through six decades from its peak value.

The mass flow rate of the fuel vapor, W, calculated for adiabatic flow of a perfect gas through a nozzle can be shown to be a function of the time-dependent fuel-vapor density, $\rho(t)$, in the reactor free-flow volume. If this flow starts at time t_2 from initiation of the accident, then at time t the mass of fuel vapor expelled from the reactor is

$$M = \int_{t_2}^{t} W\,[\rho(t)]\,dt$$

The time derivative of the thermal flux can now be expressed as

$$\frac{d}{dt}\phi_{th}(t) = \frac{(\Delta k/k)_0 - \delta \int_{t_2}^{t} W\,[\rho(t)]\,dt - \beta}{l}\,\phi_{th}(t) \qquad (4)$$

where:

δ = the reactivity worth of a unit mass of fuel
l = the average neutron generation time
β = the average effective delayed neutron fraction

The time derivative of $\rho(t)$ is dependent on:

1. Initial power level at the start of the runaway.
2. Neutron flux level.
3. Reactor free-flow volume.
4. Cross-sectional area of the free-flow volume.
5. Vapor exit nozzle cross-sectional area.
6. Vapor mass flow rate.
7. Clapeyron-type relation between fuel vapor temperature and equilibrium vapor density.

This functional relation can be written for a given reactor as

$$\frac{d\rho(t)}{dt} = F\,[\rho(t), \phi_{th}(t)] \qquad (5)$$

The integration of equation (5) is initiated by a Runge-Kutta numeric integration process and is continued by Milne's method.

Program 0031 thus analyzes a runaway by the simultaneous solution of differential equations (4) and (5). For each time iteration, a record is presented of the elapsed time, the flux level, integrated power, integrated vapor mass flow rate, vapor temperature inside the reactor, and $d\rho/dt$.

Program 0129 presents a fine analysis of the nuclear kinetics of the runaway. The gas dynamics of the fuel vapor are simply treated as being always directly proportional to the

CONFIDENTIAL

DECLASSIFIED

DECLASSIFIED

integrated power in stages 2 and 3 of the runaway. Program 0031, on the other hand, performs a detailed study of the gas dynamics and excludes some effects of delayed neutrons. Program 0031 thus imposes limitations on the reactivity input mode, is valid only for above-prompt-critical runaways, and oversimplifies stage 3 of the runaway by the equivalents of the total energy contribution.

Program 498

IBM 704 or 7090 Program 498[4] was evolved from two existing production programs, No. 0129 and No. 0031. The program was written with the intention of retaining the desirable features of both production programs while combining them into one unified calculational scheme.

The basic analytical treatment is fully presented in APEX-457,[2] -213,[3] and -585.[4]

Program 498 should not be used for analysis of transients taking more than a few minutes of actual time or of excursions so slow that geometry change (meltdown) occurs rather than fuel vaporization and expulsion. This limitation is due to the fact that the numerical technique in the main program is not designed to handle efficiently semi-steady-state situations where the decay of delayed neut[illegible]

DECLASSIFIED

CONFIDENTIAL

4.3 HAZARDS TO SURROUNDING AREA

In general, there are three sources of radiation from fission products that have been released to the atmosphere during a reactor excursion. These are: (1) irradiation of the entire body from fission fragments in the radioactive cloud, (2) irradiation of the lungs from inhaled fission fragments, and (3) irradiation of the entire body from fission fragments that are deposited on the ground by rainout from a radioactive cloud.

In all cases the fission fragments are considered to originate at a point source at the top of the stack (the height of the stack is 30 meters) of the test cell and then to diffuse according to Sutton's distribution equation for diffusion from an instantaneous point source.

Sutton's equation is used to determine the distribution of the fission fragments in the radioactive cloud. Knowing the distribution, it is possible to calculate the dosage received by a receptor from the three sources mentioned above. In computing total body dosage, it is necessary to consider both the gamma and beta radiation; in computing inhalation dosages, only the beta radiation need be considered since the lungs will receive all the betas but only a small part of the gammas.

In the analysis for total body dosage from a distributed source, consideration must be given to the attenuation due to the inverse-square law, to air absorption, and to the buildup due to air scattering. The dosage from the whole cloud requires a triple integration over the volume of the cloud as well as an integration over time to account for fission fragment decay and the motion of the cloud past the receptor, who is located on the ground.

The working equations developed from the above analysis involve approximation, chief among which is that the radiation emission from and the spatial distribution in the cloud

DECLASSIFIED

4.5 REFERENCES

1. "HTRE Hazards Report, " GE-ANPD, APEX-180, December 15, 1954.
2. Mezger, F. W., "Simple Reactor Runaway Analysis," GE-ANPD, APEX-457, November 7, 1958.
3. Mezger, F. W., "Analysis of LPT and ZPT Reactor Runaways," GE-ANPD, APEX-213, June 1, 1953.
4. Becker, R. A., "Runaway Analysis for a Gas-Cooled Reactor," GE-ANPD, APEX-585, July 1960.

DECLASSIFIED

DECLASSIFIED

[redacted]

[redacted]

DECLASSIFIED

DECLASSIFIED

CONFIDENTIAL

5. REACTOR EXPERIMENTS

5.1 DESIGN-CONFIRMATION NUCLEAR MOCKUPS

5.1.1 R-1 REACTOR MOCKUP

The first nuclear mockup built by General Electric for an aircraft type of nuclear reactor was for the heterogeneous R-1 reactor. (See APEX-902.) Prior to construction of the R-1 reactor the nuclear mockup was to be fully investigated at essentially zero power to verify nuclear characteristics, particularly power distributions. The R-1 nuclear mockup,[1] shown in Figure 5.1, was a vertical right cylinder that was split axially into two halves, one of which was on a movable table. The core consisted of concentric cylindrical rings, alternating between aluminum water tanks of 1-inch radial thickness and fuel rings containing U_3O_8 in a fluorocarbon matrix. The uranium-235 inventory was 72.43 kilograms. The fuel ring thickness was varied to flatten the power radially. The 12-inch reflector and shield was in two sections to permit filling with demineralized and borated light water. Poison-type control, safety, and manually placed rods worth a total of 14 dollars were provided. Because of a redirection of the ANP program in 1953, the mockup was not used.

5.1.2 HTRE NO. 1 MOCKUP

The concurrent development of the concentric-ring fuel element and the requirement for a more compact reactor led to the basic design of HTRE No. 1. (See APEX-904.) A mockup for critical experiments was built for this reactor and operated initially at Oak Ridge National Laboratory (ORNL)[2] and then in Evendale. The mocked-up core was moderated and shielded with light water, and had a beryllium side reflector and light-water end reflectors. The core consisted of a hexagonal array of 37 concentric-ring fuel elements. A front (top) view of the core is shown in Figure 5.2, and the mockup fuel element, in Figure 5.3.

Major shutdown reactivity control was provided by draining or, during scram, dumping the water moderator and end reflector. The initial inventory of uranium-235, as fully enriched U_3O_8 in fluorocarbon, was 25.4 kilograms. To achieve the necessary excess reactivity of 3.5 percent for HTRE No. 1, the mockup had to be reloaded to 38.0 kilograms of uranium-235, which yielded an excess reactivity for the reactor with prototype elements of 3.9 percent. This close reactivity match indicated improvement of analytical techniques.[2]

A series of shielding material studies and an investigation of Pentalene as a moderator were also undertaken in the HTRE No. 1 mockup.[3]

5.1.3 HTRE NO. 3 MOCKUP (TSM)

The experience gained from the HTRE No. 1 reactor concentric fuel elements and the hydrided-zirconium-moderator reactors led to their combination in HTRE No. 3. (See APEX-906.) A true physical and nuclear mockup of HTRE No. 3, the TSM, shown in

CONFIDENTIAL

DECLASSIFIED

DECLASSIFIED

CONFIDENTIAL

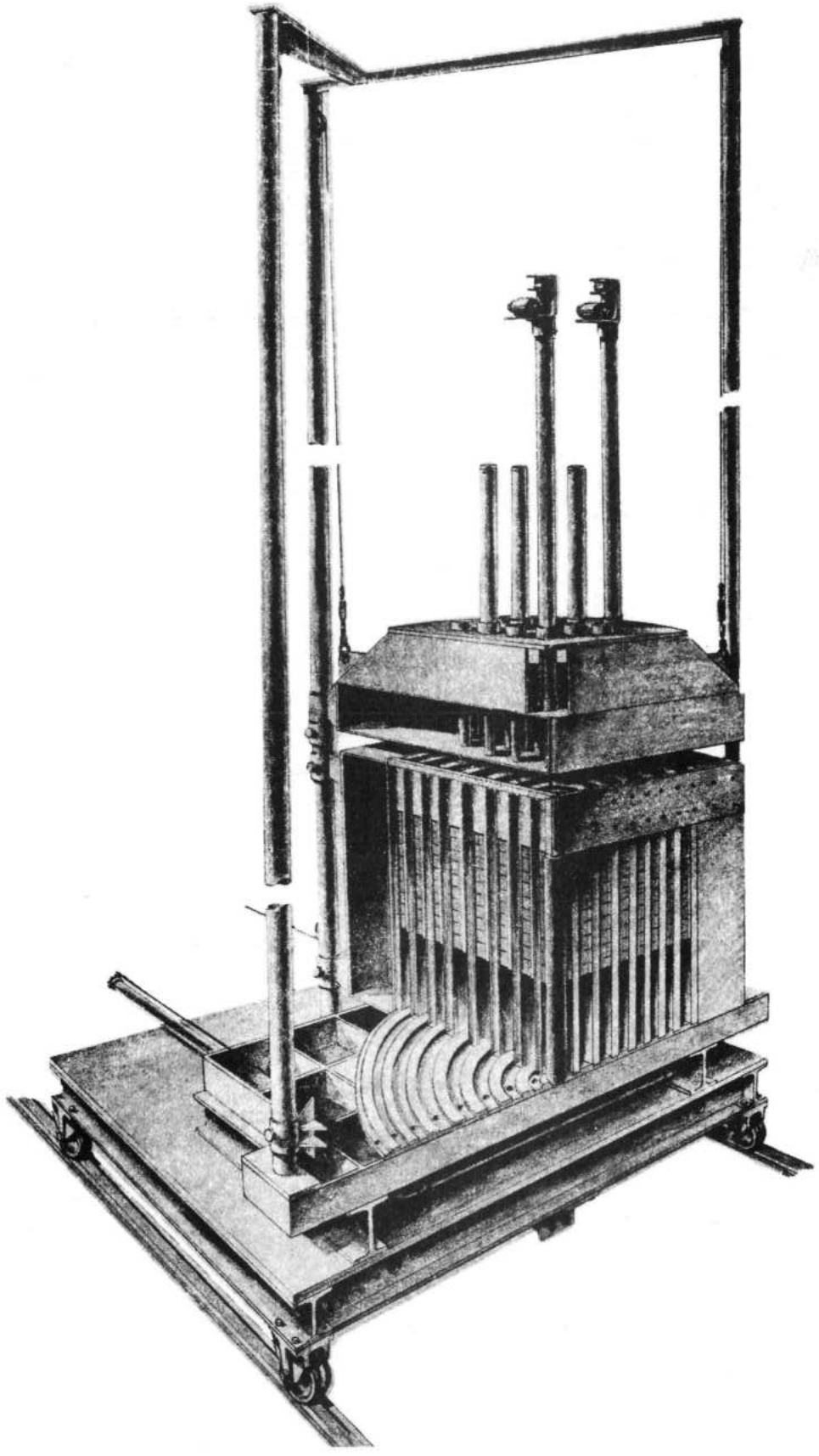

Fig. 5.1—Cutaway view of R-1 reactor mockup

CONFIDENTIAL

DECLASSIFIED

DECLASSIFIED
CONFIDENTIAL

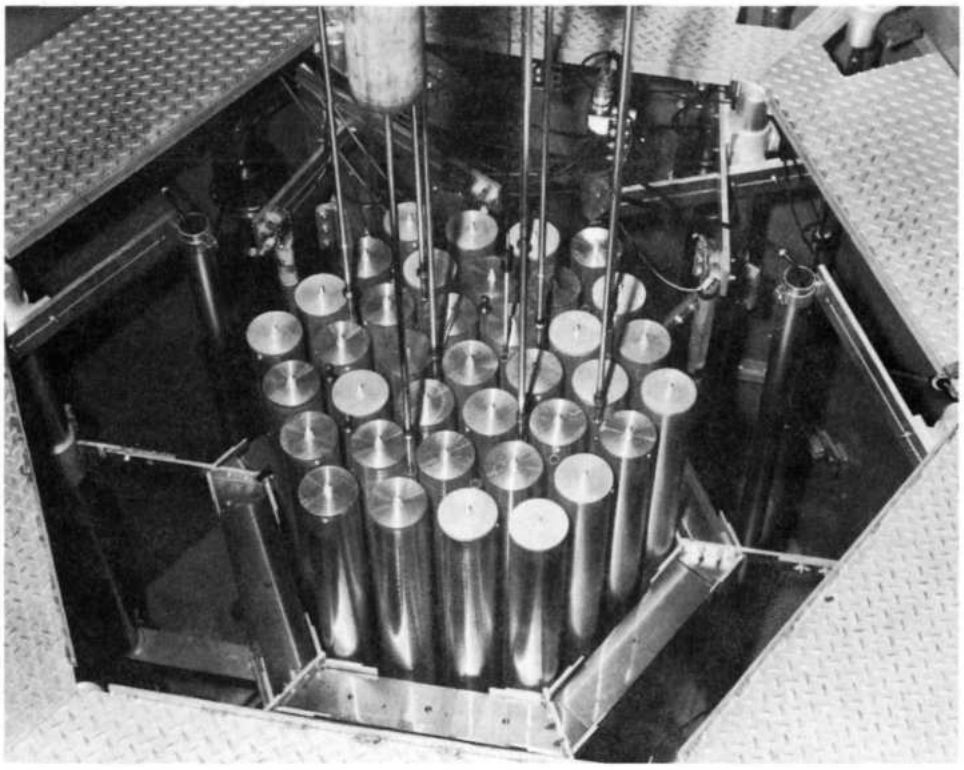

Fig. 5.2 – HTRE No. 1 mockup with fuel elements inserted and beryllium reflector in place

Figure 5.4, was constructed for critical experiments. A limited number of material substitutions, such as 304 stainless steel for Inconel X tube sheets,[4] were made.

Including a mockup of the HTRE No. 3 reactor based on preliminary design specifications, five different core configurations were built and tested to evaluate power distributions and reactivity worths of various control rod patterns and core materials.

The HTRE No. 3 reactor was initially designed to have the moderator clad primarily with a molybdenum hydrogen barrier next to the hydrided zirconium. One of the chief experimental results, and a surprising one, was reactivity loss due to the addition of this molybdenum. During the analytical evaluation to determine the reason for this high reactivity loss, new cross section data were received. These data indicated a larger resonance in molybdenum at an energy level of about 40 electron volts than had previously been reported. The neutron population in this reactor at this energy was extremely important because this energy level was close to the mean energy of fission-producing neutrons. As a consequence of this large reactivity loss due to molybdenum, a major design change was instituted. Basically this change was the removal of the molybdenum and the addition of more cooling area to bring the moderator temperature down to that allowable for unclad moderator.

The moderator was rehydrided and machined to simulate final hydrogen distributions and primary-air cooling slots. The resultant change in the power distributions in the core achieved the desired flattening.[5] The required increase in excess reactivity was gained by raising the fuel inventory in the core from 365 to 390 pounds of uranium-235.

Two configurations of the modified mockup were tested to veryify the final design. A measure of the improvement in techniques is provided by comparing the measured and

CONFIDENTIAL
DECLASSIFIED

DECLASSIFIED

CONFIDENTIAL

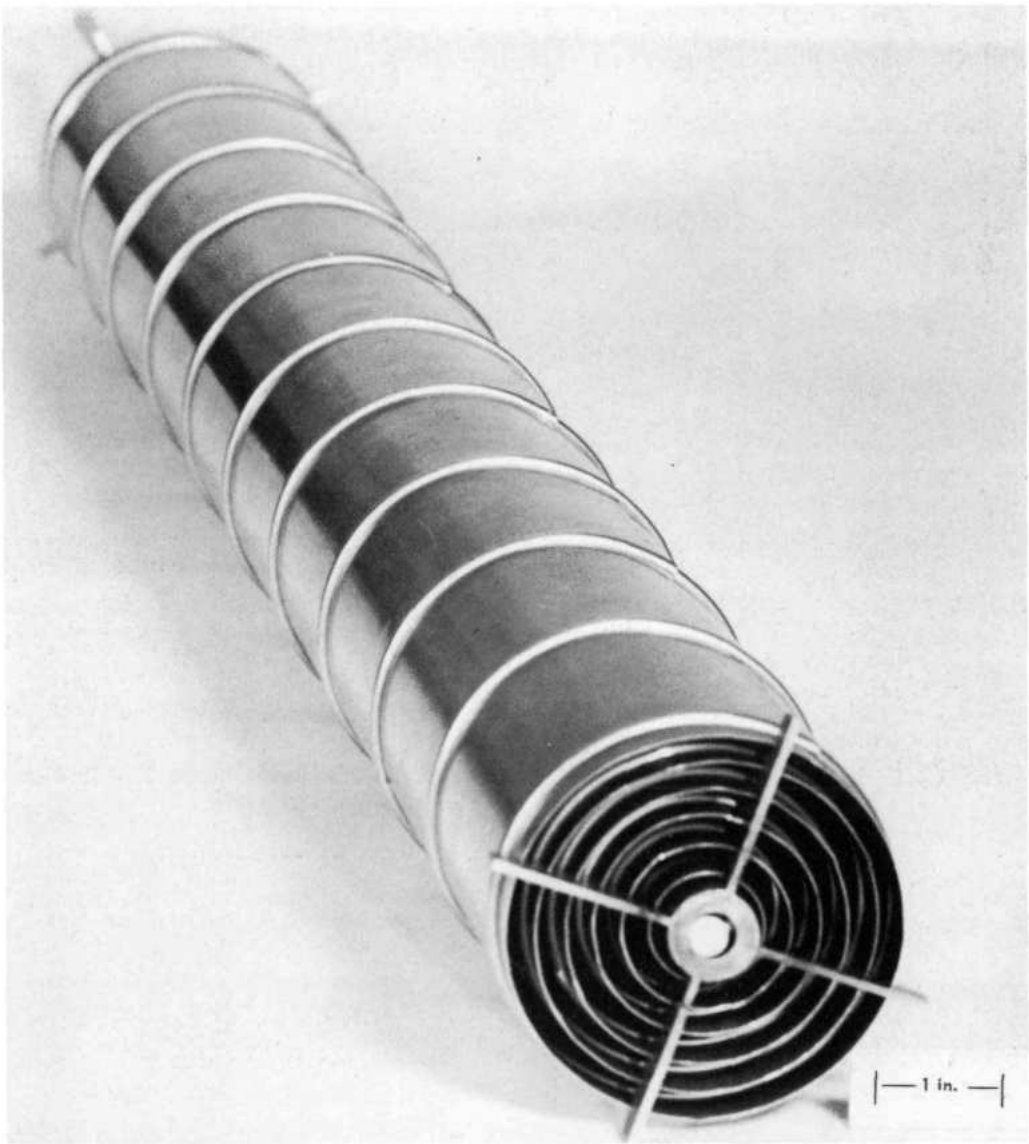

Fig. 5.3 – Fuel element support structure

predicted excess reactivity of the successive core configurations of the mockup. The difference between predicted and experimental reactivity of the first configuration was 1.48 percent $\Delta k/k$, whereas that of the final configuration was only 0.36 percent $\Delta k/k$.[6]

After design-confirmation experiments and some shield-mockup studies for the HTRE No. 3 were completed, a sector of the core was modified to test several proposed design configurations for the XMA-1A reactor.[7] This technique of using a sector of the parent core to test relatively small design changes or more-exact prototype models was a fast and economical method for design-confirmation studies and was used extensively in other critical experiments at GE-ANPD.

5.1.4 XMA-1A MOCKUP (ASM)

The XMA-1A power plant, the design of which approached that of a final ground-test prototype, had to meet much more stringent performance specifications than the HTRE

CONFIDENTIAL

DECLASSIFIED

DECLASSIFIED

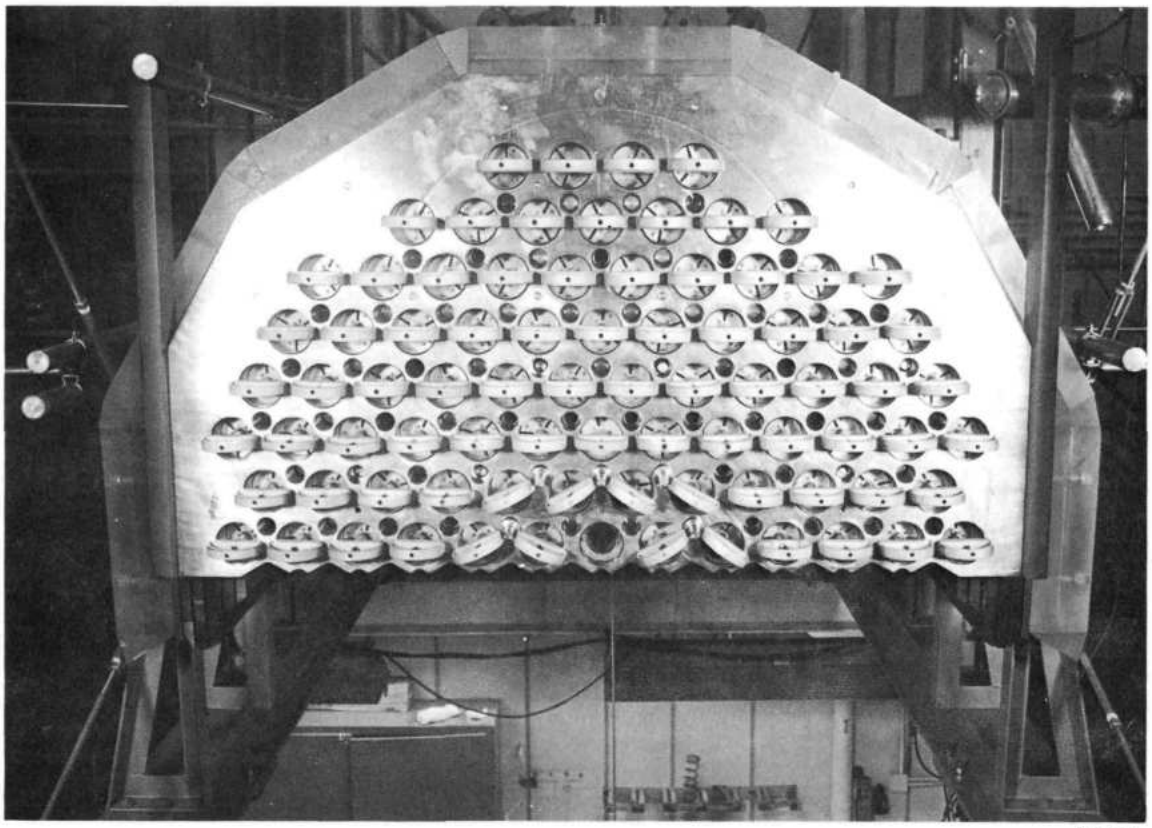

C-04541

Fig. 5.4 – Partial rear view of TSM

No. 3. (See APEX-907.) The XMA-1A reactor nuclear mockup, the ASM, was consequently built as closely to actual design specifications as time and experimental flexibility permitted. In many respects the reactor, Figures 5.5 and 5.6, closely resembled that of the HTRE No. 3.[8] Major differences were in radially and longitudinally nonuniform fuel distribution, reduced moderator volume fraction, and a very detailed hydrogen density distribution variation.

The total experiment was broken down into three phases. During the first phase the off-design moderator provided experimental base points from which moderator specifications could be established.[9] The reactor was then rebuilt and corresponded in the second phase to the then-current design with respect to moderator volume fraction and distribution; fuel loading and distribution; and nuclearly equivalent front and rear shields, end reflectors, and radial shield. Measurements in phases 1 and 2 consisted generally of detailed power-distribution and reactivity studies. In a third set of experiments the final design of the reactor and shield were simulated, and studies were conducted on problem areas such as power measurements in critical longitudinal locations at several poison insertion depths in addition to the usual reactivity and core power-mapping studies.[10] Also included were measurements of gamma heating in several core materials[11] and shielding measurements[12] such as fast and slow neutron and gamma flux mappings through and outside the radial and end shields.

After the termination of these experiments, which led to the issuance of design specifications for the XMA-1A, another experimental program evolved. The basic philosophy of this program was to use the mockup reactor as a radiation source for a number of shielding experiments. Inasmuch as most of the shielding data previously obtained in the ANP

DECLASSIFIED

DECLASSIFIED

CONFIDENTIAL

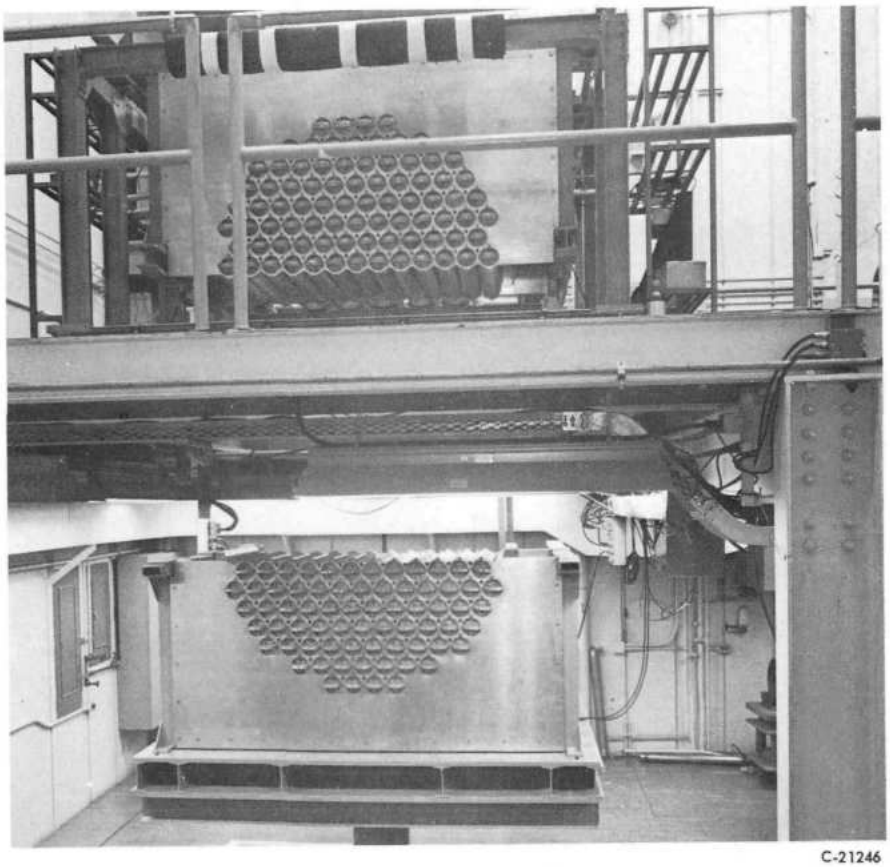

C-21246

Fig. 5.5 – Rear view of ASM

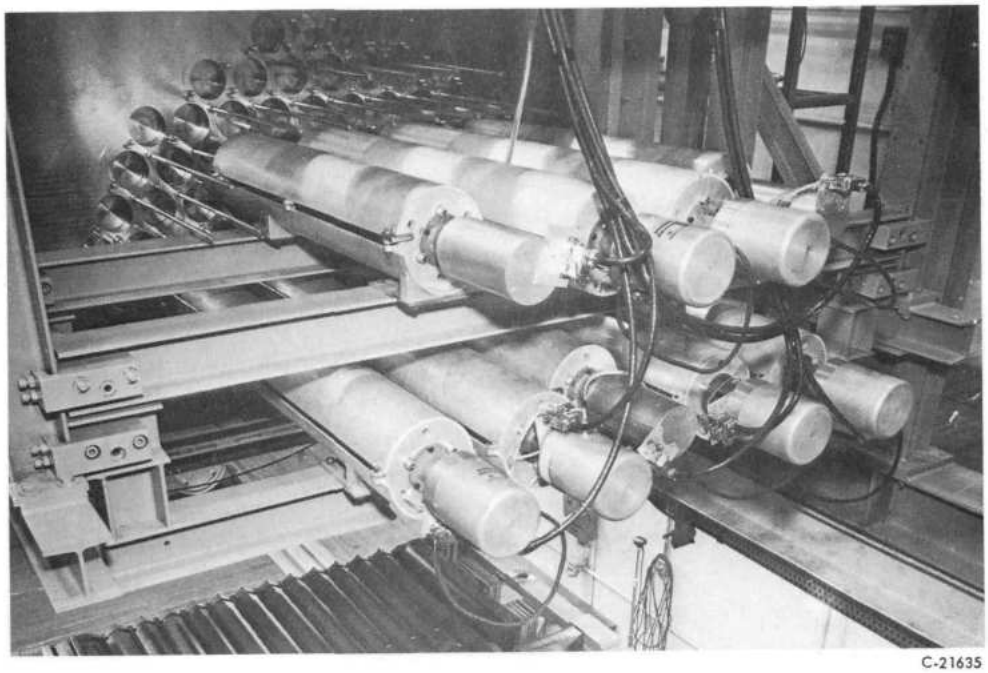

C-21635

Fig. 5.6 – Front view of ASM

CONFIDENTIAL

DECLASSIFIED

DECLASSIFIED

development program had been obtained with water-moderator reactors with essentially a zero void fraction, the additional tests were conducted for air-cooled reactors.[12,13]

5.1.5 ADVANCED XMA STUDIES

A ceramic reactor assembly (CERA) was built[14] as a mockup of a feasibility test for an advanced core for the XMA system. Although the feasibility test was soon shelved to prevent a diversion of the Department from the then primary effort (the XMA-1A), it was decided to operate the mockup, shown in Figure 5.7, to test analytical techniques for ceramic reactors and to develop a valid technique for nuclear measurements in such a device. A basic set of reactivity and power-mapping data confirmed the feasibility of the design and the relative flatness of the radial power profile.[15] In view of the subsequent emphasis on ceramic (BeO) GE-ANPD reactors, a major benefit derived from these mockup tests was the finding of an unexpectedly large fraction of nuclear poisons such as boron and lithium in the BeO obtained from vendors.

5.1.6 ADVANCED CONFIGURATION STUDIES

During the latter half of 1959 preliminary mockups of three different ceramic-core reactors were constructed and operated in the SMR matrix facility. The designs studied were of the offset twin engine (P127), offset single engine (P141), and shaft-through single engine (P140). The preliminary critical assemblies were known as the MOP-I; ACT-I, and SIC-I, respectively. The cores of all three mockups were constructed of beryllium oxide tubes and half-hexagonal prisms with metallic Oralloy fuel foils. Each core had beryllium oxide end reflectors and beryllium metal or oxide radial reflectors. Metallic, longitudinal combination tie rods and guide tubes were mocked up on 7-inch centers in all three configurations.

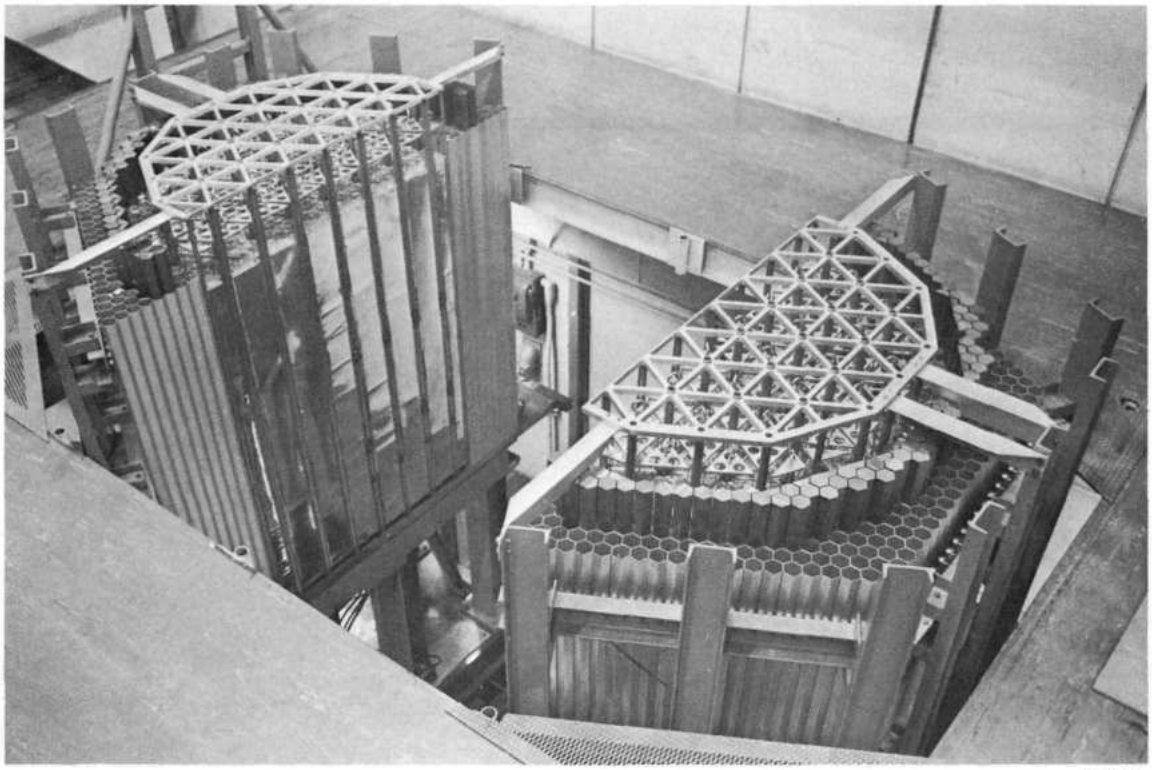

C-21247

Fig. 5.7 – Top, rear view of CERA

DECLASSIFIED

DECLASSIFIED

CONFIDENTIAL

5.1.6.1 P127 Ceramic Reactor Mockup (MOP-I)

The Be-U^{235} atomic ratio was varied from 529 to 1 to 247 to 1 in four concentric regions in the MOP-I reactor, shown in Figures 5.8 and 5.9, in order to present some degree of power flattening. The moderator volume fraction was 0.54 in all regions of the core. The total uranium-235 loading was 49.9 kilograms. The diameter of the active core was 52.2 inches, and its length was 29.8 inches. The radial reflector was composed of 3.81 inches of beryllium. There was no mockup of the shield in the MOP-I configuration.[16,17]

5.1.6.2 P141 Mockup

The Be-U^{235} atomic ratio was held constant at 181 to 1 in each of the four concentric-core regions of the P141 mockup. Power flattening was accomplished by varying the volume fraction of the coolant void in the core regions, from 0.53 to 0.48. The total uranium-235 loading was 50.5 kilograms. The diameter of the active core was 40.9 inches, and its length was 31.9 inches. The reflector was 1.67 inches of BeO backed up by 3.01 inches of beryllium. A shield mockup was constructed of stainless steel, lead, boral and acrylic plastic to approximate the nuclear characteristics of the Core Test Facility.[18,19,20]

5.1.6.3 Preliminary XNJ140E Reactor Mockup (SIC-I)

The Be-U^{235} atomic ratio was held constant at 183 to 1 in each of the five concentric-core regions of SIC-I (see Figures 5.10 and 5.11). Power flattening was accomplished by varying the volume fraction of the coolant void in the core regions from 0.53 to 0.48.

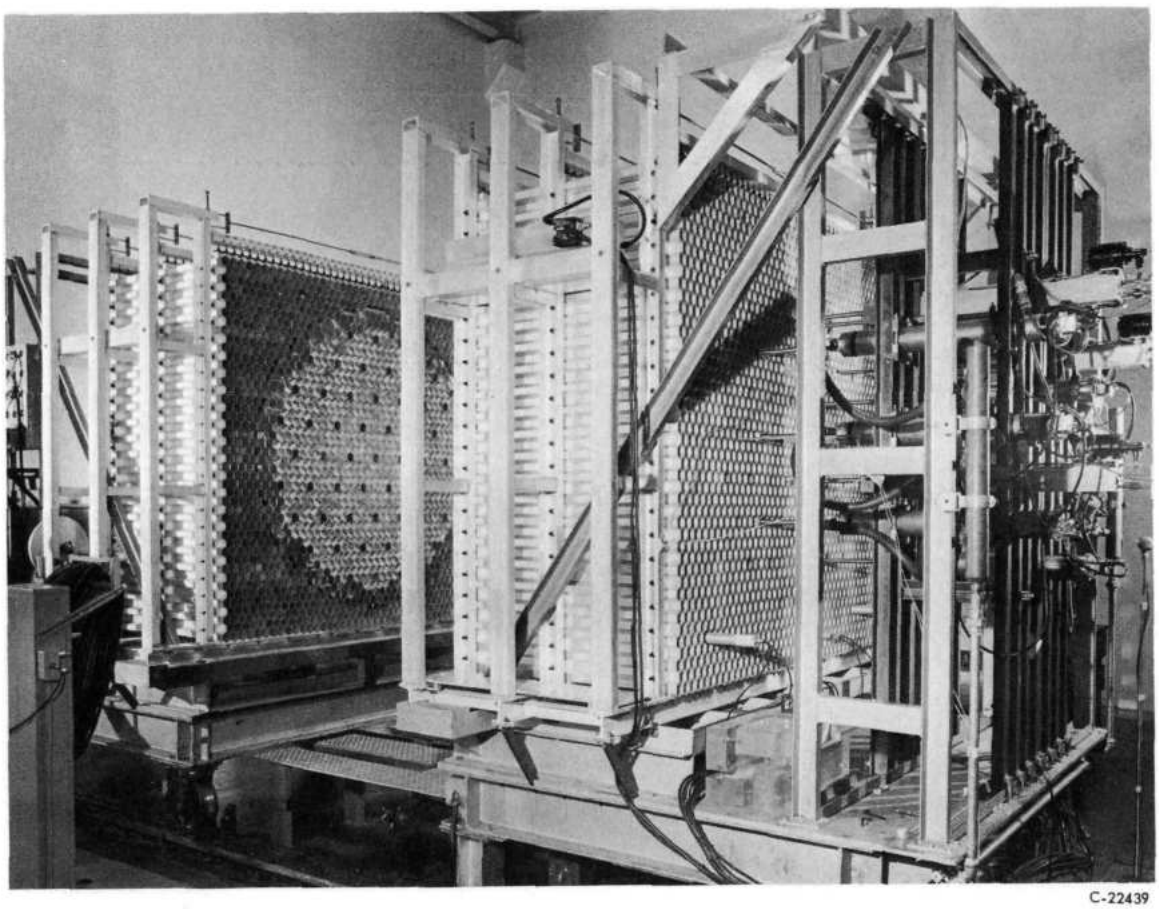

C-22439

Fig. 5.8 – MOP-1 reactor

CONFIDENTIAL

DECLASSIFIED

DECLASSIFIED

CONFIDENTIAL

C-22426

Fig. 5.9 – Quadrant of MOP-1 core

CONFIDENTIAL

DECLASSIFIED

DECLASSIFIED

CONFIDENTIAL

The total uranium-235 loading was 54.6 or 55.5 kilograms according to slight loading variations made during study of the shaft region of the core. The inner diameter of the active core was 16.04 inches; the outer diameter was 45.1 inches, with a 6.14-inch-thick radial reflector of beryllium and 1.22 inches of BeO; and the core length was 31.9 inches. The control system of the design core was mocked up by 42 europium or boron carbide rods in the radial reflector. The shaft materials studied were 304 stainless steel and Inconel X. Shaft insulators were mocked up with AlSiMag-196, beryllium oxide, or aluminum oxide. The shaft shield was beryllium metal. The radial shield consisted of 0.84 inch of type 304 stainless steel. The front shield was 304 stainless steel containing 1 weight percent natural boron. The rear shield was beryllium metal faced with boral.[21]

5.1.7 XNJ140E REACTOR MOCKUP

The nuclear mockup for the XNJ140E-1 reactor was approached on a different basis from that of previous mockups. Prior to the construction of this mockup, a full-scale assembly had always been constructed with physical as well as nuclear details being closely copied. Only those aspects concerned with airflow and high temperatures were ignored, the use of high temperature fuel elements being avoided because of the increased potential hazard. The result, in general, was an excellent mockup for obtaining directly applicable data. The prime disadvantages were (1) the long time required between freezing the design and operation of the mockup, (2) the expense, (3) the difficulty in modification for late design changes, and (4) the fact that low-temperature fuel elements using metallic fuel are not good representations of ceramic elements. In the new approach to these prob-

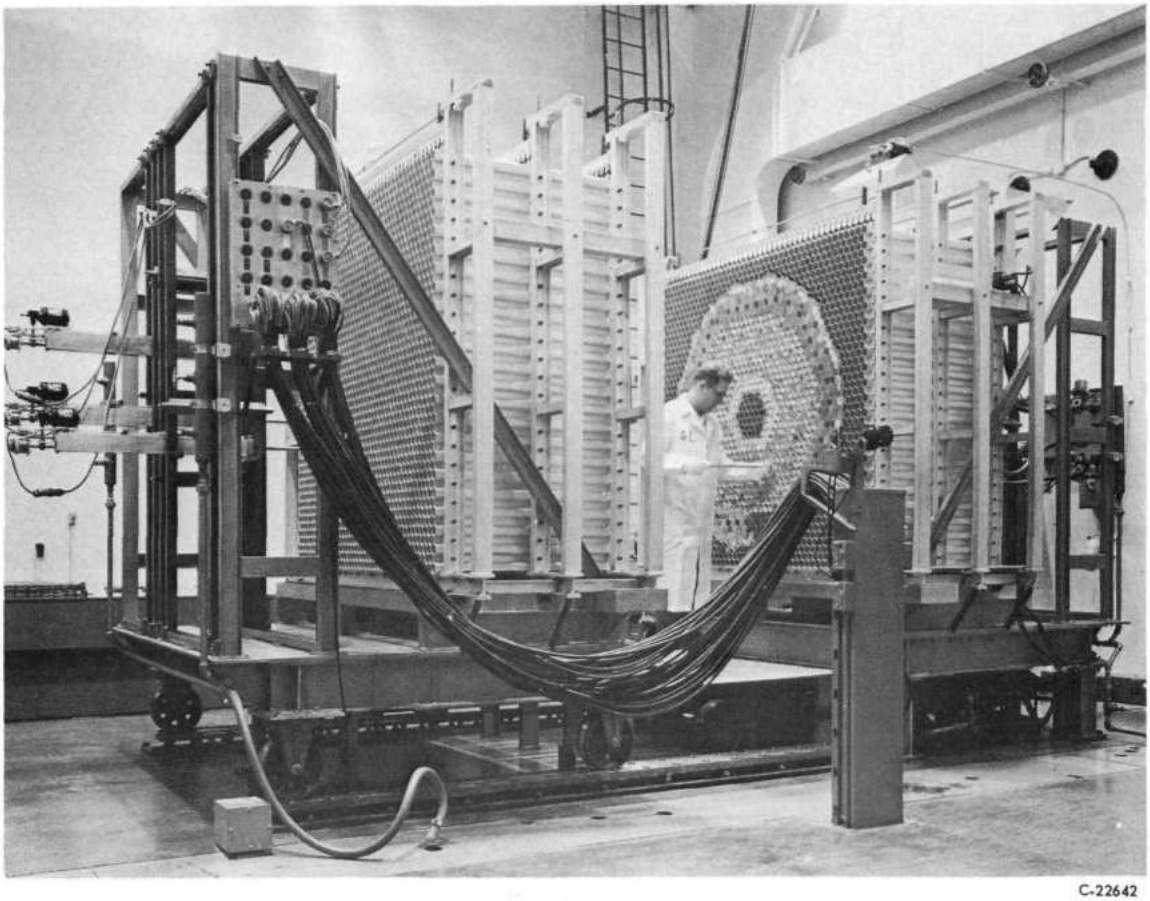

C-22642

Fig. 5.10 – SIC-1 reactor

CONFIDENTIAL

DECLASSIFIED

DECLASSIFIED

CONFIDENTIAL

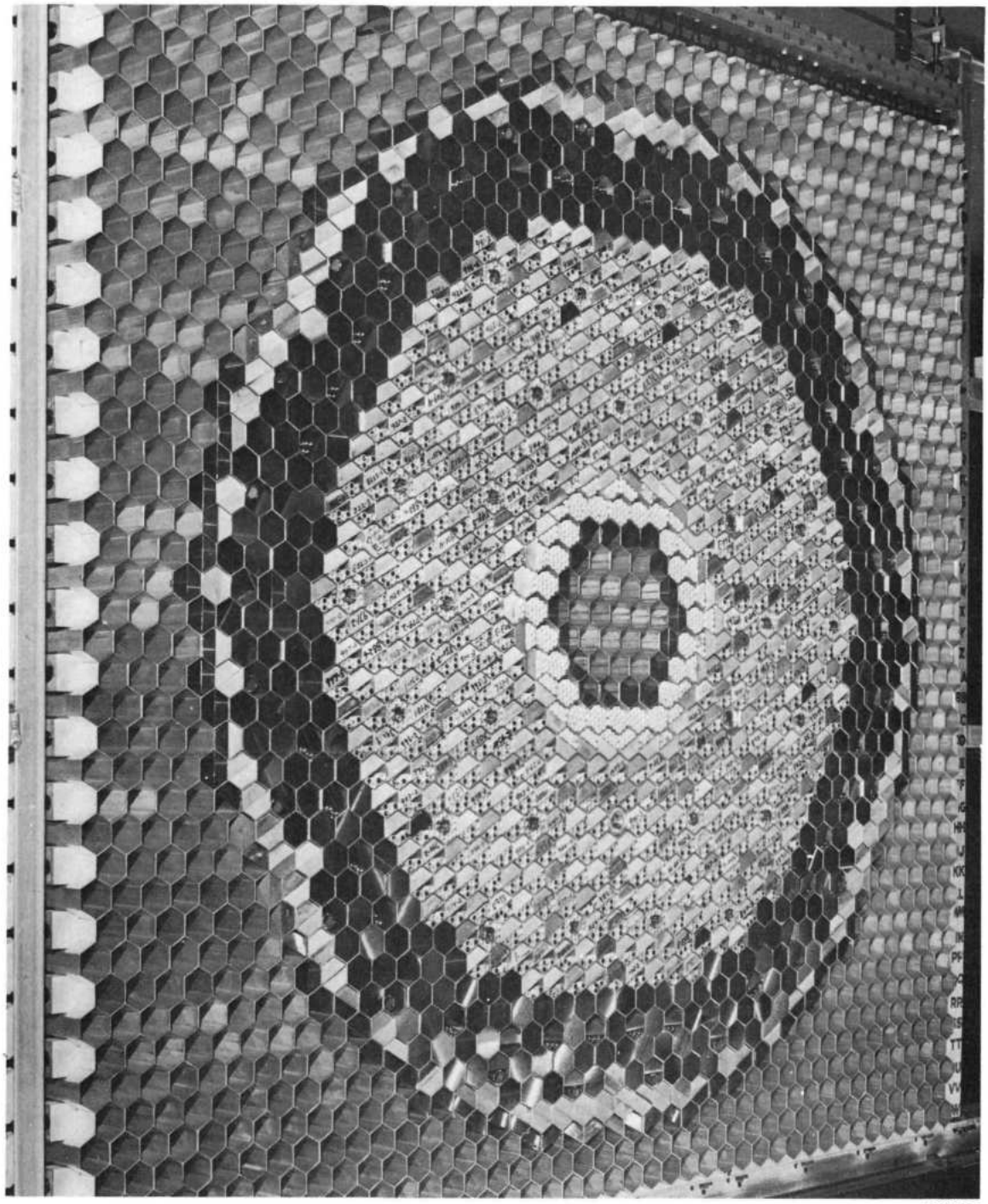

C-22736

Fig. 5.11 – Transverse cross section of SIC-1

CONFIDENTIAL

DECLASSIFIED

DECLASSIFIED

CONFIDENTIAL

lems it was assumed that gross measurements such as total excess reactivity and rod-bank worths are primarily a function of the gross properties of the assembly and do not require a mockup of fine details. It was also assumed that fine measurements of power distribution, rod scalloping, etc., are dependent primarily on local detail.[22,23]

The mockup was installed in the KEY matrix facility. This facility consisted of hexagonal aluminum tubes, each 1.75 inches across flats, stacked to form a square array approximately 8 feet on a side. The total length of the array was 7 feet. Half of this length rested on a fixed table, and the remaining half on a movable table. Thus the assembly halves could be separated.

Into this matrix was installed a core, Figure 5.12, consisting of approximately 5/6 gross mockup with low-temperature fuel elements and 1/6 fine mockup with modified design-type ceramic tube elements. Actually, the ceramic tube area occupied slightly more than a true 1/6 of the core in order to provide a buffer zone between the fine and gross regions.

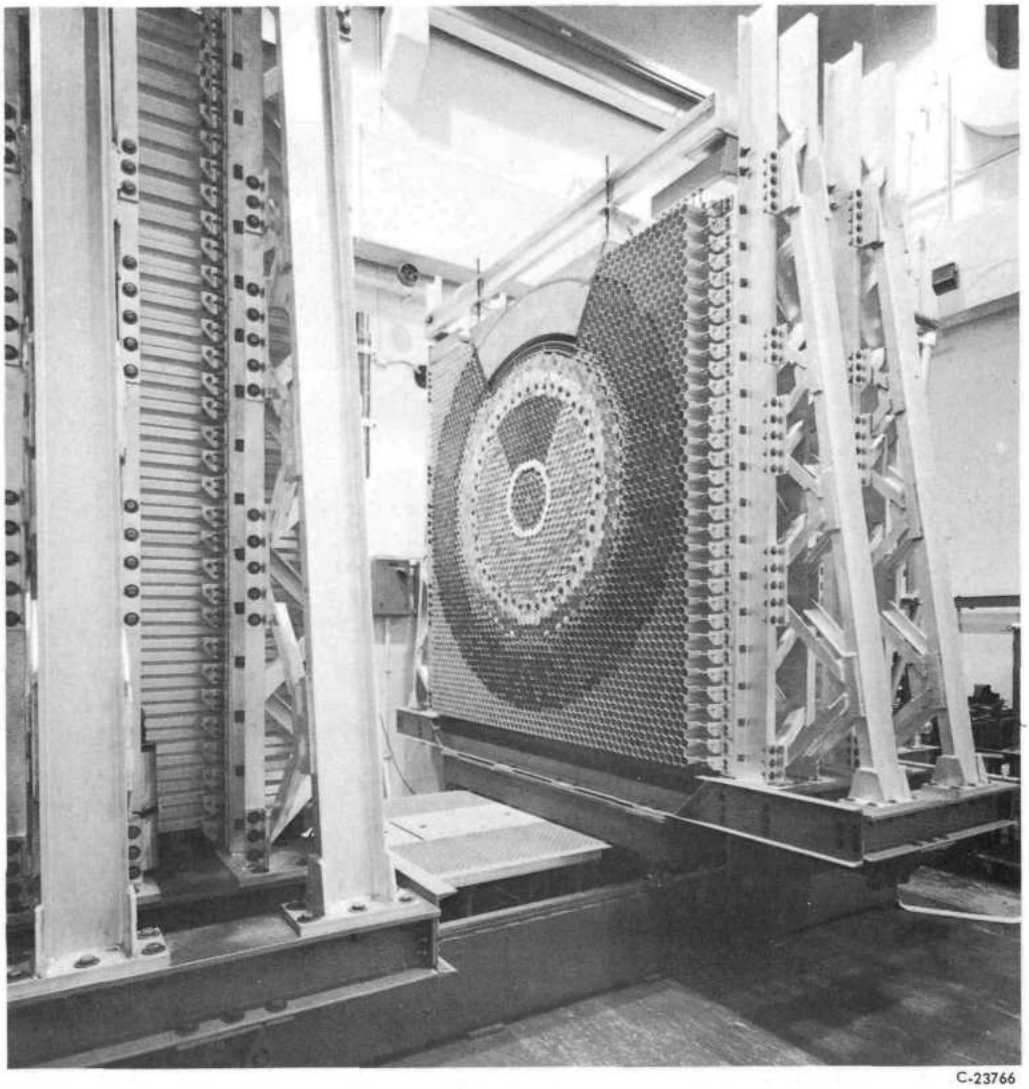

C-23766

Fig. 5.12 – XNJ140E-1 partial mockup in KEY facility

CONFIDENTIAL

DECLASSIFIED

DECLASSIFIED

This solution overcame most of the disadvantages of a completely detailed mockup. It also retained the possibility of making both gross and fine measurements. The fact that most of the fuel elements were of low-temperature design was in effect a safety feature. It was necessary, of course, to provide a reasonably close nuclear mockup in the gross portion of the core since the applicability of the fine measurements in the detailed mockup sector would be affected by the neutron environment provided by the surrounding region.

The KEY facility was designed so that the hexagonal matrix tubes could be removed from the top to provide the versatility required for building a variety of assemblies. For example, for the XNJ140E-1 critical experiment some matrix tubes were removed in a 1/6 sector at the top of the assembly to allow installation of a stainless steel can containing design-shield materials.

The various parts of the XNJ140E-1 mockup were installed as shown in Figures 5.12 and 5.13. Progressing radially from the center, the regions shown represent the (1) shaft void, (2) shaft and shaft liner material, (3) shaft insulation, (4) fueled core, (5) reflector, (6) pressure-pad spring and pressure-shell materials, and (7) shield.

Surrounding the core in the reflector are shown the 48 rod positions, which represent the control and safety rod positions in the design core. The nine shown at the top, just outside the detailed-measurement sector of the core, are exactly positioned by virtue of specially cut reflector parts. The rod positions surrounding the remainder of the core are approximately correct and were obtained by removing reflector from a half cell.

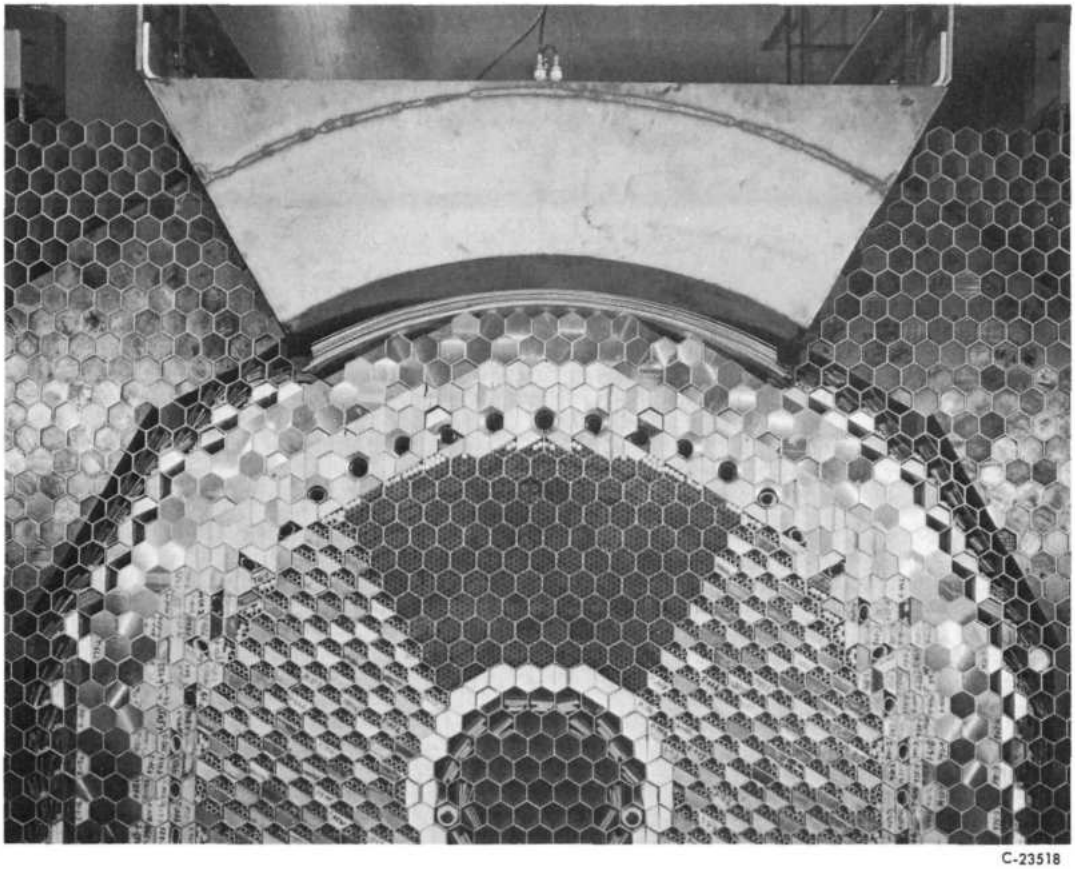

C-23518

Fig. 5.13 – Detail of XNJ140E-1 mockup measurements sector

DECLASSIFIED

DECLASSIFIED

The poison rods used to mock up the design control system were not automatically actuated in the critical experiment. Instead they were manually positioned to required insertion depths. The control rods and safety rods for the critical experiment were located in the shaft region and lower half of the core. In most cases the same cell contained two rods, one actuated from either end.

The detailed-measurement sector, shown in Figure 5.13, consisted of approximately 1/6 of the assembly. In the core portion of this sector fueled BeO tubes that closely mocked up the design-core tubes were installed. The remainder of the core contained elements similar to those used in the SIC-I assembly. The rod positions in the measurement sector, as previously mentioned, were near the correct design positions. The other major difference between the measurement sector and the remainder of the mockup was in the shield area. As shown in Figure 5.12, the matrix tubes were removed and replaced with a can containing LiH shield material. Initial criticality of the XNJ140E-1 critical experiment was attained with the entire assembly as a gross mockup. The fine-measurement sector was installed later.

The front and rear shields of the XNJ140E-1 were represented in the mockup to a thickness sufficient for determination of their effect on the core and for shield heating measurements in the problem areas. The front shield region consisted of a mockup of the tapered, borated stainless steel region nearest the core, backed up with approximately 8 inches of beryllium. The rear shield and grid plate were represented by appropriate amounts of boral, stainless steel, and beryllium inserted to approximate the correct shapes and locations. This mockup was also extended to a thickness of about 8 inches.

Many design-study measurements were made with the XNJ140E-1 mockup.[24] Included were measurements of nuclear heating in the radial and rear shields, the reactivity loss from thermocouple wires, a hypothetical fuel-meltdown mockup, the asymmetry caused by the slight mismatch between fine and gross sectors, and a three-dimensional power profile. In addition, of course, the control system and the excess reactivity of the mockup were evaluated.

As measured with the assembly that best represented the XNJ140E-1, the critical experiment had a reactivity excess of 5.07 percent $\Delta k/k$. The mockup bank of 48 rods had a measured value of 4.77 percent $\Delta k/k$ at 12-1/2-inches of insertion. Using a single-rod calibration curve to extrapolate to the full XNJ140E-1 insertion depth of 24 inches, a calculated worth of 10.7 percent $\Delta k/k$ was obtained.

5.2 EXPERIMENTS TO CONFIRM ANALYSIS METHODS

5.2.1 SMR EXPERIMENTS

Many method-confirmation experiments were conducted in the SMR matrix facility at Evendale. The SMR facility, shown in Figure 5.14, contains 1868 hexagonal aluminum tubes, each 1-3/4 inches across flats and 72 inches long. These tubes are stacked horizontally in honeycomb fashion to produce a matrix having dimensions of 70 by 70 by 72 inches. The matrix is hydraulically separable about a vertical plane dividing the assembly into two identical halves. The nuclear assemblies were loaded into the two halves so that matrix separation produced a gross change in the reactivity of the assembly and allowed access to a plane at or near the longitudinal center of the configurations. Also provided for in the facility are channels suitable for instrumentation for control, safety, and information and provisions for the appropriate safety and control mechanisms.[25]

The successful design of the HTRE No. 1 led to the investigation of the feasibility of a flight prototype using a solid hydrogenous moderator (AC-107). Hydrided zirconium was

DECLASSIFIED

DECLASSIFIED
CONFIDENTIAL

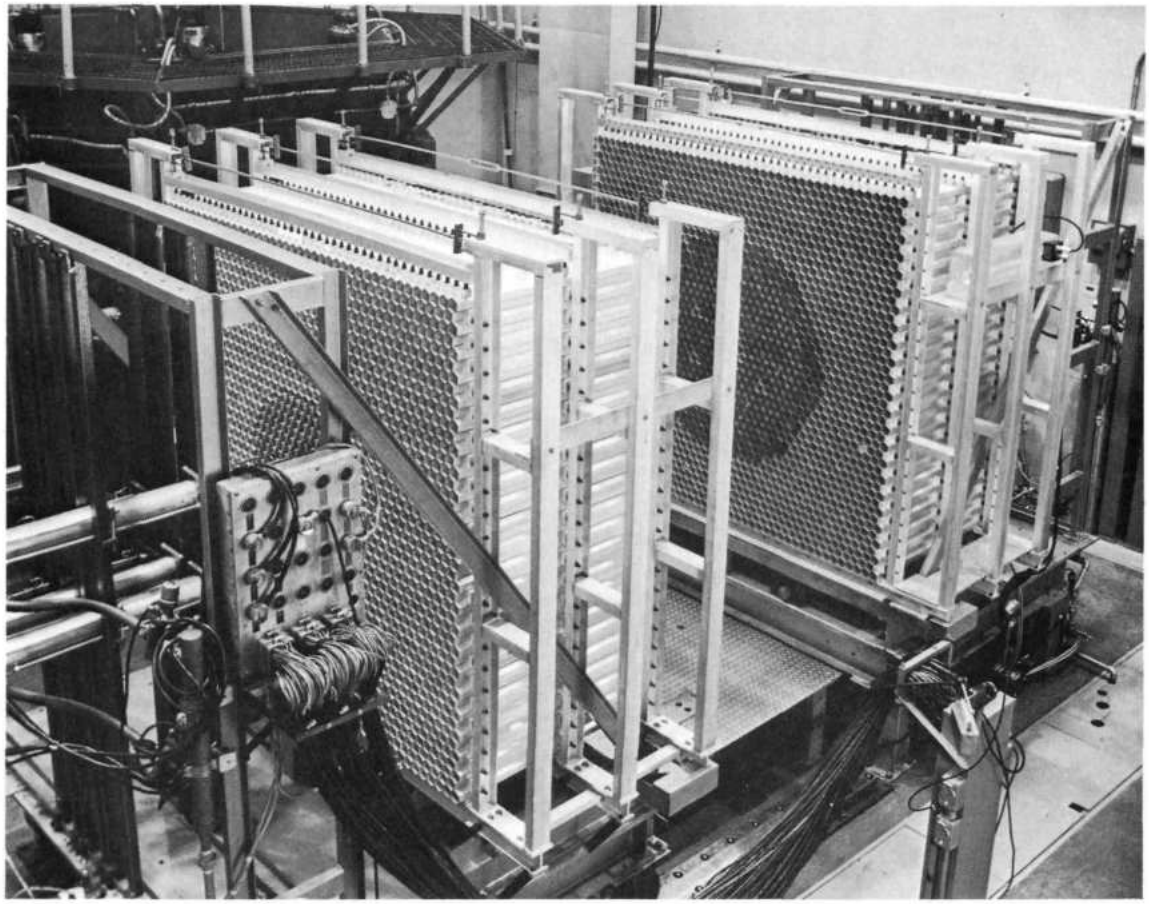

C-03553

Fig. 5.14 – SMR facility

chosen as the moderator for the preliminary design study. When the AC-107 design was discontinued, the mockup assembly installed in the flexible critical experiment assembly was retained for general investigation of the nuclear properties of ZrH_x-moderator reactors. The reactors for these experiments were typically made critical by reflector-thickness adjustments and reflector-fuel cell exchanges, and operational reactivity control was achieved by remotely actuated removal of fuel-moderator assemblies. Fine reactivity adjustments were made manually by aluminum-boron poison strips. The resultant clean cores were relatively easy to define analytically and therefore provided sound theory correlations.

5.2.1.1 Hydride-Zirconium Systems

The initial experimental verification of the slowing-down model to be used for hydrided-zirconium systems came from data obtained from the solid-moderator assemblies, SM-1[26,27] and SM-2.[28] Core diameters ranged from 19.2 to 32.5 inches, fuel loadings from 16.2 to 46.9 kilograms of uranium-235, and thickness of the beryllium metal radial reflectors from 2.4 to 9.3 inches. The core length remained constant at 30.0 inches, and the moderator (ZrH_x, $N_H = 3.97$) volume fraction was 0.36 in all the cores. A typical core configuration is shown in Figure 5.15, and fuel element detail in Figure 5.16.

The SM-1 and SM-2 series of configurations also provided data on the following effects:

1. In-core control rods and their interaction.[29,30]
2. Reflector control rods and drums.[31]

CONFIDENTIAL
DECLASSIFIED

DECLASSIFIED

CONFIDENTIAL

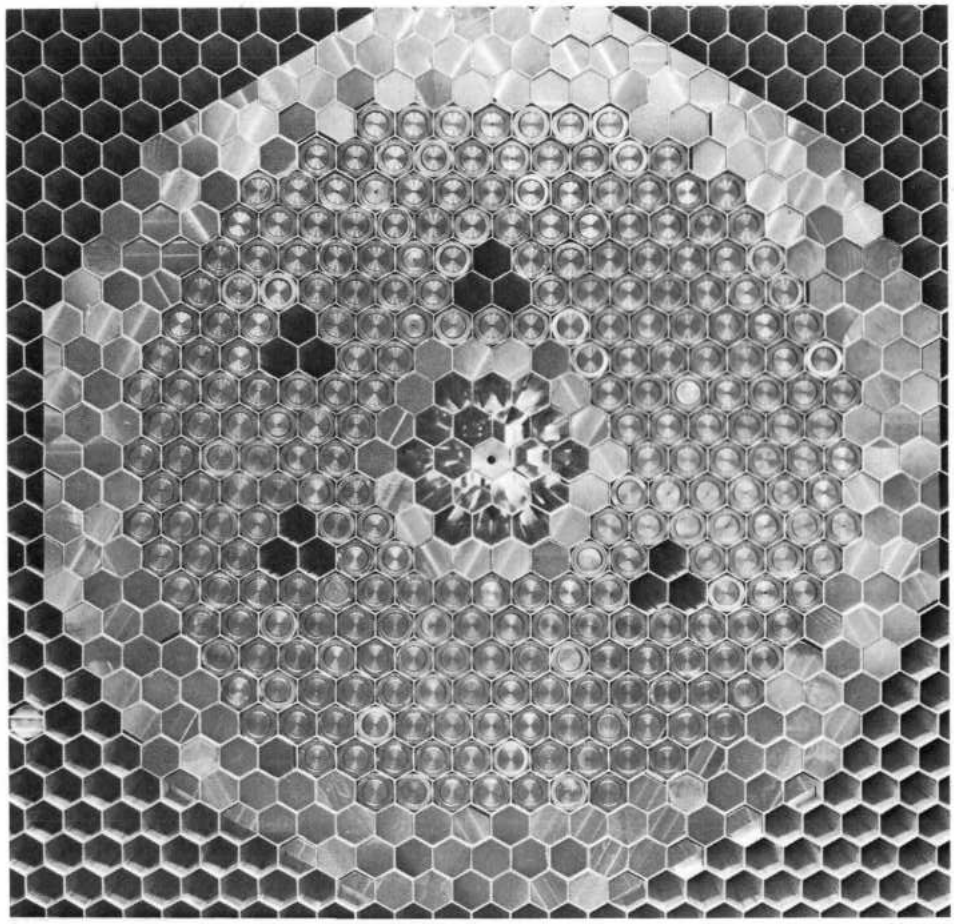

C-03607

Fig. 5.15 – Typical hydrided-zirconium-moderated core in SMR facility

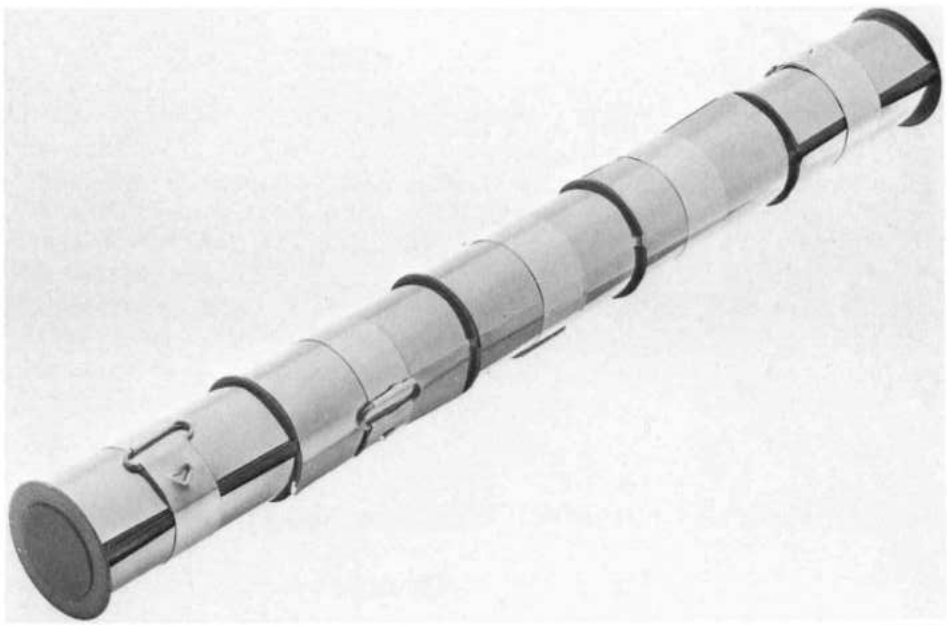

C-20570

Fig. 5.16 – Solid-moderator-type fuel element with central moderator bar

CONFIDENTIAL

DECLASSIFIED

DECLASSIFIED

3. Reflector savings.[29,32]
4. Moderator, poison, and structure annuli at the core-reflector interface.[33]
5. Axial voids and islands.[28]
6. Flux peaking in core.[34]

5.2.1.2 Hydrided Yttrium System

To provide the necessary high-temperature capability for the XMA-1C flight-prototype power plant, hydrided yttrium (YH_X) was selected as a possible moderator. One of the assemblies in the SMR matrix facility was replaced by an assembly identical except for the substitution of hydrided yttrium (YH_X, $N_H = 5.5$) for the hydrided zirconium on a volume-for-volume basis. This yttrium assembly was designated as the RAM-I. The reactivity, flux, and power were found to be almost identical for the two reactors.[35]

Initial theory-experiment correlation of 0.5 percent $\Delta k/k$ excess reactivity, 3.3 percent cell reactivity, and 0.177 rms fractional-power-density correlation indicated that existing analysis tools, such as the Program 1017-G-2 sequence, were sufficient for YH_X reactors; but the general need for refinement of the treatment of beryllium reflectors was again apparent.[36]

5.2.1.3 Acrylic Plastic System

One other hydrogen system was constructed and operated in the SMR facility. It was the safety-orientated design study (NTGS) of the Nuclear Test Gage.[37]

5.2.1.4 Beryllium Metal Systems (BEM-I and BEM-II)

The best slowing-down model to be used and the magnitude of the (n, 2n) reaction in beryllium-metal-moderated systems were determined from the BEM-I and BEM-II systems.

The BEM-I cores, Figures 5.17 and 5.18, were 30.0 inches long and 39.2 or 46.2 inches in diameter. Core excess reactivity was established by variations in the beryllium-metal radial-reflector thickness and by uniform poisoning of the core with cadmium wires. The moderator volume fraction was a constant 0.60, and the beryllium-to-uranium-235 atomic ratio was 1426 to 1. The subcadmium fission fraction was 0.69 for the smaller-diameter core and 0.83 for the larger cores.[38,39]

In the BEM-II cores the moderator volume fraction was 0.83. The core length was 32.0 inches, and the diameter varied from 15.7 to 21.7 inches. The beryllium metal reflector thickness varied from 3.0 to 8.4 inches. Critical fuel loadings varied from 14.5 to 1.7 kilograms of uranium-235 to give beryllium-to-uranium-235 atomic ratios from 288 to 1 to 4592 to 1. The subcadmium fission fraction varied from 0.45 to 0.92.[40,41]

5.2.1.5 Beryllium Oxide Systems

The beryllium-metal moderator of two of the BEM-II cores was replaced on a volume-for-volume basis with beryllium oxide, as shown in Figure 5.19. The resultant cores were designated BEOM-II. The 33.7-inch-long cores were 20.2 and 15.7 inches in diameter. They contained 4.5 kilograms and 14.5 kilograms of uranium-235 for beryllium-to-uranium-235 atomic ratios of 908 to 1 and 170 to 1. Subcadmium fission fractions were approximately the same as those for metal-moderator cores. The loss of reactivity of the cores, as compared to that for the beryllium-metal-moderator cores, was compensated for by increasing the reflector thickness. The effectiveness of beryllium metal and beryllium oxide as reflector materials was also compared in these configurations.[42]

A third BEOM-II core was designed and built so as to be particularly sensitive to impurities in the beryllium oxide moderator. This 27.1-inch-diameter core contained 5.4 kilograms of uranium-235 for a beryllium-to-uranium-235 atomic ratio of 1362 to 1 and

DECLASSIFIED

DECLASSIFIED

CONFIDENTIAL

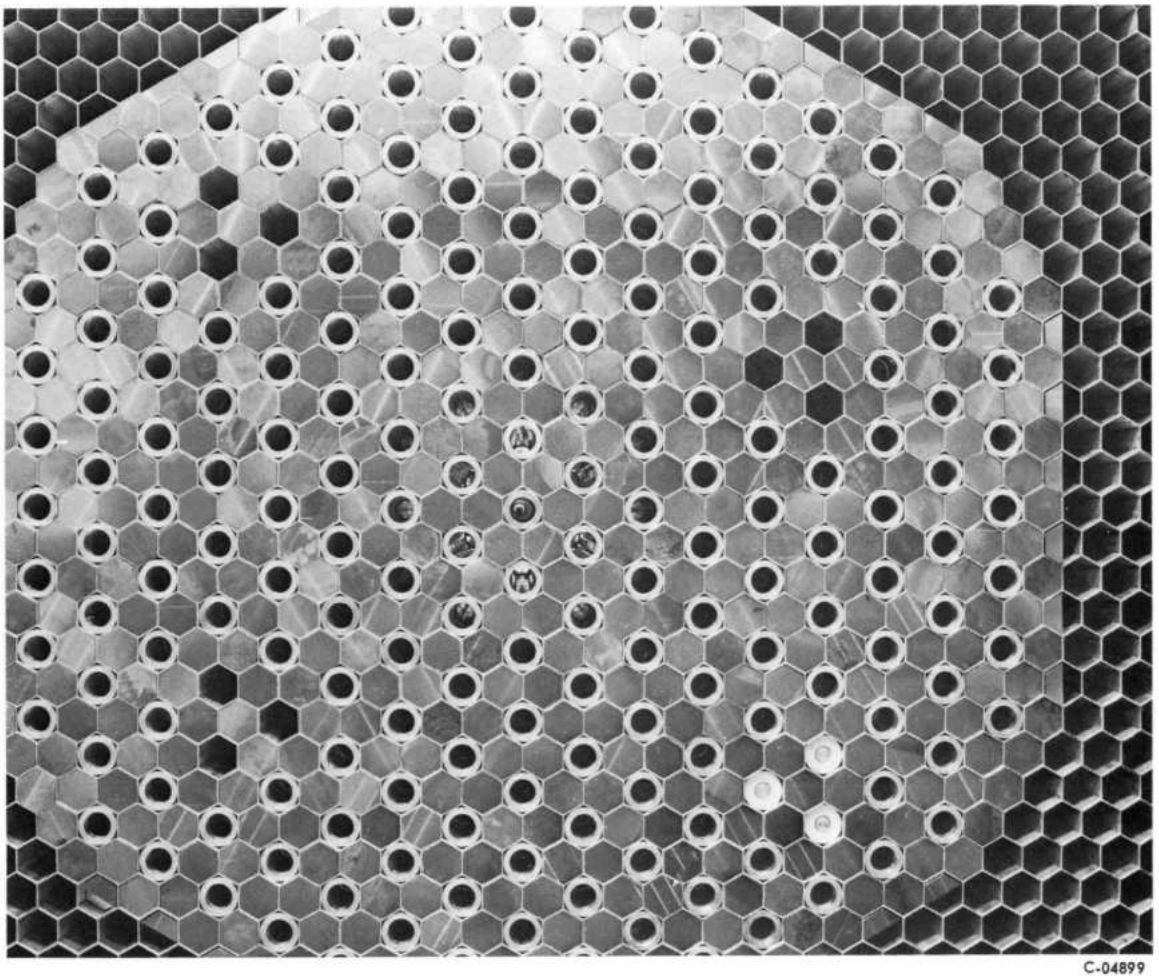

C-04899

Fig. 5.17 – Cross section at central transverse gap of BEM-I reactor

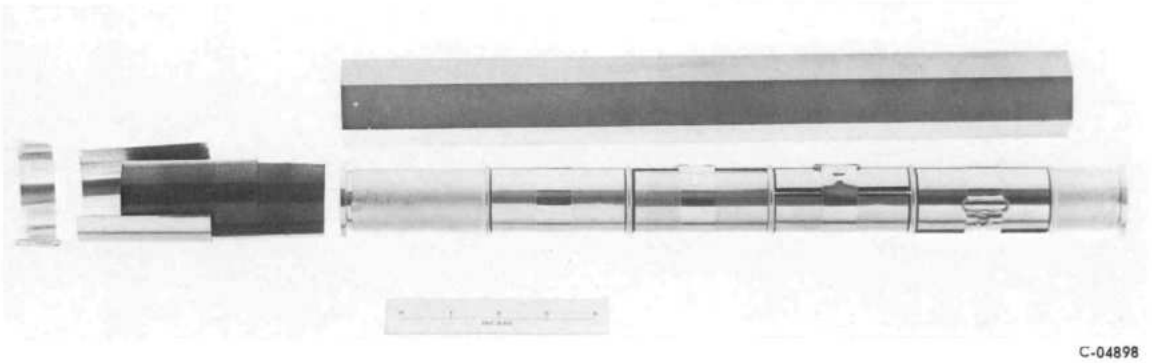

C-04898

Fig. 5.18 – Half-length fuel element and beryllium bar for BEM-I reactor

CONFIDENTIAL

DECLASSIFIED

DECLASSIFIED

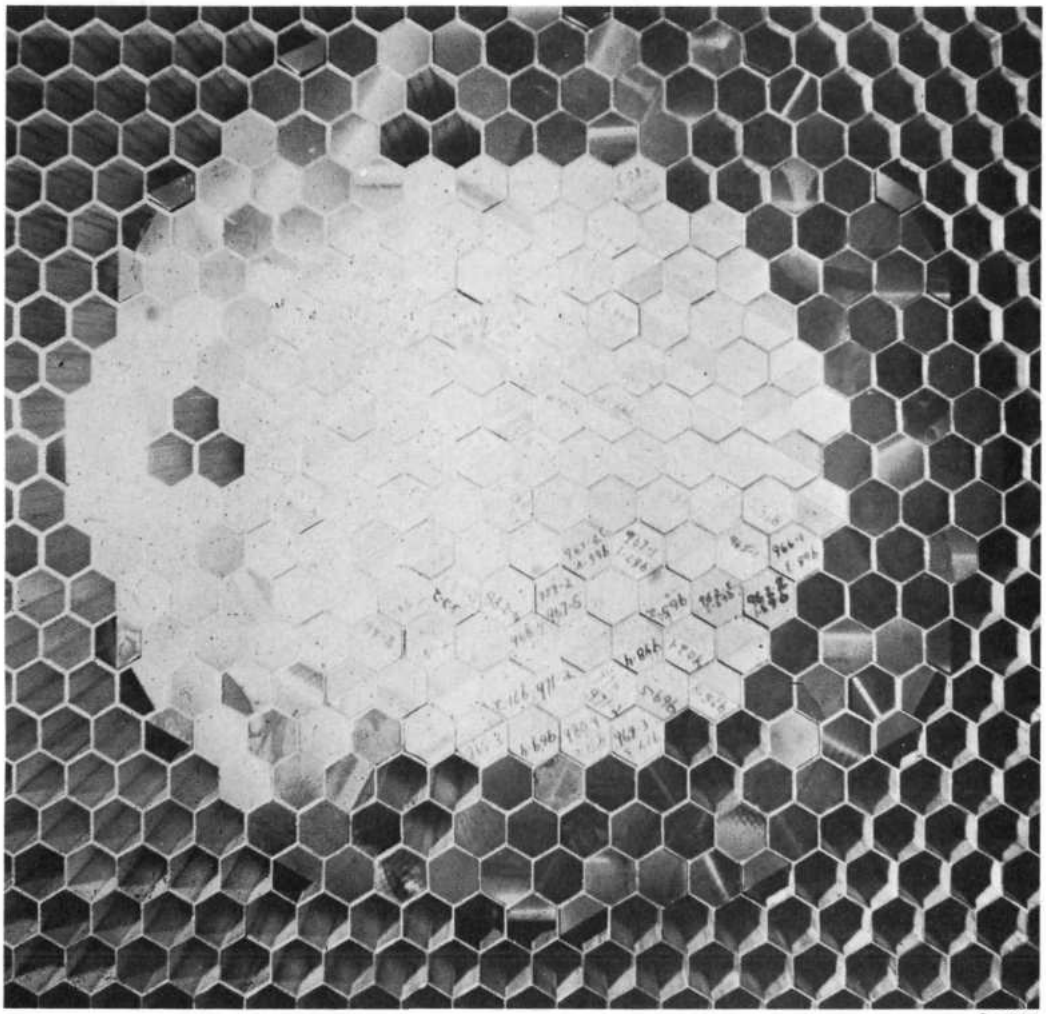

C-21228

Fig. 5.19 – Cross section at central transverse gap of BEOM-II reactor

a resultant subcadmium fission fraction of 0.85. Appreciable changes in the assembly reactivity were noted when beryllium oxides manufactured by different vendors were used as moderator.[43]

5.2.1.6 Beryllium-Hydrogen Systems

Experimental information required for determining optimum safe masses and atomic ratios of ceramic fuels was obtained from subcritical and critical assemblies in the SMR matrix facility.

Properties of a core equivalent to a 1-cubic-foot sphere containing 805* grams of uranium-235 at a 254 to 1 beryllium-to-uranium-235 atomic ratio were determined. The maximum observed multiplication of this sphere was 2.5 with 12 inches of acrylic plastic reflector and sufficient acrylic plastic in the core to establish a hydrogen-to-uranium-235 atomic ratio of 355 to 1 in the core. These were the maximum conditions obtainable with the materials available. Reasonable extrapolation indicated an expected multiplication of 3.3 at a hydrogen-to-uranium-235 atomic ratio of 500 to 1.

*An anticipated batch size of 350-grams times a safety factor of 2.3.

DECLASSIFIED

DECLASSIFIED

CONFIDENTIAL

Additional fuel was added to the 12-inch acrylic-plastic-reflected core having a hydrogen-to-uranium-235 ratio of 355 to 1. The system multiplication at a loading of 1780 grams of uranium-235 per cubic foot was found to be only 4.35, and the method of attack was discontinued as the predicted criticality was at fuel loadings in excess of 3 kilograms per cubic foot.

The 1-cubic-foot core was surrounded with the best reflector obtainable (16-inch beryllium-metal end reflectors, 6.1 inches of beryllium metal plus 9.5 inches of acrylic-plastic radial reflector). Criticality was achieved at three different fuel loadings by varying the moderator content. The reactive worths of uranium-235, acrylic plastic, and beryllium oxide were measured in each case. It was concluded that (1) the minimum critical mass of a 1-cubic-foot spherical system having a beryllium-to-uranium-235 atomic ratio of 250 to 1 is 830 grams at a hydrogen-to-uranium-235 atomic ratio of 500 to 1, and (2) at this concentration of hydrogen and below, the addition of beryllium oxide to the system at the expense of an equal volume of water will decrease the assembly reactivity.

5.2.2 HIGH-TEMPERATURE CRITICAL EXPERIMENT REACTOR

The HOTCE (hot critical experiment), Figure 5.20, is a reactor designed to study high-temperature effects while retaining the experimental advantages of a critical experiment assembly. It was assembled and operated in the Low Power Test facility at the General Electric Idaho Test Site.[44,45]

The HOTCE core consists of 151 fuel cells in a modified hexagonal array. For ease and safety in working with the assembly and to permit faster cooling of the heated core, the reactor was separated into two parts at shutdown. For this purpose, approximately one-half of the reactor was mounted on a movable table.

The moderator is zirconium hydrided to a hydrogen-atom density of 4.1×10^{22} atoms per cubic centimeter. A 4-inch beryllium reflector surrounds the core except at the ends. The active core is 30 inches long and has an effective diameter of 51.6 inches. The hydrided zirconium extends 2.75 inches beyond the fueled portion of the core to furnish a partial end reflector.

This reactor makes use of a unique fuel element design that has a dual purpose. Each element is of a helix made from 1/8-inch-diameter, fuel-bearing, stainless-steel wire. The fuel, contained within the wire, is 93.2 percent enriched uranium dioxide (UO_2). The total uranium-235 inventory is 41.9 kilograms.

In addition to providing nuclear fuel, the wire fuel elements heat the core. With electrical connections at the ends of the elements, they serve as resistance heaters. Thus, no extraneous materials are required in the core to act as heating strips.

The fuel elements may attain a temperature of 1600°F during a heating cycle. The moderator is heated by radiation and convection and is designed to withstand temperatures to 1300°F. The reflector pieces are separately heated by resistance-strip heaters located in grooves around the outer perimeter of the reflector. The entire core and reflector are insulated from the ambient air by a 4-inch blanket of high-temperature, refractory-fiber insulation.

The control system uses combination control-scram actuators. Poison-tip rods are connected to the actuators by electromagnets and are scrammed, upon release of the magnets, by a compressed spring. For control the electromagnets, with rods attached, are moved with motor-driven lead screws. From one to three of the stainless-steel-clad boron carbide rods may be driven by a single actuator.

This reactor was designed and built to obtain information on the effects of temperature upon reactor performance and to develop high-temperature-reactor measurement tech-

CONFIDENTIAL

DECLASSIFIED

DECLASSIFIED

CONFIDENTIAL

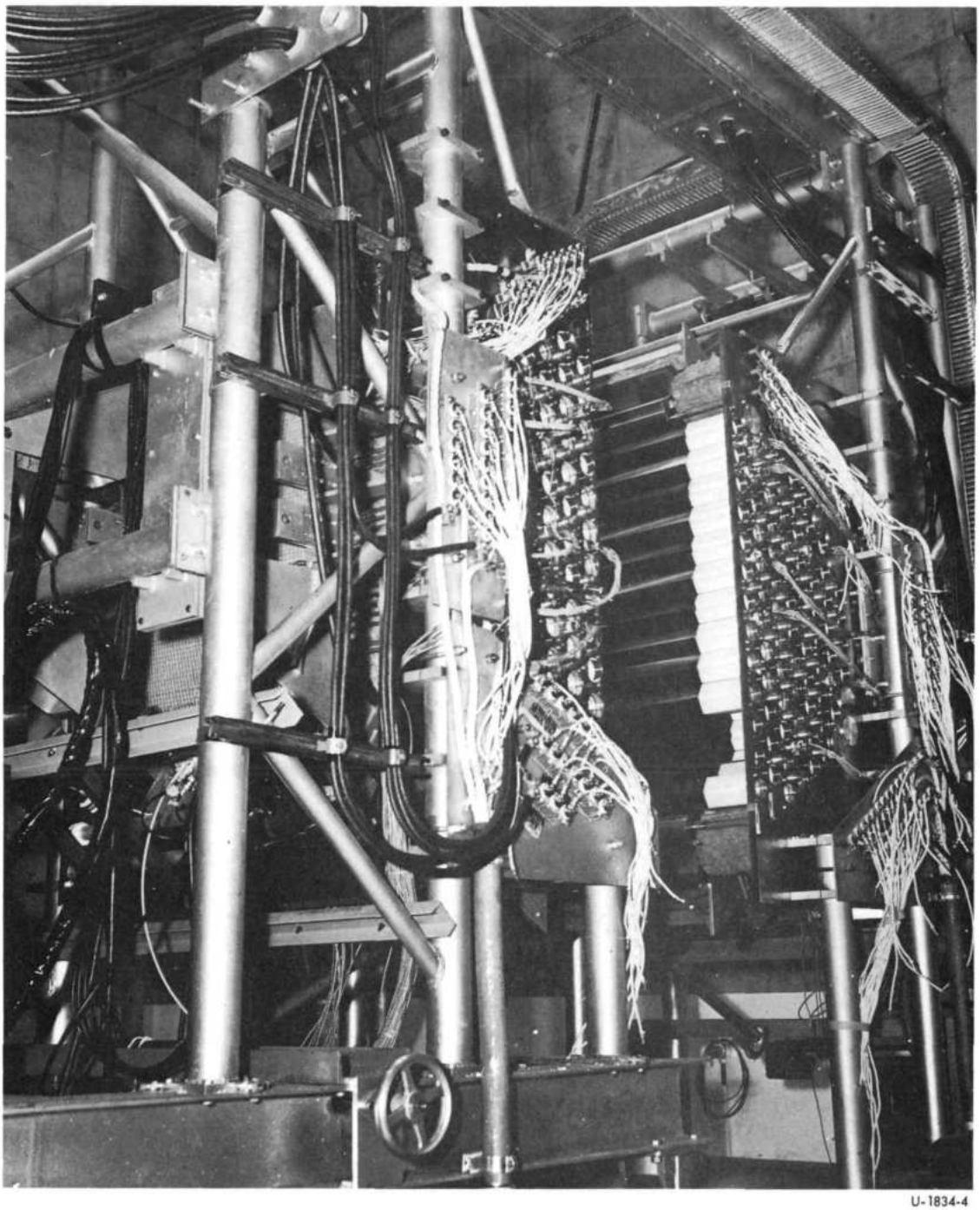

U-1834-4

Fig. 5.20 – HOTCE reactor in Low Power Test facility (LPT) at Idaho Test Station

CONFIDENTIAL

DECLASSIFIED

DECLASSIFIED

niques. The core is simple in design: all cells are identical and large enough to provide sizable test holes for the insertion of test fuel elements, control elements, measuring devices, etc. With the fuel element removed, any fuel cell provides such a test hole.

The HOTCE attained criticality with about 2 percent $\Delta k/k$ excess reactivity. High-temperature runs show a positive temperature coefficient of reactivity changing from about 0.0035 percent $\Delta k/k$ per ^{o}F at room temperature to zero at approximately $1000^{o}F$ average core temperature.[46,47] A further increase in temperature results in an inversion with a slight negative coefficient at $1100^{o}F$, the highest temperature attained.[48]

5.2.3 REVERSE FOLDED-FLOW REACTOR MOCKUP

The folded-flow concept, shown in Figures 5.21, 5.22, and 5.23, is a departure from conventional compact reactors in two principal areas, (1) the intricate coolant gas flow pattern and heat transfer system and (2) the unique core arrangement with its high-leakage design. The critical experiment work was accordingly split into two phases. The first phase was a feasibility check with an acrylic plastic moderator and with the reflector void volume lumped in the exit-air gaps.[49] Reactivity and power-distribution measurements from this assembly, the RAG-1 (Radial Air Gap),[50] served primarily as checks on

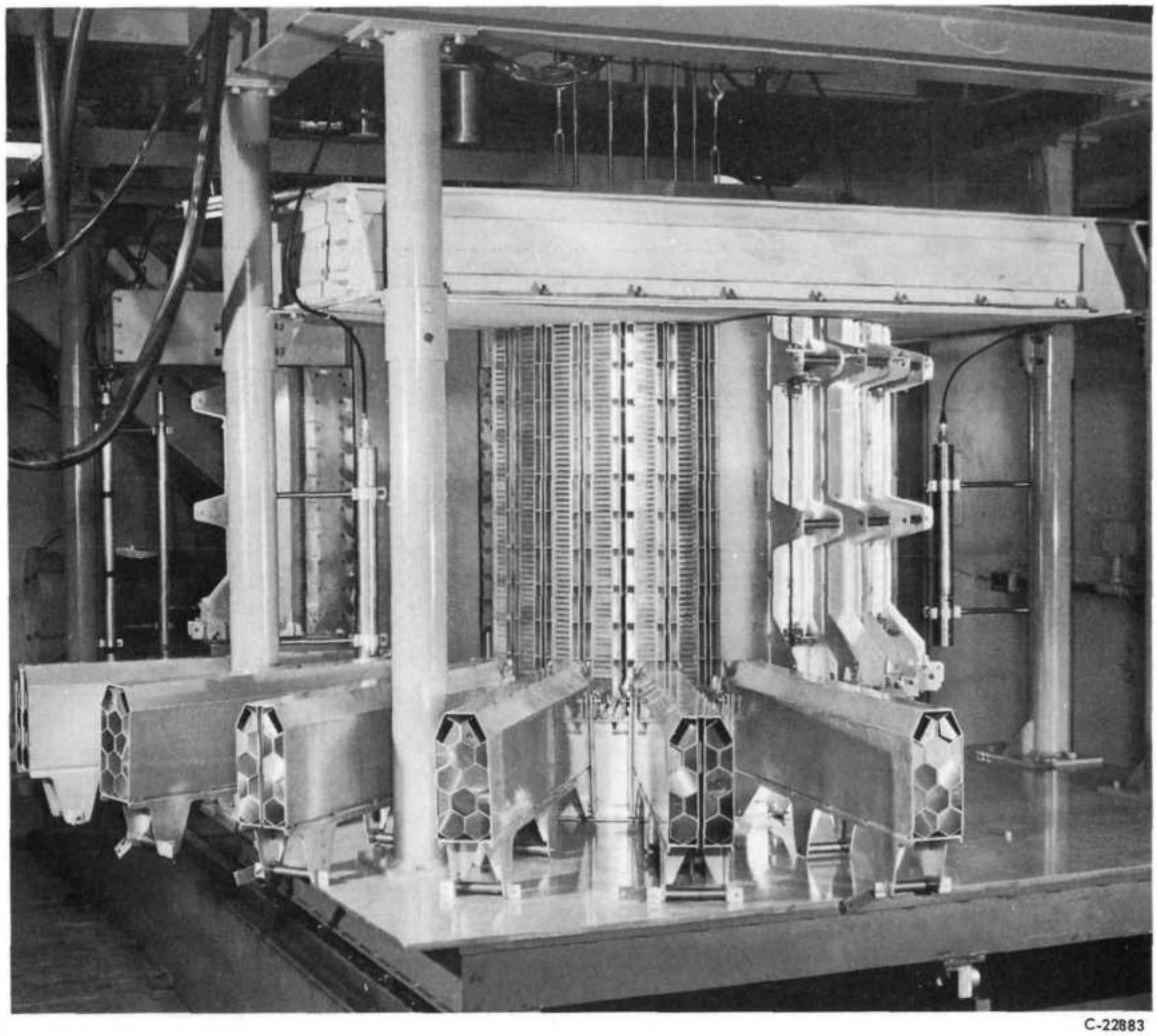

C-22883

Fig. 5.21 – RAG-1 folded-flow mockup for critical experiments, shown with six reflector sections dropped down

DECLASSIFIED

DECLASSIFIED

CONFIDENTIAL

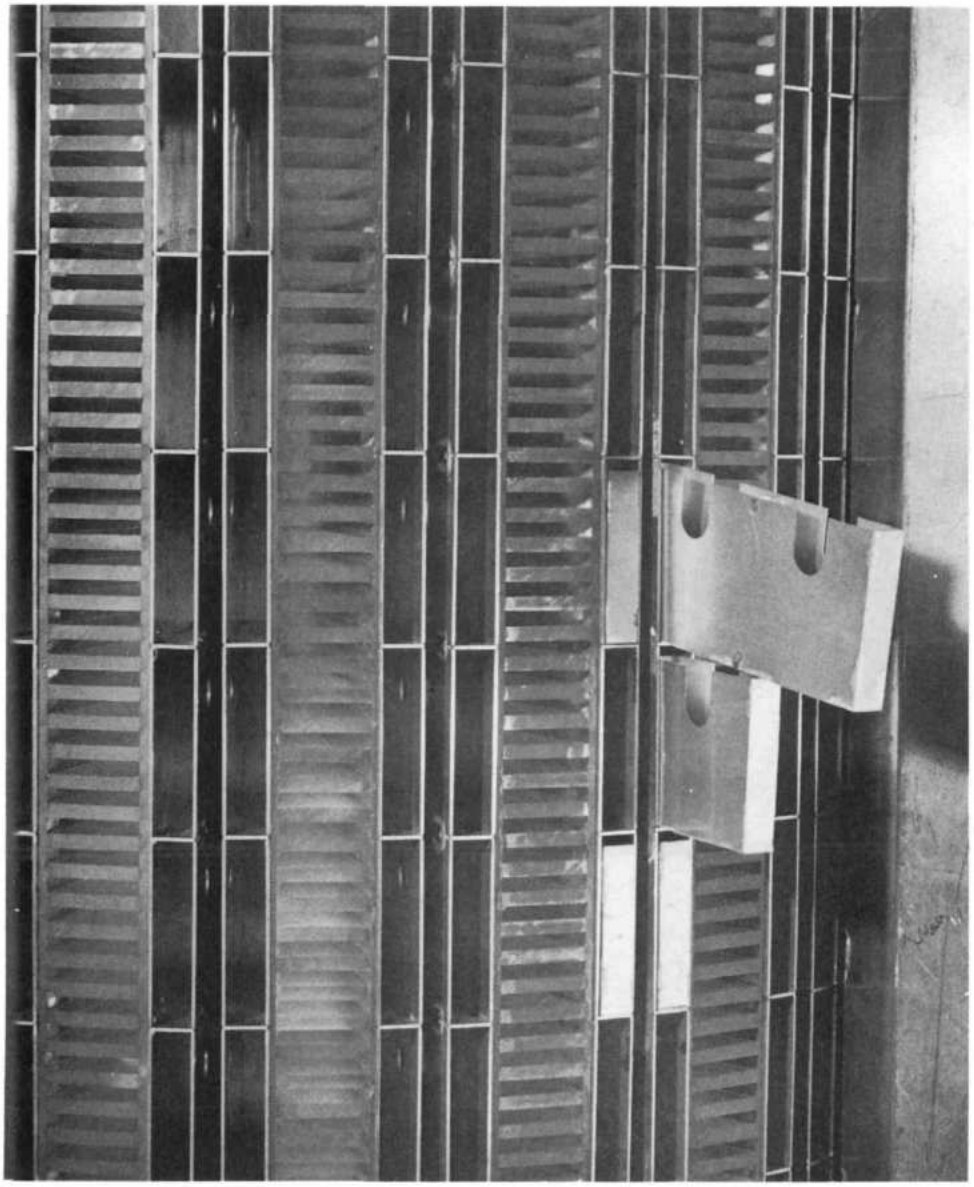

C-22882

Fig. 5.22 – RAG-1 reactor fuel-moderator region showing acrylic plastic moderator plates and shelves with aluminum boxes for uranium and 80Ni – 20Cr sheets

CONFIDENTIAL

DECLASSIFIED

DECLASSIFIED

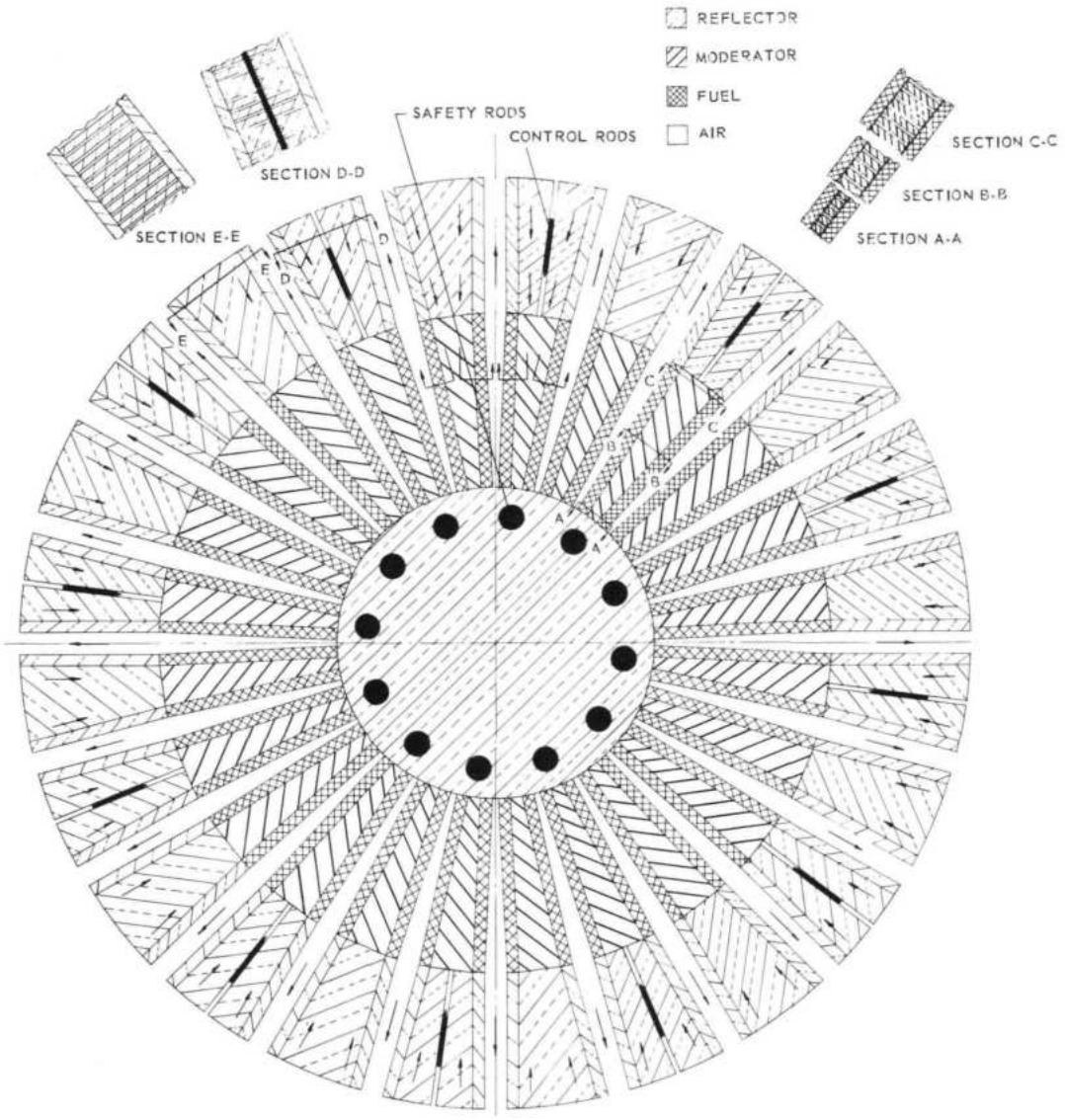

Fig. 5.23 – RAG-1 reactor schematic cross section

the applicability of conventional analytical techniques.[51] Sufficient data were obtained to serve as a base for the preliminary P122 folded-flow design and its design-confirmation mockup. For this second phase a 60-degree sector of the reactor was rebuilt with a hydrided zirconium moderator, improved slotted radial-reflector segments, and a sectional mockup of the borated-stainless-steel primary shield. Detailed power distribution and reactivity measurements were obtained,[52] and the more-difficult-to-predict secondary gamma heating distributions were determined.[53]

The folded-flow reactor is discussed in detail in APEX-909, "Aircraft Nuclear Propulsion Systems Studies."

DECLASSIFIED

DECLASSIFIED

5.3 REFERENCES

1. "Summary Hazards Report with the R-1 Mockup Reactor," GE-ANPD, APEX-110, October 1952.
2. Minnich, S. H., "C. E. Data and Supporting Analysis for the AC100A," GE-ANPD, APEX-229, December 1955.
3. Kerkhoff, R. E., "Critical Experiment with the HTRE No. 1 Nuclear Mockup (TRA)," GE-ANPD, APEX-311, June 1957.
4. Link, B. W., and Clark, R. G., "The Critical Experiment for the HTRE No. 3," Transactions of the American Nuclear Society, Vol. 3, No. 2, 1-6, Dec. 1960; Hoefer, J. A., "Summary Hazards Report for Critical Experiments with the TSM Reactor," GE-ANPD, APEX-254, July 1956.
5. Bermanis, H. L., "Power Distribution Studies in the Critical Experiment for the HTRE No. 3," Transactions of the American Nuclear Society, Vol. 3, No. 2, Dec. 1960, 1-7.
6. Orr, W. L., and Keppler, J. G., "Nuclear Design Summary of the D102A Reactor," GE-ANPD, PREDC-588, December 1959.
7. Bermanis, H. L., Clark, R. G., Link, B. W., "TSM Measurements Report No. 8," GE-ANPD, DC 58-11-3, November 1958.
8. Milburn, E. L., "ASM Summary Hazards Report," GE-ANPD, APEX-412, September 1958.
9. Bermanis, H. L., Link, B. W., "ASM Measurements Report No. 1," GE-ANPD, DC 59-2-134, February 1959.
10. Bermanis, H. L., and Link, B. W., "ASM Measurements Report No. 2, No. 3 and No. 4," GE-ANPD, DC 59-7-181 (July 1958), DC 59-8-163 (August 1958), and DC 60-2-42 (February 1960), respectively.
11. McVey, C. I., "Gamma Heating Measurements in the ASM-3-J Critical Experiment Reactor," GE-ANPD, DC 60-3-94, March 1960.
12. Brooks, E. H., and Milburn, E. L., "Shield Measurements About the ASM-3," GE-ANPD, DC 60-9-97, September 1960.
13. Brooks, E. H., Milburn, E. L., "Shielding Measurements About the SSR," GE-ANPD, DC 61-2-3, February 1961.
14. Milburn, E. L., "CERA Summary Hazards Report," GE-ANPD, APEX-367, May 1958.
15. Bermanis, H. L., Link, B. W., "Preliminary Nuclear Measurements with the CERA," GE-ANPD, DC 59-3-26, March 1959.
16. "Nuclear Development Laboratories Quarterly Task Report, July - September 1959," GE-ANPD, DC 59-9-9, September 1959.
17. Fraembs, D. H., "Experimental Results, P127 Preliminary Critical Experiment," GE-ANPD, APEX-638, August 1960.
18. "Nuclear Development Laboratories Quarterly Task Report, October - December 1959," GE-ANPD, DC 59-12-9, December 1959.
19. "Project 101 Quarterly Task Report, January - March 1960," GE-ANPD, DC 60-3-1, March 1960.
20. Fraembs, D. H., "Experimental Results, P141 Critical Experiment," GE-ANPD, APEX-703, October 1961.
21. Fraembs, D. H., "Experimental Results, Part One, P140B Preliminary Critical Experiment," "... Part Two..." and "... Part Three...," GE-ANPD, DC 60-4-112 (April 1960), DC 60-6-42 (June 1960), and DC 60-6-128 (June 1960), respectively.
22. Brown, H. E., "A Description of the D140E1 Mockup in the KEY Facility," GE-ANPD, DC 60-8-54, August 1960.
23. Link, B. W., "Summary Hazards Evaluation of the Keyhole Facility," GE-ANPD, APEX-559, May 1960.

DECLASSIFIED

DECLASSIFIED

24. Andrews, J. L., et al., "Experimental Results from a Gas Cooled Beryllia Critical Experiment," GE-ANPD, APEX-647, October 1961.
25. Simpson, J. D., "Summary Hazards Evaluation of the SMR Facility," GE-ANPD, APEX-536, December 1959.
26. Bermanis, H. L., "SM-1 Measurements Report No. 1," GE-ANPD, DC 56-4-44, April 1956.
27. Renaker, J. N., et al., "SM-1 Measurements Report No. 2," GE-ANPD, DC 56-4-151, April 1956.
28. Bermanis, H. L., Link, B. W., Renaker, J. N., "SM-2 Measurements Report No. 1," GE-ANPD, DC 56-8-5, August 1956.
29. Fraembs, D. H., "Reflector and Control Rod Studies," GE-ANPD, APEX-526, November 1957.
30. Zwick, J. W., "Control Rod Theory Evaluation Based Upon Measurements of Control Rod Worths in SM-1-2 Reactor Assemblies," GE-ANPD, APEX-578, April 1959.
31. Fraembs, D. H., Renaker, J. N., Bermanis, H. L., "SM-2 Measurements Report No. 3," GE-ANPD, DC 56-12-64, December 1956.
32. Stanley, M. J., "Post Analysis of SM-1-A Critical Assemblies," GE-ANPD, XDC 58-3-98, March 1958.
33. Fraembs, D. H., Renaker, J. N., Bermanis, H. L., "SM-2 Measurements Report No. 2," GE-ANPD, DC 56-12-51, December 1956.
34. Bermanis, H. L., Renaker, J. N., "SM-2 Measurements Report No. 5," GE-ANPD, DC 57-7-113, July 1957.
35. Stratton, V. J., Renaker, J. N., Fraembs, D. H., "RAM-1 Nuclear Measurements Report," GE-ANPD, DC 58-7-198, July 1958.
36. Wenstrup, F. D., "Preanalysis and Initial Postanalysis of the RAM-1 Critical Experiment," GE-ANPD, XDC 58-10-107, October 1958.
37. Renaker, J. N., Stratton, V. J., "Nuclear Test Gage Safety Experiment," GE-ANPD, APEX-414, February 1958.
38. Clark, R. G., et al., "BEM-1 Measurements Report No. 1," GE-ANPD, DC 58-2-119, February 1958.
39. Fraembs, D. H., "BEM-1 Measurements Report No. 2," GE-ANPD, XDC 58-7-196 (July 1958), with addendum DCL 58-7-197 (July 1958), and errata XDC 58-9-98 (September 1958).
40. "Nuclear Development Laboratories Quarterly Task Report, July - September, 1958," GE-ANPD, DC 58-9-9, September 1958.
41. "Nuclear Development Laboratories Quarterly Task Report, January - March, 1959," GE-ANPD, DC 59-3-9, March 1959.
42. "Nuclear Development Laboratories Quarterly Task Report, October - December, 1958," GE-ANPD, DC 58-12-9, December 1958.
43. "Nuclear Development Laboratories Quarterly Task Report, April - June 1959," GE-ANPD, DC 59-6-9, June 1959.
44. Hoefer, J. A., "Summary Hazards Report for Critical Experiments with the HOTCE Reactor," GE-ANPD, APEX-345, November 1957.
45. Brown, H. E., "As-Built Specifications of the HOTCE," GE-ANPD, DC 58-6-144, June 1958.
46. Skow, K. J., "Interim Report on Revised Hot Critical Experiment, Phase I Testing," GE-ANPD, DC 59-2-701, February 1959.
47. Kinkaid, R. M., "Reactivity Measurements During Phase II Tests with the HOTCE Reactor," GE-ANPD, DC 59-7-700, July 1959.
48. Wetzel, D. E., "Nuclear Analysis of the HOTCE Reactor, Part 1 - Reactivity-Temperature Relationship," GE-ANPD, XDC 59-10-201, October 1959.
49. Sundin, R. L., "RAG-1 Specifications Report," GE-ANPD, DC 60-3-93, March 1960.

DECLASSIFIED

DECLASSIFIED

CONFIDENTIAL

50. Fraembs, D. H., Hoefer, J. A., "Summary Hazards Report, Nuclear Mockup of P122 Folded Flow Reactor, RAG-1," GE-ANPD, APEX-537, January 1960.
51. Bermanis, H. L., et al., "Nuclear Measurements Report No. 1," GE-ANPD, DC 60-6-145, June 1960.
52. Bermanis, H. L., Link, B. W., "RAG Nuclear Measurements Report No. 2," and "...No. 3..." GE-ANPD, DC 60-10-57 (October 1960), and DC 60-11-160(November 1960); respectively and Clark, R. G., and Page, W. W., "RAG Nuclear Measurements Report No. 4," GE-ANPD, DC 61-5-19, April 1961.
53. Bermanis, H. L., Link, B. W., McVey, C. I., "Secondary Heating Measurements with the RAG Assembly," GE-ANPD, DC 60-11-169, November 1960.
54. Smith, M. R., "Experiment-Theory Correlation for RAG Power Distribution," GE-ANPD, DC 60-10-127, October 1960.

CONFIDENTIAL

DECLASSIFIED

RECEIVED

RECEIVED

DECLASSIFIED
CONFIDENTIAL

6. NUCLEAR-MEASUREMENT TECHNIQUES

6.1 INTRODUCTION

Inasmuch as the design of aircraft reactors by GE-ANPD was carried on by a combined analytical-experimental approach, great emphasis was laid on the measurement of fission-power distributions. During design iterations, fission-power distributions were often measured with as many as 7000 points. This measurement sequence was repeated with the various conditions of power plant operation, i.e., control rods out, simulation of xenon build-up, or different phases of the design iteration. Consequently, much effort was made to automate procurement, reduction, and reporting of this information. A 10-channel proportional counting system was procured for this purpose.[1]

As more types of information were procured, precise knowledge of the absolute reactor power was obviously required. Data described above were generally used as relative information. However, data such as those required for shield design were required in absolute terms. Data of this form were received by measuring power distributions throughout the reactor, integrating these distributions over the reactor fueled volume, and determining the average value of this integrated quantity.[2,3] Inasmuch as the distribution functions were in terms of corrected counting rates, this provided the average counting rate per gram of uranium in the reactor. The counting rate per gram of uranium to fission rate per gram was converted by exposing uranium and a catcher foil in a sigma pile, measuring the counting rate in the activation catcher foil, and calculating the fission rate in the uranium from which this counting rate was obtained. This calculation was initially performed in 1954; data obtained at a later date indicated a strong liklihood of a large error. The fission rate in the uranium was calculated again in the early part of 1961, and all data obtained prior to March 1961 and reported in any references on an absolute or per-watt basis had to be divided by 1.38.[4] The only exception to this would be fission rates in portions of the reactor external to the reactor core.

6.2 FISSION POWER MEASUREMENTS

Three primary methods for measuring power, or uranium-sensed neutron flux, were used at GE-ANPD.

Fission fragment catcher foils were utilized on all critical experiment reactors in which the uranium fuel sheets were accessible. This was the case with all metallic fuel element reactors. The foils were precision-punched discs of aluminum with a nominal diameter of 0.5645 inch or, for more detailed distribution studies, 0.25 inch. The foils were exposed in selected locations in intimate contact with uranium whose surface had been reduced of the oxide. During activation in the reactor, fission fragments would be imbedded in the soft 2S aluminum foil in proportion to the fission density near the uranium surface underneath the foil. The decay radiation was then counted in beta-proportional counters with preset time control. Data readout was automatically punched by an IBM 026 keypunch unit to facili-

CONFIDENTIAL

DECLASSIFIED

DECLASSIFIED

tate data reduction on the IBM 704 computer.[1] Decay correction was by an experimentally determined table of values for a 20-minute reactor run and corrected to an average decay time of 50 minutes after shutdown.

When foils could not be used because the metallic fuel was not accessible, long sections of uranium wire were used. The wire had a core consisting of a mixture of uranium, 80 Ni - 20 Cr and vanadium and was clad with 5-mil-thick 80 Ni - 20 Cr. The enriched-uranium content was about 1 gram for each 5 feet of wire. The wires were grouped in batches in accordance with their activity after uniform exposure to a reactor leakage flux in a rotating acrylic-plastic mounting disc. The precision of slug data for single point values was somewhat poorer than for catcher foils; fractional standard deviations for the two methods at 95 percent confidence were 8 and 4 percent, respectively.[5,6] The main difficulty with wire slugs was the nonuniformity of the clad.

A method was developed in which the activity of catcher foils, i.e., relative fission density, was correlated with absolute reactor power level through an empirical conversion factor[4] and through measured power distributions in the reactor to an accuracy of 7 percent.

6.3 FLUX MEASUREMENTS

The usual flux-detector materials, such as gold, indium, copper, and uranium, were used either as foils or wires to measure thermal neutron flux distributions. Cross calibration with the standard flux in the sigma pile provided absolute flux values. The technique of using wire flux detectors was improved by the development of several automatic wire scanners. Two wire scanners were developed in which the activated wire was mounted on a rotating wheel, which moved the wire under a scintillation-crystal detector. One of these scanners had a builtin analog-type decay-correction device in which a special template actuated a high-precision linear resistor, which attenuated the signal in relation to the decay time. Readout on this scanner was on an X-Y recorder. The other rotary wire scanner employed a single-crystal detector with a specially developed shape for high spatial resolution. This wire scanner was designed to work into a multichannel pulse-height analyzer. The mode of operation is as follows. The wire was mounted on the periphery of the wheel. As the wire passed over the crystal, the pulses generated by the crystal and the photomultiplier were fed to an appropriate scaling section of the pulse-height analyzer. The pulse-height analyzer, however, was modified so that it operated as a time analyzer with external gating for the time-channel switching. As the wheel containing the wire was rotated, another disc rigidly mounted to the same shaft would, of course, also turn. A number of small holes were drilled through the disc that served as a light passage between a light source and a phototube. Thus, in essence this disc acted as a light interrupter. The pulses generated by the interruption of the light beam provided the channel switching gates previously referred. Thus, the periphery of the wire would be transformed from spatial coordinates to a time-coordinate system for purposes of data accumulation.[7] Decay correction was thus avoided, and even short-half-life detector materials could be used. Data readout was either by cathode ray tube, strip-chart recorder, paper-tape printer, or IBM 026 card punch.

A tabulated linear carriage in the third wire scanner moved the wire past three equally spaced scintillation crystals, which also had high-resolution shape. The wire was counted incrementally with preset count control. Data readout was again through an IBM 026 on cards.[13]

Experiments were also undertaken to measure fast neutron energy distributions by means of threshold foil response as well as the other methods outlined in section 6.6.2.

DECLASSIFIED

DECLASSIFIED
CONFIDENTIAL

Foil types used were fission foils, such as thorium-232, uranium-238, plutonium-239 and resonance and threshold detectors, such as sulphur-32, bare and cadmium-covered copper, sodium in the form of sodium chloride, and nickel. The foils were counted on beta and gamma scintillation counters. Activations at the critical experiment power levels were satisfactory except those for nickel.[8,9]

The development of measurement techniques tended toward automation and high precision. This was necessitated by the large volume of data associated with the capability of the critical experiment facility for handling four reactors and by the close integration of critical experiment data with the confirmation efforts of reactor-design and analysis methods.

6.4 REACTIVITY MEASUREMENTS

Techniques used for reactivity measurements in the critical experiment work at ANPD were for the most part conventional and straightforward. The methods were primarily (1) positive-period evaluation of a control rod or other reactor components and (2) comparison of differences in positions of the control rods with the reactor critical under varying conditions.

The positive-period method was adopted because of the high concentration of beryllium generally used in ANPD reactors. Negative periods were initially evaluated and were found to be too dependent on power history. Consequently, the positive periods were used almost exclusively for all reactivity measurements. The period could be measured by a slope measurement on a logarithmic power recorder by timing marks between factors of 10 on linear direct-current recorders, or by a rapid-readout scaling system. The last method, which shows promise of being the most precise technique, consists of a fission chamber feeding into an externally gated scaler. With the reactor on a positive period, the scaler would be set up to count for 6 seconds, read out on punched cards in the next 6 seconds, and then initiate the next 6-second counting cycle. The punched cards could then be fed to a computer. The computer would be programmed to compute the slope and evaluate the uncertainty associated with the data.

The above-described methods were, as usual, useful for evaluating reactivity of the order of 0.1 $\Delta k/k$. Because the nuclear mockup is required to have the same amount of reactivity associated with it as was needed for the operation of the reactor, various means of inhibiting this reactivity in the mockup are used. One means might be simply the insertion of control rods to the appropriate depth. This method was useful for evaluating the power distribution of the reactor in the cold, clean condition. However, it was necessary to evaluate the reactor during various phases of the operating cycle. For this purpose uniformly distributed absorber wires were inserted throughout the nuclear mockup to simulate the effects of xenon absorption and fuel depletion. To evaluate the worth of these many pieces of wire, a statistical sampling technique was evolved. This technique consists of establishing the position of the control rods with all the wires in place and the reactor critical. A small randomly selected number of wires would then be removed from the reactor, and the reactivity addition due to this wire removal would be evaluated by restoring the control rods to their previous position at criticality and measuring the period by one of the above methods. The reactivity worth per wire would then be determined. By repetition of this sequence 10 to 15 times, a distribution curve of the average worth per wire was obtained. By subjecting this distribution curve to standard statistical-analysis procedures, one could obtain the extrapolated worth of all the poison wires and the uncertainty associated with this determination. Since the sample was small, the effect of interactions by the wires was not significantly disturbed, and a truer evaluation of the

CONFIDENTIAL
DECLASSIFIED

DECLASSIFIED

effects of these wires on the multiplication constant of the reacting system was consequently possible.

The method of comparing differences in control rod position due to a change in the reactor was in general felt to be accurate within 0.001 percent $\Delta k/k$ if just the reproducibility of the system is considered. Moreover, with reactors containing a high concentration of beryllium a definite correlation appeared in variations between presumably identical reactor configurations and power history. This apparently can only be attributed to a buildup of an external flux contribution due to the (γ, n) reaction in beryllium.

6.5 DOSIMETRY

During the experiments outlined in section 5 many measurements of the biological dose in the vicinity of the reactor were made. The doses measured were due to fast neutrons and penetrating radiation such as gamma rays.

6.5.1 GAMMA DOSE RATE

Two techniques were used for the determination of the radiation levels around the experimental reactors. The first was the use of conventional film badges. The film packets were located at various points along the core axis and along radii about the axis. Conventional development methods and photometric determinations of film darkening were used to convert this information into roentgens per hour per watt of reactor power as a function of various configurations about the reactor. The second method for determining these gamma dose rates the use of air-equivalent carbon-wall ionization chambers. These ionization chambers would drive directly into micro-microammeters, and the data would be obtained in the control rooms.[10,11]

6.5.2 NEUTRON DOSE

Experimental procedures very similar to those for determining gamma dose rates were used for determining fast neutron dose rates.[12] The doses were obtained in units of energy deposition in polyethylene per unit of reactor power. A Hurst-type fast neutron dosimeter was modified for these experiments. The modifications to the dosimeter reduced the sensitivity of the chamber to gamma radiation and thus extended the range of usefulness of the dosimeter. The dosimeter was fed into a Convair-type integrator for rough correlation of energy to dose. In this circuitry counts are accumulated in a manner proportional to the height of the pulse output of the dosimeter. This pulse-output height is proportional to the energy of the proton, which in turn is related to the energy of the incident neutrons. The counts accumulated after a given period of time are proportional to the energy deposition in polyethylene at the experimental points in question. Another method of converting dosimeter response to rate of energy deposition was to feed the dosimeter output into a multichannel pulse-height analyzer that provided a finer resolution of energy distributions. No analyzer data was in turn converted into equivalent polyethylene dose.

6.6 SECONDARY HEATING MEASUREMENTS

Techniques for measuring gamma heating with Bragg-Gray detectors in various reactor materials have been demonstrated and may be considered proved on the basis of performance and comparisons with alternative detection methods.

Theoretically, a Bragg-Gray detector[14,15,16] consists of an infinitestimally small gas-filled cavity in material being heated by the kinetic-energy loss of charged particles tra-

DECLASSIFIED

DECLASSIFIED

versing the region. In the gamma-heating detector the charged particles are betas produced by the gamma interaction processes with matter, as in Compton scattering, pair production, and the photoelectric effect. The amount of heating produced in the chamber material is determined by measuring the amount of ionization produced by the betas in the gas-filled cavity and theoretically relating it to the energy deposition in the surrounding chamber-wall. To simplify the theoretical treatment of the problem, certain restricting conditions must be applied to the chamber design. The main principle to be followed is that the beta energy distribution must be continuous and uniform over the path length of the betas that traverse the gas-filled cavity. A second principle, which is more easily met in practice, is that the primary charged-particle production in the gas-filled cavity must be negligible in comparison to the production in the chamber-wall material. These principles are met in the chamber design by making the wall thickness greater than the range of the beta particles in the material and by making the mean linear cavity dimension very much smaller than the range of the traversing betas in the gas. This second design condition can be experimentally validated by varying the gas density in the cavity while the chamber is in a constant gamma field and noting the linear variation in cavity ionization.

A necessary assumption is that an insulated collecting electrode can be introduced into the gas cavity without violating the basic chamber principles.[17] However, if the principles are violated by the inclusion of the electrode, the effect on the chamber response can be calculated and a correction factor applied. The ionized particles are collected by means of an electric field maintained between the collecting electrode and the chamber wall. The electric field is so arranged that the ions are collected without recombination or multiplication. This is experimentally demonstrated by observing the extent of ion collection as a function of the applied electric field and operating the chamber in the region of saturated ionization.

The Bragg-Gray type of detector has been used for some years as a device for the detection of gamma rays in air and materials that can be considered air-equivalent. The carbon ion chamber and the Victoreen Condenser r-Meter ionization chambers are examples of Bragg-Gray gamma dosimeters in common use. The latter are considered secondary standards, being calibrated against NBS radium. Carbon ion chambers are commonly calibrated against the Victoreen chambers and used for reactor measurements. Instruments of this type are referred to as secondary measuring devices since an experimental calibration is performed against either another secondary standard or a primary standard.

Using the Bragg-Gray type of detector to measure gamma heating in nuclear reactor components is somewhat more complicated than using a simple air or air-equivalent chamber, since reactor components are generally far from air-equivalent. Specialized techniques are required to calibrate the detectors with a standard source, thus allowing them to be used as standard absolute detectors. This admittedly is a complication, since it requires each chamber to be constructed to more rigid specifications than would be the case if the chambers were to measure gamma heating relative to some standard device.

An advantage in using the detectors as standards is the elimination of the experimental error in any calibration. With the recent theory improvements and advances in the design and construction of cavity ionization chambers, it is doubtful that an experimental calibration of a Bragg-Gray detector would make the device more accurate than a chamber operated as a standard.

A useful check on the absolute methods of determining gamma heating is provided by a comparison of calorimetric and ionization measurements made at the same point in the

DECLASSIFIED

DECLASSIFIED

radiation field. In one such comparison[18] the gamma heating in graphite at a point in a beam of cobalt-60 gamma rays was determined first from the rise in temperature of a hollow graphite cylinder and then from the ionization in an air-filled cavity in a similar graphite cylinder at the same location. The two measurements were found to agree within about 3 percent. In another such comparison[19] performed at ORNL, gamma heating was determined using CO_2 in a graphite-walled cavity ionization chamber and a calorimeter that measured the rate of vaporization of liquid nitrogen. The results of the two methods agreed within 3 percent.

That cavity-ionization theory remains valid with materials having higher z numbers than graphite was verified at the Hanford Atomic Products Operation by experiments in which the responses of graphite, aluminum, copper, silver, and lead ionization chambers were experimentally determined with cobalt-60 gamma radiation and were compared with the calculated responses with excellent agreement.[20]

The use of cavity ionization chambers for the measurement of reactor gamma heating has been quite limited. At Knolls Atomic Power Laboratory such chambers of beryllium, aluminum, and steel were used to measure gamma heating in the Preliminary Pile Assembly (PPA) reactor. The results were in reasonable agreement with the simple gamma heating analytical calculations used on the reactor.[21] However, gamma-heating measurements were abandoned when it was decided that for the purposes concerned the analytical methods were adequate. Measurements of gamma heat generation were made in the Engineering Test Reactor[22] (ETR) in 1958 with pedestal- and rod-type calorimeters and carbon ionization chambers (operated as standard detectors). The carbon ionization chambers were determined to be the most useful devices in measuring the gamma heating, and an extensive mapping of the ETR core was performed with apparently excellent agreement with analytically predicted values.

Bragg-Gray chambers were used to measure gamma heating in HTRE No. 3 assemblies in Idaho in order to obtain a comparison with calorimetrically determined nuclear heating rates.[16] In 1958 a Bragg-Gray chamber of hydrided zirconium and calorimeters containing hydrided zirconium sensing slugs were used in the first HTRE No. 3 assembly. The two methods of determining gamma heating rates agreed to within 9 percent with the calorimeters indicating the higher heating rates. Unfortunately, the calorimeter portion of the testing was terminated by a power excursion before the completion of the measurements, and it was necessary to use the distribution of the predicted nuclear heating rate to correct for differences in chamber and calorimeter locations and to subtract from the calorimeters the heating contribution due to the kinetic energy loss of the reactor neutrons. The limit of error in the comparison was consequently larger than the 9 percent discrepancy between the methods of determination.

A second comparison was made late in 1959 in the rebuilt HTRE No. 3 between zirconium Bragg-Gray chambers and hydrided-zirconium calorimeters. The discrepancy between the values from the Bragg-Gray chambers and those from the calorimeters was about 5 percent.

In the first HTRE No. 3 comparison the values of the heating rates measured by the Bragg-Gray chambers and the calorimeters were a factor of about 2.5 higher than the analytically predicted values. However, this is not considered significant since the power excursion prevented a final reactor power calibration by the heat-balance method. In the second HTRE No. 3 comparison the heating rates measured with the Bragg-Gray device were 12 percent higher than the predicted values[23] on the basis of power determined from the heat balance performed on the reactor.

Fabrication of Bragg-Gray detectors from certain materials such as alumina, beryllia, and lithium hydride is difficult. A means of circumventing this problem is to use an alter-

DECLASSIFIED

DECLASSIFIED
CONFIDENTIAL

native detector and calculate a correction factor based upon the theoretical response of the Bragg-Gray detector used and the response of the material in which the gamma-heating measurement is desired. This method was used at Kellogg Radiation Laboratory,[24] where the relative response of Bragg-Gray detectors was calculated as a function of Z number, barrier effectiveness, and gamma energy absorption cross section. The gamma-heating correction factor used was simply the ratio of the barrier-effectiveness values of the wall materials of the chambers. By means of this method a beryllium or aluminum chamber can be used to determine gamma heating in other materials such as lithium hydride or water. Implicit in the conversion from relative cavity ionization to relative gamma energy deposition is the assumption that the Bragg-Gray chamber used is only sensitive to first-collision gamma interactions in its wall material. This is accomplished by a design restriction on the detector that the wall thickness be very much smaller than the mean-free-path length of the gamma radiation. Naturally the design restriction (previously stated) that the chamber wall thickness be greater than the range of the beta particle in the material must also be followed.

In summary, the technology for measuring gamma heating in nuclear reactor components has been adequately demonstrated and substantiated by correlation experiments performed at GE-ANPD and at other facilities.

6.7 SPECTRAL MEASUREMENTS

In several critical experiment assemblies determinations were made of the fast neutron spectrum and the gamma ray spectrum. These data were to be of use in the detailed design of the aircraft shield.

6.7.1 GAMMA SPECTROMETRY

Gamma spectral determinations were made by the use of a sodium iodide thallium-activated crystal. The crystal was 5 inches in diameter by 7 inches long. The photomultiplier was coupled to the crystal by means of a thin lucite cap, and the output was transmitted through a cathode follower into a multichannel pulse-height analyzer. The crystal tube and preamplifier were mounted in a collimator composed of lead, iron, and lucite. The entrance hole was on the crystal axis and was 1/4 inch in diameter. The length of the collimator hole was approximately 20 inches. Crystal responses were calculated by Argonne National Laboratory using their George computer.[25] Experimental response functions at various discrete energies were also determined by means of various sources for the lower-energy gamma rays and the positive-ion Van de Graaf at WADD.[26]

6.7.2 NEUTRON SPECTROMETRY

Fast neutron spectrum data were obtained from the ASM and the KEY facility. Lithium-loaded Ilford emulsion plates were used to obtain the spectrum. By operating the reactor at very low power in order to preclude significant gamma clouding of the film, a number of reaction tracks were produced in the emulsion. These plates were then sent to Convair, Fort Worth Division of General Dynamics Corporation, where track lengths and angles were computed. By the imposition of suitable restrictions on those tracks that were counted, such as angle of track with respect to emulsion surface, a neutron spectrum could be erected. The angular dependence of the reaction track with regard to the incident angle of the neutron was eliminated by this restriction of counter tracks to those of a fairly small angle.[9]

Another promising method of determining neutron spectrum was under development when the work was terminated. The technique involved used a pair of solid-state ionization detectors, surface-junction back-biased silicon diodes on either side of a thin wafer of

CONFIDENTIAL
DECLASSIFIED

DECLASSIFIED

CONFIDENTIAL

lithium-6. Neutrons incident upon this layer of lithium-6 produced the alpha-particle reaction, or track, and tritium. These particles would then be totally absorbed in the ionization chambers on either side of the wafer. By summing these pulses and subtracting reaction energy value, the energy of the incident neutron could be determined.[27]

6.8 NONFISSION NEUTRON HEATING

During the operation of the KEY assembly, described in section 5.1, one item of information desired was the reaction rate of neutrons in the borated sections of the reactor assembly. Consequently, measurements were made using two detectors to determine this rate. One detector was simply a miniaturized BF_3 counter that was moved through appropriate places in the assembly to provide a reaction density-distribution curve. The other technique was similar to that described in section 6.6 for neutron spectroscopy. However, one solid-state detector would be used with the junction faced by a layer of boron. Approximately one-half the reaction products from the interaction of boron-10 with the neutrons would produce ionizing particles incident on the detector. If this detector were coupled to suitable pulse-counting electronic equipment, the counting rate would be proportional to the reaction rate in the boron facing the detector. One difficulty apparent in this technique was that most silicon diodes produced for this purpose appear to have a small amount of boron in them, presumably as doping. The reaction of this boron is identical to that of the purposely superimposed layer. Moreover, the pulse height distribution from these internal boron reaction rates was different than that from the external boron reaction rates. Consequently, it became difficult to separate the two reactions and to provide information as to what the true boron reaction-rate distribution was.

6.9 NUCLEAR TEST GAGE

The procurement of materials to go into or near a nuclear reactor core presents special problems inherent with the need for low-nuclear-cross-section materials. Often the vendor is not equipped to make analyses of the quality desired. When such analyses are obtained, they are usually expensive and time consuming, and the test sample is destroyed. The need to avoid these disadvantages suggested the building of the Nuclear Test Gage (NTG).

The NTG is a subcritical assembly consisting of a core containing fully enriched uranium and moderated and reflected by acrylic plastic. The fuel-bearing volume is cylindrical, 24 inches in diameter and 24 inches long. It contains 4.2 kilograms of uranium-235 in the form of uranium foil approximately 93 percent enriched. A 6-inch-diameter sample hole extends longitudinally through the unit, although normally this hole is plugged in the end-reflector region, and only a 2-inch hole penetrates the plug.

The NTG is loaded in a configuration calculated to achieve a flat neutron-flux profile across the exact center of the core in order that the scattering cross section of the sample and minor variations in its location shall have a minimum effect. It is somewhat more important to have a reasonable length of flattened flux longitudinally than radially since the sample carrier mechanism precludes the possibility of significant radial sample shift. Neutron flux profiles, both radial and longitudinal, were measured with indium foils. The longitudinal flux was measured along the center of the sample hole, but the radial flux map, not easily obtained from the NTG, was measured in a mockup assembly installed in a hexagonal-matrix critical experiment facility. This full-scale mockup provided a means of checking safety features in addition to a final check of the design.

CONFIDENTIAL
DECLASSIFIED

DECLASSIFIED

Four 0.25-curie radium-beryllium sources are equally spaced around and inserted into the fueled annulus. Surrounding the cylindrical fueled volume on the side and both ends is a 6-inch layer of acrylic plastic to act as reflector. The assembly has a multiplication of approximately 70 and a thermal flux in the center of the sample hole of about 5×10^4 n/cm^2 -sec.

Samples inserted into the sample hole have an effect on the multiplication of the assembly. The amount and sign of the change depends on any of a number of variables, e.g., the amount of material, its neutron cross section, and the fuel loading. The resultant small change in neutron level is measured with sensitive instrumentation connected to the equivalent of four gamma-compensated ionization chambers. The detectors actually consist of eight separate ionization chambers connected so that the current from the four that are sensitive only to gamma radiation will compensate the others and only the neutron flux is measured. In addition, three separate channels, two neutron- and one gamma-sensitive, are used in a scram system connected to boron-bearing safety sheets at either end of the active core. These sheets, which effectively separate the end reflectors from the fueled core, are held out of the assembly against the forces of gravity and a compressed spring by electromagnets in a typical safety-actuator design. The scram system protects against the unlikely possibility that the assembly attains criticality because of the insertion of a sample.

DECLASSIFIED

DECLASSIFIED

6.10 REFERENCES

1. Beene, J. L., and Bermanis, H. L., "A Nuclear Data Reduction System," Transactions of the American Nuclear Society, Vol. 2, No. 1, 13-6, June 1959.
2. Bermanis, H. L., and Link, B. W., "ASM Measurements Report No. 2," GE-ANPD, DC 59-7-181, July 1959.
3. Baumgardt, N. R., "Critical Experiment Stage Average Calculations," GE-ANPD, DC 58-11-41, November 1958.
4. Bermanis, H. L., " A Method for the Absolute Power Calibration of Nuclear Reactors," GE-ANPD, DC 61-7-34, June 1961.
5. Bermanis, H. L., "A Discussion of the Precision of Relative Power Measurements in the D103A Mockup," GE-ANPD, DC 59-12-84, December 1959.
6. Andrews, J. L., "Precision of Relative Power Measurements in the D140E-1 Mockup (SIC-II)," GE-ANPD, DC 61-6-6, June 1961.
7. Beene, J. L., et al., "High-Speed Wire Scanner," GE-ANPD, DC 61-6-12, May 1961.
8. Brooks, E. H., and Milburn, E. L., "Measurement of Foil Activation Rates in the SIC-II-2 Critical Assembly," GE-ANPD, DC 61-2-51, February 1961.
9. Brooks, E. H., and Milburn, E. L., "Shielding Measurements about the SSR," GE-ANPD, DC 61-2-3, January 1961.
10. Brooks, E. H., "Gamma Dose Rate Measurements for the ASM-I," GE-ANPD, DC 59-2-18, February 1959.
11. Brooks, E. H., and Mikelson, D. L., "ASM-1 Gamma Dose Rate Measurements," GE-ANPD, DC 59-2-29, February 1959.
12. Brooks, E. H., "Measurements of Fast Neutron Dose Rates," GE-ANPD, XDC 58-3-176, March 1958.
13. Beene, J. L., "Digital Type Radioactive Wire Scanner," GE-ANPD, DC 61-6-2, April 1961.
14. Bragg, W. H., Studies in Radioactivity, The Macmillan Co., London, 1912, p 94 et seq.
15. Gray, L. H., "The Absorption of Penetrating Radiation," Proc. Roy. Soc. A122, 1929, 647-688.
16. Gray, L. H., "An Ionization Method for the Absolute Measurement of α-ray Energy," Proc. Roy. Soc. A156, 1936, 578-596.
17. Lawrence, G. C., "The Measurement of Extra-Hard X-Rays and Gamma Rays in Roentgens," Can. J. Research 15A, No. 5, 1937, 67-78.
18. Bernier, J. B., Skarsgard, L. D., Cormack, D. V., and Johns, H. E., Radiation Research 5, 1956, 613.
19. Jenks, H. G., Breezeale, W. M., and Hairston, J. J., Oak Ridge National Laboratory, ORNL-923, January 1959.
20. Myers, I. T., "An Ionization Chamber Method for Absolute Gamma Ray Dose Measurements," Hanford Atomic Products Operation, HW-29732, October 1953.
21. Stehn, J. R., "The Physics of Intermediate Spectrum Reactors," Naval Reactors Branch, Division of Reactor Development, USAEC, 1958, p 23-3.
22. Hogg, C. H., Weber, L. D., and Echo, M. W., Phillips Petroleum Company, IDO-16519, April 1959.
23. Keppler, J. G., "Calculated Secondary Heat Generation in the D102A Reactor," GE-ANPD, DC 58-8-191, August 1958.
24. Fowler, W. A., Lauritsen, C. C., and Lauritsen, T., Rev. Mod. Phys. 20, 1948, 236.
25. Brooks, E. H., "Calculated Response Functions of Gamma Ray Spectrometer," GE-ANPD, DC 60-12-26, November 1960.

DECLASSIFIED

DECLASSIFIED

CONFIDENTIAL

26. Brooks, E. H., "Experimental Response Functions of a Gamma Ray Spectrometer," GE-ANPD, DC 61-1-54, January 1961.
27. Baum, J. J., "Development of a Fast Neutron Spectrometer Using Silicon Surface Barrier Diodes," APEX-639, August 1961.

CONFIDENTIAL

DECLASSIFIED

DECLASSIFIED

DECLASSIFIED

DECLASSIFIED

CONFIDENTIAL

PART 2 - SHIELD PHYSICS

7. INTRODUCTION

The design of a highly efficient aircraft reactor-shield system involves a series of complicated nuclear problems that are inseparable from the over-all design of both the power plant and the aircraft. The nuclear problems associated with the shield fall into two broad categories: (1) the optimum placement of shield materials to reduce the radiation levels in all important regions to acceptable levels consistent with the best compromise between minimizing the weight and maximizing the power plant thrust-to-weight ratio, and (2) the calculation of specific nuclear data, such as nuclear heating and activation, that will allow power plant designers to achieve an efficient, safe design which can be easily maintained. Problems in both categories require highly accurate calculations to determine the total flux and the angle and energy distribution of the neutrons and gamma rays, at any position within and in the vicinity of the reactor-shield assembly.

The shielding technology available from stationary and marine nuclear reactor development efforts was not adequate for the solution of the problems associated with aircraft shield design. Accordingly, the ANP Department conducted an extensive shield-physics program in order to develop the necessary shielding technology. This effort resulted in the development of a variety of shield nuclear-analysis methods and computer programs for use in the ANP program. Development of reactor-shield analysis methods was emphasized, but because it is not possible to design an optimum aircraft reactor-shield system without simultaneous consideration of the air-scattering and crew-shield penetration problems, some effort was also devoted to these problems. The development work emphasized a high degree of integration of experiments and theory. Major accomplishments in both these areas are summarized in this volume.

The status of the shielding technology can be briefly summarized as follows: solution of the nuclear problems had progressed to the point where a shield system could be designed for an aircraft near the size of a heavy bomber. Shield design improvements were most likely to take the form of more efficient ways of combining and distributing shield materials and in reducing the weight of supporting structures.

Experiments have demonstrated the validity and versatility of the shield technology developed for ANP application. These experiments were conducted at the Battelle Memorial Institute, the Nuclear Aircraft Research Facility operated by Convair, the Oak Ridge National Laboratory and the Shield Test Pool Facility at the General Electric Idaho Test Station. In the theoretical shield physics area, the Nuclear Development Corporation of America made many key theoretical contributions. In fact, a combination of their efforts and the shield-physics effort at GE-ANPD provided most of the technology applied in the design of shields for the various power plant designs.

Specific applications are described in other volumes devoted to descriptions of the individual power plants. The closely related development of shield materials is discussed in APEX-915.

CONFIDENTIAL

DECLASSIFIED

DECLASSIFIED

Most of the ANP shielding technology can be usefully applied in the analysis and design of any nuclear radiation shield. Many of the computer codes developed here, especially the point kernel and single-scattering codes, have already been used extensively on numerous other nuclear energy projects; and some of the Monte Carlo codes, which have been developed recently, are being distributed to other installations.

DECLASSIFIED

DECLASSIFIED
CONFIDENTIAL

8. SHIELD DESIGN CONSIDERATIONS

Stationary nuclear power plants typically have shield weights many times greater than the weights of the heaviest bombers. Even in marine propulsion applications, shield weights greater than the total weights of heavy bombers can be tolerated. Thus, providing adequate shielding for aircraft applications consistent with high performance and with sufficiently low weight has long been recognized as a task many times more difficult than that for other applications.

The design of a highly efficient aircraft reactor-shield system involves a series of complicated nuclear problems which are inseparable from the over-all design of both the power plant and the aircraft. (See APEX-908 for a discussion of shield design as applied to a specific, high performance power plant.) These problems must be solved with greater sophistication than has been necessary in the design of shields for stationary or marine reactors.

The individual nuclear problems associated with an aircraft shield fall into two broad categories: (1) the optimum placement of shield materials to reduce the radiation levels in all important regions to acceptable levels consistent with the best compromise between minimizing the weight and maximizing the power plant thrust-to-weight ratio, and (2) the calculation of specific nuclear data, such as nuclear heating and activation, that will allow power plant designers to achieve an efficient, safe design which can be easily maintained. Problems in both categories require highly accurate calculation of several important nuclear quantities:

1. Heating rates due to absorption of nuclear radiation at all points within the reactor-shield assembly.
2. Activation of power plant components, both within the basic reactor-shield assembly and external to the reactor-shield assembly.
3. Radiation quantities required for evaluating radiation damage to power plant components and materials.
4. Activation of aircraft materials.
5. Radiation quantities required for evaluating radiation damage to aircraft components and materials.
6. Biological dose rates, both internal and external to the crew compartment.

The calculation of these quantities requires a capability for determining the nuclear environment at all points, e.g., within the reactor-shield assembly, external to the reactor-shield assembly, and within the crew-shield assembly. It must be possible to determine the total flux and the angle and energy distribution of the neutrons and gamma rays as well as the response of any detector used to measure the effect of the radiation.

8.1 INTEGRATED SHIELD DESIGN

The primary function of an aircraft shield system is, of course, to provide protection from the radiation emitted from the reactor. The first consideration is usually given the

CONFIDENTIAL

DECLASSIFIED

DECLASSIFIED

flight crew which must be protected from biological damage during flight operations. In order to achieve minimum weight, a divided-shield system was conceived with the crew shield being the prime responsibility of the airframe manufacturer and the reactor shield the responsibility of the power plant manufacturer. In arriving at the radiation constraints, the protection of aircraft components from radiation damage and excessive induced activation must be considered.

The reactor shield usually also provides some protection of the ground handling and maintenance crews even though it may not have been specifically designed to do so.

Once a shield is provided for these functions, it must also perform other functions which make it compatible with the power plant. For example, for a direct-cycle power plant, it must provide for transmission of the working air. It must also provide for the penetration of control rods, and turbomachinery shafts.

Since it operates at fairly elevated temperatures, the problem of providing a sound structure to hold the shield together at a minimum weight is a challenging one. Structural weights are high partly because of uncertainty in predicting nuclear heating of the shield. Use of compressor-air to cool the shield clearly causes a loss in thrust. If ram air is used as the coolant, the coolant passages become large and radiation leakage out of the channels increases. Also, the fact that some of the shield material is necessarily moved out to a larger radius results in more weight for the same attenuation.

Thus, it was imperative that the nuclear design of the aircraft reactor shield be integrated closely with all the other phases of the over-all power plant design, and with the over-all airframe design.

8.2 DIVIDED SHIELD

Adequate radiation protection of the flight crew and aircraft components can be provided in one of three ways: (1) by distributing enough shielding around the reactor so that everything outside the reactor-shield assembly is protected, (2) by distributing all of the shielding around the areas or components requiring protection, or (3) by dividing the shielding between the reactor-shield assembly and the areas or components that require protection. The method of shielding chosen greatly affects the total shield system weight and the power plant performance. The method chosen should maximize power plant performance within the radiation level constraints established for each application. These may apply to either the operating conditions, after-shutdown conditions, or both.

For a high-speed bomber application, a divided-shield concept promises the highest performance. The division of the shield is determined by the radiation constraints; dimensions of the aircraft, crew compartment, and reactor, and the nuclear and physical properties of the shield materials. At least enough shielding is placed around the reactor to prevent excessive induced-activation and radiation damage of aircraft and power plant components. The remainder of the shielding required to limit the crew dose rate is divided between the crew shield and reactor shield so that maximum performance is achieved.

The crew dose rates are established by the mission requirements. Radiation constraints external to the reactor-shield assembly are established mutually by the power plant and airframe manufacturers. The constraints can vary depending upon maintenance procedures established, components chosen, and the placement of these components relative to operating life established. There is, of course, a trade-off between over-all operating performance and the maintenance factors. This is particularly true in the air-cycle system since the amount of shielding placed around the reactor affects the thrust as well as the over-all weight.

DECLASSIFIED

DECLASSIFIED

8.3 DUCTING SYSTEMS

Efficient transmission of the working air from the compressor through the shield to the reactor and from the reactor through the shield to the turbine is especially difficult because of conflicting requirements. The ducts should be as straight and large as possible to minimize pressure loss, but they should be as small and tortuous as possible to minimize radiation leakage. Naturally each design must be the result of compromise.

Several designs were considered. Annular ducts with multiple bends probably received the most attention, although various porous shield plugs were studied seriously. Among the latter were: (1) wavy-wall plugs, in which the air flowed between corrugated plates of the shield material, (2) assemblies of struts with streamlined cross sections, (3) alternate assemblies of rods of shield material and tube sheets of shield materials, (4) assemblies of hexagonal shield pieces with helical air passages machined the full length around each hexagonal piece, (5) assemblies of serpentine tubes with shield material located between the tubes, and (6) plugs with many parallel straight air passages of small diameter. All of these were analyzed for possible application, and mockups of most were tested in various reactor and source plate facilities.

8.4 ITERATIVE DESIGN PROCEDURE

All nuclear design of shields was accomplished by iterative design procedures. No computer programs were developed for direct determination of shield requirements to satisfy specified radiation constraints.

The iterative design procedure that was usually followed starts with establishing a complete description of the source. In addition to defining all physical dimensions, calculations are made using reactor analysis methods and programs to establish the spatial and energy distribution of neutron and gamma ray sources throughout the reactor assembly. Secondary gamma rays from thermal neutron capture are included.

Next, approximate thicknesses of the selected shield materials are established by perturbation of a previous design, by calculations using the comparison method described in section 9.1, or by interpolating from a family of curves of fast neutron and gamma ray dose rate as a function of neutron and gamma shield material thicknesses. Curves of this type are prepared using the point kernel methods described in section 9.2.

A shield is then sketched around the reactor assembly with these approximate thicknesses, and dose rates are computed for positions around the shield using point kernel programs. Comparison of the computed dose rates with specified dose rates allows perturbation of the first approximate shield. With experience, only a few iterations of this type are necessary to achieve the desired radiation-leakage pattern.

The effects of secondary gamma rays generated in the shield are determined by using a combination of point kernel and multigroup diffusion programs to establish secondary sources throughout the shield. Point kernal programs are used in turn to compute the dose rate outside the shield due to these secondary sources. The spacing of neutron and gamma shield materials and the proper location of strong neutron absorbers to limit secondary effects are established by iterative calculations of this type.

Air-scattered contributions to dose rates outside the shield are determined by using point kernel results as input to single-scattering programs. Other single-scattering programs are used to compute dose rates inside specified crew shields. If a crew shield needs to be designed, this also is done by iteration.

DECLASSIFIED

DECLASSIFIED

No single document describes all the methods, computer programs, and nuclear data used for shield nuclear analysis at ANPD in recent years. However, individual topical reports cover all these areas. They will be referenced throughout this report. Earlier methods are described fully in the literature,[1] as are the early computer programs,[2] and the fundamentals of shield physics.[3]

DECLASSIFIED

DECLASSIFIED

8.5 REFERENCES

1. Carver, J. G., Edwards, W. E., and MacDonald, J. E., "GE-ANPD Methods of Shield Design," GE-ANPD, APEX-230, December 30, 1955.
2. Capo, M. A., "Shielding Computer Programs," GE-ANPD, APEX-387, October 29, 1957.
3. Haffner, J. W., and Aschenbrenner, F. A., "Nuclear Radiation Shielding," GE-ANPD, DC 57-1-65, January 15, 1957.

DECLASSIFIED

DECLASSIFIED

DECLASSIFIED

DECLASSIFIED

9. THEORETICAL SHIELD PHYSICS AND COMPUTER PROGRAMS

Summary descriptions of the methods and computer programs developed at the GE-ANP Department for nuclear analysis of aircraft shield systems are described in this section.

A comparison method, which applied water-centerline data from the Bulk Shielding Facility (BSF), was used for most reactor-shield calculations prior to 1955. It is still used occasionally for quick estimates. Since 1955, however, various digital computer programs have been used singly and in combination for most calculations.

Essentially, two generations of computer programs, for use with the IBM 704 or 7090, were developed here for shield nuclear analysis. Programs of the first generation are based on phenomenological or empirical methods. These programs were used extensively for analysis and iterative design of aircraft shields. Second-generation programs, coded and checked for coding errors, all apply Monte Carlo methods. Although these programs have not been used extensively for design purposes, it is believed that their validity and versatility will be limited only by the availability of adequate basic nuclear data.

The discussion of these methods begins with a brief description of the comparison method. This is followed by discussions of point kernel, combined point kernel multigroup diffusion, single-scattering, duct analysis, and two-component methods and programs. Finally, specialized reactor-shield, flexible, and air-scattering Monte Carlo codes are described.

During the last year of the ANP program, an investigation of Program S-VII (ANP Program 414)[1] for shielding calculations, was begun. Program S-VII is a one-dimensional transport theory code which constructs neutron and photon transport-theory solutions having plane, cylindrical, or spherical geometry. It represents an extension of ideas originated by B. G. Carlson in the Los Alamos SN neutron codes. This investigation showed that for studies in which the many limitations are not too severe, S-VII is a valuable tool for shielding calculations. A description of this investigation was published.[2]

9.1 COMPARISON METHODS

A comparison method may be used for determining, by iterative hand calculation, first trial thicknesses of materials required to shield against neutrons and gamma rays emitted by a reactor during operation. The method essentially corrects empirical data for differences in source strength, source distribution, source leakage characteristics, source-receiver distance, and materials separating the source and receiver.

Although the comparison method could be used to apply empirical radiation penetration data from any experiment or theoretical calculation, it has been applied most frequently

DECLASSIFIED

DECLASSIFIED

to water-centerline data from the Bulk Shielding Reactor (BSR). The basic equation for applying these data to the computation of dose rates[3] is as follows:

$$D(\rho) = D_{BSR}(t) \left(\frac{t + d_{BSR}}{\rho + d_{design}}\right)^2 \left(\frac{L_{design}}{L_{BSR}}\right) P_{design} \exp \sum_i \left(\frac{t_i}{\lambda_{H_2O}} - \frac{t}{\lambda_i}\right) \quad (1)$$

where $D(\rho)$ = direct-beam dose rate
$D_{BSR}(t)$ = BSR dose rate at water thickness t per watt of power
t = total shield thickness, cm
ρ = distance from design-reactor surface to receiver point, cm
d = small distance correction to account for source depth, cm
L = total leakage rate per watt of reactor power
t_i = normal thickness of material i, cm
λ_i = relaxation length in material i, cm
P_{design} = power of design reactor, watts

The term $(t + d_{BSR}/\rho + d_{design})^2$ is a geometrical correction factor which is really composed of two parts, $(t + d_{BSR}/\rho + d_{BSR})^2$ and $(\rho + d_{BSR}/\rho + d_{design})^2$. The first of these corrects the dose rate measured in the BSF at distance t to that dose rate corresponding to a distance ρ from the BSR surface, and the latter corrects for the fact that the theoretical center of radiation is shifted in going from the BSR core to a core having a different geometry and self-absorption coefficient. The terms d_{BSR} and d_{design} represent the distances from the reactor surfaces to the theoretical centers of radiation in the BSR and design reactors, respectively. They form a small correction and can usually be neglected without serious error.

Leakage factors and effective source depths for the BSR were computed and reported for both fast neutrons and gamma rays.[3,4]

The comparison method is subject to considerable error when the design and experimental sources differ greatly or when a large portion of the experimental shield material is replaced by other materials. The results of calculations involving comparison of cylindrical or spherical and slab shields are also open to question and require additional complex corrections.

9.2 POINT KERNEL METHOD

A method of shield analysis which is versatile and reasonably accurate for the calculation of neutron and gamma ray energy spectra and dose and energy-absorption rates in and around reactor shields combines the use of point-to-point attenuation functions with integration over source regions. This method is readily adapted to digital computer solution. Consequently, the method can be used to perform quick shield analyses.

Since neither neutrons nor gamma rays arriving at a receiver from separate sources interact appreciably, this method can be assumed to be correct if the point-to-point attenuation functions are known accurately. However, a point-to-point attenuation function, in general, is a complicated functional which is defined along all possible paths for the particle between the source and receiver points. This functional can only be approximated in any actual situation.

It may be assumed, to a reasonably good approximation, that the point-to-point attenuation function depends only on the quantity of each material encountered by the primary ray proceeding from the source point directly to the receiver point. A point-to-point attenuation function, based on this assumption, can be expressed as a function of the

DECLASSIFIED

DECLASSIFIED

source-receiver path length, ρ, the path length, ρ_m, in each of the M materials, the source energy, E_j, the detector energy, E, and the macroscopic cross section, $\Sigma_m(E_j)$, as follows:

$$\Phi = \Phi\left[\Sigma_1(E_j), \ \ldots, \ \Sigma_M(E_j), \ \rho_1, \ \ldots, \ \rho_M, \rho, E_j, E\right] \tag{2}$$

Henceforth, this function will be written as $\Phi = \Phi[\Sigma_m(E_j), \rho_m, \rho, E_j, E]$ and called a point kernel. $\Phi[\Sigma_m(E_j), \rho_m, \rho, E_j, E]$ equals the flux of particles of energy E at the receiver, due to particles of energy E_j emitted by a point source of unit strength.

If it is assumed that the point source emits isotropically, the point kernel can be written as the product of a material attenuation function $\Psi[\Sigma_m(E_j), \rho_m, E_j, E]$ and a geometrical attenuation function $1/4\pi\rho^2$, i.e.,

$$\Phi[\Sigma_m(E_j), \rho_m, \rho, E_j, E] = \frac{\Psi[\Sigma_m(E_j), \rho_m, E_j, E]}{4\pi\rho^2} \tag{3}$$

Material attenuation functions can be established by fitting attenuation data obtained by either theoretical or experimental methods. The functions may be either purely mathematical or based on some physical analysis.

The response of an isotropic point detector to particles of energy E from a small element of volume dV_S is

$$dD(E) = \frac{S(\vec{\rho}_S, E_j)\, \Psi[\Sigma_m(E_j), \rho_m, E_j, E]\, dV_S\, dE_j}{4\pi\rho^2} \tag{4}$$

where $S(\vec{\rho}_S, E_j)\, dE_j$ is the source density at position $\vec{\rho}_S$ for particles of energy E_j in range dE_j. The calculated detector response will obviously be in units determined by the units of the source, material attenuation function, and spatial dimensions. Integrating the above equation over the source energy spectrum and the source volume yields the following equation for the total detector response at energy E:

$$D(E) = \int_{\substack{\text{source} \\ \text{energy} \\ \text{spectrum}}} \int_{\substack{\text{source} \\ \text{volume}}} \frac{S(\vec{\rho}_S, E_j)\, \Psi[\Sigma_m(E_j)\, \rho_m, E_j, E]\, dV_S\, dE_j}{4\pi\rho^2} \tag{5}$$

9.2.1 DIGITAL COMPUTER POINT KERNEL PROGRAMS

Several point kernel programs were developed at GE-ANPD for calculating neutron and gamma ray penetration of source-shield assemblies. Shielding Computer Programs 14-0, 14-1, and 14-2[5,6] are the latest in this series; and, with one exception, they provide equal or greater capability than all the previous point kernel programs. They all evaluate point kernels and integrate over source regions to compute neutron and gamma ray fluxes and dose and energy-absorption rates for positions in and around complex source-shield configurations. In addition, the programs can compute shield weight. An earlier code,[7] Program 04-4, contains one unique option for summing computed dose rates from an assembly of isotropic point sources. Since this option was seldom used, the 14-series of programs essentially replaced 04-4 for all new problems. Therefore, only the 14-series programs will be described in this summary report.

Enough physical and source-description capability is provided by these programs so that nuclear analysis of source-shield assemblies containing sources described in either a cylindrical or rectangular coordinate system should involve little uncertainty except that associated with the point kernels and secondary-source distributions. The programs

DECLASSIFIED

DECLASSIFIED

are comprised of numerous subroutines to facilitate any possible future modifications. They are available for use on either an IBM 704 or 7090 having 32,768 magnetic core memory locations. Magnetic tape units are used for the production package and output. Input may be either on cards or tape. No magnetic drum memory is required.

Reactor and shield geometries are described in these programs by combinations of regions formed by rotation of rectangles and trapezoids about the source-shield axis or parallel axes or by translation of convex quadrilaterals parallel to any axis of the rectangular coordinate system. Compositions are expressed as volume fractions for each material in the source-shield assembly and are associated with the appropriate geometrical regions by code numbers.

Programs 14-0 and 14-1 can be used for shields containing multiple sources described in a cylindrical coordinate system. Source-region integration limits are specified for each of as many as six source types, and location dimensions are specified for the axis of each of a possible 200 source regions. Source-region nodal points (source points) are located by intersection of axial lines in shells concentric about the source-region axes and planes normal to the axes. The provisions for spacing these lines, shells, and planes permit description of cylindrical volume, cylindrical or plane surface, axial or radial line, or point sources. A different source-point spacing is permitted for each source type.

Source-density distributions must be the same for neutrons and gamma rays in both programs. Source-density distributions must be identical in all regions of a given type, but they may differ in the different source types. Gamma ray source energy spectra are assumed independent of position, but they too may differ in the different source types.

Source-density distributions are assumed independent of angular position in both programs. They are assumed separable along the axis and radius of regions of each source type in Program 14-0, and they may be described by either cosine or exponential functions. The functions may differ in as many as four ranges along either the axis or radius of a source region. The source density must be specified as input in Program 14-1 for each ring of source points in each different source type.

Program 14-2 can be used for shields containing sources described in a rectangular coordinate system. Integration limits, which are specified for each space variable, may be equal for any or all variables. Planes of source points may be equally or unequally spaced between the integration limits of each space variable. Consequently, rectangular parallelepiped volume, rectangular plane surface, line, or point sources may be described.

Source-density distributions, which must be identical for neutrons and gamma rays, are assumed to be nonseparable. They must be continuous over x, but they may be discontinuous over Y and Z. A table of source densities is required as input data. Gamma ray source energy spectra are assumed independent of position.

9.2.1.1 Fast Neutron Dose Rate

A modification of a material attenuation function suggested by R. D. Albert and T. A. Welton[8,9,10] is used for computing fast neutron dose rates from fission sources in mixtures of hydrogenous and heavy shield materials. This theory combines a theoretical hydrogen cross section with integration over the fission neutron spectrum to obtain the uncollided flux as a function of penetration distance into the shield medium. The attenuation effects of materials other than hydrogen are included by assuming exponential attenuation and treating the cross section as energy-independent adjustable parameters to be determined by the "best fit" to experimental data. This treatment is

DECLASSIFIED

DECLASSIFIED

based on the assumption that all heavy materials are followed by sufficient hydrogenous material so that the use of effective removal cross sections is valid. The material attenuation function used in these programs for fast neutrons is

$$\Psi_n(\Sigma_m, \rho_m) = \alpha_1\left(\sum_{m=1}^{L} \eta_m \rho_m\right)^{\alpha_2} \exp\left[-\alpha_3\left(\sum_{m=1}^{L} \eta_m \rho_m\right)^{\alpha_4}\right] \exp\left(-\sum_{m=1}^{M} \rho_m \Sigma_m\right) \qquad (6)$$

where α_1, α_2, α_3, and α_4 are constants and η_m is the ratio of the hydrogen density in material m to that in water. Consequently, this function accounts for attenuation in hydrogen contained in as many as L hydrogenous materials. The hydrogenous materials must be among the first L materials. This equation is not energy-dependent since the method of obtaining the function results in an integration over the fission neutron energy spectrum. The dose rate is that due to neutrons of all energies detected by sensors to obtain the experimental data used to adjust the coefficients.

Since the Albert-Welton function cannot be used for small thicknesses of hydrogenous material, these programs switch to an alternate exponential function for thicknesses ranging from zero to the minimum thickness for which the Albert-Welton function is valid. Thus,

$$\Psi_n(\Sigma_m, \rho_m) = \alpha_5 \exp\left[-\alpha_7\left(\sum_{m=1}^{L} \eta_m \rho_m\right)\right] \exp\left(-\sum_{m=1}^{M} \Sigma_m \rho_m\right) \qquad (7)$$

when $\sum_{m=1}^{L} \eta_m \rho_m < \alpha_6$ which is entered as an output quantity.

Coefficients used in the Albert-Welton function and this exponential function are presented in section 10.2.

The following equation is used in Program 14-0 for integration over individual cylindrical source regions, summation over all source regions of a single type, and final summation over all source region types to compute fast neutron dose rates:

$$D_n = \frac{C}{4\pi} \sum_{t=1}^{T} \sum_{s(t)=1}^{S(t)} \int_{Z_{s1}}^{Z_{su}} S(Z_S, t)\,dZ_S \int_{r_{s1}}^{r_{su}} r_S S(r_S, t)\,dr_S \int_{\varphi_{sl}}^{\varphi_{su}} \frac{\Psi_n(\Sigma_m, \rho_m)}{\rho^2}\,d\varphi_S \qquad (8)$$

Z_{sl}, Z_{su}, r_{sl}, r_{su}, ϕ_{sl}, and ϕ_{su} are lower and upper limits of integration respectively on the source region space coordinates Z_S, r_S, and ϕ_S. The constant C is used as a multiplying factor when symmetry occurs and integration is performed over only part of a source volume. The source function is assumed independent of ϕ_S and separable in Z_S and r_S. Since the material attenuation function is energy-independent, the source function and the dose rate equation are also energy-independent.

The integrations indicated in the preceding equation are performed by the trapezoidal method when the number of source points between the integration limits for a variable ≥ 2. No integration is performed over a variable if only one source point is used for that variable. If $\phi_{sl} = \phi_{su}$, r_S is eliminated from the integration over r_S. If $r_{sl} = 0$ and $r_{su} \neq 0$,

$$r_S\, S(r_S, t) \int \frac{\Psi_n(\Sigma_m, \rho_m)}{\rho^2}\,d\phi_S \underset{=}{\text{set}} 0 \text{ at } r_S = 0$$

and $\Psi_n(\Sigma_m, \rho_m)/\rho^2$ is not computed for these points.

DECLASSIFIED

DECLASSIFIED

Similar equations are solved in the other point kernel programs for computation of fast neutron dose rates.

9.2.1.2 Gamma Ray Dose Rate

The material attenuation function used in these programs for computing gamma ray flux and dose and energy absorption rates is

$$\Psi_\gamma[\Sigma_m(E_j), \rho_m] = B\,[\Sigma_m(E_j), \rho_m] \exp\left[\sum_{m=1}^{M} \rho_m \Sigma_m(E_j)\right] \tag{9}$$

where $B[\Sigma_m(E_j), \rho_m]$ is a buildup factor used to determine empirically the scattered contributions to the computed detector response. Uncollided contributions of each discrete energy source are determined correctly by the exponential function. The buildup factors used were obtained by a moments method solution of the Boltzmann transport equation at the Nuclear Development Corporation of America. Further discussion of these factors is presented in section 10.3.

Three optional methods are provided in these programs for computing $B[\Sigma_m(E_j), \rho_m]$. Buildup in a single infinite homogeneous medium is computed by two equations in an option called the short form:

$$B[\Sigma_m(E_j), \rho_m] = \beta_0(E_j) + \beta_1(E_j)X(E_j) + \beta_2(E_j)X(E_j)^2 + \beta_3(E_j)X(E_j)^3 \tag{10}$$

$$X(E_j) = \sum_{m=1}^{M} \rho_m \Sigma_m(E_j) \tag{11}$$

Actual shields can seldom be considered infinite or homogeneous. Shields usually are composed of layers of light and heavy materials. Empirical expressions for computing buildup factors for lead-water and iron-water combinations were established by Monte Carlo techniques by the Nuclear Development Corporation of America.[11] Actually, the expressions were determined for plane sources, but it is assumed that the same functional forms hold for point sources. Also, it is assumed that the expressions are suitable for other material combinations where the attenuation properties are similar to those of iron, lead, and water.

The buildup factor for the case of lead or iron followed by water is computed by the following long form equation:

Long Form 1

$$B[\Sigma_m(E_j), \rho_m] = B_2(X_2) + \left[\frac{B_1(X_1)-1}{B_2(X_1)-1}\right]\left[B_2(X_1 + X_2) - B_2(X_2)\right] \tag{12}$$

where X_1 = thickness of first material encountered (lead or iron) in terms of number of relaxation lengths.

B_1 = buildup factor for first material encountered.

X_2, B_2 = corresponding quantities for second material encountered (water).

The buildup factor for the case of water followed by lead or iron is computed by the following long form equation:

Long Form 2

$$B[\Sigma_m(E_j), \rho_m] = B_2(X_2) + \left[\left(\frac{B_1(X_1)-1}{B_2(X_1)-1}\right)\exp C_2X_2 + \frac{(\mu_{cs}/\mu_t)_1}{(\mu_{cs}/\mu_t)_2}\,(1-\exp C_3X_2)\right] \cdot \left[B_2(X_1 + X_2) - B_2(X_2)\right] \tag{13}$$

DECLASSIFIED

DECLASSIFIED

where μ_{cs} = attenuation coefficient for Compton scattering in the material.
μ_t = total attenuation coefficient for the material.

Other symbols have the same definition as in the previous equation except that the first material encountered is now water.

Buildup factors are computed from the cubic polynomial:

$$B_p(X_p) = {}_p\beta_0(E_j) + {}_p\beta_1(E_j)X_p + {}_p\beta_2(E_j)X_p^2 + \beta_3(E_j)X_p^3 \tag{14}$$

where p equals 1 or 2 and refers to the first or second material encountered. The number of relaxation lengths of the p^{th} material encountered is represented by X_p.

If ${}_1\beta_0$ and ${}_2\beta_0$ equal 1.0, either expression for the combined buildup factor becomes indeterminate when X_1 equals zero. The programs are coded so that $B[\Sigma_m(E_j), \rho_m]$ reduces to $B_2(X_2)$ in either case.

It may be necessary, for shields containing more than two materials, to consider the sum of the relaxation lengths of several similar materials as first and second materials encountered. This is accomplished by application of the following equation:

$$X_p(E_j) = \sum_{m=1}^{M} {}_p\tau_m \rho_m \Sigma_m(E_j) \tag{15}$$

where ${}_p\tau_m$ is a screening constant and is either 0 or 1 depending on whether material m is to be recognized as the p^{th} material encountered.

Cubic polynomial coefficients currently available for the computation of gamma ray buildup factors are not valid for greater than 20 relaxation lengths for light materials or 15 relaxation lengths for heavy materials. Consequently, these programs are coded to make the following checks and substitutions:

1. Short Form

   If $X(E_j) > 20$, $X(E_j) \overset{\text{set}}{=} 20.$

2. Long Form 1

   If $X_1(E_j) > 15$, $X_1(E_j) \overset{\text{set}}{=} 15$, and if $X_2(E_j) > 20$, $X_2(E_j) \overset{\text{set}}{=} 20.$

3. Long Form 2

   If $X_1(E_j) > 20$, $X_1(E_j) \overset{\text{set}}{=} 20$, and if $X_2(E_j) > 15$, $X_2(E_j) \overset{\text{set}}{=} 15.$

The number of substitutions is included in the output for each receiver point.

Although these substitutions are not desirable, they may be less serious than extrapolation beyond the valid range of the polynomials. If a substitution is required for only an occasional source point, the effect should be negligible.

The following equation is used in Program 14-0 for integration over individual cylindrical source regions, summation over all source regions of a single type, summation over source-region types, and final summation over source energies to compute gamma ray flux and dose and energy-absorption rates

$$D_\tau = \sum_{j=1}^{J} \frac{C}{4\pi} \sum_{t=1}^{T} \sum_{s(t)=1}^{S(t)} K(E_j)\, \Gamma(E_j, t) \int_{Z_{sl}}^{Z_{su}} S(Z_s, t)\, dZ_s \int_{r_{sl}}^{r_{su}} r_s S(r_s, t)\, dr_s \int_{\varphi_{sl}}^{\varphi_{su}} \frac{\Psi_\gamma[\Sigma_m(E_j), \rho_m]}{\rho^2} d\varphi_s \tag{16}$$

DECLASSIFIED

DECLASSIFIED

$\Gamma(E_j, t)$ is a source intensity term for each source energy and each source region type. $K(E_j)$ is a conversion factor for converting from flux due to photons of source energy E_j to any desired units. The flux or dose rate is computed and printed for each source energy. Finally, the total flux or dose rate is computed and printed. Integration is performed as discussed previously.

Similar equations are used in the other programs for computing gamma ray flux and dose and energy-absorption rates.

9.2.1.3 Neutron Spectra

The material attenuation function used in these programs for computing differential neutron number flux is

$$\Psi_n(E_n, \rho_m) = \exp \sum_{k=0}^{K} \left[\sum_{i=0}^{I} b_{ki}(p) \, (X_p)^i \right] (E_n)^k \tag{17}$$

where E_n is the scattered neutron energy and X_p is the effective material thickness. The coefficients, $b_{ki}(p)$, of the bivariant polynomial can be obtained by fitting the natural logarithms of differential neutron number spectra computed by moments method solution of the Boltzmann transport equation. Differential number spectra are available for point U^{235} fission neutron sources in several infinite homogeneous media. Limited data are available for discrete-energy neutron sources.

A set of coefficients, $b_{ki}(p)$, may be specified in input for each of two ranges of energy E_n for each of three possible materials. A maximum of 20 values of E_n are allowed as input. Maximum valid E_n's for the lower energy sets of coefficients also must be specified as input.

The effective material thickness is computed for each value of p from

$$X_p = \sum_{m=1}^{M} {}_p\nu_m \rho_m \tag{18}$$

where ${}_p\nu_m$ is an effective factor. It is necessary that ${}_p\nu_m$ be an effective material density if X_p is required in gm/cm^2. The largest X_p is used in the computation of the differential number flux. Also, the polynomial coefficients are used for that value of p which gives the largest X_p.

Since differential spectra are currently not available for thicknesses greater than 120

DECLASSIFIED

In addition to printing results from these equations, the programs are coded to compute and print normalized differential neutron number fluxes if fast neutron dose rates are requested in the same problem. The normalization is carried out as follows:

$$\text{Normalized } I_o(E_n) = \frac{I_o(E_n)\, D_n}{\int_{E_1}^{E_n} K(E_n)\, I_o(E_n)\, d\, E_n} \tag{20}$$

when $K(E_n)$ is a specified conversion factor, and the integration is performed by the trapezoidal method.

9.2.1.4 Gamma Ray Energy Spectra

The material attenuation function used in these programs for computing the gamma energy flux in the energy interval $E_q \leq E \leq E_{q+1}$ is

$$\Psi_\gamma(E_q \leq E \leq E_{q+1},\ \rho_m) = \left(\sum_{\substack{\text{All } E_j \\ \geq E_q}} \Gamma(E_j, t) \left\{ \sum_{v=0}^{V} \left[\sum_{u=0}^{U} A_{vu}(E_j, m)\, X(E_j)^u \right] E_q{}^v \right\} \exp -X(E_j) \right.$$

$$\left. + \sum_{\substack{\text{All } E_j \\ \geq E_{q+1}}} \Gamma(E_j, t) \left\{ \sum_{v=0}^{V} \left[\sum_{u=0}^{U} A_{vu}(E_j, m)\, X(E_j)^u \right] (E_{q+1})^v \right\} \exp -X(E_j) \right) \frac{(E_{q+1} - E_q)}{2}$$

$$+ \sum_{\substack{\text{All } E_q \\ < E_j \leq \\ E_{q+1}}} \Gamma(E_j, t)\, E_j \exp -X(E_j) \tag{21}$$

where the first part gives the scattered gamma ray energy flux and the second part gives the uncollided energy flux due to gamma rays originating with energies between E_q and E_{q+1}. The first and second parts of the expression for the scattered gamma ray energy flux give the differential scattered gamma ray energy flux at energies E_q and E_{q+1}, respectively. The final term of the expression for the scattered gamma ray energy flux represents a trapezoidal integration over the energy interval. $\Gamma(E_j, t)$ is the source intensity term that was defined earlier. $X(E_j)$ is the shield thickness in relaxation lengths and is given by

$$X(E_j) = \sum_{m=1}^{M} \Sigma_m(E_j)\, \rho_m \tag{22}$$

which is identical with that used in the short form for the gamma ray dose rate.

The coefficients, $A_{vu}(E_j, m)$, of the bivariant polynomial can be obtained by fitting differential scattered gamma ray energy spectra computed by moments method solution of the Boltzmann transport equation. Differential scattered gamma ray energy spectra are available for several discrete-energy sources in many infinite homogeneous media.

A set of coefficients, $A_{vu}(E_j, m)$, may be specified in input for each of two energy ranges for each of three possible materials. Maximum valid energies for the lower energy sets of coefficients must be included in input. Material numbers of the materials for which coefficients are specified also must be included in input. The coefficients used for a source-receiver path are those for the material, for which coefficients are specified, which has the greatest ρ_m for that path.

DECLASSIFIED

DECLASSIFIED

Since differential scattered gamma ray energy spectra are currently not available for material thicknesses greater than 20 relaxation lengths, these programs are coded to set $X(E_j)$ equal to 20 if a larger value is computed. The reasons for this substitution are the same as those discussed previously. The number of substitutions is included in the output for each receiver point.

The following equation is used in Program 14-0 for integration over individual cylindrical source regions, summation over all source regions of a single type, and final summation over all source region types to compute the gamma ray energy flux in the energy interval $E_q \leq E \leq E_{q+1}$:

$$I_o(E_q \leq E \leq E_{q+1}) = \frac{C}{4\pi} \sum_{t=1}^{T} \sum_{s(t)=1}^{S(t)} \int_{Z_{sl}}^{Z_{su}} S(Z_s, t)\, dZ_s \int_{r_{sl}}^{r_{su}} r_s S(r_s, t)\, dr_s \int_{\varphi_{sl}}^{\varphi_{su}} \frac{\Psi_\gamma(E_q \leq E \leq E_{q+1}, \rho_m)}{\rho^2}\, d\varphi_s , \tag{23}$$

and similar equations are used in the other programs.

The programs compute and print $I_o(E_q \leq E \leq E_{q+1})$ for $1 \leq q \leq Q$ where $Q \leq 20$. $Q+1$ detector energies must be included in input. If gamma ray dose rates are requested in the same problem, the programs also compute and print the following normalized energy fluxes:

$$\text{Normalized } I_o(E_q \leq E \leq E_{q+1}) = \frac{I_o(E_q \leq E \leq E_{q+1})\, D_\gamma}{\sum_{q=1}^{Q} K(E_q)\, I_o(E_q < E < E_{q+1})} \tag{24}$$

9.2.1.5 Calculation Procedure

The general calculation procedure in Program 14-0 is as follows:

1. The total source-receiver distance and the distance through each material are calculated for the source point located at the lower integration limits of all three space coordinates.
2. Each desired attenuation function is evaluated for the computed total and material distances. Those functions which are energy dependent are evaluated for each source energy.
3. Operations 1 and 2 are repeated for source points at successively larger values of azimuthal angle until all the functions have been evaluated for all values of the azimuthal angle and the lower integration limits of the radius and length.
4. A trapezoidal integration over azimuthal angle is performed for each of the attenuation functions.
5. Operations 1, 2, 3, and 4 are repeated for successively larger radii until integrals over azimuthal angle are obtained for each function and each radius at the lower limit of the length variable.
6. Each integral over azimuthal angle is multiplied by the appropriate radius and radial source density, and a trapezoidal integration over the radius is performed for each attenuation function.
7. All previous operations are repeated for successively larger values of the length until double integrals over azimuthal angle and radius are obtained for each value of the length variable.
8. Each double integral is multiplied by the appropriate axial source density, and a trapezoidal integration over the length is performed for each attenuation function.
9. The triple integrals are multiplied by any appropriate conversion factor and source intensities.

DECLASSIFIED

DECLASSIFIED

10. The preceding procedure is repeated for all source regions and source types.
11. Summations over source regions, types, and energies are performed, and the results are multiplied by a symmetry factor to achieve the desired detector responses.

The procedure in Program 14-1 is slightly different since a source density is entered in input for each ring of source points. Except for integration over a rectangular coordinate system, the procedure in Program 14-2 is also similar.

9.2.1.6 Limitations of Programs

The material attenuation functions used in these programs are primarily infinite-media functions. The use of an infinite-medium attenuation function has the effect of surrounding the source and receiver points with an infinite medium of the same composition as the shielding which lies along the source-receiver path. The constants used in the function are those determined for such an infinite-medium case and include the effects of scattering to the receiver from all regions in the medium. The density of each material in this medium is determined effectively by distributing the intervening shield material uniformly over the total distance between the source and receiver points. Consequently, a shield-air boundary (assuming air outside the shield) may cause the actual detector-response to be substantially different from that computed, assuming an infinite homogeneous medium.

The effect of the shield-air boundary is simplest for the case of a receiver point on the shield surface. Here the calculation of a detector response includes scattering to the receiver from regions of the medium which are outside the shield boundary and which do not exist in the real situation. The densities of the materials in the medium will obviously be the same in the calculation as in the actual shield since the entire source-receiver path is filled with shielding material. The shield-air boundary has the effect of removing part of the material assumed to be present in the calculation. The material removed is from regions which do not affect the direct-beam attenuation but can only act to increase the computed detector response through scattering. Hence, attenuation calculations for this case will yield a detector response which is too high.

The same effect is present for a receiver point located in air at some distance from the shield-air boundary. Here, however, other effects occur as a consequence of the "smearing out" of the shield material into a uniform distribution along the source-receiver path and the subsequent use of the resulting reduced densities in the inifinite medium which is assumed for the calculation. The attenuation calculations will predict fewer scatterings than will actually occur in the regions filled by the actual shield; and it will predict, for such scatterings, an attenuation which is too high because the calculation assumes some material in the regions actually occupied by air space. Both of these effects tend to make the calculated detector response too low. It is not possible to determine, for the general case, whether the net result of all these effects is to make the calculated detector response too high or too low.

The above discussion relates the effect of the finite extent of the shield on a detector-response prediction by the point kernel method. Inhomogeneous regions in the shield may present even more serious difficulties to the method. Obviously, the greater the difference in the attenuation characteristics of the various regions of inhomogeneity, the greater the uncertainty in using homogeneous attenuation functions. Attenuation calculations for paths through highly-attenuating regions bordered by poorly attenuating regions are likely to yield low answers because of scattering (short circuiting) around the highly-attenuating regions. This effect is observed behind shadow shields and in regions adjacent to large void coolant passages which penetrate the shield.

Calculations for paths through poorly attenuating regions bordered by highly attenuating regions are likely to yield high answers since calculated scattered contributions from the

DECLASSIFIED

DECLASSIFIED

adjacent regions may be much greater than actual contributions. Since equal thicknesses of most shield and structural materials attenuate neutrons at approximately the same rate, regions of inhomogeneity (except for voids) are not expected to seriously affect neutron dose rate calculations. Similar gamma ray calculations are subject to more doubt. This effect is observed along source-receiver paths which penetrate large void coolant passages or which penetrate weak shield regions adjacent to shadow shields. The effect was clearly observed in analyses of experiments performed in the General Electric Outside Test Tank. Uncollided calculations gave more nearly correct results in some of the measured configurations.

The Albert-Welton function is restricted to hydrogenous media or to shields in which non-hydrogenous materials are backed with sufficient thickness of hydrogenous materials to validate the use of the function. The function has frequently been used when the last material was not hydrogenous. Tests in the Outside Test Tank have indicated that the order in which some material combinations are penetrated does not seriously affect the penetration of the materials.

Additional uncertainty is associated with gamma ray calculations involving more than two layers of materials. Also, the gamma ray attenuation functions do not account for secondary gamma ray generation in shields. Secondary gamma ray sources must be treated separately.

The attenuation functions coded in these programs for computing neutron and gamma ray spectra are expected to be reasonably accurate for infinite homogeneous media. Since few spectra computed by these methods for finite heterogeneous shields have been compared with experimental spectra, little is known about their validity for such shields. Nevertheless, the methods are included for development purposes.

Numerous cases of acceptable agreement between calculated and measured fast neutron and gamma ray dose rates in pool and source-plate facility experiments and outside reactor shields have been achieved. See section 11.3 and references 12, 13, 14, and 15 for typical comparisons.

9.2.1.7 Input Data Check

A special program[16] (Program 14-3) was prepared to check input data to the other programs of the series. Experience proved this program to be a valuable accessory, since many problems for this series of programs require vast amounts of input data and long running times.

9.2.2 PROPOSED ALTERNATE POINT KERNELS

Several alternate point kernels were proposed and studied for possible application to neutron-penetration calculations. Each would require relatively minor modification of the point kernels already programmed. Some were proposed to make fast neutron dose rate calculations more rigorous and accurate, and others were proposed to provide greater versatility in addition to better accuracy.

The ethylene neutron single-collison response function[17] was fitted by

$$R = 2.69 \times 10^{-5} - \exp\left[-0.38245\,(E + 27.8)\right] \frac{\text{rads/hr}}{\text{n/cm}^2\text{-hr}} \qquad (25)$$

and incorporated in a modification of the Albert-Welton function. In this modification, the theoretical hydrogen cross section was reduced so that only scattering outside a certain narrow cone[10] results in removal from the beam. Derivation of the modified function and comparisons with experiments were published.[18] It is shown that reasonable agreement with experiment can be achieved without the usual adjustment of the coefficients to fit experimental data.

DECLASSIFIED

DECLASSIFIED

Three methods of calculating fast neutron dose rates were compared and the results published.[19] The methods applied are: (1) the Albert-Welton function fitted to fast neutron dose rate data, (2) neutron buildup factors in conjunction with exponential attenuation, and (3) a polynomial approximation to fast neutron dose rate data. All are based on a curve of fast neutron dose rate as function of depth in hyrogen which was obtained at the Nuclear Development Corporation of America by a moments method solution of the Boltzmann transport equation.

The polynomial function is quite similar to the one described previously for computation of neutron spectra. In fact, the function coded in the 14-series program can easily be reduced to that used in the referenced study.[19] It is simply

$$f(X) = \exp \sum_{i=0}^{3} a_i X^i + \epsilon_i(X) \qquad (26)$$

where X is the penetration distance.

It was concluded from this study and a later one,[9] that the polynomial function offers several attractive advantages. It is easier to fit to basic penetration data; it can even be fitted at zero penetration. It can be used for media other than hydrogen, and it can be used to compute responses other than dose rates. It offers the possibility of combining several of the functions in describing fast neutron attenuation through a combination of materials. It has the disadvantage that it cannot be extrapolated safely.

A recent Monte Carlo study[20] of neutron penetration in lithium hydride from a monoenergetic, point source resulted in a proposed plan for parametric neutron penetration calculations and modification of the polynomial functions coded in the 14-series programs for neutron spectra calculation. The proposed program modification would permit a flexible source description by combining monoenergetic sources. The proposed parametric calculations would provide data which could be fitted by the polynomial functions for efficient application to design or analysis. Of course, such data should be verified by experiment as much as possible.

9.3 COMBINED POINT KERNEL-MULTIGROUP DIFFUSION METHOD

Program G-2, a multi-energy diffusion code, was extended for use in reactor-shield assemblies. Combined with a method for normalizing the G-2 flux, the program will compute the neutron spectrum and integrate any known response function over the spectrum at specified points. Thus, the technique may be used to determine important quantities such as neutron heating rate, activation rate, and secondary gamma sources. The methods for normalization include point-to-point normalization to calculated fast-neutron dose rates, normalization to the power level of the fission source, and using the uncollided flux from the fission source to calculate a distributed source strength throughout the shield. Comparisons with measured values indicate that no one method of normalization always gives the best results. Thus, care must be exercised when applying the program to various situations.

9.3.1 DIFFUSION THEORY USED IN PROGRAM G-2

Assuming that there is no energy loss in the non-isotropic portion of the scattering cross section, the one-dimensional diffusion equation can be shown to be a P_1 approximation to the Boltzmann transport equation.[21] Since laboratory coordinates (not center-of-mass coordinates) are used in the transport equation, the requirements for no energy loss for non-isotropic scattering are rather severe. Also, the P_1 approximation does not include the transients which extend several mean free paths on each side of a boundary.

DECLASSIFIED

DECLASSIFIED

The one-space-variable diffusion equation used in Program G-2 has the form

$$-\frac{1}{r^{\alpha}}\frac{d}{dr}\left(r^{\alpha} D_n \frac{d\varphi_n}{dr}\right)+\left(\Sigma_{a,n} + D_n K_{\perp,n}^2\right)\varphi_n = S_n F - \left(\frac{\partial q}{\partial u}\right)_n \quad (27)$$

where

- u is the lethargy
- n is the lethargy level
- D_n is the diffusion coefficient
- φ_n is the flux
- $\Sigma_{u,n}$ is the absorption cross section
- $K_{\perp,n}^2$ is the perpendicular buckling which is used to estimate the perpendicular losses
- q is the slowing down density
- $S_n F = S_n \int \nu/k\, \Sigma_f \varphi du$ is the fission source.

The term α in the diffusion equation has the value 0, 1, or 2 for slab, cylindrical, or spherical geometry.

A relationship between flux and slowing-down density may be estimated by using a slowing-down model. Either the modified age or Coveyou-Macauley slowing-down model may be used in Program G-2. Discussions of the slowing-down models were published.[21] For the modified age model one obtains

$$q_n + \left(\frac{\partial q}{\partial u}\right)_n = \xi \Sigma_{s,n} \varphi_n \quad (28)$$

where

- ξ is average logarithmic energy decrement and
- $\Sigma_{s,n}$ is the scattering cross section

The Coveyou-Macauly model gives

$$\frac{q_n}{\xi} + \left(\frac{\partial q}{\partial u}\right)_n = \Sigma_{s,n}\, \varphi_n. \quad (29)$$

The value of $(\partial q/\partial u)_n$, determined by one of the above equations, may be substituted in the diffusion equation. For the modified-age slowing-down model, this gives

$$\frac{1}{r^{\alpha}}\frac{d}{dr}\left(r^{\alpha} D_n \frac{d\varphi_n}{dr}\right)+\left(\Sigma_{a,n} + D_n K_{\perp,n}^2 + \xi\Sigma_{s,n}\right)\varphi = q_n + S_n F \quad (30)$$

Integrating equation (28) trapezoidally yields

$$q_n = \frac{(q_{n-1})[1 - (u_n - u_{n-1})/2] + [(u_n - u_{n-1})/2]\,(\xi \Sigma_{s,n}\phi_n + \xi \Sigma_{s,n-1}\phi_{n-1})}{1 + (u_n - u_{n-1})/2} \quad (31)$$

Substituting this value of q_n in equation (30) gives, for modified age theory, the diffusion equation

$$-\frac{1}{r^{\alpha}}\frac{1}{dr}\left(r^{\alpha} D_n \frac{d\phi_n}{dr}\right) + A_n \phi_n = S_n^* \quad (32)$$

where

$$A_n = \Sigma_{a,n} + D_n K_{\perp}^2 + \frac{\xi \Sigma_{s,n}}{1+(u_n - u_{n-1})/2} \quad (33)$$

and

$$S_n^* = S_n F + \frac{(q_{n-1})\,[1 - (u_n - u_{n-1})/2] + [(u_n - u_{n-1})/2]\,(\xi \Sigma_{s,n-1}\phi_{n-1})}{1 + (u_n - u_{n-1})/2} \quad (34)$$

DECLASSIFIED

DECLASSIFIED

The following technique is used to solve the multilevel diffusion equations. The source spectrum at lethargy level 0 is taken as zero. Thus, $q_0(r)$ and $\varphi_0(r)$ are zero. An initial power density, F(r), of unity is assumed at each lattice point. From these values equation (34) is used to determine S_1^*. The diffusion equation (32) is then solved for φ_1 using finite difference approximations[22] subject to given albedo conditions at the right and left hand boundaries. The slowing-down density q_1 can be found from equation (31). F, φ_1, and q_1 may be used to calculate S_2^* using equation (34), and ϕ_2 and q_2 are computed from equations (31) and (32). After the fluxes at each lethargy level are calculated, F is computed by a trapezoidal integration over lethargy.

A trapezoidal integration over the volume (in one dimension) is completed to give the reactivity. If the criteria for convergence on reactivity and power density are not met, F is normalized to an integrated value of unity by dividing by the reactivity and the new value of F is used to go through the next iteration.

9.3.2 DESCRIPTION AND USE OF PROGRAM G-2

Program G-2 is a multi-region, multi-energy, one-dimensional diffusion computer program. The program has a lethargy lattice of 19 levels and a thermal group. Fifty compositions, each composed of 16 materials, are allowed in a system of as many as 50 regions and 100 lattice points. The output may include any desired quantity (e.g., fast-neutron dose rate, subcadmium activation, and thermal-neutron flux) for which the response functions are known. A description of the original program[21] and the information required for applying the program to shielding calculations[22] were published.

The program will handle slab, cylindrical, or spherical geometry. The receiver points, however, in all cases must lie on a single straight line. Since the program is one-dimensional, the perpendicular neutron losses must be estimated. In order to determine these losses, the curvature of the flux for each lethargy level (perpendicular buckling) must be approximated. The perpendicular buckling may be entered into the program for each lethargy level or estimated by the program from the geometry of the configuration. In the latter case, it is assumed that the flux goes to zero at the extrapolated boundary. This assumption may give a poor approximation if the configuration is surrounded by a scattering medium.

If the configuration consists of water, Be, BeO, or LiH, the neutron spectrum part of Program 14-0[23] may be used to estimate the perpendicular buckling. In this case, the neutron spectrum is calculated at receiver points on the axis at the mid-point of each region and at four points equally spaced on a circle whose center lies on the axis and whose plane is perpendicular to the axis. Symmetry, however, may reduce the number of required points. A discussion of this technique, which was applied to a BeO slab array, was published.[24]

The term in the diffusion equation which represents the gain of neutrons due to slowing down from higher energies is determined by a slowing-down model. Either the Coveyou-Macauley or modified age model may be used. The Coveyou-Macauley model is recommended for light non-absorbing nuclei in a region where the perpendicular losses are small. The modified age model is recommended otherwise.[22]

The nuclear data for Program G-2 are contained on a nuclear data tape in the form of individual records for each element, compound, mixture, and spectrum. Tape data came largely from AECU-2040 and BNL 250. Where BNL 325 data were noted to differ markedly from earlier data, the original values on the IBM tape were revised. The nuclear data and formulae were published.[25,26,27] The technique for modifying the data on the tape was published.[28]

DECLASSIFIED

DECLASSIFIED

In applying Program G-2 to nuclear radiation shielding problems, the G-2 calculations can be normalized to the fast-neutron dose rates determined by Program 14-0.[23] Using the Hurst response[29] and the G-2 spectrum, the program calculates the fast-neutron dose rates at the specified lattice points. The ratio of the 14-0 dose rates to the G-2 dose rates is used to normalize the diffusion results. Thus, the point kernel approximation (Program 14-0) is used to obtain the spatial distribution, and the diffusion approximation is used to obtain the energy distribution of the neutrons. A discussion of this technique was published.[22]

The G-2 flux may also be normalized to the power level of the source. In this case, the diffusion approximation also determines the spatial distribution. The application of this method to a source plate was published.[24]

In addition to the above methods, the uncollided flux per unit lethargy may be used to calculate sources along the axis of the shield configuration. Program 14-0 may be used to calculate the uncollided fluxes. In this case, total neutron cross sections are used in place of gamma ray absorbtion coefficients. By choosing regions sufficiently small, the source strength as a function of lethargy calculated at the center of a region may be considered constant along the axis within the region. The fixed sources are entered into Program G-2, and the fluxes are normalized to the sources. A discussion of this method was published.[24]

Program G-2 was originally programmed for the IBM 704 computer. This version, however, has been converted to run on the IBM 7090. When the conversion was made a few minor improvements were incorporated. A discussion of the IBM 7090 version was published.[30]

9.3.3 COMPARISON OF G-2 CALCULATIONS WITH MEASUREMENTS

Thermal-neutron flux traverses measured at the Lid Tank Shielding Facility were compared with calculated traverses using Program G-2. The comparisons included traverses in water, oil, and in water and in oil behind 1, 2, 3, and 4 inches of stainless steel. The G-2 fluxes were normalized to calculated fast-neutron dose rates at each point. Agreement between measured and calculated values was in the neighborhood of a factor of two. The details of the calculations and the graphs showing the comparisons were published.[31]

Additional calculations using Program G-2 were published.[32] These calculations were made in several of the slab arrays used in the Outside Test Tank located at Convair in Fort Worth. A comparison with measured sulfur activation indicated that point-to-point normalization to fast-neutron dose rates gave better results than normalization to a single fast-neutron dose rate. The effects of lattice point spacing, different slowing down models, and homogeneous materials were studied.

Program G-2 was used to calculate the water centerline thermal-neutron flux traverse measured at the GE-ANPD Source Plate Facility located at the Battelle Memorial Institute.[33] The G-2 fluxes were normalized point-to-point to the calculated first-neutron dose rates. The comparison is shown in Figure 9.1.

A number of calculations were compared with measured thermal-neutron fluxes within BeO and in water behind various thicknesses of BeO.[24] The measured data were obtained at the GE-ANPD Source Plate Facility. The modified age model and the Coveyou-Macauley model were used to calculate the centerline thermal-neutron flux traverse through 21 inches of BeO. All three techniques for normalizing the G-2 flux were used. Normalization to measured fast-neutron dose rates gave poor results indicating that the slowing-down models are not adequate for the higher energy levels in BeO. However, normalization to power and use of the uncollidated flux to calculate distributed sources gave values agreeing with measured values within a factor of two. The comparisons for the Coveyou-Macauley model are shown in Figure 9.2. In water behind the BeO, power normalization gave better agree-

DECLASSIFIED

DECLASSIFIED

CONFIDENTIAL

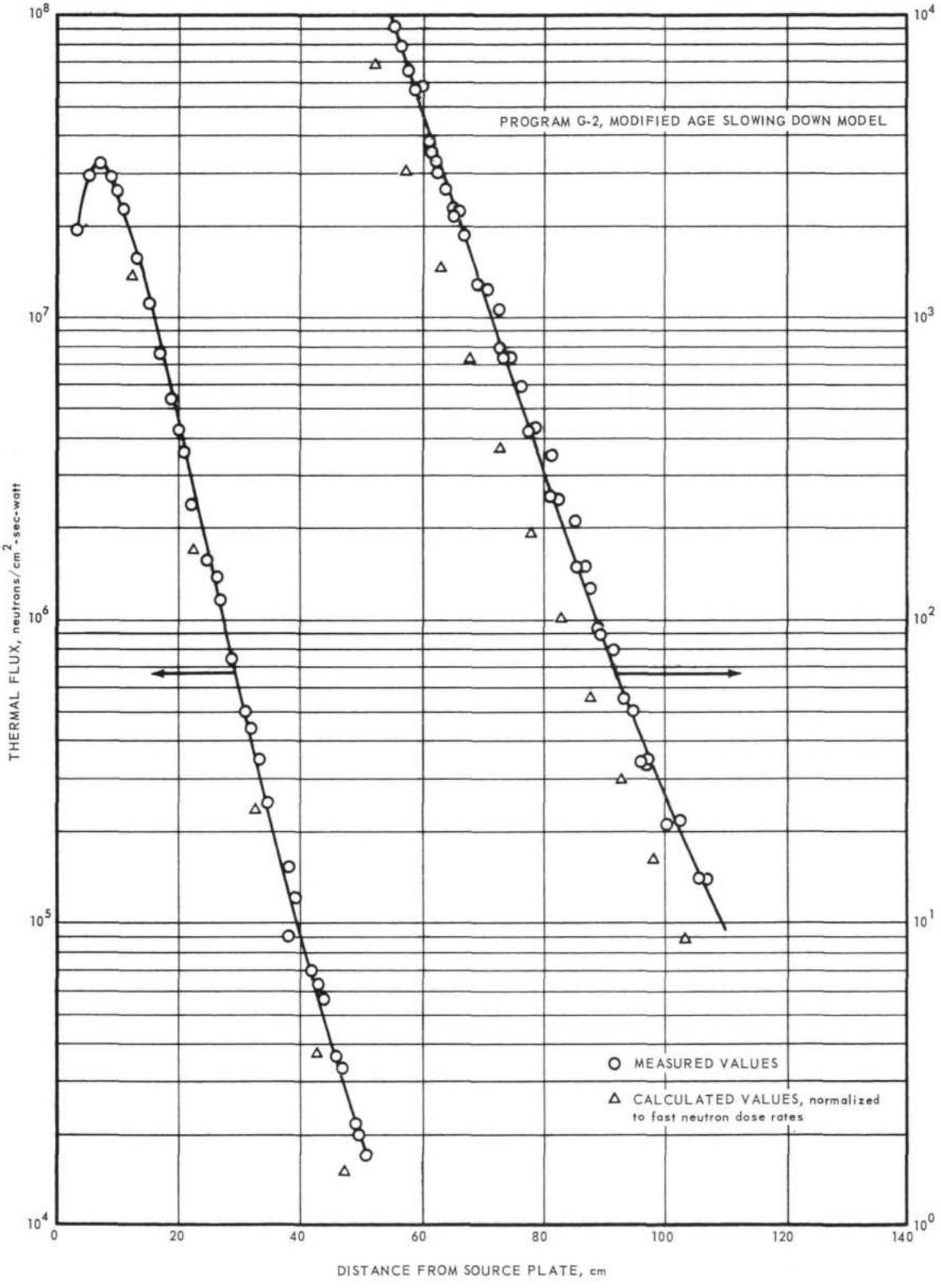

Fig. 9.1 – Comparison of measured and calculated thermal fluxes in water

CONFIDENTIAL

DECLASSIFIED

DECLASSIFIED

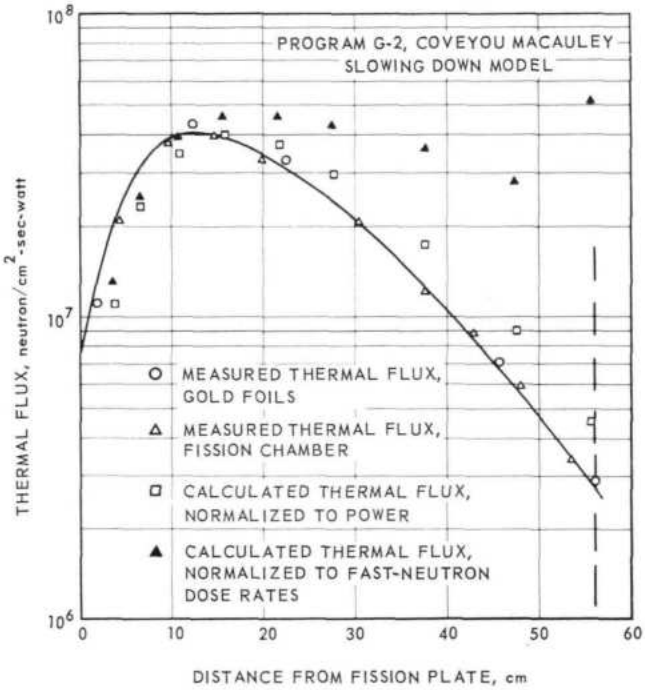

Fig. 9.2 – Comparison of measured and calculated thermal fluxes within 21 inches of beryllium oxide

ment near the BeO-water interface, but normalization to measured fast-neutron dose rates gave better agreement as the penetration in water increased. A comparison with sulfur activation measured within BeO indicated that normalization to fast-neutron dose rates gave the better results.

Similar calculations were made for beryllium slab arrays in the shielding tank at the GE-ANPD Source Plate Facility.[34] Normalization to fast-neutron dose rates gave poor results for thermal-neutron flux and resonance foil activation traverses within beryllium. A comparison between measured and calculated thermal-neutron flux traverses is shown in Figure 9.3. Similar results were obtained for resonance foil activation traverses. Again, normalization to source plate power gives the better results.

The comparisons with experimental data indicate that no one technique can be used for all situations. The successful use of the program requires experience and good judgment.

9.4 SINGLE SCATTERING METHOD

Significant amounts of radiation may leak from the reactor-shield assembly of a divided shield system. It is necessary, therefore, to determine radiation levels in the vicinity of the power plant and at the crew position in order to evaluate the effect of such radiation on the ground handling problem, the extent of radiation damage and activation of various aircraft components, and the total mission dose received by the crew.

Two radiation components are usually distinguished in determining radiation effects at points external to the reactor-shield assembly: a direct-beam component due to radiation which has not undergone any air scattering, and a scattered component due to radiation which has suffered one or more scatterings in air.

DECLASSIFIED

DECLASSIFIED

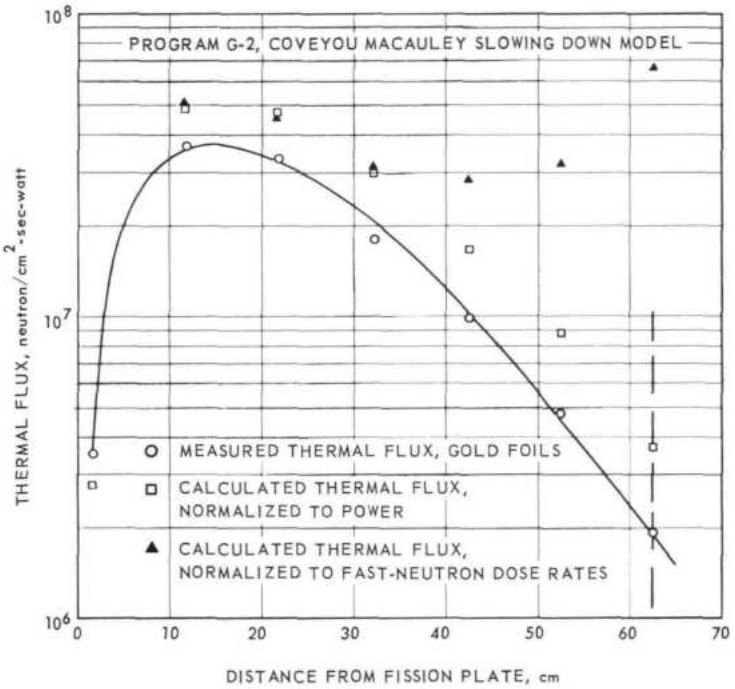

Fig. 9.3 – Comparison of measured and calculated thermal fluxes within 24 inches of beryllium

Many situations of interest can be adequately treated by considering only the direct-beam component and the single-scattered portion of the scattered component. This section describes methods for computing the first or single-scattered contribution to isodoses around reactor-shield assemblies and dose rates within a crew shield.

Discussion of single-scattering methods for computing air-scattered radiation have been published.[35] A discussion of the assumptions involved in these methods and ensuing errors is given in the same reference.

The work at GE-ANPD on the single-scattering methods for computing air-scattered radiation resulted in four single-scattering model computer programs. Use of digital computers for this work effected a reduction in the number of assumptions and the computing time necessitated by a practical hand calculational procedure.

Programs 05-0 and 09-0 calculate the gamma ray and neutron dose rate, respectively, at any specified unshielded point detector due to single-scattered radiation in a homogeneous infinite medium from an anisotropic point source. The source energy spectrum may be approximated by ten discrete values of the energy. Exponential attenuation may be considered on either scattering leg as desired. The dose rate arising from the source spectrum is obtained by summation of the dose rates computed for each initial energy.

Programs 05-0 and 09-0 solve the following equation:

$$D(\rho, \Lambda, \Gamma) = \frac{nR^2}{\rho} \sum_{j=1}^{J} K(E_j)$$

$$\left[\int_{\gamma_o}^{\pi} d\gamma \int_{\beta_o}^{\pi-\gamma} \frac{d\sigma}{dr}(\theta, E_j) \frac{\exp\left(k_1 \Sigma(E_j) \sin\beta + k_2 \Sigma(E_j) \sin\gamma\right)}{K(E_j^s)} d\beta \int_{o}^{2\pi} D_R(E_j, \gamma, \psi)\, d\psi \right] \quad (35)$$

CONFIDENTIAL

DECLASSIFIED

DECLASSIFIED

The reader is referred to Figures 9.4 and 9.5 for clarification of the following definitions of quantities appearing in this equation:

j = subscript identifying source energy value. j takes on the integer values 1 through J.

γ = angle between direction of unscattered radiation leaving the source and source-detector axis.

β = angle between direction of radiation scattered to detector and source detector axis.

θ = angle between direction of unscattered radiation and direction of scattered radiation. $\theta = \gamma + \beta$

ψ = angle between x′ axis and projection of $\vec{r}_1$ on x′-y′ plane

dV_P = scattering volume element at P.

r_1 = separation distance between point source and scattering point, P.

r_2 = separation distance between scattering point, P, and point detector.

ρ = separation distance between point source and point detector.

$\frac{d\sigma}{dr}$ = differential scattering cross section. In program 05-0 this is the Klein-Nishina formula. In program 09-0 it has the form: $\frac{d\sigma}{dr} = \sum_{n=1}^{3} P_n(E_j) \cos^n \theta$.

$D_R(E_j, \gamma, \psi)$ = direct beam dose rate at (R, γ, ψ) due to radiation of energy E_j.

$K(E)$ = conversion factor from dose rate to particle flux for radiation of energy E.

E^S = energy of scattered radiation.

$\Sigma(E)$ = In program 05-0 this is the total absorption coefficient in the medium for gamma rays of energy E; in program 09-0 it is the total macroscopic cross section of the medium.

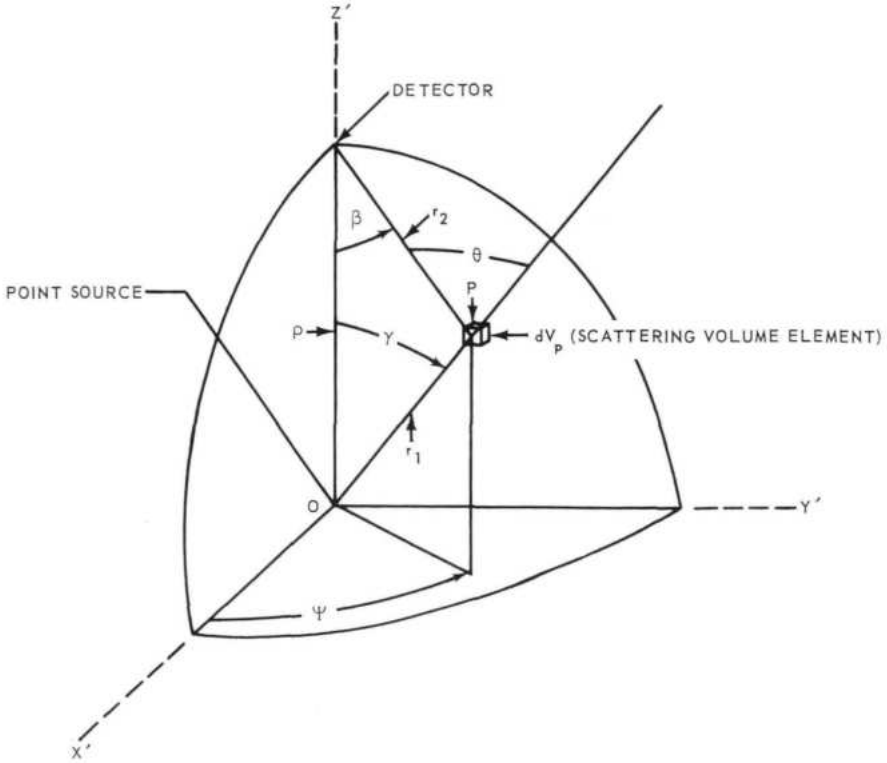

Fig. 9.4 – Coordinate system for air scattering geometry

DECLASSIFIED

DECLASSIFIED

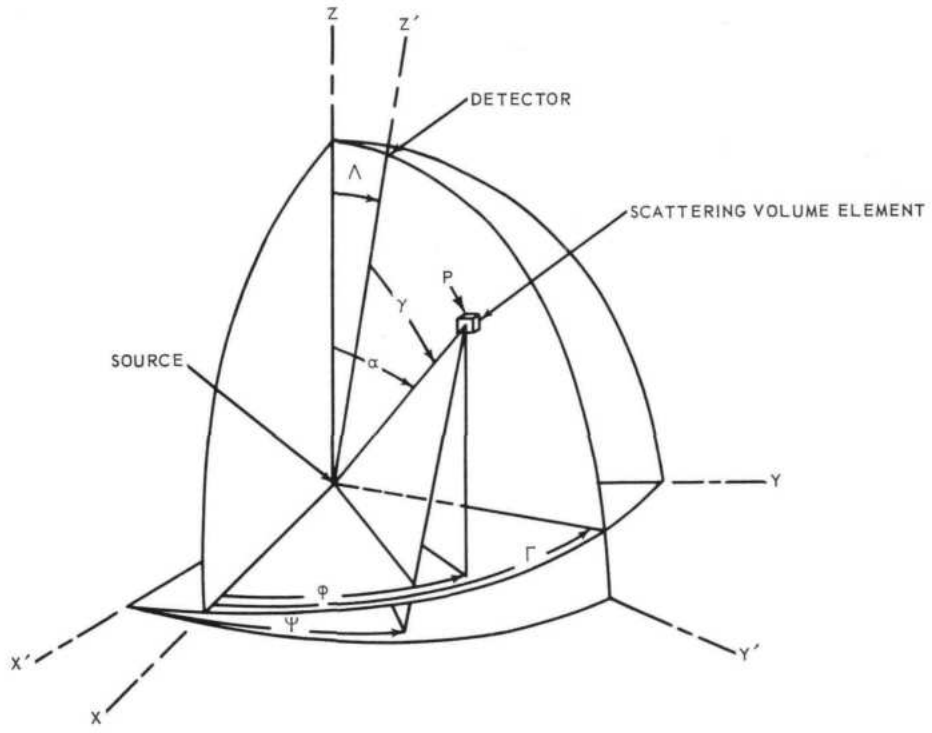

Fig. 9.5 – Angle relationships between source-detector and source system coordinate systems

n = scatterer density of the medium.

ρ, Λ, Γ = detector point coordinates.

k_1, k_2 = screening constants: equal to 1 if medium attenuation is desired; equal to 0 if no medium attenuation is desired.

γ_o, β_o = input quantities giving desired lower limits on integration over angles γ and β, respectively.

The values for the direct beam dose rates at a distance, R, from the point source are most conveniently obtained as functions of coordinates related to a reference system which is fixed with respect to the source system. For example, in the case of an extended source such as a reactor-shield assembly, a convenient fixed reference system might have its origin at the geometric center of the reactor and Z-axis along some symmetry axis of the assembly. These coordinates are usually the angles (α, ϕ) referred to a right-hand cartesian coordinate system (XYZ) with the Z axis being a symmetry axis of the source system (see Figure 9.5). In order to transform $D_R(E_j, \gamma, \psi)$ to $D_R(E_j, \alpha, \phi)$, it is necessary to obtain the transformation for $(\gamma, \psi) \rightarrow (\alpha, \phi)$. The program accomplishes this using the system of equations

$$\cos \alpha = \cos \Lambda \cos \gamma - \sin \Lambda \sin \gamma \sin \psi \quad (36)$$

$$\sin \alpha \cos \varphi = \sin \Gamma \sin \gamma \cos \psi + \cos \Lambda \cos \Gamma \sin \gamma \sin \psi + \sin \Lambda \cos \Gamma \cos \gamma \quad (37)$$

$$\sin \alpha \sin \varphi = - \cos \Gamma \sin \gamma \cos \psi + \cos \Lambda \sin \Gamma \sin \gamma \sin \psi + \sin \Lambda \sin \Gamma \cos \gamma \quad (38)$$

The derivation of equation (35) and complete descriptions of program 05-0 and 09-0 were published.[36,37]

Shielding programs 07-1 and 10-0 calculate the gamma ray and neutron dose rate, respectively, at a shielded point detector due to both direct-beam and single-scattered radiation in a homogeneous, infinite medium from an anisotropic point source. The detector

DECLASSIFIED

DECLASSIFIED

shield and the angular distribution associated with the point source are both assumed to be symmetric about the source-detector axis. The source energy spectrum may be approximated by ten discrete values of the energy. Exponential attenuation may be considered on either scattering leg as desired. The dose rate arising from the source spectrum is obtained by summation of the dose rates computed for each initial energy and for the rear, side, and front wall of the detector shield. The most general form of the detector shield that can be treated by the programs is shown in Figure 9.6.

Programs 07-1 and 10-0 solve the following equation for the single-scattered radiation:

$$D = \frac{2\pi n R^2}{\rho} \sum_{j=1}^{J} K(E_j) \sum_{i=1}^{3} \int_{\gamma 1i}^{\gamma 2i} d\gamma \int_{\alpha_{oi}}^{\pi-\gamma} \frac{D_R(E_j, \alpha)}{K(E_j^S)} \frac{d\sigma}{dr}(\theta, E_j)$$

$$\exp\left[\frac{-\rho}{\sin(\gamma+\alpha)}\left(k_1\Sigma_a(Ej)\sin\gamma + k_2\Sigma_a(E_j^S)\sin\alpha\right)\right] \psi_1 \, d\alpha \quad (39)$$

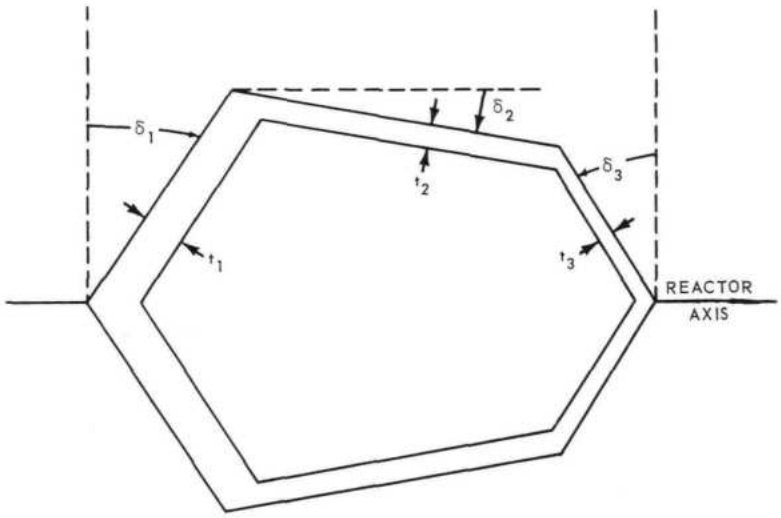

Fig. 9.6 – Detector shield configuration

The reader is referred to Figures 9.6 and 9.7 for clarification of the following definitions of quantities appearing in equation 39:

- j = subscript identifying source energy value. j takes on the integer values 1 through J.
- i = subscript identifying wall of detector shield. The rear wall is identified by i = 1, the side wall by i = 2, and the front (windshield) wall by i = 3.
- α = angle between direction of unscattered radiation leaving the source and source-detector axis.
- γ = angle between direction of radiation scattered to detector and source-detector axis.
- θ = angle between direction of unscattered radiation and direction of scattered radiation; $\theta = \gamma + \alpha$.
- φ = angle between x axis and projection of $\vec{r}_1$, on x-y plane.
- dV_P = scattering volume element at P.
- r_1 = separation distance between point source and scattering point P.
- r_2 = separation distance between scattering point P and point detector.

DECLASSIFIED

DECLASSIFIED

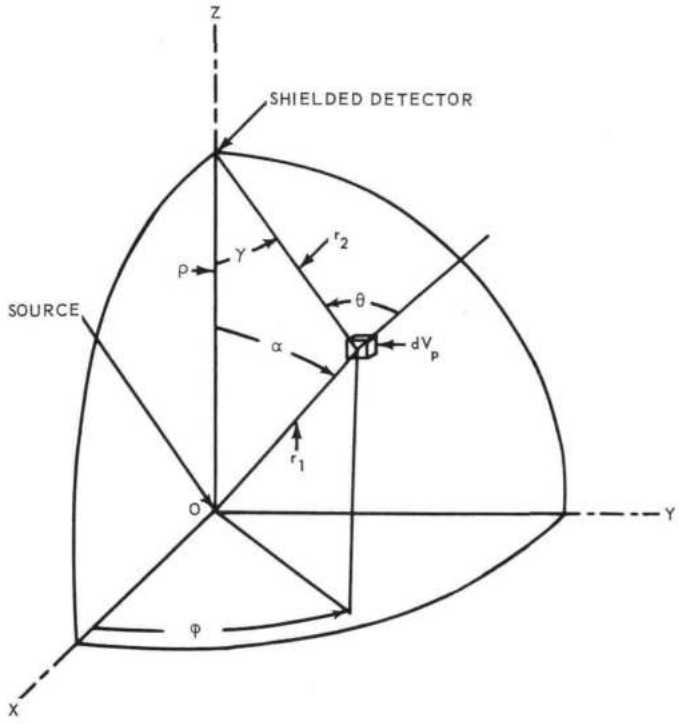

Fig. 9.7 – Coordinate system for single scattering

ρ = separation distance between point source and point detector.

$\frac{d\sigma}{dr}$ = differential scattering cross section. In program 07-1 this is the Klein-Nishina formula. In program 10-0 it has the form $\frac{d\sigma}{dr} = \sum_{n=1}^{3} P_n(E_j) \cos^n \theta$.

$D_R(E_j, \alpha)$ = direct beam dose rate at (R, α) due to radiation of energy E_j.

$K(E)$ = conversion factor from dose rate to particle flux for radiation of energy E.

E^S = energy of scattered radiation.

$\Sigma_a(E)$ = in program 07-1 this is the total absorption coefficient in air for gamma rays of energy E; in program 10-0 it is the total macroscopic cross section in air for neutrons of energy E.

n = scatterer density of medium.

k_1, k_2 = screening constants: equal to 1 if air attenuation is desired; equal to 0 if no air attenuation is desired.

α_{oi} = lower integration limit on alpha for wall i.

γ_{1i} = lower integration limit on gamma for wall i.

γ_{2i} = upper integration limit on gamma for wall i.

ψ_i = detector shield penetration function for wall i.

The form for the shield penetration functions used in program 07-1 is suitable for detector shields composed of one or two layers of materials on a side and are based on empirical expressions for computing buildup factors for water-lead and water-iron combinations established by Monte Carlo techniques.[38] It is assumed that these expressions are suitable for other material combinations for which the attenuation properties are similar

DECLASSIFIED

DECLASSIFIED

to those of water-iron or water-lead combinations. The form for ψ_i used in program 07-1 is

$$\psi_i = B_{i2}(\mu_{i2} S_{i2}) + \left[C_{i1}\, e^{P_1 \mu_{i2} S_{i2}} + C_{i2}\left(1 - e^{P_2 \mu_{i2} S_{i2}}\right)\right] \times \left[B_{i2}(\mu_{i1} S_{i1} + \mu_{i2} S_{i2}) - B_{i2}(\mu_{i2} S_{i2})\right] \exp\left[-\sum_{g=1}^{2} \mu_{ig}(E_j^s)\, Sig\right] \tag{40}$$

where:

$$C_{i1} = \frac{B_{i1}(\mu_{i1} S_{i1}) - 1}{B_{i2}(\mu_{i1} S_{i1}) - 1} \text{ and } C_{i2} = \frac{\mu_{i1}^{c.s.}(E_j^s)/\mu_{i1}(E_j^s)}{\mu_{i2}^{c.s.}(E_j^s)/\mu_{i2}(E_j^s)}$$

$$S1_g = \frac{t1_g}{\cos(\gamma - \delta_1)} \text{ and } S2_g = \frac{t2_g}{\sin(\gamma - \delta_2)} \text{ and } S3_g = \frac{-t3_g}{\cos(\gamma + \delta_3)}$$

$\mu_{i1}^{c.s.}$ = attenuation coefficient for Compton scattering in first material at i-th wall encountered by gamma ray.

$\mu_{i2}^{c.s.}$ = attenuation coefficient for Compton scattering in second material at i-th wall encountered by gamma ray.

μ_{i1} = total absorption coefficient for first material at i-th wall encountered by gamma ray.

t_{i1} = normal thickness of first material at i-th side encountered by gamma ray.

t_{i2} = normal thickness of second material at i-th side encountered by gamma ray.

B_{i1} = buildup factor for first material at i-th side encountered by gamma ray.

B_{i2} = buildup factor for second material at i-th side encountered by gamma ray.

$\delta_1, \delta_2, \delta_3$ = the angles which determine the half-angle for rear, side, and front conical sections of detector shield. A right cylindrical shield is obtained by setting $\delta_1 = \delta_2 = \delta_3 = 0$. (See Figure 9.6).

P_1, P_2 = constant coefficients used in computation of ψ_i functions.

The subscripts g and i refer to a particular material of which that part of the shield is composed. The normal thicknesses, t_{ig}, of each region is assumed to be constant for a given value of i and g. The S_{ig} appearing in the expression for the shield penetration functions are the thickness of each region seen by a scattered gamma ray that has a path that is at an angle γ with the source-detector axis.

The form for the shield penetration function used in program 10-0 is based on the assumption that the attenuation of the radiation through the detector shield walls can be adequately represented by an exponential. It is further assumed that the detector shield contains hydrogen and that the dependence of the relaxation length is controlled by the hydrogen in the shield. These assumptions lead to the following form for ψ_i in program 10-0.

$$\psi_i = \exp\left[-\sum_{g=1}^{G_i} \frac{S_{ig}}{\lambda_{ig}(E_j)\,(C_6 + C_7 \cos\theta)^{C_8}}\right] \tag{41}$$

where

$$S1_g = \frac{t1_g}{\cos(\gamma - \delta_1)} \text{ and } S2_g = \frac{t2_g}{\sin(\gamma - \delta_2)} \text{ and } S3_g = \frac{-t3_g}{\cos(\gamma + \delta_3)}$$

DECLASSIFIED

DECLASSIFIED

G_i = the number of regions for wall i.
$\lambda_{ig}(E_j)$ = neutron-dose-rate relaxation length in material comprising region g, wall i, for neutrons of energy E_j.
t_{ig} = normal thickness of region g, wall i.
C_6, C_7, C_8 = constant coefficients used in computation of ψ_i.
δ_i = angle which determines the half angle for conical section forming wall i.

Program 07-1 and 10-0 solve the following equation for the direct beam component:

$$D_d = \frac{R^2}{\rho^2} \sum_{j=1}^{J} D_R(E_j, \alpha = 0)\, \psi_1\, (\gamma=0) \qquad (42)$$

where
$D_R(E_j, \alpha=0)$ = direct beam dose rate at (R, 0) due to radiation of energy E_j.
$\psi_1(\gamma=0)$ = detector shield penetration factor for rear wall (i = 1).

The detector shield penetration factor, $\psi_1(\gamma = 0)$, used in program 07-1 is obtained from equation (40) by setting i = 1 and $\gamma = 0$. The value of this factor used in program 10-0 is obtained from equation (41) in a similar manner.

The derivations of the preceding equations and complete description of programs 07-1 and 10-0 are given in references 39 and 40, respectively.

9.5 DUCT ANALYSIS METHODS

Direct-air cycle reactors require reactor shields with relatively large air ducts. The calculation of the effects of such ducts on radiation leaking from a reactor shield constitutes one of the most difficult problems in shield analysis and design. Because of the difficulty of such calculations, duct analysis methods are usually very crude. The adequacy of a particular method must, therefore, be tested against experimental data from duct mockups which approximate closely the ducting configuration for which the method was developed.

The method employed at GE-ANPD for determining the effect of ducts on the fast neutron dose rate calculates the radiation level incident on an element of duct surface area using a point kernel program. The radiation emitted by the element of duct surface area is determined by adjusting the incident radiation level by an albedo obtained from data supplied in reference 41. In this manner a surface source distribution is obtained for the entire duct wall. This source distribution is then used as input to a point kernel program, which performs a surface integration over the duct wall to obtain radiation levels at detector positions outside the duct. This method was developed very recently, and no reference exists describing it nor have any results from the method been compared with experimental data to verify its adequacy.

An earlier method for determination of the effect of ducts on fast neutron dose rate, developed by Henderson and Patterson,[42] utilizes a point kernel program to obtain the radiation level at volume elements in regions adjacent to and forming the duct wall. Volume sources for these volume elements are then obtained using a single-scattering model. Radiation levels outside the duct are obtained by using the volume sources as input to a point kernel program and integrating over the entire region surrounding the duct. This method was applied to analysis of experimental data from the OTT duct configuration.[43] For this configuration, the single-scattering approximation gives acceptable agreement with the experimental data.[42]

DECLASSIFIED

DECLASSIFIED

A more sophisticated approach to the problem of analysis of ducts was initiated by A. Prince.[44] This approach applied the Hilbert-Schmidt theory of integral equations and the Fermi[45] albedo concept to analysis of the effect of cylindrical or annular ducts on fast neutron dose rate and thermal neutrons. A comparison of results of this analysis with data from a series of annular duct scattering experiments performed at Convair were made. The comparison indicated that the approach is a feasible one; the analytical results approached the experimental data to within the experimental error.[44]

The method in current use has been used to estimate the effect of ducts on gamma ray leakage. The results show that this effect is small for the ducted shields of interest. This result has been confirmed by Monte Carlo studies of the D140E reactor-shield assembly using program 18-0.

9.6 TWO-COMPONENT METHOD

The two-component method[46] of shield analysis considers the arrival of radiation at a detector located outside a finite shield from two distinct source regions. In the case of neutrons, the first component, which is obtained by a volume integration over the active core of the reactor, consists of neutrons that are essentially uncollided and neutrons that have undergone very low-angle elastic scattering. This is the collimated component. The second component, which is obtained by a surface integration over the major shield exterior surfaces, consists of neutrons that have undergone large-angle elastic scattering and neutrons that have been inelastically scattered. This is called the diffuse component.

Consider the case of a point source located in a finite shield as shown in Figure 9.8. The radiation calculated at some detector point will consist of a contribution from the collimated component, which considers only the linear path connecting the source and the detector, plus, usually, a larger contribution by the diffuse component from the surface. The difference in magnitude may be attributed primarily to the following factors: (1) the detector subtends a larger solid angle of the surface source than the point source, (2) the detector, at a certain distance from the surface, may see areas of high radiation on the shield surface over large detector angles near the reactor center, (3) the collimated component may, at certain angles, see local thicker-than-average portions of the shield along the linear path, and (4) the cross sections used for each component are not the same. This difference in the two components is not pronounced in nearly spherical solid shields but becomes important in engineered cylindrical shields that contain voids.

To illustrate the importance of the neutron angular distribution in elastic scattering with lightweight nuclei for the calculation of neutron transport through shields, typical distributions for several different neutron energies in the center-of-mass coordinate system are shown in Figure 9.9. There will be a slight shift in the distribution when it is plotted in the laboratory system, but the trend for the forward scattering with increasing energy is about the same. For very low neutron energies, the elastic scattering will be nearly isotropic. At approximately 2.7 Mev, the backscattering is much larger than at the higher energies. It is evident that the bulk of the forward neutron scattering becomes larger with increasing neutron energy. This important effect is considered in calculating the energy dependent removal cross section that is used to obtain the "removal" group in the BEPO neutron penetration calculations.[47, 48]

The removal cross section for all elements other than hydrogen is defined as

$$\Sigma_R(E) = \Sigma_{ne}(E) + \Sigma_{el}(E)\left[1 - \overline{\mu(E)}\right] \qquad (43)$$

DECLASSIFIED

DECLASSIFIED

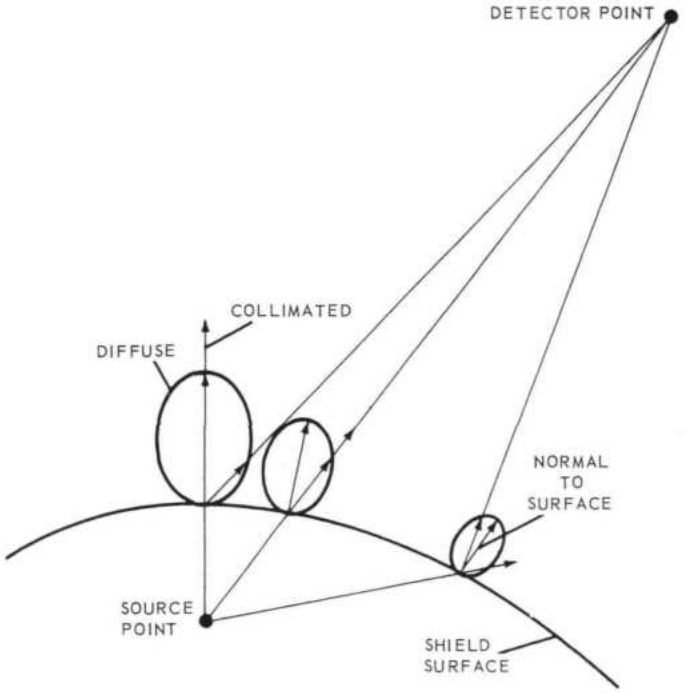

Fig. 9.8 – Sketch illustrating the two-component concept

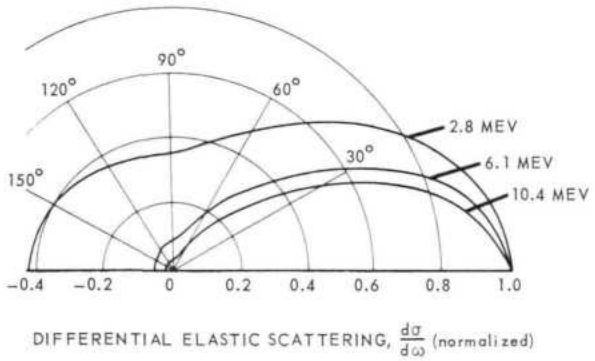

Fig. 9.9 – Typical differential angular distribution for elastic scattering with lightweight nuclei (C. M. System)

$\Sigma_{ne}(E)$ = Non elastic scattering cross section

$\Sigma_{el}(E)$ = Elastic scattering cross section

$\overline{\mu(E)}$ = Mean cosine of the scattering angle in the laboratory system

Using these energy dependent removal sections for lithium hydride, treating the hydrogen as in reference 48, the neutron spectrum of the collimated component is calculated for several positions in an infinite media for a point fission source. Figure 9.10 shows the collimated neutron spectrum for three positions. Included in the figure are the values obtained by the Nuclear Development Corporation of America in an infinite media of lithium hydride by the use of the moments method.[49] By subtracting the collimated component

DECLASSIFIED

DECLASSIFIED

CONFIDENTIAL

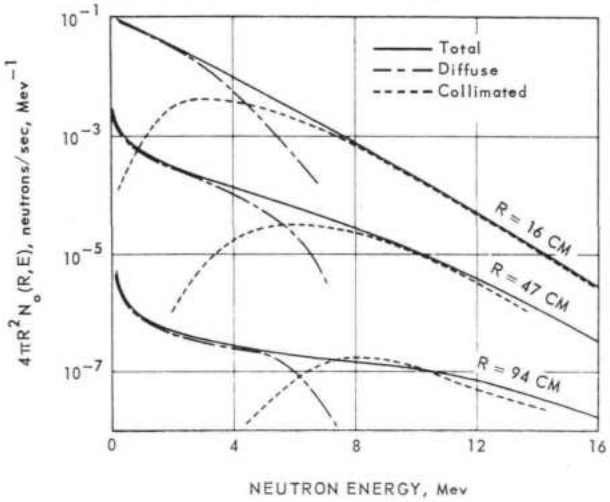

Fig. 9.10 – Differential neutron spectrum in an infinite medium

from the NDA data, it is possible to obtain the diffuse component of the neutron spectrum at those positions for an infinite media. Note that most of the diffuse neutrons have energies below 4 to 6 Mev.

Using these differential neutron spectra for various positions in an infinite media of lithium hydride and the response of fast neutron dosimeter, the diffuse and collimated dose rates as a function of thickness are plotted in Figure 9.11. Due to the dosimeter energy response, a large portion of the total dose is attributed to the diffuse component. After a certain thickness, the dose comes into equillibrium with the collimated component. This is to be expected since the collimated component essentially represents the fast neutrons that are transported large distances and subsequently are slowed down and migrate as lower energy neutrons. Figure 9.11 also illustrates the effect of a finite shield on the fast neutron dose near the boundary. The collimated component is not affected by the boundary, however, the diffuse component due to the migration is slightly depressed. Preliminary Monte Carlo calculations[50] performed by Convair-Fort Worth indicate that this flux depression near the surface of the shield does exist.

The problem of calculating neutron penetration, migration, and diffusion in materials is much easier when considering infinite media. Since engineered shields require finite media analysis, the infinite media neutron flux calculations must then be corrected for finite geometries. This correction factor represents the ratio of the neutron current leaving the surface of the shield to the total flux that would be calculated in an infinite media at that particular position. Since the migration characteristics of the neutrons vary with energy, this correction factor generally is not a constant. Typical ratios of the current to the flux and also the flux to the flux for a finite hydrogenous medium to that for an infinite hydrogenous medium at a fixed position is shown in Figure 9.12. Studies such as these were performed with the use of Monte Carlo by NDA under contract with GE-ANP. This figure illustrates the fact that if a flux measurement device such as a large dosimeter chamber were to be placed close to the surface of a shield, the correction required for the experiment-theory correlation for the finite case may be fairly small. However, if a current measurement device such as a very thin foil were to be placed on the surface, the correction may in some cases approach 50 percent.

In addition to the ratio of the current to the flux for analysis in finite shields, it is also important to know the angular distribution of the neutrons leaving the surface of the shield.

CONFIDENTIAL

DECLASSIFIED

DECLASSIFIED

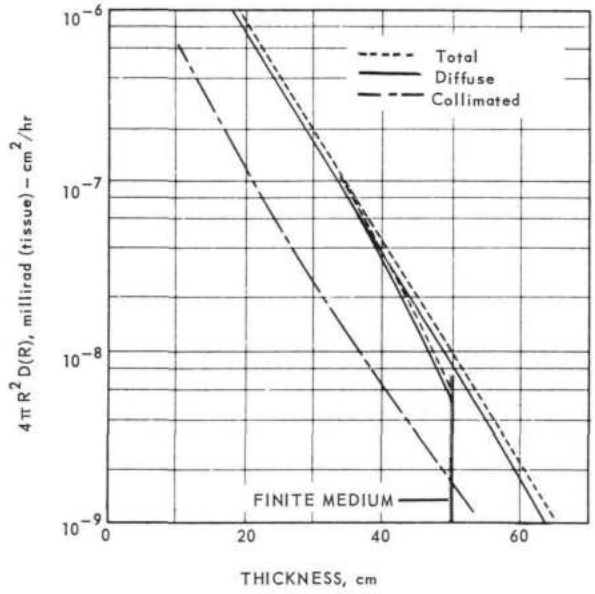

Fig. 9.11 – Fast neutron dose rate as a function of thickness

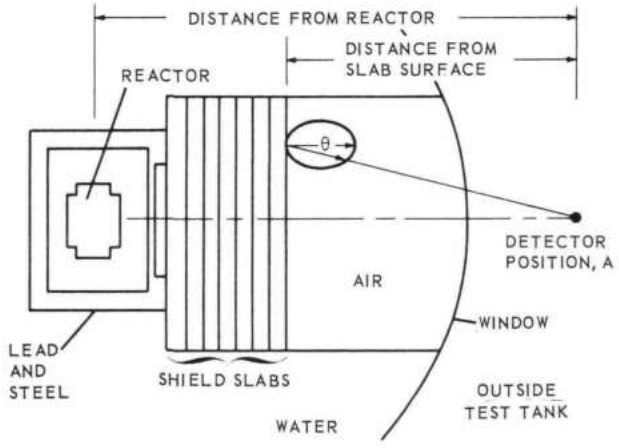

Fig. 9.12 – Outside test tank shield experiment geometry

Convair-Fort Worth has performed some preliminary calculations[50] of the angular distribution of fast dose neutrons leaving a finite hydrogenous shield. These Monte Carlo data are plotted as histograms in Figure 9.13. Using the neutron density as a function of thickness away from the boundary as a source of scattering centers[51] an analytical approximation to the angular distribution of the diffuse neutrons leaving the surface may be given as:

$$F(\Theta) \sim \text{Cos}\,\Theta + 5.5\,\text{Cos}^3\,\Theta$$

where Θ is the angle away from the normal to the surface. This curve is normalized to the histogram data as shown in the figure. The difference between the analytical fit and histogram data from 0 to 20 degrees was approximated by a $\text{Cos}^{50}\,\Theta$ distribution which is assumed to represent the collimated component of the fast dose. An integration of both angular distributions over the complete outward solid angle indicates that the diffuse component accounts for about 87 percent of the total dose neutrons. The collimated compon-

DECLASSIFIED

UNCLASSIFIED

CONFIDENTIAL

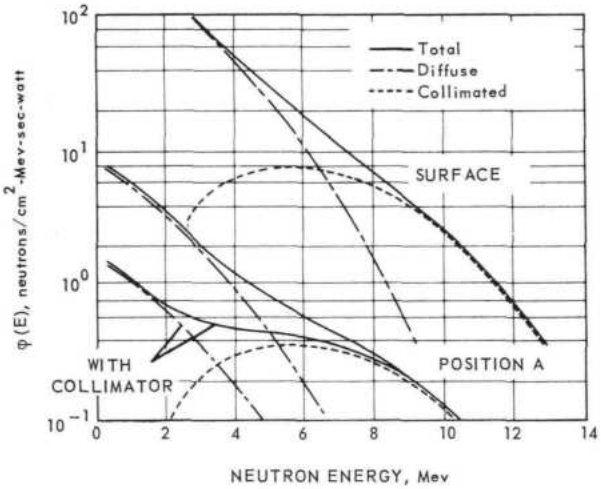

Fig. 9.13 – Differential neutron spectrum for a typical OTT experiment

ent represents about 13 percent of the total dose neutrons of which about 1 percent is calculated to be the uncollided contribution. This distribution of the diffuse and the collimated components appear to agree with other observations.

Many experiments have been performed that would permit a correlation of the two-component method of analysis with experiment. Specifically, tests that were performed by Convair under a GE-ANP contract using the Outside Test Tank indicated that the fall-off of the radiation that was measured in air appeared to originate near the surface of the shield slabs rather than from the center of the reactor. The two-component method was able to demonstrate this effect, and the correlation of analysis with experiment was good.

A schematic diagram illustrating a typical test arrangement is shown in Figure 9.14. External measurements were made at positions ranging from 9 feet to 100 feet along a centerline from the center of the reactor. Additional measurements were made at different angles about the tank. In addition, threshold and slow neutron detector foils were used to measure the neutron environment within the slabs and on the slab surface. In several test configurations, photographic plate neutron spectrum measurements in the energy range from about 0.7 to 11 Mev were made. In these tests, a detector collimator was required to reduce background and to establish the direction of the measured neutrons.

With the use of the energy dependent removal cross sections, the collimated neutron spectra to the surface for the case of lithium hydride for one particular experiment was calculated. By the use of the NDA moments data corrected for a finite media the diffuse component at the slab surface was also obtained. The total surface neutron spectrum with the two components are shown in Figure 9.15. If a dosimeter or any other neutron detector were placed at the 12 foot position, (Figure 9.14) this detector would be in a radiation field having a neutron spectrum as indicated in Figure 9.15. It is clear that on the slab surface the diffuse component represents a large portion of the total neutron flux; however, at the 12 foot position, due in part to the radiation decrease with increasing distance from the surface, the diffuse component is not a large contributor for this particular shield arrangement.

When the photographic plate measurements were made, the collimators that were employed subtended a small portion of the complete slab surface. Therefore only a small fraction of the total surface diffuse neutrons were detected by the photographic plate. Fig-

CONFIDENTIAL

UNCLASSIFIED

DECLASSIFIED

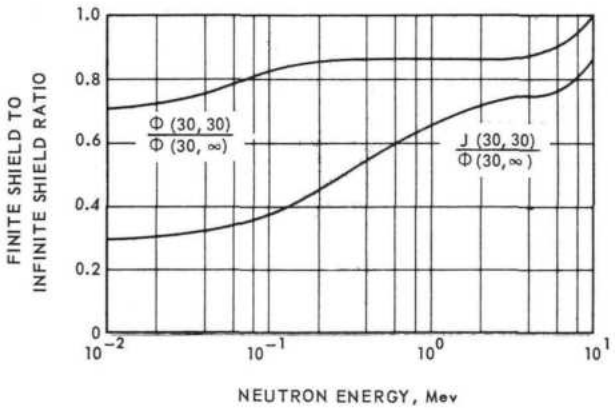

Fig. 9.14 – Infinite to finite shield correction factors

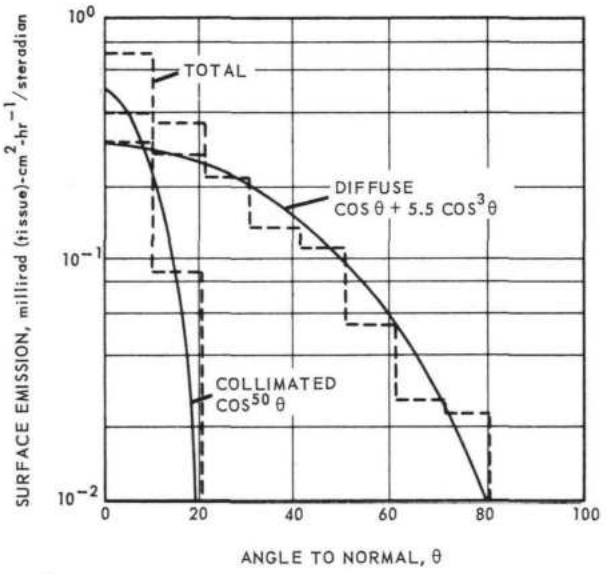

Fig. 9.15 – Surface emission angular distribution for fast neutrons

ure 9.15 demonstrates that the spectrum of the collimated flux remains unchanged when using the collimator, but the intensity of the diffuse portion is considerably reduced. As the detector collimator angle becomes smaller, the measured neutron flux approaches the collimated value for this geometry. If a measurement were made at some other angle so that the collimator would not see the reactor core, most of the neutrons detected would be in the diffuse component category and the predominant neutron energy would be much less than in the case where a measurement is made normal to the slab for this geometrical arrangement.

To facilitate rapid analysis, a computer program was developed, under subcontract,[52] by Convair-Fort Worth to integrate the particle flux over the entire surface of a shield that is symmetrical about the X-axis. Either of two modes of surface emission are possible with the code:

Mode 1. Radial emission from the center of the core, with the angular distribution based on a line drawn from the core center through a point on the surface.

DECLASSIFIED

DECLASSIFIED

Mode 2. Normal emission from the shield surface, with the angular distribution based on the normal to the surface at the point considered.

Figure 9.16 illustrates the geometry that is used in this surface integration program. The input simply requires the particle current at the respective x-y coordinate on the shield surface, the type of emission angular distribution considered, and detector positions defined by the angle and radius.

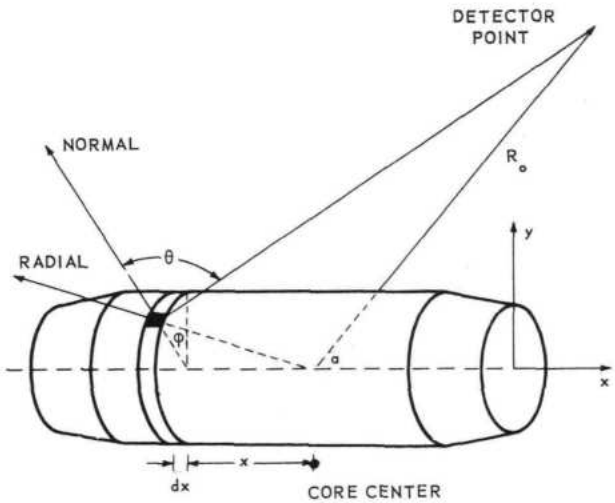

Fig. 9.16 – Geometry for surface integration program

Although the present analysis using the two-component method appears to give good correlation with experimental data, improvements are required in the following areas: (1) prediction of the angular distribution of particle flux leaving the surface of shields, (2) calculation of the neutron current on the surface of finite shields, and (3) obtaining better data on the differential elastic scattering cross sections of shield material nuclei.

9.7 MONTE CARLO METHODS

Until recently, nearly all shield nuclear analysis was accomplished with phenomenological or empirical methods based largely on bulk shielding experiments. Because of the many limitations of these approaches, the rapid improvement of digital computers, and the expanding knowledge of basic nuclear data, development of Monte Carlo codes for use in shield analysis was undertaken a number of years ago at GE-ANPD.

The Monte Carlo method is a statistical technique used in the analysis of physical and mathematical processes that are probabilistic in nature or can be so interpreted.

The transport of neutrons and gamma rays in a shield is an example of a physical process, probabilistic in nature, which can be conveniently handled by the methods of Monte Carlo. Average quantities for neutrons and gamma rays, such as current, absorption, flux, heating, dose rate, and leakage tallies, are determined in this approach by tracing individual histories chosen from appropriate distributions for a sufficiently large number of histories.

There are a number of ways in which the Monte Carlo method can be used in shield analysis and design. Because, in theory, it is an exact method, the technique can be used to

DECLASSIFIED

DECLASSIFIED

check the adequacy of basic nuclear data through application to suitable experimental situations. The flexibility of the method in handling complex geometry and material configurations allows application to the analysis and design of reactor-shield systems. If the basic nuclear data used in Monte Carlo studies are known to be adequate, the method may also be used as a substitute for experiment in providing parametric data for establishing semi-empirical methods of shield design.

The Shielding Unit's effort along these lines has resulted in five Monte Carlo codes in use on the IBM 7090. These include one specialized code, program 18-0,[53] for analysis of reactor-shield assemblies; two general purpose codes, programs FMC-N and FMC-G,[54] for analysis of reactor or crew shields or for use as development tools to generate parametric data; a gamma ray air-scattering code, program 15-2;[55] and a neutron air-scattering code, program 16-0.[56]

Specialized Monte Carlo program 18-0 is a digital computer code that applies Monte Carlo methods to simulate neutron and gamma ray histories in reactor-shield assemblies. This program is designed to investigate and determine nuclear heating rates in reactor-shield systems and neutron and gamma ray leakage distributions in energy and angle for an equivalent point source.

The flow charts for program 18-0 were prepared by the Nuclear Development Corporation of America under NDA Subcontract AT-74.[57,58] Coding of the program was done by the Mathematical Analysis Unit of GE-ANPD. The original flow charts supplied by NDA were modified somewhat as coding progressed.

The program is coded for an IBM 7090 with a fast memory capacity of 32,768 storage locations. Seven magnetic tape units are required, but no magnetic drum storage is necessary.

The shield portion of a reactor-shield assembly is described by regions which are formed by rotation of a class of simply connected quadrilaterals about the reactor-shield assembly axis. Each region is composed of a homogeneous mixture of the basic materials of which the region is composed.

Two reactor description capabilities are provided by the program. The shield region geometry routine can be utilized to describe reactors that can be approximated by contiguous regions of homogenous composition which possess cylindrical symmetry about the reactor-shield assembly axis. A reactor geometry subroutine is not required when this manner of describing a reactor is used.

A reactor geometry subroutine, separate from the shield geometry subroutine, is provided in the program for the description of reactors with off-axis cylindrical fuel tubes. The treatment of the geometry of reactors of this type by the reactor geometry subroutine is approximate only. Source particles are generated in fuel tubes, and their histories are followed through the correct source tube configuration detail until they escape the reactor by leakage down the source tube or penetrate a specified distance into the moderator region beyond the fuel tube. When either of these events occurs, the remainder of the particle history spent in the reactor is followed by the reactor geometry routine using a less detailed description of the reactor geometry and composition.

The spatial and energy coordinates of source neutrons and gamma rays whose histories are to be determined by the program are selected from the appropriate probability distributions by an auxiliary code, program 20-0.[59] In addition to these state parameters, the complete set of parameters generated by program 20-0 for a source particle includes a source tube and region number. Program 20-0 places the source particle parameters on tape for use as input to program 18-0. The direction coordiantes of a source particle are not chosen by program 20-0. These parameters are chosen by program 18-0 from an isotropic distribution in the laboratory system.

DECLASSIFIED

DECLASSIFIED

A neutron or gamma ray collision event is selected by random sampling from the appropriate discrete distributions for all neutron or gamma ray events allowed in the program. Thus, no weighting of a neutron or gamma ray is effected at a collision by the method of event selection.

Neutron events treated by the program are: (1) elastic scattering, (2) inelastic scattering, (3) radiative capture, (4) neutron capture with alpha emission, (5) n, 2n reaction in beryllium, and (6) absorption with no secondary emission.

Gamma ray events treated by the program are: (1) Compton scattering, (2) absorption (photoelectric effect and pair production), and (3) gamma ray absorption with neutron emission (photoneutron reaction).

The angular distribution of elastically scattered neutrons may be isotropic or anisotropic in the center-of-mass system at the discretion of the user.

Inelastically scattered neutrons, neutrons from the beryllium n, 2n reaction, and secondare gamma rays are assumed to be emitted isotropically in the laboratory system.

The angular distribution of scattered gamma rays is assumed to be that given by the Klein-Nishina formula. The angular distribution of neutrons from photoneutron reactions is described by a second degree polynomial in the cosine of the polar scattering angle in the center-of-mass system.

The important sampling techniques of splitting and Russian roulette on energy and region for neutrons and on region for gamma rays are optionally allowed in the program. The only way in which neutrons or gamma rays acquire a weight other than 1 is through application of this technique.

Output available from the program includes: energy deposition in each shield region due to certain neutron and gamma ray reactions; energy-angle leakage distribution for neutrons and gamma rays for a point source equivalent to the assembly, or, optionally, a tape record of the parameters of escaping particles.

Also included in the output for each shield region are the number of: (1) neutron and gamma ray particles absorbed, (2) neutron and gamma ray particles suffering energy cutoff, (3) neutron and gamma ray particle currents across specified shield boundaries, (4) n, α reactions, (5) n, γ reactions, and (6) inelastic scattering events.

Parameters of the generated secondary particles may form part of the output when desired.

A complete description of program 18-0 was published.[53]

Program 18-0 has been used to calculate gamma ray heating rates in the D140E reactor-shield assembly.[60] Comparisons were made between these results and similar results using GE-ANPD point kernel programs for certain specified regions of the assembly. The comparison showed that results from the two calculations agree to within 20 percent.

The D140E study using program 18-0 indicated that a complete gamma ray heating rate analysis of such an assembly could be performed in 12 to 15 hours on the IBM-7090.

Flexible Monte Carlo programs FMC-N and FMC-G are digital computer programs which apply Monte Carlo methods to simulate neutron and gamma ray histories, respectively, in a source-shield configuration. As the names imply, the programs are designed for flexibility in the geometrical, material, nuclear, and source descriptions of source-shield configurations and variance reduction techniques.

The programs are coded for an IBM 704 computer with a fast memory capacity of 32,768 storage locations and eight magnetic tape units and for an IBM 7090 computer with a fast

DECLASSIFIED

DECLASSIFIED

memory capacity of 32,768 storage locations and ten magnetic tape units on two data channels. No magnetic drum storage is necessary.

Flow charts for the programs were obtained from a report by F. Mozer and E. Leshan.[61] Although their flow charts were followed directly for most of the coding, several changes were made to make the codes more suitable for specialized reactor and shield analysis. The more important changes are:

1. Inclusion of a modified version of the GMC source generator.[62]
2. Elimination of the particle similarity indicator, τ.
3. Elimination of the option for using the rejection technique for sampling from the evaporation model.
4. Consistent use of energy rather than velocity.
5. Introduction of energy and weight cutoffs and a number-of-collisions cutoff following energy cutoff to replace census time.
6. Insertion of a fixed nuclear mass of 20 in FMC-N to distinguish between light and heavy nuclei (nuclei with a mass equal to or greater than 20 are considered heavy).
7. Introduction of reflecting boundaries to simplify some geometry descriptions.
8. Modification of the history tally to count on a collision basis rather than a region basis.
9. Modification of the absorption tally to be tallied by energy and region rather than by region alone.
10. Inclusion of the option of obtaining the energy deposition in conjunction with the absorption tally.
11. Modification of the neutron fission routine to save the fission neutron's parameters with the option of processing these neutrons by generations or saving the fission neutron's parameters on magnetic tape for faster analysis.
12. Inclusion of the option of including or excluding the expectation calculations.
13. Inclusion of the option of Monte Carlo or expectation flux tallies.

Any number of regions, of a variety of geometrical shapes, are enclosed by a number of surfaces described by the general equation:

$$A X^2 + X_0 X + BY^2 + Y_0 Y + C Z^2 + Z_0 Z - K = 0 \qquad (44)$$

Each region is composed of a homogeneous mixture of any number of materials.

The direction, spatial, and energy parameters of source neutrons and gamma rays may be selected by a source particle generator, or they may be entered as input from cards or magnetic tape.

It is often desirable to have the same source distribution available for several runs on a Monte Carlo program and to alter the random number sequence at the start of each run to vary the history of each particle. In many instances, the time spent in generating the source spectrum will be fairly long, and a considerable amount of time will be wasted if the distribution must be generated for each run. Therefore, the source generator contained in the FMC programs has been made available as an auxiliary code.

Flexible Monte Carlo Source Generator (GE-ANPD program 707) provides three methods for generation of the source particle's direction cosines, three methods for generation of the source particle's spatial coordinates, and one method for generation of the source particle's energy. In addition, any or all of these parameters may be entered as input. Separability is assumed between the direction cosines, spatial coordinates, and energy. Additional separability is assumed in some of the various options for the source particle's direction cosines and spatial coordinates.

Parameters of any number of source particles for any number of source regions may be generated. These parameters are stored on magnetic tape for later analysis and pro-

DECLASSIFIED

DECLASSIFIED

cessing by the FMC programs. The program is coded in FAP for an IBM 7090 computer with a 32-K memory capacity and two data channels.

A complete description of program 707 was published.[63]

The neutron collision routine uses random sampling from the appropriate discrete distributions to select either an elastic-scattering event, an inelastic-scattering event, or a fission event. Thus, the subset of the set of all possible neutron events consisting of these three events is assumed to occur with probability 1. A neutron emerging from a collision is given a weight equal to the probability that it escaped absorption at that collision, multiplied by the probability that it escaped absorption at all prior collisions. This is necessary to eliminate the bias introduced by the event-sampling scheme which does not allow absorption to occur. Further adjustment of the weight is necessary when one or more of the optional variance reduction techniques are used. The angular distribution of scattered neutrons may be isotropic or anisotropic in the center-of-mass system at the discretion of the user.

For a fission event, the weight of the incident neutron is considered in determining the actual number of neutrons to be produced, thereby producing neutrons of weight 1. The angular distribution of the fission-produced neutrons is assumed isotropic in the laboratory system. Parameters of these neutrons are stored on magnetic tape for later analysis. The weight of the incident neutron is tallied in the absorption tally, and the history is terminated.

The emission of gamma rays due to neutron absorption, inelastic scattering, and fission is optionally allowed. The weight of the incident neutron is considered in determining the actual number of gamma rays to be emitted, thereby emitting gamma rays of weight 1. The angular distribution of the emitted gamma rays is assumed to be isotropic in the laboratory system. Parameters of these gamma rays are stored on magnetic tape for later analysis.

The gamma ray collision routine treats all collisions as Compton-scattering collisions, i.e., Compton scattering is assumed to occur with probability 1. A gamma ray emerging from a collision is given a weight equal to the probability that it escaped absorption at that collision, multiplied by the probability that it escaped absorption at all prior collisions. This is done in order to eliminate the bias introduced by assuming all collisions to be Compton scattering collisions. The absorption probabilities are equal to the sums of the photoelectric and pair-production probabilities.

Cumulative probability tables are used to determine the angular distribution of the Compton-scattered gamma rays. The gamma ray collision routine optionally allows the emission of 500 kev gamma rays following absorption by pair-production of the primary gamma ray. These gamma rays are then processed in their turn by the code.

Several variance reduction techniques are optionally allowed in addition to the non-optional statistical estimation technique of weighting for absorption escape at each collision. An optional statistical estimation technique may be used for scoring entrance tallies and mandatory leakage tallies. Flexibility in sampling from source spectra is achieved by using energy group-averaged constants called acceleration factors. The other options, which are forms of importance sampling, are splitting and Russian roulette performed on the spatial variables at region boundary crossings and on the energy, spatial and direction variables at collisions, Russian roulette on particles whose weight falls below the weight cutoff, and the exponential transformation.

Output available from these programs includes independently optional absorption or energy deposition tallies, Monte Carlo entrance and leakage tallies, expectation entrance

DECLASSIFIED

DECLASSIFIED

and leakage tallies, Monte Carlo or expectation flux tallies, and history tallies of particles reaching selected regions. Monte Carlo and optional expectation leakage tallies are made for all regions external to the source-shield configuration. The absorption or energy deposition, entrance, leakage, and flux tallies are made by region and energy group. These programs also optionally print the source particle's direction cosines, spatial coordinates, and energy. The printing of the history tallies is also optional.

Output data from flexible Monte Carlo programs FMC-N and FMC-G can be converted to heating rates, dose rates, or both by means of the FMC flux conversion program (GE-ANPD program 585). The program also computes the flux per energy interval per unit volume per neutron or gamma ray. A set of input data for up to 100 energy levels and 48 regions can be handled in a single run of the computer. The program was written in Fortran for the IBM 704 and IBM 7090 computers. A complete description of this program was published.[64]

Appropriate history tally data from the flexible Monte Carlo program can be converted to energy-angle distribution at any point in configurations possessing spherical symmetry by means of the Histangle program (GE-ANPD program 737). This program has been written but has not yet been checked out. A report describing the program is in preparation.

A complete description of programs FMC-N and FMC-G was published.[54]

Data from FMC-G were compared with Spencer-Fano Moments method data[65] for differential spectra in infinite media for several materials at various distances from an isotropic, monoenergetic point source of gamma rays. Results of the study showed good agreement between results from the two methods. This is illustrated in Figure 9.17 which shows the agreement obtained for iron. Since the comparison was made for checkout purposes only, no error analysis was performed on the data.

Similar comparisons were made with FMC-N and moments method data for differential neutron spectra in infinite media of beryllium,[66] beryllium oxide,[66] and lithium hydride[67] at various distances from a point isotropic fission neutron source. Input was taken from references 68 and 66 for the beryllium and beryllium oxide studies. Reference 69 contains references to the input data used in the lithium hydride study. Good agreement was obtained between FMC-N and moments method results.

Comparisons were made between program 18-0 and program FMC-G machine computation times. These studies show that program 18-0 is approximately three times faster than the FMC programs for complex geometrical configurations.

A method was devised for handling the n,2n reaction in FMC-M. It involves treating the reaction as a fission and adjusting the fission secondary neutron spectrum and heating constant appropriately. A weighted average heating constant is based on the expected proportion of reactions for each energy group. The secondary neutron spectrum from the beryllium n,2n reaction was adjusted in reference 70 to fit the limited experimental data fairly well and still maintain some semblance of correlation with the theoretical modes of reaction.

Program 15-2 employs both Monte Carlo and numerical methods to calculate the energy-angle distribution of gamma rays at a point detector due to single and multiple scattering in air from a monoenergetic, monodirectional point source. The program is coded for an IBM 7090 computer with a fast memory capacity of 32,768 storage locations.

Gamma ray events allowed in program 15-2 are photoelectric effect, pair production, and Compton scattering.

DECLASSIFIED

DECLASSIFIED

CONFIDENTIAL

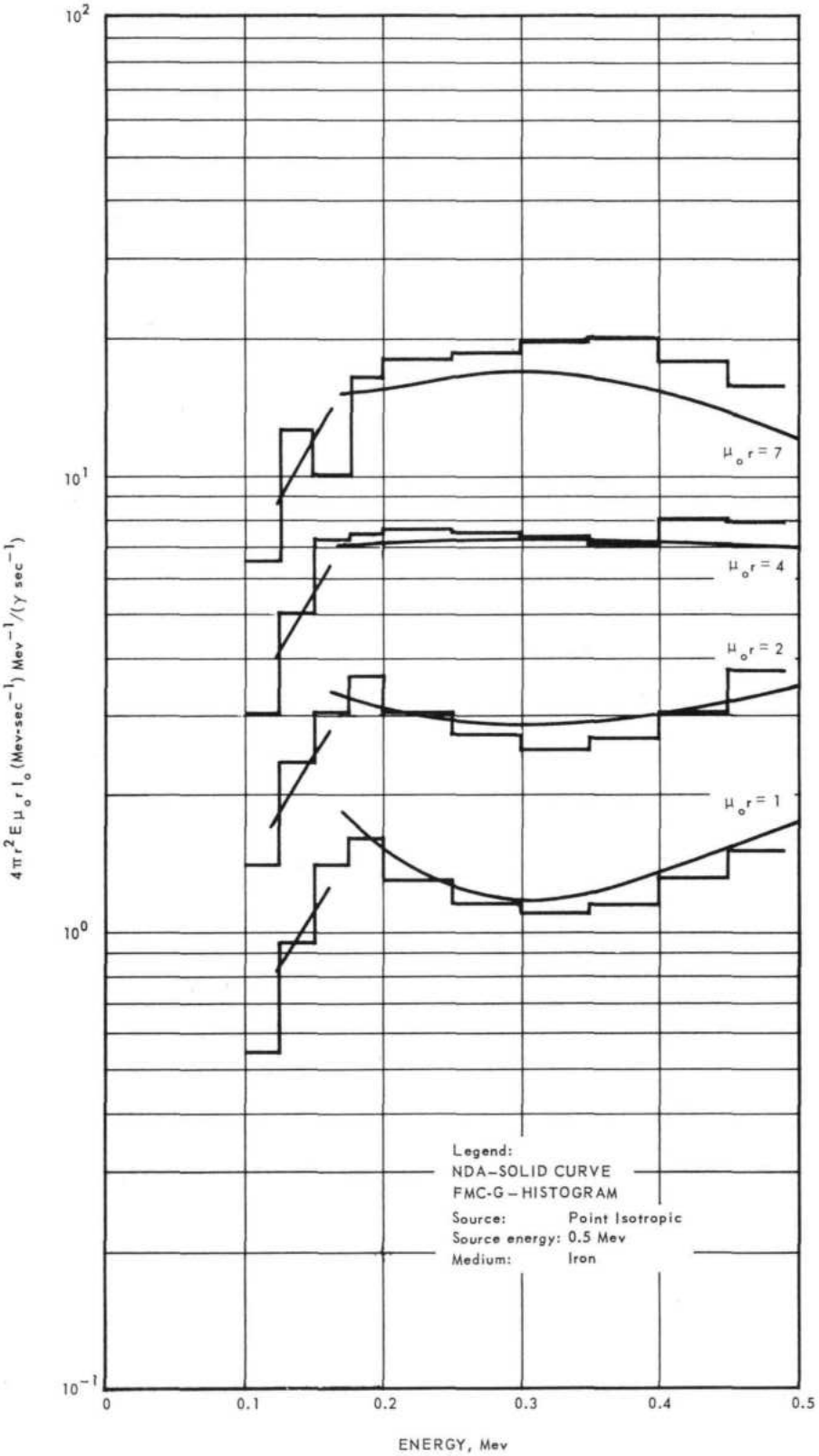

Fig. 9.17 – Differential gamma ray energy spectra

CONFIDENTIAL

DECLASSIFIED

DECLASSIFIED

The collision routine treats all collisions as Compton scattering collisions, i.e., Compton scattering is assumed to occur with probability 1. Since all collisons are biased in favor of Compton scattering, a gamma ray emerging from a collision is given a weight equal to the probability that it escaped absorption at the collision, multiplied by the probability that it escaped absorption at all prior collisions. The weight of a particle may be adjusted further if one or both of the importance sampling options described below are used.

The single-scattered contribution to the detector energy-angle distribution is computed by numerical integration, while the contribution due to second and higher order scattering is determined using Monte Carlo techniques.

First collision points for the Monte Carlo calculations are obtained using systematic sampling. Subsequent collision points are determined randomly. A quota sampling scheme, which assigns N_K histories to the k-th first collision point, is used to allow a more intensive study of those histories that contribute the most error to the problem. Scoring is done at the second and the higher order of collision points using a statistical estimation technique; at each collision point the product of the weight of the particle and the conditional probability that the particle will reach the detector without further collision is scored for the appropriate detector energy-angle bin. The detector angle bins are determined by dividing the space about the detector into a number of solid angles with the apex at the detector.

A gamma ray history is terminated at the n-th collision if the number of collisions exceeds a prescribed number of collisions, the energy or weight of the particle fall below an energy or weight cutoff valve, or the distance of the particle from the detector exceeds a prescribed distance.

Two options in the program provide for further possible reduction of the variances of the estimates in addition to the sampling schemes mentioned above. One of these is the biased sampling of the scattering angle from the isotropic distribution. The program uses an isotropic distribution and corrects by weighting the particle properly according to the Klein-Nishina relationship. The other option is given the name exponential transformation. In this option the mean free path of a gamma ray is altered depending on the energy of the gamma ray, its position, and direction with respect to the detector.

Still another option in the program allows the generation and tracking of 0.5 Mev photons following pair-production events.

Printout includes the detector energy-angle distribution due to single scattered gamma rays, the detector energy-angle distribution due to total scattered radiation, a tabulation of various counts made in the course of the calculation, and a record of the contribution to the total flux by each order of scattering.

A complete description of program 15-2 was published.[55]

Program 16-0 employs both Monte Carlo and numerical methods to calculate the energy-angle distribution of neutrons at a point detector due to single and multiple scattering in air from a monoenergetic, monodirectional point source. The program is coded for an IBM 7090 computer with a fast memory capacity of 32,768 storage locations.

Neutron events allowed in program 16-0 are isotropic elastic scattering, anisotropic elastic scattering, inelastic scattering, radiative capture, and absorption without secondary emission. Parameters of gamma rays born during the course of a neutron history are recorded for future use in a gamma ray air-scattering program.

DECLASSIFIED

DECLASSIFIED

A neutron collision event is selected by random sampling from the appropriate discrete distribution for all neutron events allowed in the program. Thus, no weighting of a neutron is effected at a collision by the method of event selection.

The single-scattered contribution to the detector energy-angle distribution is computed by numerical integration, while the contribution due to second and higher order scattering is determined using Monte Carlo techniques.

First collision points for the Monte Carlo calculation are obtained using systematic sampling. Subsequent collision points are determined randomly. A quota sampling scheme, identical to the one used in program 15-2, is used in program 16-0. Scoring is done at second and higher order collision points using a statistical estimation technique. At each collision point, after selection of one of the allowed events, the probability that the particle will reach the detector without further collision is scored for the appropriate detector energy-angle bin. The detector angle bins are determined in the same manner as in program 15-2.

Neutron histories are always forced to terminate after a finite number of collisions because of one of the following factors: an absorption event, radiative capture, neutron energy below cutoff, the distance between detector and collision point exceeding a prescribed distance, or the neutron having had more than a prescribed number of collisions.

Printout from program 16-0 includes the energy-angle distribution for the single-scattered component, the energy-angle distribution for the total scattered radiation, and a record of the contribution to the total flux by each order of scattering.

A complete description of program 16-0 was published.[56]

DECLASSIFIED

DECLASSIFIED

9.8 REFERENCES

1. Duane, B. H., "Neutron and Photon Transport, Plane-Cylinder-Sphere, GE-ANPD Programs, Variational Optimum Formulation," GE-ANPD, XDC 59-9-118, September 1959.
2. Hanchon, K. B., "An Investigation into the Use of Program S-VII in Shielding Calculations," GE-ANPD, DC 61-1-92, January 20, 1961.
3. Capo, M. A., "Calculations of Leakage from the Bulk Shielding Reactor," GE-ANPD, DC 55-11-110, November 22, 1955.
4. Carver, J. G., Edwards, W. E., and MacDonald, J. E., "GE-ANPD Methods of Shield Design," GE-ANPD, APEX-230, December 30, 1955.
5. Martin, J. T., Yalch, J. P., and Edwards, W. E., "Shielding Computer Programs 14-0 and 14-1, Reactor Shield Analysis," GE-ANPD, XDC 59-2-16, January 23, 1959.
6. Martin, J. T., Yalch, J. P., and Edwards, W. E., "Shielding Computer Program 14-2, Reactor Shield Analysis," GE-ANPD, XDC 59-6-173, June 15, 1959.
7. Capo, M. A., Edwards, W. E., Loechler, J. J., and Paine, K. A., "Shielding Computer Program 04-4, Reactor Shield Analysis," GE-ANPD, XDC 59-7-150, March 1958.
8. Albert, R. D., and Welton, T. A., "A Simplified Theory of Neutron Attenuation and Its Application to Reactor Shield Design," Westinghouse Electric Corporation, WAPD-15, November 30, 1950.
9. Casper, A. W., "Modified Fast Neutron Attenuation Functions," GE-ANPD, XDC 60-2-76, February 3, 1960.
10. Haffner, J. W., and Van Valkenburg, H., "Modification of the Albert-Welton Point Kernel," GE-ANPD, XDC 55-9-150, September 20, 1955.
11. Kalos, M. H., "A Monte Carlo Calculation of the Transport of Gamma Rays," Nuclear Development Corporation of America, NDA 2056-10, March 15, 1957.
12. Belcher, J. A., "Comparison of Predicted and Experimental Dose Rates for Configurations Tested at the OTT," GE-ANPD, DC 59-10-76, November 6, 1959.
13. Casper, A. W., "Comparison of BSF Water Centerline Measurements with Predictions," GE-ANPD, XDC 58-11-208, November 6, 1958.
14. Schreiber, P. W., and Kodras, F. D., "Measured and Calculated Radiation Levels Within and Behind Beryllium Oxide," GE-ANPD, XDC 61-1-14, February 1961.
15. Schreiber, P. W., "Measured and Calculated Radiation Levels Within and Behind Beryllium," GE-ANPD, APEX-701, July 1961.
16. McDonald, M. D., "Shielding Computer Program 14-3, Data Check for Shielding Computer Programs 14-0, 14-1 and 14-2," GE-ANPD, XDC 59-3-52, December 10, 1958.
17. Henderson, B. J., "Conversion of Neutron or Gamma Ray Flux to Absorbed Dose Rate," GE-ANPD, XDC 59-8-179, August 14, 1959.
18. Hanchon, K. B., "Fast Neutron Dose Rate Calculations Incorporating Energy Dependence of Detector Response," GE-ANPD, DC 60-9-76, September 12, 1960.
19. Capo, M. A., "Comparison of Methods for Computing Fast Neutron Dose Rates," GE-ANPD, DC 59-10-77, October 8, 1959.
20. Casper, A. W., "A Plan for Parametric Neutron Penetration Calculations," GE-ANPD, DC 61-3-162, March 1961.
21. Campbell, D. J., "Program G-2," GE-ANPD, XDC 58-4-63, April 1958.
22. Haffner, J. W., "Use of Program G-2 for Shielding Calculations," GE-ANPD, DC 59-7-170, July 1959.
23. Martin, J. T., Yalch, J. P., and Edwards, W. E., "Shielding Computer Programs 14-0 and 14-1, Reactor Shield Analysis," GE-ANPD, XDC 59-2-16, January 1959.
24. Schreiber, P. W., and Kodras, F. D., "Measured and Calculated Radiation Levels Within and Behind Beryllium Oxide," GE-ANPD, XDC 61-1-149, February 1961.

DECLASSIFIED

DECLASSIFIED

25. Ferry, M. S., "Supplement 2 to APEX-515, Cross Sections for Reactor Analysis," GE-ANPD, XDC 60-6-148, April 1960.
26. Henderson, W. B., and Stanley, M. J., "Cross Sections for Reactor Analysis," GE-ANPD, APEX-515, December 1960.
27. Stanley, M. J., "Supplement I to APEX-515, Cross Sections for Reactor Analysis," GE-ANPD, XDC 59-11-72, October 1959.
28. Henderson, W. B., "Use of Decimal Input to Modify Program G-2 Composition Data," GE-ANPD, DCL 61-1-119, January 1961.
29. Henderson, B. J., "Conversion of Neutron or Gamma Ray Flux to Absorbed Dose Rate," GE-ANPD, XDC 59-8-179, August 1959.
30. Henderson, W. B., "Conversion of Program G-2 to IBM-7090," GE-ANPD, DCL 61-4-48, April 1961.
31. Haffner, J. W., "Thermal Flux Calculations," Proceedings of 5th Semiannual ANP Shielding Information Meeting," III, LNP-NR-47, May 14-15, 1958.
32. Gerado, H. A., and Belcher, J. A., "Preliminary Analysis of OTT Configurations Using Diffusion Theory," GE-ANPD, DC 58-11-147, November 1958.
33. Casper, A. W., "Data Report and Analysis of Battelle Pool Mapping," GE-ANPD, XDC 59-8-228, August 1959.
34. Schreiber, P. W., "Measured and Calculated Radiation Levels Within and Behind Beryllium," GE-ANPD, APEX-701, July 1961.
35. Goldstein, H., "Air Scattering of Gamma Rays and Neutrons," Nuclear Development Corporation of America, NDA Memo 12-3, April 20, 1953.
36. Loechler, J. J., MacDonald, J. E., and Van Valkenburg, H. M., "704 Program Report, Aircraft Nuclear Propulsion Shielding Program 05-0," GE-ANPD, XDC 59-8-218, July 31, 1959.
37. Haffner, J. W., Loechler, J. J., and MacDonald, J. E., "IBM 704 Program Report, Aircraft Nuclear Propulsion Shielding Program 09-0," GE-ANPD, APEX-533, December 1958.
38. Kalos, M. H., "Gamma Ray Penetration in Composite Slabs," Nuclear Development Corporation of America, NDA 2056-10, March 15, 1957.
39. Loechler, J. J., and MacDonald, J. E., "704 Program Report, Aircraft Nuclear Propulsion Shielding Program 07-1," GE-ANPD, XDC 60-3-103, February 2, 1960.
40. Haffner, J. W., Loechler, J. J., and MacDonald, J. E., "An IBM 704 Program Report, Aircraft Nuclear Propulsion Shielding Program 10-0," GE-ANPD, APEX-503, March 1958.
41. Spencer, Journal of Research of the National Bureau of Standards, "Physics and Chemistry," September-October 1959.
42. Henderson, B. J., and Patterson, H. W., "Single Scattering of Neutrons Through Ducts," GE-ANPD, DC 59-12-121, December 11, 1959.
43. Zoller, L. K., "Water Centerline Data Within the OTT," GE-ANPD, XDC 59-8-174, August 21, 1959.
44. Prince, A., "The Scattering of Neutrons by Air Ducts in Shields," GE-ANPD, XDC 59-7-119, July 17, 1959.
45. Fermi, E., "On the Motion of Neutrons in Hydrogenous Substances," NP-2385, 1951 (Translated from Ricerca Scientificia VII-2, 13, 1936).
46. Moteff, J., "Two-Component Method," American Nuclear Society Topical Meeting on Nucleonics in Flight, Dallas, Texas, March 29, 1961.
47. Avery, A. F., Bendall, D. E., Butler, J., and Spinney, K. T., "Methods of Calculation for Use in the Design of Shields for Power Reactors," SWP/P52, 1960.
48. Avery, A. F., "A Multigroup Method for Calculating Neutron Attenuations in Water," SWP/P60, 1959.
49. Henderson, B. J., and Gerardo, H. A., "Penetration of Neutrons from a Point Fission Source Through Lithium Hydride," GE-ANPD, DC 60-7-114, July 21, 1960.

DECLASSIFIED

DECLASSIFIED

50. Humphries, C. E., Warren C. S., and Wells, M. B., Private Communication, Convair.
51. Fermi, E., "On the Motion of Neutrons in Hydrogenous Substances," NP-2385, 1951. (Translated from Ricerca Scientificia VII-2, 13, 1936).
52. Lawil, F., "Surface Integration IBM Code," Convair, FZK-127, 1961.
53. MacDonald, J. E., Martin, J. M., and Yalch, J. P., "Specialized Reactor-Shield Monte Carlo Program 18-0," GE-ANPD, XDC 61-1-91, January 26, 1961.
54. MacDonald, J. E., and Loechler, J. J., "Flexible Monte Carlo Programs FMC-N and FMX-G," GE-ANPD, APEX-706, August 1961.
55. Baumgardt, N. R., Trampus, A., and MacDonald, J. E., "Program 15-2, Monte Carlo Calculation of Gamma Ray Scattering in Air," GE-ANPD, XDC 61-5-1, May 1961.
56. MacDonald, J. E., Baumgardt, N. R., and Trampus, A., "A Monte Carlo Calculation of Air Scattered Neutrons," GE-ANPD, DC 60-7-119, July 26, 1960.
57. Oswald, F. J., Schaffer, R., and Waldinger, H. V., "A Description of Monster, A Digital Computer Program for a Monte Carlo Reactor Shielding Calculation," Nuclear Development Corporation of America, NDA 2092-5, June 1958.
58. Rabinowitz, G., "Inclusion of Splitting as a Function of Energy, Photoneutron Production, and Variance Calculation in Program 18-0 (Monster)," Nuclear Development Corporation of America, NDA Memo 2123-1, April 18, 1960.
59. MacDonald, J. E., and Martin, J. M., "Shielding Computer Program 20-0," GE-ANPD, DC 60-10-98, October 21, 1960.
60. Capo, M. A., "Efficiency Studies With Specialized Reactor-Shield Monte Carlo Program 18-0," GE-ANPD, APEX-707, August 1961.
61. Mozer, F., Lockheed Missile Systems Division, and Leshan, E. J., American Standard, Atomic Energy Division, "A General Monte Carlo Code for Shielding Calculations," LNP-NP-47, Vol. II, Proceedings 5th Semiannual ANP Shielding Information Meeting, May 14-15, 1958.
62. Leshan, E. J., "A General Purpose Monte Carlo Program for the IBM 704, Part I, Method," American Radiation and Standard Sanitary Corporation, Atomic Energy Division, September 1956.
63. Loechler, J. J., "Flexible Monte Carlo Source Generator," GE-ANPD, XDC 61-4-52, April 1961.
64. Scherer, L. H., "FMC Flux Conversion," GE-ANPD, DC 60-10-26, October 4, 1960.
65. Goldstein, H., and Wilkins, J. E., "Calculations of the Penetration of Gamma Rays," Nuclear Development Corporation of America, NYD 3075, June 30, 1954.
66. Goldstein, H., and Krumbein, A. D., "Moments Method Calculation of the Penetration of Neutrons from a Point Fission Source Through Be and BeO," Nuclear Development Corporation of America, NDA Memo 2124-1, May 27, 1960.
67. Henderson, B. J., and Gerardo, H. A., "Penetration of Neutrons From a Point Fission Source Through Lithium Hydride," GE-ANPD, DC 60-7-114, July 21, 1960.
68. Goldstein, H., and Mechanic, H., "Penetration of Neutrons from a Point Fission Source Through Beryllium and Beryllium Oxide," Nuclear Development Corporation of America, NDA 2092-9, June 23, 1958.
69. Goldstein, H., "Information on the Cross Sections Used for Moments Method Calculations in LiH," Nuclear Development Corporation of America, NDA Memo 2125-1, April 1, 1960.
70. Code, C. J., Jr., "Description of Beryllium n, 2n Reaction for FMC-N," GE-ANPD, August 1961.

DECLASSIFIED

DECLASSIFIED

DECLASSIFIED

DECLASSIFIED
CONFIDENTIAL

10. SHIELD NUCLEAR DATA

Shield nuclear data summarized and referenced in this section are: (1) source data, (2) neutron penetration data, (3) gamma ray penetration data, and (4) conversion factors. The work completed on the effort to compile adequate basic nuclear data for Monte Carlo shield analysis is described and referenced. Some early shield nuclear data, now nearly obsolete, are also referenced to provide a complete history of the shield physics program.[1, 2]

10.1 SOURCE DATA

In order to predict with any degree of realism, the heat generation in reactor shield assemblies, as well as the radiation leakage, it is necessary to know the distribution of the total energy released per fission between the fission fragments, fission neutrons, gamma radiation, and beta radiation. Consequently, several important compilations of source data were prepared in support of the reactor and shield physics efforts.

Data defining the distribution of the fission energy of uranium-235 were published.[3] Later, more comprehensive data on prompt fission gamma rays were compiled.[4] Summarizing from these two reports, the energy released, when a nucleus of uranium-235 undergoes thermal neutron-induced fission, is distributed among the six components as shown in Table 10.1

The thermodynamically available energy per thermal fission, therefore, is 191.48 Mev. This does not include the energy from processes which may follow fission, such as neutron inelastic scattering or neutron radiative capture. For power level determinations, this corresponds to 3.26×10^{10} fissions per watt-second.

The latest and possibly the most accurate data available on the gamma rays associated with the fission of uranium-235 both during fission and for long times afterward were published in a manner convenient for use in shielding calculations.[4] The gamma rays are categorized as: (1) the so-called "prompt" gamma rays occurring within a period of 5×10^{-8} seconds after fission, (2) the gamma rays emitted between 5×10^{-8} seconds and 10^{-6} sec-

TABLE 10.1

ENERGY DISTRIBUTION FOR THERMAL U-235 FISSION, Mev

Kinetic energy of fission fragments	165.
Kinetic energy of fission neutrons	4.75
Prompt gamma radiation	7.53
Fission product decay gamma radiation	6.55
Fission product decay beta radiation	7.65
Neutrino energy	10.
Total energy per fission	201.48

CONFIDENTIAL
DECLASSIFIED

DECLASSIFIED

CONFIDENTIAL

onds after fission (the so-called "short half-life" gamma rays), (3) the gamma rays emitted between 10^{-6} seconds and 1 second after fission (which may be termed intermediate life gamma rays), and (4) the gamma rays usually referred to as "delayed" gamma rays, which are emitted at times greater than 1 second after fission.

No experimental or theoretical quantitative data on the intermediate life gamma rays were found; therefore, several possible schemes of interpolation between the known endpoints of the time interval were considered. It was finally assumed that the estimated energy release of 0.68 Mev per fission can be neglected compared to the 7.53 Mev of prompt gamma radiation.

Source strengths of gamma rays from fission of uranium-235 for an operating time of 100 hours are summarized in Tables 10.2 and 10.3. Alternate group structures are given for the energy range 0 to 3 Mev.

TABLE 10.2

SOURCE STRENGTHS OF GAMMA RAYS FROM FISSION OF U-235 FOR OPERATING TIME OF 100 HOURS

			Source Strengths (Mev per fission)				
(1) Group Designation	(2) Energy Range, Mev	(3) Typical Energy Of Group, Mev	(4) Prompt	(5) Short Half-Life	(6) Invariant Part = (4) + (5)	(7) Delayed	(8) Total = (6) + (7)
A	0-1	0.5	(3.146)	(0.224)	(3.370)		
B	1-2	1.5	(2.229)	(0.082)	(2.311)		
C	2-3	2.5	(1.183)		(1.183)		
Subtotal	0-3.0		(6.558)	(0.306)	(6.864)		
1	0-0.4	0.3	0.965	0.129	1.094	0.336	1.430
2	0.4-0.9	0.7	1.873	0.086	1.959	1.465	3.424
3	0.9-1.35	1.0	1.320	0.033	1.353	1.093	2.446
4	1.35-1.8	1.5	0.878	0.033	0.911	0.964	1.875
5	1.8-2.2	2.0	0.656	0.025	0.681	0.665	1.346
6	2.2-2.6	2.5	0.503		0.503	0.534	1.037
7	2.6-3.0	2.8	0.363		0.363	0.351	0.714
Subtotal	0-3.0		6.558	0.306	6.864	5.408	12.272
8	3-4	3.5	0.559		0.559	0.554	1.113
9	4-5	4.5	0.252		0.252	0.216	0.468
10	5-6	5.5	0.111		0.111	0.040	0.151
11	6-7	6.5	0.040		0.040		0.040
12	7-7.5	7.0	0.015		0.015		0.015
	>7.5		<0.003				
Total	0-7.5		7.535	0.306	7.841	6.218	14.059

Source strengths of fission product decay gamma rays for shutdown calculations are available in references 5, 6, and 7. Graphs of decay rate as a function of shutdown time for seven energy groups and reactor operating times of 0.25, 1, 3, 10, 30, 100, 300, and 1000 hours were published.[5] Shutdown times range from 167 seconds to 100 days. With the exception of the curves for 0.25 hours of operation, the data were all taken or interpolated from a paper by J. F. Perkins and R. W. King.[8] The data for 0.25 hours of operation were taken from a report by J. F. Scoles.[9] These data have been used in most recent shielding calculations for shutdown times exceeding 25 minutes.

Data from a report by M. R. Smith[6] have been used in calculations for shutdown times of less than 25 minutes. These data were obtained by integrating data reported by Knabe and Putnam[10] over specific reactor histories. Knabe and Putnam combined the experimental results of Maienschein, et al., at the Oak Ridge National Laboratory[11] and the computed data of Perkins and King. The decay gamma data reported by Knabe and Putnam

CONFIDENTIAL

DECLASSIFIED

TABLE 10.3

SOURCE STRENGTHS OF GAMMA RAYS FROM FISSION OF U-235 FOR OPERATING LIFE OF 100 HOURS

			Source Strengths (Photons per fission)				
(1) Group Designation	(2) Energy Range, Mev	(3) Typical Energy Of Group, Mev	(4) Prompt	(5) Short Half-Life	(6) Invariant Part = (4) + (5)	(7) Delayed	(8) Total = (6) + (7)
A	0-1	0.5	(8.055)	(1.059)	(9.114)		
B	1-2	1.5	(1.619)	(0.0547)	(1.674)		
C	2-3	2.5	(0.493)		(0.493)		
Subtotal	0-3		(10.167)	(1.114)	(11.281)		
1	0-0.4	0.3	4.629	0.898	5.527	1.121	6.648
2	0.4-0.9	0.7	3.102	0.151	3.253	2.325	5.578
3	0.9-1.35	1.0	1.196	0.0306	1.227	0.994	2.221
4	1.35-1.8	1.5	0.568	0.0207	0.589	0.622	1.211
5	1.8-2.2	2.0	0.330	0.0132	0.343	0.334	0.677
6	2.2-2.6	2.5	0.211		0.211	0.224	0.435
7	2.6-3.0	2.8	0.131		0.131	0.128	0.259
Subtotal	0-3.0		10.167	1.114	11.281	5.748	17.029
8	3-4	3.5	0.164		0.164	0.161	0.325
9	4-5	4.5	0.0575		0.0575	0.0492	0.107
10	5-6	5.5	0.0203		0.0203	0.00762	0.0279
11	6-7	6.5	5.25(-3)		5.25(-3)		5.25(-3)
12	7-7.5	7.0	2.12(-3)		2.12(-3)		2.12(-3)
	>7.5						
Total	0-7.5		10.416	1.114	11.530	5.966	17.496

CONFIDENTIAL

CONFIDENTIAL

DECLASSIFIED

gives the time variation of the photon number release rate for an instantaneous thermal fission event for uranium-235 and also states the time dependence of the average energy per photon for the various energy groups considered. Smith reported the decay gamma energy release rate as a function of time after shutdown for nine different reactor operating histories ranging from one second to 10^8 seconds at one watt. He reports energy release rates for six groups in the energy range 0 to 2.6 Mev and for six groups in the energy range 2.6 to 5.5 Mev. Data are also given for the combination of the upper six groups and for the combination of all 12 groups.

A later report[7] by M. R. Smith supplements and in part supersedes his earlier report.[6] The later report represents an attempt to remove basic data discrepancies and improve the treatment of the decay gamma activity in the six groups of the energy range 2.6 to 5.5 Mev. Decay gamma energy release rates are presented as a function of time after shutdown for reactor operation times of 1 second, 1 hour, and 10^8 seconds at a constant power level of one watt. The results are presented in both tabular and graphic form.

The energy spectra of gamma rays resulting from thermal neutron capture were compiled for 48 elements.[12] The data are presented in both graphical and tabular form. Thermal neutron-capture cross sections, isotopic abundances, binding energies of the extra neutron in the isotopes, and weighted-average binding energies are also tabulated.

10.2 NEUTRON PENETRATION DATA

The modified Albert-Welton function used in the point kernel programs for computing fast neutron dose rates in hydrogenous materials was given in section 9.2 as follows:

$$\Psi_n(\Sigma_m, \rho_m) = \alpha_1 \left[\sum_{m=1}^{L} \eta_m \rho_m\right]^2 \exp\left\{-\alpha_3 \left[\sum_{m=1}^{L} \eta_m \rho_m\right]^{\alpha_4}\right\} \exp\left[\sum_{m=1}^{M} \rho_m \Sigma_m\right] \exp \sum_{m=1}^{L} \eta_m \rho_m < \alpha_6: \quad (1)$$

Recommended values of the coefficients of this function are:

$\alpha_1 = 6.944 \times 10^{-5}$
$\alpha_2 = 0.34921$
$\alpha_3 = 0.42231$
$\alpha_4 = 0.69842$

These coefficients give dose rates in ethylene rads per hour for a source of 1 fission per second. Distances must be in centimeters.

These coefficients were obtained by fitting dose rate data measured in water at the GE-ANPD Source Plate Facility at Battelle Memorial Institute. The data were published,[13] as was the derivation of the above coefficients.[14] The effect of oxygen was eliminated[15] by assuming a removal cross section of 0.92 barns ±.05. Coefficient α_4 was assumed to be $2\alpha_2$.

Computations using these coefficients were compared with measurements made at the Bulk Shielding Facility and the Lid Tank Facility at Oak Ridge National Laboratory.[14] Table 10.4 summarized the agreement obtained.

Monte Carlo calculations were made at the Nuclear Development Corporation of America under subcontract.[16] The calculations showed that the dose rate integrated over the surface of a sphere, a large distance from the surface of a finite sphere of lithium hydride surrounding a point-fission source, is 0.71 times that at the same depth of lithium hydride in an infinite medium. Later Monte Carlo calculations made here as part of a more ex-

DECLASSIFIED

DECLASSIFIED

TABLE 10.4

COMPARISON OF COMPUTED AND MEASURED FAST NEUTRON DOSE RATES IN WATER

Facility	Range, centimeters	Maximum Difference, %	Average Difference, %
GE-ANPD Source Plate	12.1 - 97	7.3	3.2
ORNL Bulk Shielding Facility	10 - 130	16.4	7.4
ORNL Lid Tank	10 - 120	15.9	9.1

tensive investigation gave ratios between 0.6 and 0.65. Therefore α_1 is usually arbitrarily reduced 30 percent for calculating dose rates outside finite hydrogenous shields.

Effective fast-neutron-removal cross sections used in the modified Albert-Welton function for elements other than hydrogen are given in Table 10.5. The interpolated values were calculated by using the equations

$$\Sigma/\rho = 0.19\ Z^{-0.743} \quad \text{for } Z \leq 8 \tag{2}$$

and

$$\Sigma/\rho = 0.125\ Z^{-0.565} \quad \text{for } Z > 8, \tag{3}$$

which are the equations of curves positioned by eye to best fit measured broad-beam removal cross sections. The cross section for lithium in lithium hydride was measured in the GE-ANPD Source Plate Facility and was reported.[17] It gives good agreement with experiment when used in conjunction with the Albert-Welton function and the coefficients presented in this section. All other measured cross sections were taken from the references indicated in the table. Interpolated values are included in the table for elements for which measured values are available, in order to show the accurace of the fit. Measured values are always used when available.

Since the Albert-Welton function is not valid for very small thicknesses of hydrogenous material, the point kernel programs switch to the following alternate function when

$$\Psi_n(\Sigma_m, \rho_m) = \alpha_5 \exp\left\{-\alpha_7 \left[\sum_{m=1}^{L} \eta_m \rho_m\right]\right\} \exp\left[-\sum_{m=1}^{M} \Sigma_m \rho_m\right] \tag{4}$$

A value of 8.262 is somewhat arbitrarily used for α_6. This corresponds to a lithium hydride thickness of 10 centimeters where the Albert-Welton curve begins to deviate sharply from the actual dose rate curve.

Coefficient α_5 equals $4\pi\rho^2$ times the dose rate at the source position. Although this is not exactly the same in all materials, the same value is used for consistency. However, different values are used for internal and external receiver positions. The values of α_5 used were established by extrapolating to zero the exponential approximations of theoretical dose rate curves in beryllium and beryllium oxide. Such curves were computed for infinite media by the Nuclear Development Corporation of America and were published.[18] Later Monte Carlo calculations were made for both finite and infinite media; the infinite media results agree closely with the NDA moments method results. Effective removal cross sections, which were determined from these curves, are used for computing dose rates in these materials by using Equation (4) and equating α_7 to zero.

Coefficient α_7 for hydrogenous materials is adjusted so that Equations (4) and (1) are in coincidence at α_6 which equals 8.262. Here again, separate values are used for internal and external receiver positions.

DECLASSIFIED

DECLASSIFIED

CONFIDENTIAL

TABLE 10.5

EFFECTIVE BROAD BEAM NEUTRON REMOVAL CROSS SECTION

Element	Atomic Number Z	Σ/ρ, cm^2/gm (Measured)	Σ/ρ, cm^2/gm (Interpolated)
Aluminum	13	0.0292 ± 0.0012[4]	0.0293
Antimony	51		0.0136
Argon	18		0.0244
Arsenic	33		0.0173
Barium	56		0.0129
Beryllium	4	0.0717 ± 0.0043[4]	0.0678
Bismuth	83	0.0101 ± 0.0010[4]	0.0103
Boron	5	0.0540 ± 0.0054[4]	0.0575
Bromine	35		0.0168
Cadmium	48		0.0140
Calcium	20		0.0230
Carbon	6	0.0407 ± 0.0024[4]	0.0502
Cerium	58		0.0126
Cesium	55		0.0130
Chlorine	17	0.020 ± 0.014[4]	0.0252
Chromium	24		0.0208
Cobalt	27		0.0194
Copper	29	0.0194 ± 0.0011[4]	0.0186
Dysprosium	66		0.0117
Erbium	68		0.0115
Europium	63		0.0120
Fluorine	9	0.0409 ± 0.0020[4]	0.0361
Gadolinium	64		0.0119
Gallium	31		0.0180
Germanium	32		0.0176
Gold	79		0.0106
Hafnium	72		0.0112
Helium	2		0.1135
Holmium	67		0.0116
Indium	49		0.0139
Iodine	53		0.0133
Iridium	77		0.0107
Iron	26	0.0214 ± 0.0009[4]	0.0198
Krypton	36		0.0165
Lanthanum	57		0.0127
Lead	82	0.0103 ± 0.0009[4]	0.0104
Lithium	3	0.094 ± 0.007[13]	0.0840
Lutetium	71		0.0112
Magnesium	12		0.0307
Manganese	25		0.0203
Mercury	80		0.0105
Molybdenum	42		0.0151
Neodymium	60		0.0124
Neon	10		0.0340
Nickel	28	0.0190 ± 0.0010[4]	0.0190
Niobium	41		0.0153
Nitrogen	7		0.0448
Osmium	76		0.0108
Oxygen	8	0.031 ± 0.002[12]	0.0405

CONFIDENTIAL

DECLASSIFIED

DECLASSIFIED

TABLE 10.5 (Cont'd.)

EFFECTIVE BROAD BEAM NEUTRON REMOVAL CROSS SECTION

Element	Atomic Number Z	Σ/ρ, cm^2/gm (Measured)	Σ/ρ, cm^2/gm (Interpolated)
Palladium	46		0.0144
Phosphorus	15		0.0271
Platinum	79		0.0107
Potassium	19		0.0237
Praseodymium	59		0.0125
Radium	88		0.0100
Rhenium	75		0.0109
Rhodium	45		0.0145
Rhubidium	37		0.0163
Ruthenium	44		0.0147
Samarium	62		0.0121
Scandium	21		0.0224
Selenium	34		0.0170
Silicon	14		0.0281
Silver	47		0.0142
Sodium	11		0.0322
Strontium	38		0.0160
Sulfur	16		0.0261
Tantalum	73		0.0111
Tellurium	52		0.0134
Terbium	65		0.0118
Thallium	81		0.0104
Thorium	90		0.0098
Thullium	69		0.0114
Tin	50		0.0137
Titanium	22		0.0218
Tungsten	74	0.00821 ± 0.00181[4]	0.0110
Uranium	92	0.0091 ± 0.0010[4]	0.0097
Vanadium	23		0.0213
Xenon	54		0.0131
Ytterbium	70		0.0113
Yttrium	39		0.0158
Zinc	30		0.0183
Zirconium	40		0.0156

Coefficients established by these procedures are summarized in Table 10.6 for finite and infinite media for beryllium, beryllium oxide, and hydrogenous materials.

The material attenuation function coded in the 14-series programs for computing differential neutron number flux (from section 9.2) is:

$$\Psi_n(E_n, \rho_m) = \exp \sum_{\beta=0}^{K} \left[\sum_{i=0}^{I} b_{ki}(p) \, (X_p)^i \right] (E_n)^k \qquad (5)$$

Differential neutron number spectra computed by moments method solution of the Boltzmann transport equation for infinite homogenous media of water,[19] beryllium,[18] beryllium oxide,[18] and lithium hydride[20] were fitted by the above expression. The coefficients, b_{ki}, for each material are presented in Tables 10.7, 10.8, 10.9, and 10.10. The source

DECLASSIFIED

CONFIDENTIAL

TABLE 10.6

FAST NEUTRON DOSE RATE FUNCTION COEFFICIENTS

Receiver	α_1 rad(ethylene)-cm^2-sec / hr-fission	α_2	α_3	α_4	α_5 rad(ethylene)-cm^2-sec / hr-fission	α_6	α_7	Σ/ρ cm^2/gm
Internal Receiver								
Hydrogenous	6.944×10^{-5}	0.34921	0.42231	0.69842	1.4×10^{-4}	8.262	0.2188	
Beryllium					1.4×10^{-4}			0.071
Beryllium oxide					1.4×10^{-4}			0.045
External Receiver								
Hydrogenous	4.861×10^{-5}	0.34921	0.42231	0.69842	7.5×10^{-5}	8.262	0.1863	
Beryllium					7.5×10^{-5}			0.0745
Beryllium oxide					7.5×10^{-5}			0.0478

CONFIDENTIAL

DECLASSIFIED

CONFIDENTIAL

TABLE 10.7

BIVARIANT POLYNOMIAL COEFFICIENTS FOR COMPUTING DIFFERENTIAL NEUTRON NUMBER SPECTRA IN WATER

Source: Isotropic, Point U^{235} Fission - one neutron per second
Range: $0 \leq X \leq 120$ gm/cm^2
Energy Range: 0.33 Mev $\leq E_n \leq$ 10.9 Mev

k \ i	0	1	2	3
0	-8.02010/-1	-8.43334/-2	-6.84948/-4	3.90014/-6
1	-1.36141/-1	-5.09570/-2	4.70700/-4	-1.02522/-6
2	-7.11817/-2	1.91231/-2	-1.10198/-4	-1.25674/-7
3	-6.38719/-4	-2.39958/-3	9.59928/-6	5.41859/-8
4	2.75980/-4	9.86242/-5	-2.69196/-7	-3.39646/-9

Note: Maximum absolute percent deviation at discrete values = 36.7
Mean absolute percent deviation at discrete values = 6.6

TABLE 10.8

BIVARIANT POLYNOMIAL COEFFICIENTS FOR COMPUTING DIFFERENTIAL NEUTRON NUMBER SPECTRA IN BERYLLIUM

Source: Isotropic, Point U^{235} Fission - one neutron per second
Range: $10 \leq X \leq 180$ gm/cm^2

Energy Range: 0.066 Mev $\leq E_n \leq$ 1.63 Mev

k \ i	0	1	2
0	3.3829/0	-5.83640/-2	-8.82617/-5
1	-1.04453/1	-1.03148/-2	7.88869/-5
2	1.73345/1	3.74824/-3	-1.17541/-4
3	-1.36715/1	8.74276/-3	6.11033/-5
4	3.78860/0	-4.36956/-3	-1.09195/-5

Note: Maximum absolute percent deviation at discrete values = 37.3
Mean absolute percent deviation at discrete values = 12.0

Energy Range: 1.63 Mev $\leq E_n \leq$ 17 Mev

k \ i	0	1	2	3
0	4.5275/0	9.49075/-3	-5.36033/-4	1.59023/-6
1	-4.42937/0	-4.88438/-2	1.96995/-4	-7.46214/-7
2	1.23290/0	1.03856/-2	-2.87897/-5	1.88894/-7
3	-1.79488/-1	-9.44268/-4	1.53373/-6	-2.47215/-8
4	1.15565/-2	3.81766/-5	2.10757/-9	1.50819/-9
5	-2.6869/-4	-5.57700/-7	-1.48842/-9	-3.40779/-11

Note: Maximum absolute percent deviation at discrete values = 25.8
Mean absolute percent deviation at discrete values = 7.73

CONFIDENTIAL

DECLASSIFIED

UNCLASSIFIED

CONFIDENTIAL

TABLE 10.9

BIVARIANT POLYNOMIAL COEFFICIENTS FOR COMPUTING DIFFERENTIAL NEUTRON NUMBER SPECTRA IN BERYLLIUM OXIDE

Source: Isotropic, Point U^{235} Fission - one neutron per second
Range: $20 \leq X \leq 210$ gm/cm^2

Energy Range: 0.066 Mev $\leq E_n \leq$ 2.44 Mev

k \ i	0	1	2	3	4
0	2.80081/0	6.98856/-3	-6.89484/-4	3.38955/-6	-6.01244/-9
1	-6.79955/0	-7.63398/-2	6.89303/-4	2.29194/-6	2.44231/-9
2	7.42073/0	7.95360/-2	-4.3500/-4	-2.07216/-7	3.61096/-9
3	-4.06749/0	-3.76861/-2	1.23484/-4	9.53758/-7	-3.94186/-9
4	7.80211/-1	6.74247/-3	-1.69318/-5	-2.38693/-7	9.07269/-10

Note: Maximum absolute percent deviation at discrete values = 18.6
Mean absolute percent deviation at discrete values = 9.9

Energy Range: 2.44 Mev $\leq E_n \leq$ 16 Mev

k \ i	0	1	2
0	2.1368/0	6.77527/-2	-3.76588/-4
1	-1.50501/0	-7.14633/-2	2.12941/-4
2	1.43574/-1	1.47608/-2	-4.18866/-5
3	-1.13215/-2	1.18203/-3	3.24569/-6
4	2.99331/-4	3.18483/-5	-8.55890/-8

Note: Maximum absolute percent deviation at discrete values = 40.4
Mean absolute percent deviation at discrete values = 14.7

TABLE 10.10

BIVARIANT POLYNOMIAL COEFFICIENTS FOR COMPUTING DIFFERENTIAL NEUTRON NUMBER SPECTRA IN LITHIUM HYDRIDE

Source: Isotropic, Point U^{235} Fission - one neutron per second
Range: $11.4 \leq X \leq 103$ gm/cm^2

Energy Range: 0.0603 Mev $\leq E_n \leq$ 2 Mev

k \ i	0	1	2	3
0	1.95376/0	-2.22241/-1	-6.32306/-5	4.47879/-6
1	-5.96583/0	5.64267/-2	-9.22977/-4	4.72108/-6
2	5.84584/0	-8.25182/-2	1.57925/-3	-8.88733/-6
3	-1.79414/0	2.99882/-2	-5.88268/-4	3.36041/-6

Note: Maximum absolute percent deviation at discrete values = 11.1
Mean absolute percent deviation at discrete values = 4.5

Energy Range: 2 Mev $\leq E_n \leq$ 18 Mev

k \ i	0	1	2	3
0	6.1359/-1	-2.43672/-1	3.78118/-4	2.23514/-6
1	-9.81261/-1	2.90514/-2	-5.03296/-4	2.46920/-6
2	2.70911/-2	-2.25179/-3	6.30391/-5	-3.63487/-7
3	-9.76967/-4	6.51995/-5	-2.04231/-6	1.23150/-8

Note: Maximum absolute percent deviation at discrete values = 13.4
Mean absolute percent deviation at discrete values = 3.2

CONFIDENTIAL

UNCLASSIFIED

DECLASSIFIED

strength is normalized to 1 fission neutron per second. The criterion of minimization was the sum of the squared magnitude deviations.

Comparisons of calculations which were made using data presented in Tables 10. 1 through 10. 10, and measured data in beryllium and beryllium oxide were published.[21, 22]

Data similar to those in Table 10. 10 were determined by Monte Carlo methods and reported for monoenergetic 1, 2, 4, 6, 8, and 10 Mev sources in lithium hydride.[23] However, the calculations were part of a pilot study to establish a program of parametric penetration calculations and may not be statistically accurate.

Graphs of neutron dose rate and heating rate versus penetration depth may be conveniently applied by means of the comparison method for preliminary shielding calculations. Penetration data for beryllium, beryllium oxide, and lithium hydride were computed by a moments method solution of the Boltzmann transport equation by the Nuclear Development Corporation of America under subcontract. Their results were reported.[17, 18] The results are summarized in Figures 10. 1, 10. 2, and 10. 3. Because of its importance as a nuclear rocket propellant, a curve of fast-neutron absorbed dose rate versus penetration depth is presented in Figure 10. 4 for hydrogen. These data also are the result of NDS moments calculations. Fast neutron attenuation curves for several hydrogenous materials were published.[24,25] They were all computed using the modified Albert-Welton function. Even though earlier, less accurate coefficients were used for the calculation, the curves may still be useful for preliminary predictions.

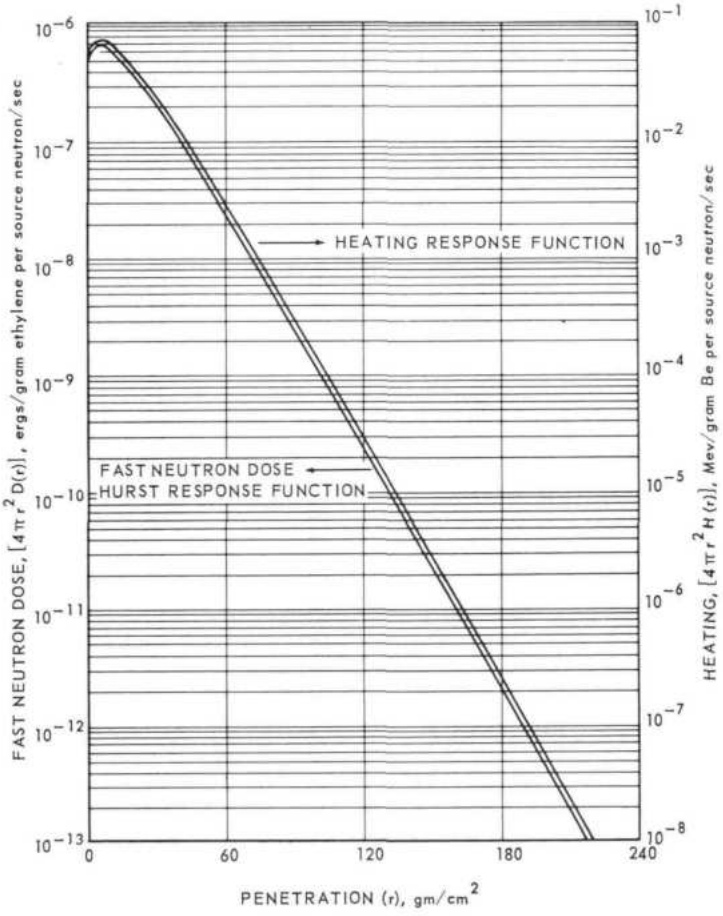

Fig. 10.1 – Fast neutron dose and heating ($4\pi r^2$) versus penetration due to a unit, point, isotropic fission neutron source in Be

DECLASSIFIED

DECLASSIFIED

CONFIDENTIAL

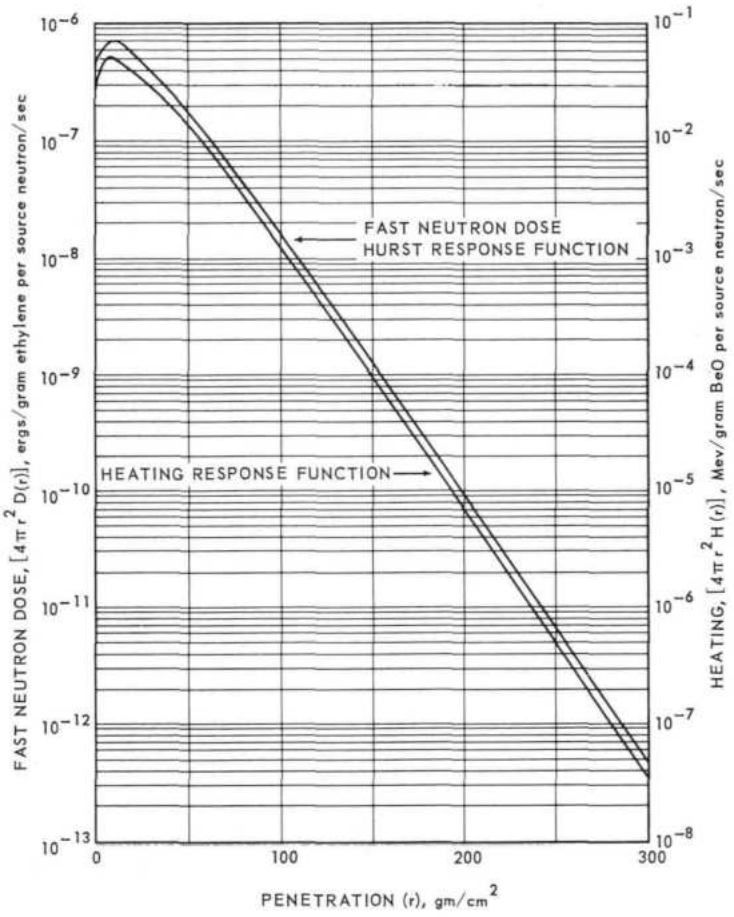

Fig. 10.2 – Fast neutron dose and heating ($4\pi r^2$) versus penetration due to a unit, point, isotropic fission neutron source in BeO

10.3 GAMMA RAY PENETRATION DATA

The compilation of basic gamma ray cross section data published[26] by G. White Grodstein, is reasonably adequate for most shielding requirements, and there is little need for reproduction of those data here. However, several GE-ANPD documents, which reported rather unique manipulations or tabulations of these and other data, are worthy of reference.

Photoelectric, pair-production, Compton, and total gamma ray cross sections were published[27] for 33 energy levels over the range 0.01 Mev to 10 Mev. Data are presented for several elements, mixtures, and compounds. Interpolated or extrapolated data are included for many energy levels and elements not listed by Grodstein. Also tabulated in the referenced work are the ratios of the Compton scattering cross section to the total cross section. Values of the differential Compton scattering cross section, $d\sigma/\Omega$, are tabulated for 30 angles over the range 0 to 180 degrees for the same 33 energy levels. In addition, the Compton scattering cross section, reduced to a normalized cumulative density function for various energy groups, is included for use in the flexible Monte Carlo program (FMC-G).

CONFIDENTIAL

DECLASSIFIED

DECLASSIFIED

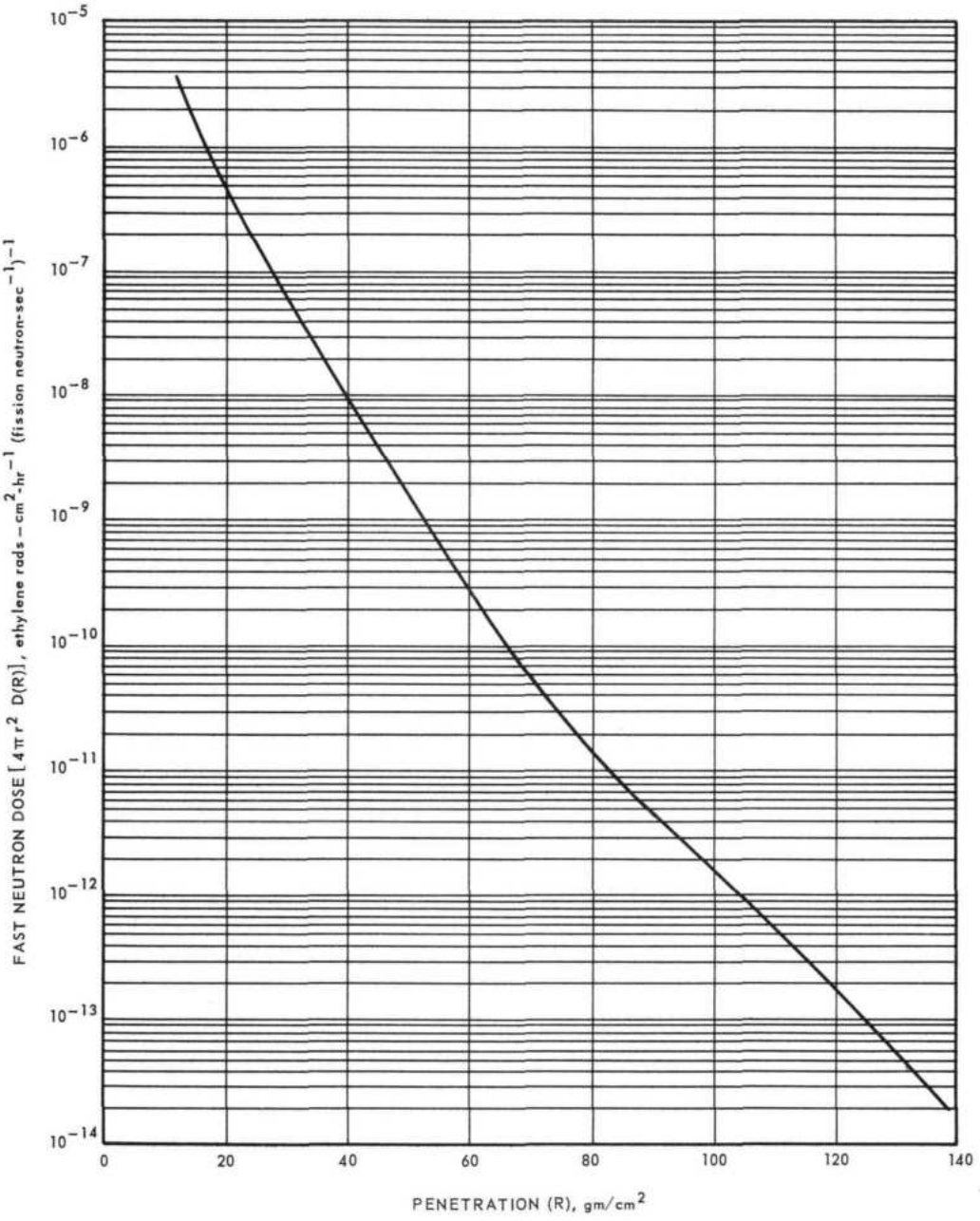

Fig. 10.3 – Fast neutron dose ($4\pi r^2$) versus penetration due to a unit, point, isotropic fission neutron source in air

DECLASSIFIED

DECLASSIFIED

CONFIDENTIAL

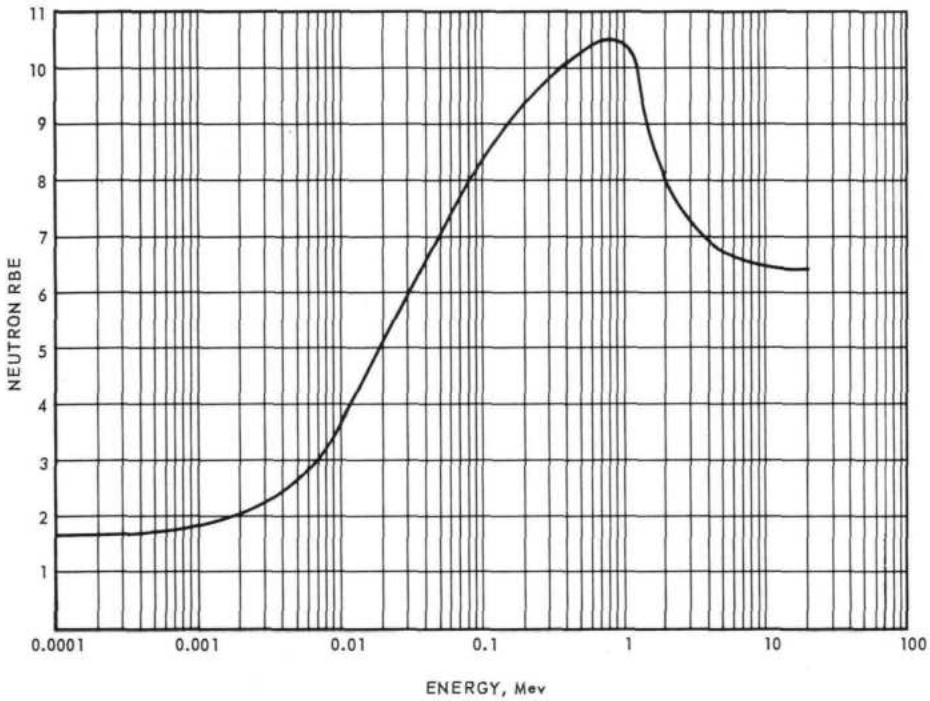

Fig. 10.4 – Maximum neutron relative biological effectiveness

Mass gamma ray total and energy absorption coefficients were tabulated as a function of energy from 0.2 Mev to 10 Mev for various elements, mixtures, and compounds. Most of these data for elements were taken from Grodstein,[26] but data for certain elements and energy levels were interpolated by using bivariant polynomial expressions fitted to his data. Absorption coefficients for elements of atomic number 1 to 11 were accurately approximated by:

$$\mu/\rho_{calc}(1/Z, E) = \sum_{i=0}^{I} \sum_{j=0}^{J} a_{ij}(1/Z)^i(E)^j = \mu/\rho_{meas} - \epsilon_{ij}(1/Z, E) \qquad (6)$$

where:

Z = atomic number
E = gamma ray energy, Mev
μ/ρ calc = approximated mass absorption coefficient, cm^2/gm
μ/ρ meas = NBS-583 mass absorption coefficient, cm^2/gm

For elements of higher atomic numbers, 20 to 92, a modification of the form of the independent variables, Z and E, was required:

$$\mu/\rho_{calc}(Z, 1/E) = \sum_{i=0}^{I} \sum_{i=0}^{J} a_{ij}(Z)^i(1/E)^j = \mu/\rho_{meas} - \epsilon_{ij}(Z, 1/E) \qquad (7)$$

For both ranges of atomic number (1 to 11 and 20 to 92), it was necessary to fit the above expressions over two ranges of energy (0.2 Mev to 2 Mev, 2 Mev to 10 Mev) to obtain a good approximation. No suitable expression was obtained to approximate the absorption coefficients for elements of atomic numbers 12 to 19. Coefficients of the above expressions were derived by the method of least squares. The criterion of minimization was the sum of the squared percent deviations.

Coefficients of polynomials fitted to linear gamma ray total absorption coefficients (both including and excluding coherent scattering) for use in the single-scattering programs dis-

CONFIDENTIAL

DECLASSIFIED

DECLASSIFIED

cussed in section 9.4, were published.[28] Coefficients are presented for air, water, lead, aluminum, lithium hydride, and polyethylene over several energy ranges.

As discussed in section 9.2, buildup factors, which were computed by a moments method solution of the Boltzmann transport equation by the Nuclear Development Corporation of America, are used in the point kernel programs for dose rate, energy flux, and energy absorption rate calculations. The buildup factors are approximated by cubic polynomials. Reference 29 contains tables of buildup polynomial coefficients for each type buildup and each material considered in NYD-3075[30] for point isotropic sources. In order to tabulate coefficients for source energies not considered in reference 30, the NDA data were fitted by bivariant polynomials which were then evaluated at the energies of interest to obtain coefficients of the cubic polynomial used in the point kernel programs.

For low Z materials the buildup factor was approximated by:

$$B_{calc}(\mu_{or}, 1/E) = \sum_{j=0}^{J}\sum_{i=0}^{I} C_{ij}\left[\mu_{or}\right]^{i}\left[1/E\right]^{j} = B_{meas} - \epsilon_{ij}(\mu_{or}, 1/E) \qquad (8)$$

where:

μ_{or} = number of relaxation lengths
E = gamma ray energy
B_{calc} = approximated buildup factor
B_{meas} = NYD-3075 buildup factor

For high Z materials a modification of the independent variable, E, was necessary:

$$B_{calc}(\mu_{or}, E) = \sum_{j=0}^{J}\sum_{i=0}^{I} C_{ij}\left[\mu_{or}\right]^{i}\left[E\right]^{j} = B_{meas} - \epsilon_{ij}(\mu_{or}, E) \qquad (9)$$

Complete tabulations of the bivariant polynomial and the cubic polynomial coefficients are included in the reference. Cubic polynomial coefficients for computing dose rate in water, iron, and lead are presented in Tables 10.11, 10.12, and 10.13 typical frequently used data.

Coefficients C_2 and C_3, of Equation (13) in section 9, for combining buildup factors for water followed by lead or iron are -1.7 and -1, respectively.

Reference 31 discusses several of the different types of buildup factors which have been defined and tabulated and examines the criteria for choice of a particular type for use in computing gamma ray heating rates. NDA energy absorption buildup factors are recommended for single-material shields, and energy buildup followed by energy absorption buildup is recommended for two-material shields.

The material attenuation function coded in Shielding Computer Programs 14-0, 14-1, and 14-2 for calculating gamma ray energy spectra includes a bivariant polynomial of the following form:

$$\sum_{v=0}^{V}\left[\sum_{u=0}^{U} A_{vu}(E_j, m)\,(X(E_j))^{u}\right](E_q)^{u} \qquad (10)$$

where:

E_j = source energy, Mev
E_q = detector energy, Mev
m = material

$X(E_j)$ = shield thickness in relaxation lengths. The coefficients, A_{vu}, were obtained by fitting the differential scattered gamma ray energy spectra, computed by moments method

DECLASSIFIED

DECLASSIFIED

CONFIDENTIAL

TABLE 10.11

WATER DOSE BUILD-UP DATA

$$B(\mu_o r) = \sum_{i=0}^{3} \beta_i [\mu_o r]^i + \epsilon_i (\mu_o r)$$

Polynomial Coefficients, β_i, For Operating Gamma Energies

E, Mev	β_0	β_1	β_2	β_3
0.5	1.00113(0)	9.36474(-1)	5.54450(-1)	1.15572(-2)
1.5	9.94795(-1)	9.28043(-1)	7.47068(-2)	-1.04320(-3)
2.5	9.96628(-1)	7.51604(-1)	2.10432(-2)	-4.41413(-4)
3.5	9.98993(-1)	6.23573(-1)	5.93758(-3)	-1.58115(-4)
4.5	1.00084(0)	5.35722(-1)	-1.79494(-4)	-2.26547(-5)
5.5	1.00223(0)	4.72985(-1)	-3.18502(-3)	4.97490(-5)
6.5	1.00330(0)	4.26265(-1)	-4.85031(-3)	9.19725(-5)
7.5	1.00415(0)	3.90231(-1)	-5.85157(-3)	1.18248(-4)
8.5	1.00483(0)	3.61640(-1)	-6.49003(-3)	1.35421(-4)
9.5	1.00538(0)	3.38419(-1)	-6.91548(-3)	1.47078(-4)

Polynomial Coefficients, β_i, For Shut-down Gamma Energies

E, Mev	β_0	β_1	β_2	β_3
0.4	9.94430(-1)	1.06903(0)	7.27189(-1)	2.63428(-2)
0.7	1.00081(0)	9.50167(-1)	3.27854(-1)	1.71770(-3)
1.0	9.96776(-1)	9.86981(-1)	1.71388(-1)	-9.76614(-4)
1.5	9.94795(-1)	9.28043(-1)	7.47068(-2)	-1.04320(-3)
2.0	9.95418(-1)	8.35691(-1)	3.83095(-2)	-6.96119(-4)
2.5	9.96628(-1)	7.51604(-1)	2.10432(-2)	-4.41413(-4)
2.8	9.97382(-1)	7.07858(-1)	1.47803(-2)	-3.31704(-4)

TABLE 10.12

IRON DOSE BUILD-UP DATA

$$B(\mu_o r) = \sum_{i=0}^{3} \beta_i [\mu_o r]^i + \epsilon_i (\mu_o r)$$

Polynomial Coefficients, β_i, For Operating Gamma Energies

E, Mev	β_0	β_1	β_2	β_3
0.5	1.00248(0)	8.60918(-1)	9.70348(-2)	-1.56599(-4)
1.5	1.01623(0)	7.11403(-1)	4.86269(-2)	-4.50817(-4)
2.5	1.00427(0)	5.87959(-1)	3.01773(-2)	-4.35074(-4)
3.5	9.98823(-1)	4.83384(-1)	2.32938(-2)	-3.02887(-4)
4.5	9.97490(-1)	4.04113(-1)	1.93460(-2)	-1.46585(-4)
5.5	9.97682(-1)	3.44126(-1)	1.66909(-2)	-4.99942(-6)
6.5	9.98413(-1)	2.97757(-1)	1.47575(-2)	1.15620(-4)
7.5	9.99307(-1)	2.61055(-1)	1.32787(-2)	2.17086(-4)
8.5	1.00021(0)	2.31372(-1)	1.21082(-2)	3.02640(-4)
9.5	1.00108(0)	2.06913(-1)	1.11574(-2)	3.75315(-4)

Polynomial Coefficients, β_i, For Shut-down Gamma Energies

E, Mev	β_0	β_1	β_2	β_3
0.4	1.00453(0)	8.86429(-1)	9.92463(-2)	4.95504(-5)
0.7	9.32798(-1)	9.23400(-1)	1.26464(-1)	-2.08625(-3)
1.0	1.00017(0)	7.88213(-1)	8.10147(-2)	-7.99320(-4)
1.5	1.01623(0)	7.11403(-1)	4.86269(-2)	-4.50817(-4)
2.0	1.00996(0)	6.49044(-1)	3.64848(-2)	-4.57877(-4)
2.5	1.00427(0)	5.87959(-1)	3.01773(-2)	-4.35074(-4)
2.8	1.00194(0)	5.53775(-1)	2.75901(-2)	-4.03225(-4)

CONFIDENTIAL

DECLASSIFIED

DECLASSIFIED

TABLE 10.13

LEAD DOSE BUILD-UP DATA

$$B(\mu_o r) = \sum_{i=0}^{3} \beta_i [\mu_o r]^i + \epsilon_i(\mu_o r)$$

Polynomial Coefficients, β_i, For Operating Gamma Energies

E, Mev	β_0	β_1	β_2	β_3
0.5	9.99929(-1)	2.44127(-1)	-1.78358(-2)	5.93192(-4)
1.5	1.01710(0)	3.79917(-1)	-5.31222(-3)	1.84649(-4)
2.5	1.00261(0)	3.60258(-1)	5.47052(-3)	-1.14309(-5)
3.5	9.91319(-1)	2.91837(-1)	1.08445(-2)	3.38460(-4)
4.5	9.92867(-1)	2.31505(-1)	9.91068(-3)	1.20429(-3)
5.5	1.00121(0)	1.99051(-1)	3.79009(-3)	2.32921(-3)
6.5	1.00413(0)	1.89990(-1)	-5.12565(-3)	3.36619(-3)
7.5	9.92788(-1)	1.88339(-1)	-1.39234(-2)	4.01480(-3)
8.5	9.71201(-1)	1.79401(-1)	-1.99175(-2)	4.15784(-3)
9.5	9.65807(-1)	1.62547(-1)	-2.13993(-2)	3.99807(-3)

Polynomial Coefficients, β_i, For Shut-down Gamma Energies

E, Mev	β_0	β_1	β_2	β_3
0.4	9.94144(-1)	2.16091(-1)	-1.89417(-2)	6.18700(-4)
0.7	1.00866(0)	2.90843(-1)	-1.54800(-2)	5.26200(-4)
[illegible]				
1.5	[illegible]	[illegible]	[illegible]	[illegible]
2.0	[illegible]	[illegible]	[illegible]	[illegible]
2.5	[illegible]	[illegible]	[illegible]	[illegible]
3.5	[illegible]	[illegible]	[illegible]	[illegible]

solution of the Boltzmann transport equation by the Nuclear Development Corporation of America. These spectra data are tabulated in NYO-3075[30] for several homogeneous infinite media for discrete energy point sources of 0.5, 1, 2, 3, 4, 6, and 10 Mev.

The spectra data in NYO-3075[30] were cross plotted to obtain data for other discrete energy sources. Due to the extensive amount of work involved in cross-plotting, coefficients were obtained only for water, iron, and lead infinite homogeneous media. In addition, a two-point formula was used to extrapolate the spectra data to 0.1 relaxation lengths for each material.

Binomial polynomial coefficients were then derived by the method of least squares. The criterion of minimization was the sum of the squared percent deviations. Coefficients were reported[31] for water, iron, and lead for one-photon-per-second sources of discrete energy 0.4, 0.5, 0.7, 1, 1.5, 2.0, 2.5, 3.0, 3.5, 4.5, 5.5, 6.5, 7.5, 8.5, and 9.5 Mev. The coefficients for water are reproduced in Table 10.14.

Graphs of gamma ray dose rate versus penetration depth may be conveniently applied by means of the comparison method for preliminary shielding calculations. Penetration data resulting from point kernel calculations were reported in references 33 and 34 for several materials. Although the source spectrum considered in these calculations was that for a specific direct-cycle reactor, the graphs are frequently useful for quick calculations.

A Monte Carlo code was described in section 9.3 for calculation of gamma ray air-scattering probabilities. Actually, extensive computation and compilation of such probabilities were made by Wright Air Development Center. Their data are reported in ORNL 2221.[35] Presented in reference 36 is an evaluation of the angular distribution data reported in

CONFIDENTIAL
DECLASSIFIED

DECLASSIFIED

CONFIDENTIAL

TABLE 10.14

BIVARIANT POLYNOMIAL COEFFICIENTS FOR COMPUTING DIFFERENTIAL GAMMA RAY ENERGY SPECTRA, $4\pi r^2 e\mu_o r I_o$

Medium: Water, $0.1 \leq \mu_o r \leq 20$
Source: Point Isotropic

Coefficients, A_{vu}, for $E_j = 0.4$ Mev, 0.2 Mev $\leq E_q \leq 0.4$ Mev

v \ u	0	1	2	3
0	8.99855(-2)	5.94146(0)	-6.81333(-2)	3.26550(-2)
1	-7.66562(-1)	-3.16542(1)	3.13363(0)	-1.38093(-1)
2	1.46131(0)	5.14699(1)	-6.61283(0)	1.55028(-1)

Coefficients, A_{vu}, for $E_j = 0.5$ Mev, 0.2 Mev $\leq E_q \leq 0.5$ Mev

v \ u	0	1	2	3
0	2.49223(-2)	4.10925(0)	2.30790(-1)	2.46439(-2)
1	-1.71641(-1)	-1.82650(1)	9.29768(-1)	-1.03909(-1)
2	2.57696(-1)	2.73258(1)	-2.80016(0)	1.09761(-1)

Coefficients, A_{vu}, for $E_j = 0.7$ Mev, 0.2 Mev $\leq E_q \leq 0.7$ Mev

v \ u	0	1	2	3
0	-4.27390(-3)	4.29364(0)	3.11775(-1)	1.66490(-2)
1	1.03189(-1)	-2.05546(1)	-1.90782(-1)	-6.69269(-2)
2	-4.22215(-1)	3.85966(1)	-4.69589(-1)	4.10185(-2)
3	3.68733(-1)	-2.17176(1)	2.93121(-1)	2.50731(-2)

Coefficients, A_{vu}, for $E_j = 1$ Mev, 0.2 Mev $\leq E_q \leq 1$ Mev

v \ u	0	1	2	3
0	5.92420(-2)	3.68085(0)	6.03515(-2)	9.54565(-3)
1	-2.96591(-1)	-1.39922(1)	7.00903(-1)	-6.07197(-2)
2	4.49251(-1)	1.99749(1)	-1.33652(0)	9.86492(-2)
3	-2.14002(-1)	-8.46826(0)	5.78827(-1)	-4.76415(-2)

Coefficients, A_{vu}, for $E_j = 1.5$ Mev, 0.2 Mev $\leq E_q \leq 1$ Mev

v \ u	0	1	2	3
0	-1.36945(-1)	7.19625(0)	-1.19845(0)	9.35311(-2)
1	1.53044(0)	-4.69779(1)	1.11097(1)	-8.52091(-1)
2	-4.95198(0)	1.19668(2)	-3.18516(1)	2.52252(0)
3	6.09576(0)	-1.28815(2)	3.67658(1)	-2.97884(0)
4	-2.54284(0)	4.96299(1)	-1.47819(1)	1.21383(0)

Coefficients, A_{vu}, for $E_j = 2$ Mev, 0.2 Mev $\leq E_q \leq 2$ Mev

v \ u	0	1	2
0	6.81000(-2)	2.58526(0)	2.76231(-2)
1	-3.78437(-1)	-8.90866(0)	-3.61052(-2)
2	6.33301(-1)	1.40652(1)	1.02257(-1)
3	-4.29366(-1)	-9.33632(0)	-8.99370(-2)
4	9.93962(-2)	2.15773(0)	2.22153(-2)

CONFIDENTIAL

DECLASSIFIED

DECLASSIFIED

TABLE 10.14 (Cont'd.)

BIVARIANT POLYNOMIAL COEFFICIENTS FOR COMPUTING DIFFERENTIAL GAMMA RAY ENERGY SPECTRA, $4\pi r^2 e\mu_o r I_o$

Coefficients, A_{vu}, for E_j = 2.5 Mev, 0.2 Mev $\leq E_q \leq$ 2 Mev

v \ u	0	1	2	3	4
0	5.52666(-2)	1.54448(0)	2.90915(-2)	1.55500(-3)	-1.48254(-4)
1	-3.00640(-1)	-4.11674(0)	-6.37353(-2)	-1.99134(-2)	1.22644(-3)
2	5.42161(-1)	5.78500(0)	2.08898(-1)	3.50743(-2)	-2.42899(-3)
3	-3.88792(-1)	-3.61705(0)	-1.50214(-1)	-2.96473(-2)	2.06168(-3)
4	9.31313(-2)	8.18072(-1)	3.07141(-2)	8.28329(-3)	-5.62539(-4)

Coefficients, A_{vu}, for E_j = 2.8 Mev, 0.2 Mev $\leq E_q \leq$ 2 Mev

v \ u	0	1	2	3
0	6.58986(-2)	1.21674(0)	5.22968(-2)	-2.49460(-3)
1	-3.79473(-1)	-2.55116(0)	-2.78939(-1)	1.28871(-2)
2	7.22011(-1)	3.24269(0)	5.33490(-1)	-2.34244(-2)
3	-5.49161(-1)	-1.86373(0)	-3.83658(-1)	1.69219(-2)
4	1.37262(-1)	3.99013(-1)	9.05035(-2)	-4.06563(-3)

Coefficients, A_{vu}, for E_j = 3.5 Mev, 0.2 Mev $\leq E_q \leq$ 3 Mev

v \ u	0	1	2	3	4
0	3.19079(-2)	1.14752(0)	-5.05693(-2)	6.64931(-3)	-2.41462(-4)
1	-1.30653(-1)	-2.18419(0)	9.24792(-2)	-1.57831(-2)	6.34486(-4)
2	1.64261(-1)	2.20231(0)	-2.68024(-2)	1.15977(-2)	-5.48550(-4)
3	-7.72234(-2)	-9.13561(-1)	-3.75054(-3)	-4.06327(-3)	2.17215(-4)
4	1.19402(-2)	1.33649(-1)	1.51282(-3)	5.60991(-4)	-3.17243(-5)

Coefficients, A_{vu}, for E_j = 4.5 Mev, 0.2 Mev $\leq E_q \leq$ 4 Mev

v \ u	0	1	2	3
0	3.18212(-2)	1.12019(0)	-3.28447(-2)	6.07125(-4)
1	-1.11760(-1)	-2.80367(0)	9.84837(-2)	-1.65015(-3)
2	1.43385(-1)	3.64517(0)	-1.17592(-1)	1.78739(-3)
3	-8.25490(-2)	-2.11379(0)	6.74343(-2)	-1.02613(-3)
4	2.14827(-2)	5.52704(-1)	-1.76576(-2)	2.77622(-4)
5	-2.04398(-3)	-5.26673(-2)	1.68912(-3)	-2.75516(-5)

Coefficients, A_{vu}, for E_j = 5.5 Mev, 0.2 Mev $\leq E_q \leq$ 5 Mev

v \ u	0	1	2	3
0	1.21845(-2)	5.12278(-1)	-6.59420(-3)	1.97037(-4)
1	-2.50558(-2)	-3.01968(-1)	-1.84673(-2)	-6.03527(-5)
2	1.14067(-2)	1.08930(-1)	1.78985(-2)	5.26472(-4)
3	-1.39837(-3)	-1.04260(-2)	-4.50863(-3)	-3.30792(-4)
4	-1.60813(-5)	-5.04442(-7)	3.84472(-4)	5.61046(-5)
5	2.93549(-6)	1.52092(-5)	-1.00861(-5)	-2.04344(-6)

DECLASSIFIED

DECLASSIFIED

TABLE 10.14 (Cont'd.)

BIVARIANT POLYNOMIAL COEFFICIENTS FOR COMPUTING DIFFERENTIAL GAMMA RAY ENERGY SPECTRA, $4\pi r^2 e^{\mu_o r} I_o$

Coefficients, A_{vu}, for $E_j = 6.5$ Mev, 0.2 Mev $\leq E_q \leq 6$ Mev

v \ u	0	1	2	3
0	1.35030(-2)	5.93428(-1)	-2.80057(-2)	6.91033(-4)
1	-3.32784(-2)	-7.19747(-1)	2.99495(-2)	-4.64188(-4)
2	2.98947(-2)	5.18207(-1)	-9.11255(-3)	-2.15493(-4)
3	-1.17303(-2)	-1.65103(-1)	-6.21278(-4)	2.33908(-4)
4	2.04144(-3)	2.45327(-2)	5.93633(-4)	-5.80120(-5)
5	-1.28903(-4)	-1.36348(-3)	-5.94416(-5)	4.45392(-6)

Coefficients, A_{vu}, for $E_j = 7.5$ Mev, 0.2 Mev $\leq E_q \leq 7$ Mev

v \ u	0	1	2	3
0	7.87972(-3)	5.67225(-1)	-3.92729(-2)	1.15068(-3)
1	-6.86943(-3)	-7.35315(-1)	6.90013(-2)	-2.13492(-3)
2	7.72548(-4)	5.29171(-1)	-5.06644(-2)	1.59739(-3)
3	5.79268(-4)	-1.64400(-1)	1.66011(-2)	-5.30938(-4)
4	-1.59648(-4)	2.31912(-2)	-2.43654(-3)	7.86341(-5)
5	1.11884(-5)	-1.20407(-3)	1.30559(-4)	-4.23312(-6)

Coefficients, A_{vu}, for $E_j = 8.5$ Mev, 0.2 Mev $\leq E_q \leq 8$ Mev

v \ u	0	1	2	3
0	1.33030(-2)	4.80793(-1)	-3.08067(-2)	8.56383(-4)
1	-1.96067(-2)	-4.88959(-1)	3.32011(-2)	-8.32585(-4)
2	1.11714(-2)	2.90521(-1)	-1.56418(-2)	3.24244(-4)
3	-2.97211(-3)	-7.40257(-2)	3.37078(-3)	-5.42092(-5)
4	3.66396(-4)	8.62239(-3)	-3.32597(-4)	3.55165(-6)
5	-1.68236(-5)	-3.71602(-4)	1.22335(-5)	-5.11324(-8)

Coefficients, A_{vu}, for $E_j = 9.5$ Mev, 0.2 Mev $\leq E_q \leq 9$ Mev

v \ u	0	1	2	3
0	1.35666(-2)	4.16520(-1)	-2.58440(-2)	7.00753(-4)
1	-2.01546(-2)	-3.82130(-1)	2.39750(-2)	-5.50116(-4)
2	1.10691(-2)	2.17225(-1)	-1.10200(-2)	2.06378(-4)
3	-2.75377(-3)	-5.26859(-2)	2.38652(-3)	-3.75207(-5)
4	3.11491(-4)	5.80816(-3)	-2.37627(-4)	3.12038(-6)
5	-1.29529(-5)	-2.35143(-4)	8.81568(-6)	-9.42887(-8)

DECLASSIFIED

DECLASSIFIED

ORNL 2292. Results of this study indicated that further reduction and utilization of the WADC energy and angular distribution data would not be beneficial for the following reasons:

1. The number of histories traced (1800) is insufficient to establish consistent angle bin data. At larger source angles as many as 8000 to 10,000 histories are indicated as necessary.
2. The angle bin data are strongly influenced by the number of particles originating at each first collision point. It is believed that originating one particle, as in the WADC data, is certainly not adequate.
3. In some areas, the treatment of the numerical integration in the single-scattering calculations is incorrect.
4. Finer polar angle bin data are required. Between 0 and 40 degrees, finer bin divisions are necessary to adequately describe the flux incident at a crew shield surface. Also, it may be possible to coalese the bin data at some of the larger detector angles.
5. The manpower required to reduce the energy bin data is prohibitive. The source energies and energy bin divisions used by WADC are not very convenient.

A preliminary study was performed later and reported in reference 37 to determine adequate source-detector parameters and to estimate the total cost of compiling useful gamma ray air-scattering probabilities. The following parameters were defined as necessary for a useful compilation:

1. Source angles of 1, 15, 45, 90, 135, and 180 degrees.
2. Source energies of 0.5, 2, 5, and 10 Mev.
3. Source-detector separation distances of 10, 40, and 100 feet.
4. Detector angle bins of a maximum of 5 degree increments from 0 to 60 degrees, with 20-degree bins from 60 to 180 degrees.
5. Detector energy bins specified so that contributions from all source energies could be added directly.

These parameters cover a wide range of each variable, and the data behave in a consistent manner so that interpolation and/or curve fitting techniques can be applied to obtain data at other values of these parameters.

10.4 CONVERSION FACTORS

Presented in this section are factors for converting gamma ray flux to absorbed dose rates in air, carbon, and tissue; neutron flux to first-collision absorbed dose rates in ethylene and tissue; and neutron flux to first-collision RBE dose rates in tissue.

The conversion factors were calculated by mathematically combining known atomic cross sections, atomic abundances, and RBE factors. The results consist of conversion factors for gamma ray energies ranging from .01 to 10 Mev inclusive, neutron conversion factors for energies ranging between .01 and 18 Mev inclusive, and RBE dose rate conversion factors for .01 to 18 Mev inclusive.

CONVERSION OF GAMMA RAY FLUX TO ABSORBED DOSE RATE FOR CARBON, AIR, AND TISSUE

To calculate these conversion factors, it was necessary to know the mass energy absorption coefficients. The mass gamma ray energy absorption coefficients were calculated by:

$$\frac{\mu_a}{\rho}(E) = \frac{\left[\sigma_{ca}(E)\right](.6025)(Z)}{A} + \left[\sigma_{pp}(E)\right] C_1 + \left[\sigma_{pE}(E)\right] C_1, \text{cm}^2/\text{gm} \quad (11)$$

CONFIDENTIAL

DECLASSIFIED

DECLASSIFIED

where:

$\frac{\mu a}{\rho}$ (E) = mass energy absorption coefficients at a given energy (E) in units of cm^2/gm

σ_{ca} (E) = energy absorption cross section for the Compton effect in units of barns/electron (taken from reference 38)

Z = atomic number

A = atomic weight

σ_{pp}(E) = cross section for pair production in barns/atom (taken from reference 39)

σ_{pE}(E) = cross section for photoelectric effect in barns/atom (taken from reference 39)

C_1 = conversion factor for each element such that barns/atom (C_1) = cm^2/gm

After the mass energy absorption coefficients were calculated, the conversion factors were calculated as follows:

For energy flux

$$\frac{1 \text{ rad}}{\text{hr}} = \frac{1 \text{ rad}}{\text{hr}} \left(\frac{1 \text{ hr}}{3600 \text{ sec}}\right) \left(\frac{100 \text{ ergs/gm}}{1 \text{ rad}}\right) \left(\frac{1 \text{ Mev}}{1.6 \times 10^{-6} \text{ ergs}}\right) \left(\frac{\text{gm}}{\mu a/\rho \text{ cm}^2}\right) \qquad (12)$$

cancelling factors gives

$$1 = \frac{\text{rads/hr}}{\text{Mev/cm}^2\text{-sec}} \left(5.76 \times 10^{-5} \frac{\mu a}{\rho}\right)$$

For photon flux

$$5.76 \times 10^{-5} \left(\frac{\mu a}{\rho}\right) \frac{\text{rads/hr}}{\text{Mev/cm}^2\text{-sec}} \left(\frac{\text{E Mev}}{\text{photon}}\right) = 5.76 \times 10^{-5} \text{ E} \left(\frac{\mu a}{\rho}\right) \frac{\text{rad/hr}}{\text{photon/cm}^2\text{-sec}} \qquad (13)$$

where:

E = photon energy in Mev.

The composition of air was taken as N(.755), O(.232), A(.013). The composition of tissue by weight was taken as O(.65), C(.18), N(.03), Ca(.013), and P(.01). These conversion factors as a function of energy are given in Tables 10.15 and 10.16. The same factors are presented graphically in reference 40.

CONVERSION FACTORS FOR CONVERTING NEUTRON FLUX TO ABSORBED DOSE RATE IN ETHYLENE AND TISSUE

These factors were calculated by the method indicated in NBS Handbook 63. The conversion factors are given by the relationship:

$$F = \sum \frac{(E\sigma_i)\ 2\ M_i\ N_i}{(M_i + 1)2} \ (5.76 \times 10^{-5}) \frac{\text{rads/hr}}{\text{neutrons/cm}^2\text{-sec}} \qquad (14)$$

Contributing Elements

where:

M_i = the atomic mass number

σ_i = the elastic scattering cross section in cm^2

E = the energy in Mev

N_i = the atomic abundance (atoms/gram)

DECLASSIFIED

DECLASSIFIED

CONFIDENTIAL

TABLE 10.15

FACTORS FOR CONVERTING GAMMA RAY ENERGY FLUX TO ABSORBED DOSE RATE (rads/hr/Mev/cm^2-sec)

E (Mev)	Air	Carbon	Tissue
0.01	2.67/-4	1.12/-4	3.38/-4
0.015	7.59/-5	2.97/-5	9.60/-5
0.02	3.03	1.16	3.88
0.03	8.58/-6	3.37/-6	1.11
0.04	3.74	1.76	4.80/-6
0.05	2.24	1.30	2.81
0.06	1.70	1.16	2.05
0.08	1.37	1.17	1.91
0.10	1.34	1.24	1.50
0.15	1.45	1.42	1.58
0.2	1.55	1.53	1.69
0.3	1.66	1.66	1.80
0.4	1.70	1.70	1.85
0.5	1.71	1.71	1.85
0.6	1.71	1.71	1.85
0.7	1.70	1.67	1.84
0.8	1.66	1.66	1.80
1.0	1.61	1.61	1.74
1.5	1.48	1.48	1.60
2.0	1.37	1.37	1.48
2.5	1.27	1.27	1.35
2.8	1.24	1.23	1.30
3.0	1.22	1.20	1.31
3.5	1.15	1.15	1.23
4.0	1.12	1.10	1.20
4.5	1.06	1.05	1.15
5.0	1.04	1.02	1.11
5.5	1.02	9.5/-7	1.07
6.0	9.92/-7	9.59	1.05
6.5	9.5	9.20	1.02
7.5	9.2	8.80	9.8/-7
8.0	9.23	8.80	9.73
8.5	9.0	8.50	9.6
9.5	8.75	8.30	9.5
10.0	8.83	8.37	9.76

CONFIDENTIAL

DECLASSIFIED

DECLASSIFIED

CONFIDENTIAL

TABLE 10.16

FACTORS FOR CONVERTING GAMMA RAY PHOTON FLUX TO ABSORBED DOSE RATE

$$\left(\frac{\text{rads/hr}}{\text{photons/cm}^2\text{-sec}}\right)$$

E (Mev)	Air	Carbon	Tissue
0.01	2.67/-4	1.12/-6	3.38/-6
0.015	1.14	4.46/-7	1.4
0.02	6.05/-7	2.33	7.75/-7
0.03	2.57	1.01	3.34
0.04	1.49	7.03/-8	1.92
0.05	1.12	6.51	1.40
0.06	1.02	6.96	1.23
0.08	1.10	9.32	1.53
0.10	1.34	1.24/-7	1.49
0.15	2.17	2.13	2.37
0.2	3.09	3.07	3.38
0.3	4.99	4.99	5.50
0.4	6.81	6.82	7.39/-7
0.5	8.55	8.55	9.27
0.6	1.02/-6	1.02/-6	1.10/-6
0.7	1.16	1.18	1.26
0.8	1.33	1.33	1.44
1.0	1.61	1.61	1.76
1.5	2.22	2.22	2.40
2.0	2.74	2.73	2.76
2.5	3.2	3.18	3.50
2.8	2.45	3.4	3.70
3.0	3.65	3.61	3.93
3.5	4.1	4.0	4.3
4.0	4.46	4.39	4.79
4.5	4.85	4.7	5.2
5.0	5.21	5.09	5.57
5.5	5.6	5.4	6.0
6.0	5.95	5.75	6.33
6.5	6.3	6.1	6.7
7.5	7.0	6.7	7.5
8.0	7.38	7.04	7.79
8.5	7.8	7.5	8.3
9.5	8.6	8.25	9.5
10.0	8.83	8.37	9.76

CONFIDENTIAL

DECLASSIFIED

DECLASSIFIED
CONFIDENTIAL

The atomic abundances taken from Table 1, of reference 41, for tissue elements are given below:

Element	Atoms Per Gram
O	2.45×10^{22}
C	0.903×10^{22}
H	5.98×10^{22}
N	0.129×10^{22}

Only the elastic scattering cross sections were considered in these calculations. Both absorption cross sections and inelastic scattering cross sections were omitted. Contributions from the former interaction are negligible, and the latter became important only at energies above 10 Mev. This omission tends to make the conversion factors low for the higher energies.

The tissue factors were calculated under the assumption that only the elements oxygen, carbon, nitrogen, and hydrogen were present. Table 10.17 shows these results, and they are shown graphically in reference 40.

CONVERSION FACTORS FOR CONVERTING FIRST-COLLISION NEUTRON FLUX TO RBE DOSE RATE

The fundamental relationship for converting absorbed dose to RBE dose is:

$$\text{REM} = \text{Rad (RBE)}$$

With the absorbed dose rate known from previous calculations, only the RBE remained to be determined. The RBE was taken from Figure 14 of NBS Handbook 63.[41] This graph gives the RBE as a function of depth in tissue and neutron energy. A separate curve is plotted for each energy, and the maximum ordinate of each curve was used as the RBE value in the calculation of the RBE dose. These maximum RBE values were then plotted as functions of energy in Figure 10.5. Values from this curve subsequently were used in conjunction with the above formula to determine the conversion factors.

The results are tabulated in Table 10.18 and shown graphically in reference 40.

Ratio of Conversion Factors

Table 10.17 gives the ratio of ethylene conversion factors to tissue conversion factors. The average value of the ratio was found to be 1.44. Statistical calculations indicated 95 percent tolerance limits of 1.44 ± 0.1 and 95 percent confidence limits of 1.44 ± 0.122.

10.5 BASIC NUCLEAR DATA

The basic nuclear data compilation effort was initiated in order to provide, as far as possible, complete and up-to-date experimental neutron cross section and allied data for use in shielding calculations.

Although this effort was intended to provide such data for general shielding use, primary attention was given to the input requirement of the Monte Carlo programs and the shielding materials of interest to the ANP effort.

Cross section data considered, refer to atoms free and at rest in the laboratory system. This means that the various effects arising from the molecular structure and its thermal motion were neglected. These effects can be of great importance in reactor analysis.

CONFIDENTIAL
DECLASSIFIED

DECLASSIFIED

CONFIDENTIAL

TABLE 10.17

FACTORS FOR CONVERTING NEUTRON FLUX TO ABSORBED DOSE RATE (rads/hr/n/cm^2-sec)

E(Mev)	Tissue	Ethylene	Ratio Of Factors E/T
0.01	3.36/-7	4.89/-7	1.45
0.1	2.26/-6	3.29/-6	1.45
0.2	3.62	5.26	1.45
0.3	3.98	5.77	1.45
0.4	5.25	7.38	1.41
0.5	5.79	8.20	1.42
0.6	6.25	9.04	1.45
0.7	6.63	9.61	1.45
0.8	7.07	1.02/-5	1.44
0.9	7.73	1.09	1.41
1.0	8.72	1.14	1.31
1.1	8.54	1.21	1.41
1.2	8.85	1.26	1.42
1.3	9.44	1.30	1.37
1.4	9.39	1.34	1.43
1.5	9.68	1.36	1.41
1.6	9.95	1.43	1.44
1.7	1.02/-5	1.47	1.45
1.8	1.07	1.52	1.42
1.9	1.09	1.58	1.44
2.0	1.08	1.57	1.44
2.1	1.15	1.86	1.61
2.2	1.12	1.64	1.46
2.3	1.14	1.68	1.47
2.4	1.12	1.68	1.49
2.5	1.18	1.71	1.46
2.7	1.21	1.78	1.47
2.9	1.28	1.98	1.55
3.0	1.27	1.83	1.44
3.3	1.43	2.02	1.41
3.4	1.45	2.04	1.40
3.6	1.51	2.10	1.39
3.75	1.59	2.18	1.37
4.0	1.49	2.15	1.45
4.1	1.48	2.19	1.48
4.3	1.63	2.25	1.38
4.7	1.51	2.22	1.47
4.8	1.56	2.20	1.41
4.9	1.50	2.19	1.46

CONFIDENTIAL

DECLASSIFIED

DECLASSIFIED

CONFIDENTIAL

TABLE 10.17 (Cont'd.)

FACTORS FOR CONVERTING NEUTRON FLUX TO ABSORBED DOSE RATE (rads/hr/n/cm^2-sec)

E(Mev)	Tissue	Ethylene	Ratio of Factors E/T
5.1	1.67	2.22	1.33
5.2	1.56	2.23	1.43
5.3	1.55	2.21	1.43
5.6	1.60	2.30	1.44
6.0	1.62	2.30	1.42
6.2	1.64	2.35	1.43
6.3	1.64	2.41	1.47
6.6	1.63	2.30	1.42
6.7	1.63	2.30	1.42
7.0	1.62	2.28	1.41
7.3	1.66	2.36	1.42
7.5	1.75	2.67	1.52
7.7	1.76	2.66	1.36
7.8	1.76	2.75	1.56
8.0	1.71	2.68	1.57
8.3	1.78	2.62	1.47
8.5	1.77	2.58	1.46
9.0	1.69	2.48	1.47
10.0	1.78	2.64	1.48
11.0	1.88	2.81	1.49
12.0	1.92	2.87	1.50
13.0	1.99	2.88	1.45
14.0	1.94	2.74	1.41
15.0	2.02	2.81	1.39
16.0	2.04	2.84	1.39
17.0	2.02	2.81	1.43
18.0	1.97	2.81	

CONFIDENTIAL

DECLASSIFIED

DECLASSIFIED

CONFIDENTIAL

TABLE 10.18

FACTORS FOR CONVERTING NEUTRON FLUX TO RBE DOSE RATE (rem/hr/n/cm^2-sec)

E(Mev)	Tissue	E(Mev)	Tissue
0.01	1.18/-6	4.0	1.04
0.1	1.95/-5	4.1	1.02
0.2	3.48	4.3	1.11
0.3	3.98	4.7	1.02
0.4	5.35	4.8	1.06
0.5	5.97	4.9	1.01
0.6	6.50	5.1	1.12
0.7	6.96	5.2	1.05
0.8	7.42	5.3	1.03
0.9	8.11	5.6	1.06
1.0	9.15	6.0	1.07
1.1	8.79	6.2	1.08
1.2	8.89	6.3	1.08
1.3	9.35	6.6	1.07
1.4	9.10	6.7	1.08
1.5	9.29	7.0	1.07
1.6	9.35	7.3	1.10
1.7	9.35	7.5	1.15
1.8	9.63	7.7	1.16
1.9	9.64	7.8	1.16
2.0	9.28	8.0	1.11
2.1	9.69	8.3	1.16
2.2	9.21	8.5	1.15
2.3	9.13	9.0	1.10
2.4	8.87	10	1.16
2.5	9.05	11	1.22
2.7	9.30	12	1.25
2.9	9.53	13	1.29
3.0	9.37	14	1.26
3.3	1.03/-4	15	1.31
3.4	1.03	16	1.33
3.6	1.07	17	1.31
3.75	1.11	18	1.28

CONFIDENTIAL

DECLASSIFIED

DECLASSIFIED

Furthermore, only those neutrons of energy less than 20 Mev were considered, since this is the range of greatest interest in shielding and reactor design.

Cross section and allied data which are expected to be important either directly or indirectly in Monte Carlo shielding calculations are:

σ_t - total

$\sigma_{n,n}$ - elastic [$\sigma_{n,n}(\theta)$ differential elastic]

σ_{non} - non-elastic

$\sigma_{n,n'}$ - inelastic [$\sigma_{n,n'}(\theta)$ or $\sigma_{n,n'}$, $\gamma(\theta)$ differential inelastic]

$\sigma_{n,\gamma}$ - radiative capture (gamma spectra)

$\sigma_{n,2n}$ - neutron in - 2 neutrons out

$\sigma_{n,p}$ - neutron in - proton out

$\sigma_{n,d}$ - neutron in - deuteron out

$\sigma_{n,\alpha}$ - neutron in - alpha particle out

$\sigma_{n,t}$ - neutron in - triton out

σ_f - fission cross section

Although other reactions exist, they may be considered unimportant in the energy range of interest.

The compilation effort covered the following materials: hydrogen, lithium, beryllium, boron, carbon, nitrogen, oxygen, aluminum, chromium, iron, cobalt, nickel, yttrium, zirconium, molybdenum, tungsten, lead, and uranium.

In addition to compiling basic experimental nuclear data, the effort consisted of extending and interpolating the available data, when necessary, and compiling the basic data in a form suitable for use in the shielding Monte Carlo codes.

All experimental data compiled during the duration of the effort are available either on IBM cards or in published reports. The status of neutron cross sections and allied data as of mid-1960 is discussed in reference 42. This report contains a brief discussion of the experimental and theoretical methods for determining the cross section data given above. Following this is a compilation of the areas of experimental data. In order to facilitate effective presentation, a bar graph is used to enable the reader to determine the status of the data for each material at a glance. A reference survey is included in the report.

Neutron cross section data compiled for hydrogen, lithium, beryllium, boron, carbon, nitrogen, and oxygen are given in reference 43; and neutron cross section data compiled for chromium, iron, nickel, yttrium, zirconium, tungsten, lead, and uranium, are given in reference 44. A discussion of the data for each of the elements is given in the published reports.

A compilation of the experimentally determined neutron radiative capture cross sections for many elements pertinent to the ANP shielding effort is given in reference 45. In general, the data cover the energy range 0 - 6.0 Mev; however, in some regions the data for some of the isotopes are not complete over the entire range.

Reference 46 presents a compilation of averaged microscopic neutron reaction cross sections for use in shield Monte Carlo codes. Available basic neutron reaction cross sections for 16 elements pertinent to the ANP shielding effort were averaged for 25 energy groups covering the energy range 10^{-8} to 20 Mev.

DECLASSIFIED

DECLASSIFIED

The tabulated cross sections for the group energy bounds are the results of a linear approximation of the basic data across each group. The straight-line approximation for each group was adjusted to give the correct average and the best slope for the group. The best slopes were determined by dividing each energy group into two equal half-groups. The average cross section for each half-group was computed and attributed to the energy at the center of the half-group. A straight line was then drawn through these two points to establish the best slope.

All basic experimental cross sections used in the averaging are listed in the report. References to the basic data are also included.

The basic data points selected for the averaging process may not be adequate. Probably sufficient points were used outside the thermal group, but possible too few points were used for the thermal group. The reader should satisfy himself of the adequacy of the data for his own purpose before using them.

Experimental data on gamma ray and neutron spectra, resulting from inelastic scattering of neutrons in various elements, are presented in reference 47. These data include nuclear level schemes, gamma ray and neutron spectra, total inelastic and differential inelastic scattering cross sections.

Experimental differential neutron elastic scattering cross sections are compiled in reference 48 for the energy range of 0.13 to 20 Mev, for 17 natural elements and isotopes pertinent to aircraft shielding calculations. Although all the experimental data available on February 28, 1961, are included, more complete data are necessary for many of the elements for accurate Monte Carlo or transport analysis.

The absolute differential cross sections are plotted in barns per steradian versus the cosine of the scattering angle, with cos $\theta = 1.0$ corresponding to forward scattering. The curves are arranged in order of increasing atomic number, with several curves for different incident neutron energies included on each page.

An important erratum to this report was issued June 21, 1961. It stated: "The data presented as ANL (to be published) should be labeled in laboratory coordinates instead of center-of-mass." This includes the following curves:

Lithium

E_n(Mev): 0.1, 0.245, 0.255, 0.26, 0.265, 0.295, 0.6, 1.65

Beryllium

E_n(Mev): 0.5, 0.63, 1.14, 1.44, 1.95, 2.25

Carbon

E_n(Mev): 0.12, 0.35, 0.725, 1.34, 1.95, 2.054, 2.076, 2.082, 2.088, 2.13

Oxygen

E_n(Mev): 0.2, 0.44, 0.76, 1.0, 1.25, 1.32, 1.61, 1.643, 1.655, 1.659, 1.6645, 1.672

Lead

E_n(Mev): 0.16, 0.36, 0.63, 0.83, 1.04, 1.24, 1.75, 1.95

It is to be noted that the above data has been published in the Annals of Physics Volume 12(1961) page 135, under the title, "The Angular Distributions of Neutrons Scattered from Various Nuclei," R. O. Lane, et al. It is recommended that the reader consult this publication for a full discussion of the experimental and analytical procedures and the actual measured values of the differential cross sections for the scattering of neutrons.

DECLASSIFIED

DECLASSIFIED

CONFIDENTIAL

10.6 REFERENCES

1. Carver, J. G., Edwards, W. E., and MacDonald, J. E., "GE-ANPD Methods of Shield Design," GE-ANPD, APEX-230, December 30, 1955.
2. Edwards, W. E., and Capo, M. A., "Nuclear Data," GE-ANPD, XDC 57-1-8, January 3, 1957.
3. Smith, M. R., "Distribution of the Energy per Fission of U^{235}," GE-ANPD, DC 60-1-177, January 11, 1960.
4. Carver, J. G., "U^{235} Fission Gamma Ray Source Data," GE-ANPD, XDC 60-11-63, October 5, 1960.
5. Capo, M. A., "U^{235} Fission Product Decay Gamma Energy Spectra," GE-ANPD, DC 59-10-135, October 19, 1959.
6. Smith, M. R., "The Activity of the Fission Products of U^{235} (Program 408)," GE-ANPD, XDC 60-1-157, December 10, 1959.
7. Smith, M. R., "The Activity of the Fission Products of U^{235} (Supplement No. 1)," GE-ANPD, XDC 60-12-46, December 6, 1960.
8. Perkins, J. F., and King, R. W., "Energy Release from the Decay of Fission Products," Nuclear Science and Engineering, Volume 3, pp. 726-746 (1958).
9. Scoles, J. F., "Calculated Gamma Ray Spectra from U^{235} Fission Products," Convair, NARF 58-37T, August 29, 1958.
10. Knabe, W. E., and Putnam, G. E., "The Activity of the Fission Products of U^{235}," Internuclear Company, INTERNUC 33, October 31, 1959, reissued as APEX-448.
11. Maienschein, F. C., Peele, R. W., Zober, W., and Love, T. A., "Gamma Rays Associated with Fission," Paper 670 in Proceedings of the Second United Nations International Conference on the Peaceful Uses of Atomic Energy, Volume 15, pp. 366-372. The same data were presented earlier in ORNL-2609, "Neutron Physics Division Annual Progress Report for Period Ending September 1, 1958," pp. 45-51.
12. Deloume, F. E. "Gamma Ray Energy Spectra From Thermal Neutron Capture," GE-ANPD, APEX-407, August 1958.
13. Casper, A. W., "Data Report and Analysis of Battelle Pool Mapping," GE-ANPD, XDC 59-8-228, August 25, 1959.
14. Casper, A. W., "Modified Fast Neutron Attenuation Functions," GE-ANPD, XDC 60-2-76, February 3, 1960.
15. Trubey, D. K., and Chapman, G. T., "Effective Neutron Removal Cross Sections of Carbon and Oxygen in Continuous Media," Oak Ridge National Laboratory, ORNL-2081, "Applied Nuclear Physics Division Annual Report for Period Ending September 10, 1956."
16. Fleishan, M. R., "A Monte Carlo Study of the Leakage from Finite Hydrogenous Regions of the Neutrons from a Point Fission Source," Nuclear Development Corporation of America, NDA-2092-6, June 2, 1956.
17. West, D. L., "Data Report and Analysis of Fast Neutron Attenuation Within LiH," GE-ANPD, XDC 60-1-17, December 30, 1959.
18. Goldstein, H., and Krumbein, A. D., "Moments Method Calculation of the Penetration of Neutrons from a Point Fission Source Through Be and BeO," Nuclear Development Corporation of America, NDA Memo 2124-1, May 27, 1960.
19. Krumbein, A. D., "Summary of NDA Unclassified Results of Moments Calculations for the Penetration of Neutrons Through Various Materials," Nuclear Development Corporation of America, NDA 92-2, August 30, 1957.
20. Henderson, B. J., and Gerardo, H. A., "Penetration of Neutrons from a Point Fission Source Through Lithium Hydride," GE-ANPD, DC 60-7-114, July 21, 1960.
21. Schreiber, P. W., "Measured and Calculated Radiation Levels Within and Behind Beryllium," GE-ANPD, APEX-701, July 1961.

CONFIDENTIAL

DECLASSIFIED

DECLASSIFIED

22. Schreiber, P. W., and Kodras, F. D., "Measured and Calculated Radiation Levels Within and Behind Beryllium Oxide," GE-ANPD, XDC 61-1-14, February 1961.
23. Casper, A. W., "A Plan for Parametric Neutron Penetration Calculations," GE-ANPD, DC 61-3-162, March 29, 1961.
24. Edwards, W. E., "Fast Neutron Attenuation in Hydrogenous Materials," GE-ANPD, XDC 57-1-32, December 28, 1956.
25. White, E., "Gamma Ray and Fast Neutron Attenuation in Hydrogenous Media," GE-ANPD, DC 60-3-105, March 7, 1960.
26. Grodstein, G. W., "X-Ray Attenuation Coefficients from 10 Kev to 100 Mev," National Bureau of Standards, NBS-583, April 30, 1957.
27. Mann, R. A., "Gamma Ray Cross Section Data," GE-ANPD, DC 60-9-75, September 7, 1960.
28. Capo, M. A., "Polynomial Approximation of Linear Gamma Ray Absorption Coefficients," GE-ANPD, DC 57-8-158, August 19, 1957.
29. Capo, M. A., "Polynomial Approximation of Gamma Ray Buildup Factors for a Point Isotropic Source," GE-ANPD, APEX-510, November 1958.
30. Goldstein, H., and Wilkins, J. E., "Calculation of the Penetration of Gamma Rays," Nuclear Development Corporation of America, NYO-3075, June 30, 1954.
31. Carver, J. G., "Interim Report on Buildup Factors for Heating Calculations," GE-ANPD, DC 58-10-161, October 22, 1958.
32. Capo, M. A., "Shielding Computer Programs 14-0, 14-1, and 14-2 - Input Data Coefficients for Computing Gamma Ray Energy and Neutron Spectra," GE-ANPD, DC 59-10-148, October 19, 1959.
33. Edwards, W. E., "Gamma Ray Attenuation Curves," GE-ANPD, XDC 57-1-101, January 2, 1957.
34. White, E., "Gamma Ray and Fast Neutron Attenuation in Hydrogenous Media," GE-ANPD, DC 60-3-105, March 7, 1960.
35. Lynch, R. E., et al., "A Monte Carlo Calculation of Air-Scattered Gamma Rays," Oak Ridge National Laboratory and Wright Air Development Center, ORNL 2292, October 7, 1958.
36. Capo, M. A., "Evaluation of the Detector Angular Distribution of Air-Scattered Gamma Rays Computed by Wright Air Development Center's Monte Carlo Code," GE-ANPD, DC 60-1-168, January 22, 1960.
37. Capo, M. A., "Determination of Suitable Parameters for Compiling Gamma Ray Air Scattering Probabilities," GE-ANPD, DC 60-10-150, October 26, 1960.
38. Goldstein, H., "The Attenuation of Gamma Rays and Neutrons in Reactor Shields," U.S. Government Printing Office, May 1, 1957.
39. Grodstein, G. W., "X-Ray Attenuation Coefficients from 10 Kev to 100 Mev," NBS Circular 583, April 30, 1957, Tables 12-35.
40. Henderson, B. J., "Conversion of Neutron or Gamma Ray Flux to Absorbed Dose Rate," GE-ANPD, XDC 59-8-179, August 14, 1959.
41. National Bureau of Standards Handbook 63, "Protection Against Neutron Radiation Up to 30 Million Electron Volts," U.S. Government Printing Office, November 22, 1957.
42. Prince, A., "The Status of Neutron Cross Sections and Related Data," GE-ANPD, XDC 60-11-164, November 30, 1960.
43. Gerardo, H. A., "Some Neutron Induced Cross Sections for Elements Pertinent to XMA," GE-ANPD, DC 59-5-45, May 5, 1959.
44. Gerardo, H. A., "Some Neutron Induced Cross Sections for Elements Pertinent to XMA, Part 2," GE-ANPD, DC 59-7-171, July 16, 1959.
45. Gerardo, H. A., "Neutron Radiative Capture Cross Section Compilation," GE-ANPD, DC 59-12-155, December 21, 1959.

DECLASSIFIED

DECLASSIFIED

46. Gerardo, H. A., "Experimental and Averaged Microscopic Neutron Reaction Cross Sections," GE-ANPD, DC 60-9-150, September 30, 1960.
47. Prince, A., "Nuclear Data From Neutron Inelastic Reactions," GE-ANPD, DC 60-10-19, October 4, 1960.
48. Gerardo, H. A., "Experimental Differential Neutron Elastic Cross Section - Angular Distributions (.13 - 20 Mev)," GE-ANPD, XDC 61-3-131, March 1961.

DECLASSIFIED

DECLASSIFIED

DECLASSIFIED

DECLASSIFIED

CONFIDENTIAL

11. BASIC SHIELD EXPERIMENTS

To provide accurate data in clean geometries which could be easily analyzed to provide checks on the theoretical and design methods, basic shield penetration measurements were needed. These measurements were the primary interest of the ANPD experimental shielding program.

Extensive gamma ray point source and calorimetric nuclear heating measurements were made as part of this supporting experimental program. Additional tests planned in both series, necessary to make the information already obtained really useful, were not completed. Nevertheless, available experimental results are described and referenced in the next two sections.

Of the basic shield experiments performed, the source plate experiments were most successful. Measurements made in the Source Plate Facility at Battelle Memorial Institute are described in some detail and referenced completely in section 11.3. Centerline thermal neutron fluxes, fast neutron dose rates, and gamma ray dose rates are presented for beryllium, beryllium oxide, and water. Centerline fast neutron dose rates are also given for lithium hydride.

11.1 GAMMA RAY POINT SOURCE EXPERIMENTS

At ITS, beginning in January, 1958, and continuing on an intermittent basis through 1960, arrays of materials were measured for penetration by gamma rays from several point sources. The experiments were undertaken to provide experimental verification of the buildup factors and differential energy spectra calculated by a moments method solution of the Boltzmann transport equation by the Nuclear Development Corporation of America.[1] The work at ITS was deemed necessary because all gamma ray penetration calculations made at ANPD were based on these buildup factors and differential energy spectra. Prior to these experiments, experimental verification was based on limited gamma ray source energies and materials of a limited range in atomic number.

The measurements were planned to cover a wide range of atomic numbers for penetration thicknesses up to 10 relaxation lengths. At the beginning of the experiments, four primary objectives were stated:[2]

1. Measure gamma ray dose rates and energy spectra behind seven single materials as a function of separation distance from available point sources of cesium-137, cobalt-60, sodium-24, and fission products.
2. Measure gamma ray dose rates and energy spectra behind layers of multiple materials as a function of separation distance from available point sources.
3. Investigate the effects of short circuiting around and through single- and multiple-layer gamma shields.
4. Take gamma ray dose rate measurements inside lead shields at various distances from point sources behind lead shadow shields in water to check single-scattering computer programs.

CONFIDENTIAL

DECLASSIFIED

DECLASSIFIED

CONFIDENTIAL

EXPERIMENTAL APPARATUS AND PROCEDURE

The measurements were conducted in the 607 fuel element storage pool (48' x 70' x 27' deep) at the Idaho Test Station. An instrument bridge 13 feet wide spanned the width of the pool. This bridge supported the source, test slabs, detector positioning mechanism, and electronic equipment. Traveling on the bridge was an instrument dolly which supported the detector and provided it with three degrees of freedom. Suspended 13 feet beneath the bridge and some 9 feet below the water level was a 5-1/2-foot-square aluminum platform used to support the source and slabs of material under test. The slabs were stacked vertically upon a three-point pedestal raised 2 feet above the platform. The source could be moved up or down or swung out from its position under the pedestal. The equipment provided a clean geometry and good position accuracy.

Dose rate measurements were taken by placing the source in contact with the lower surface of the slabs and a scintillation counter at the upper surface of the slabs. From this point the counter was raised in a vertical traverse through water above the slabs. In this way, data were obtained for penetration through a material alone and through the material in combination with water.[3,4]

DATA OBTAINED

Data were obtained in this experiment with cobalt-60 and cesium-137 sources for water, aluminum, iron, lead, Hevimet, tin, and uranium. For aluminum, iron, lead, Hevimet, and uranium, data were taken for various thicknesses up to 10 relaxation lengths, in most cases, and for geometries where both the source and the detector were in contact with the slabs, where the source was in contact with the slab but the detector was traversed in water away from the slabs, and where there was water separating the source and the slabs.

A scintillation detector was the primary instrument used for the gamma ray dose rate measurements. Originally, an anthracene crystal was used, but in May 1958, this was replaced by a Pilot-B plastic scintillator crystal containing diphenylstilbene. The crystal was 1-inch long by 1-1/2 inch in diameter, and was surrounded by about 1/8-inch of Lucite. Differential energy spectra were measured with a single-crystal, NaI(th), 3 by 3 inch spectrometer coupled with a 256-multichannel pulse-height analyzer. Data were obtained for the unshielded sources and for a number of cases after penetration through several relaxation lengths of material.[5,6,7,8]

ANALYSIS OF DATA

Analysis of the single-material dose-buildup factors was performed[9] by comparing the experimentally derived average dose-buildup factors with the average calculated dose-buildup factors. Briefly, the dose rate from a point source in an infinite medium is given by:

$$D(Z) = \frac{1}{4\pi Z^2} \sum_{j=1}^{J} A_j(E_j)\, K_j(E_j)\, B_j(X)\, e^{-X} \text{ R/hr} \qquad (1)$$

where

$X = \sum_{m=1}^{M} \mu(E_j, m) t_m$ = the number of relaxation lengths of material

Z = source-detector separation distance

$K_j(E_j)$ = Photon flux to dose-rate conversion factor at gamma ray energy E_j, (R/hr)/(photon/cm^2-sec)

$A_j(E_j)$ = number of photons per unit-time emitted by the source at energy E_j, photons/sec

$B_j(X)$ = dose buildup factor at energy E_j through X relaxation lengths, dimensionless

$\mu(E_j, M)$ = linear absorbtion coefficients at energy E_j for material m, cm^{-1}

t_m = thickness of material m, cm

CONFIDENTIAL

DECLASSIFIED

DECLASSIFIED

Now define the average dose buildup factor as:

$$\bar{B} \sum_{j=1}^{J} A_j(E_j) K_j(E_j)\, e^{-X} = \sum_{j=1}^{J} A_j(E_j) K_j(E_j) B_j(X)\, e^{-X} \tag{2}$$

i.e.,

$$\bar{B} \frac{\sum_{j=1}^{J} A_j(E_j) K_j(E_j)\, e^{-X}}{\sum_{j=1}^{J} A_j(E_j) K_j(E_j) B_j(X)\, e^{-X}} \tag{3}$$

The $B_j(X)$ are the theoretical infinite medium dose-buildup factors calculated by H. Goldstein and J. E. Wilkins.[1]

The experimentally determined average dose-buildup factors to be compared with the calculated average dose-buildup factors are found in the following manner.

From the infinite dose equation,

$$4\pi Z^2 D(Z) = \sum_{j=1}^{J} A_j(E_j) K_j(E_j) B(X)\, e^{-X} \tag{4}$$

Substituting $4\pi Z^2 D(Z)$ for $\sum_{j=1}^{J} A_j(E_j) K_j(E_j) B(X)\, e^{-X}$ in the equation for the average dose-buildup factor yields

$$\bar{B}_{ex} = \frac{4\pi Z^2 D(Z)}{\sum_{j=1}^{J} A_j(E_j) K_j(E_j)\, e^{-X}} \tag{5}$$

where $\bar{B}_{ex}$ is used to denote the experimental average dose-buildup factor.

To be useful, the denominator of the expression for $\bar{B}_{ex}$ must also be a measured quantity in order to remove the source term $A_j(E_j)$ from the expression. This was done by expressing the dose rate in terms of counts per minute multiplied by a conversion factor. The conversion factor was found by solving the infinite medium point source equation for air where the dose $D(Z)$ is equal to counts per minute, times a conversion factor. This conversion factor was used to remove the necessity for knowing the absolute value of the source by expressing the buildup factor as a ratio of the cpm in air to the cpm in water.

When the experimental average dose-buildup factors were compared with the calculated average dose-buildup factors, there were marked disagreements both in shape and in magnitude. For water, the experimental curves are low over the thickness range investigated, and the slopes of the experimental curves differ from the slopes of the theoretical curves for both cesium and cobalt sources, although to a lesser degree for cobalt. For aluminum, iron, lead and uranium samples, the behavior is similar except that at some apparently arbitrary material thickness, the experimental values of dose-buildup factors increase much more rapidly than expected from theory. Hevimet takes exception to this characteristic and behaves like water; however, there is a slight indication of an upturn in the buildup factors for a material thickness of 3 inches or more.

One of the possible sources of disagreement between experimental and theoretical average dose-buildup factors is the different energy response of the anthracene crystal relative to air. That is, the experiment measured energy absorption in anthracene, and the theoretical buildup factors refer to energy absorption in air. Accordingly, energy absorption-

DECLASSIFIED

DECLASSIFIED

buildup factors for an anthracene detector were computed for a cobalt source spectrum attenuated through water, iron, and lead.[10] When this factor was used in the comparisons, the dose-buildup factors in water improved in both magnitude and slope, especially at the deeper penetrations. The agreement between iron and water data with theory was not significantly improved.

An analysis of the gamma ray energy spectrum data for the attenuation of the monoenergetic cesium spectrum through iron was performed. The theoretical energy spectrum was calculated by a Monte Carlo computer code, FMC-G, in which the experiment was accurately portrayed as a cesium source with a crystal spectrometer placed in contact with the opposite side of a two-foot circular iron disc. The results of this calculation were converted to a pulse-height distribution of the NaI(th) experimental crystal by multiplying each energy group by a energy response function and efficiency of the crystal. The results of calculation provided a theoretical pulse-height energy spectrum that was compared to the experimental data. This comparison showed fair agreement in shape but poor agreement in absolute magnitude.

CONCLUSIONS

The results of this experiment are inconclusive. In many instances, additional experimental work would help resolve the differences between the experimentally determined average dose-buildup factors and the theoretical values.[11] This is particularly true for measurements concerning the center-of-detection of the detectors, the possibility of scattering around the slabs, background count rate in the pool, and similar values. All the point kernel programs have been used with dose-buildup factors but many of the gamma ray measurements, taken during the course of experiments, employed scintillation counters that record something other than air dose. Hence, disagreement is to be expected. Based on this experiment, no judgement can be made on the validity of the theoretical dose-buildup factors.

11.2 NUCLEAR HEATING EXPERIMENTS

In 1957, a series of experiments, analyses, and instrument-development programs were undertaken to provide calculational techniques and data to handle the problems associated with radiation heating in reactor shields.[12] Prior to these experiments, experimental shield measurements had been concentrated on biological dose rates. However, it became clear that heat generation in the reactor shield was one of the limiting factors in shield design.

In principal, with a knowledge of the biological dose and the energy spectrum of the radiation at a point in a shield, an accurate calculation of the heat generation could be made. Practically, a sufficient accurate knowledge of the energy spectrum is rarely obtainable. For that reason, direct calorimetric measurements of the heat generated in complex laminated shields were undertaken in order to develop and check simple empirical methods of calculating the heating rate.

EXPERIMENTAL APPROACH

The nuclear heating experiments consisted principally of calorimetric measurements of the heat generated in thermally isolated samples located in a laminated shield constructed of typical reactor shield materials. This was done by locating a slab array of several materials adjacent to one face of a swimming pool reactor. The first experiments were conducted at the Oak Ridge Bulk shielding facility; latter experiments were begun at the Shield Test Pool Facility at the Idaho Test Station. In the portion of the

DECLASSIFIED

DECLASSIFIED

experimental series for which data are available, the data were taken at Oak Ridge.[12,13] The shield array for this series consisted of 4 inches of beryllium followed by 4 inches of a heavy gamma shield, either lead, a tungsten alloy (Mallory 1000), or steel. This was followed by a 4-inch slab and a 12-inch slab of lithium hydride. Located in the center of each slab, along a centerline of the reactor, was a calorimetric heat rate sensor. These consisted of a small sample of the same material as the slab, suspended in a void cavity in a cylinder of the same material. The sample was thermally isolated from the case by mounting it in the center of the cavity with three ceramic supports. Thermocouples were attached to the sample and to the case. The raw experimental data taken were the temperatures of the sample and case as a function of time after the reactor was turned on. From these data a heating curve was constructed. Analysis of the heating curve then provided the heating rate.

DATA OBTAINED

Heating rates were obtained for beryllium, gamma shielding, and lithium hydride where the gamma shielding was iron, lead, or Mallory 1000.[14,15] Hence, heat rates are available for beryllium for three cases in which the material following the beryllium slab was different, and heating rates are available for the lithium hydride for three cases in which different material preceded the lithium hydride.

ANALYSIS OF DATA

The analysis of this experiment was accomplished in two steps. First, the heating rates were derived from the raw data. Second, calculations of nuclear heating in the slabs were compared with the raw data.

A computer program was prepared[16] to translate the thermocouple data to heating rates.

Calculations of the nuclear heating were subdivided into several operations:

1. Calculations of the heating caused by gamma rays emitted from the core.[17]
2. Calculations of the heating caused by direct neutron interactions.
3. Calculations of heating caused by neutron induced radiations.[18]

Core gamma heating was calculated using point kernel techniques. For this work, core gamma rays were defined as the sum of the gamma rays released as a result of fission, both prompt and fission product decay, plus the gamma rays resulting from thermal neutron capture in the core. The attenuation to the sample was calculated using linear absorption coefficients. The energy absorption was calculated using energy absorption-buildup factors, where available, and dose-buildup factors when they were not available.

Neutron heating was calculated using a one-dimensional, multigroup, diffusion code. The direct neutron heating was calculated by converting to heat the energy lost in moderation. Indirect neutron heating was calculated by using the diffusion code to calculate the thermal neutron radiative captures in the shield materials. These capture rates were then used to establish sources of secondary gamma rays which were used as input in a point kernel code to calculate the energy absorption in the samples, in the same way as for the core gamma rays.

The results of the analysis were surprisingly accurate. The ratio of the calculated heating rates to the measured heating rates in the beryllium ranged from 1.13 to 1.26 by the best method; the ratio in the gamma shield ranged from 0.83 to 1.11; and the ratio in the lithium hydride slabs ranged from 0.36 to 0.9.

DECLASSIFIED

DECLASSIFIED

CONFIDENTIAL

ADDITIONAL EXPERIMENTS

The nuclear heating experiment performed at the ORNL, Bulk Shielding Facility was a composite slab experiment which did not allow separation of the heating effects into contributions from gamma rays, fast neutrons, and thermal neutrons.[19,20] Hence, while the agreement observed in the other experiments is good, it is only a measure of the ability to calculate gamma heating, because gamma heating made up more than half the total heating. To improve heating calculations, measurements were needed in which each type of heating could be observed individually. To accomplish this, an experiment was planned for the Shield Test Pool Facility incorporating the following features:

1. Three basic slab configurations capable of emphasizing heating from gamma rays, fast neutrons, and thermal neutrons. The configuration used to observe gamma ray heating was a test slab with 12 inches of lithium hydride between the test slab and the reactor. The configuration for fast neutron heating contained 7 inches of lead and 0.75 inch of boral preceding the test slab. The configuration for thermal neutrons contained all of the fast neutron materials plus 4 inches of beryllium to moderate the fast neutrons and provide a high thermal flux.
2. In addition to direct heating measurements and biological dose measurements, measurements of neutron flux with threshold foils.
3. Improved heat rate sensors.

This experimental program[13,21,22] was begun but never finished because of the cancellation of the program.

HEAT RATE SENSOR DEVELOPMENT

From the outset, this experiment required the development of heating rate sensors. The sensors used in the first experiments at the BSF were relatively crude devices. Sensors for each of the materials in the slab array were made of a hollow cylindrical block of the shield material. A small sample of the shield material was thermally isolated in the cavity by fixing it in space with ceramic stand-offs. Thermocouples were located on both faces of the isolated sample and on the case. The accuracy and sensitivity of these sensors were less than needed for precise work. Accordingly, a sensor was designed incorporating improvements, to achieve greater sensitivity and accuracy. The principal improvements were in two areas: improvement in thermal isolation from the case[23,24] and improvement in the calibration.[25] To decrease the heat flow from the case, the shield samples in the cavity were plated to increase the reflectivity. The suspension system was changed to a thin tungsten spring wire, and the hollow cavity was evacuated to an air pressure of approximately 0.1 microns of mercury. Improvement in calibration was a result of extreme care and precision in working with the thermocouples. These improvements required many months of effort. Particular difficulty was experienced in attempting to maintain the vacuum in the cavity; this was partly because of the porous nature of some of the materials.

CONCLUSIONS

Three important contributions resulted from this experimental program: (1) it was demonstrated that simple calculational techniques could be used to calculate total nuclear heating rates in shields, (2) the requirements and techniques for refined heating rate measurements in laminated shields were outlined, and (3) a highly sensitive workable heat rate sensor was developed.

CONFIDENTIAL

DECLASSIFIED

DECLASSIFIED

11.3 SOURCE PLATE EXPERIMENTS

In 1955, an experimental shielding program using the Lid Tank Shielding Facility at Oak Ridge National Laboratory was initiated by the Shielding Unit of the General Electric Aircraft Nuclear Propulsion Department. The purpose of this program was to study the attenuation properties of advanced shielding materials. This series of experiments was completed in 1958.

The Lid Tank Shielding Facility had the advantage of a simple source geometry which simplified the analysis of the data. However, the low power (5 watts), the slow rate of obtaining data, and the lack of equipment to measure neutron and gamma spectra were disadvantages. In order to overcome these disadvantages, the design of a source plate facility at the Battelle Memorial Institute was initiated in July 1957. This facility was designed and constructed, the instruments were ordered, and the fission plate was calibrated during the first year. The second year was devoted to the calibrations of the basic instruments, mechanical calibrations, and preliminary shielding experiments. In the following two years, this facility was used to study the shielding characteristics of LiH, Be, and BeO.

LID TANK SHIELDING EXPERIMENTS

A schedule for shielding experiments using advanced shield materials was published in July 1955.[26] The materials used for this study consisted of LiH and combinations of stainless steel, Hevimet, boral, uranium, beryllium, tungsten, zirconium, and lithium hydride. The measurements included fast-neutron dose rate and gamma dose rate traverses behind the various slab arrays and thermal-neutron flux traverses using foils between the slabs. The measured data may be found in references 27 and 28. An analysis of these data[29] indicated the importance of secondary gamma sources. Additional experiments[30] were proposed to investigate the suppression of secondary gamma rays and the attenuation of thermal-neutron flux, fast-neutron dose rate, and gamma dose rate using slab arrays composed of the materials used in the first series of measurements. The data obtained from this series of tests were published.[31] Analysis of these data, which was related to Project 103 Shield Design, was completed in June 1958.[32, 33]

DESCRIPTION OF THE SOURCE PLATE FACILITY

The research reactor, located at the Battelle Memorial Institute Atomic Energy Center, was used to provide a source of thermal neutrons for the GE-ANPD Source Plate Facility. A complete description of this reactor was published.[34] The core of the pool-type reactor is composed of the MTR-type fuel elements suspended on a tower from a movable bridge. The pool is enclosed by thick concrete walls modified into a stall at one end through which beam-tubes and a thermal column give access to the core.

The thermal column is approximately 12 feet in length and 4 feet square. It is stacked with high-purity graphite blocks, and access to the thermal is provided by horizontal and vertical entrances. In order to increase the thermal-neutron current at the horizontal entrance, 29 percent of the graphite was removed from the center of the column. With this void in the center of the column, the ratio of thermal to epithermal flux was approximately 67 at the horizontal entrance. The end of the column was modified by a paraffin collimator in order to reduce the number of thermal neutrons diffusing around the source plate.

The GE-ANPD Source Plate Facility consisted of a U-235 source plate, a large open shielding tank with an instrument tower and bridge, and a control panel for the various

DECLASSIFIED

DECLASSIFIED

CONFIDENTIAL

instruments. A description of this facility was published.[35] Thermal neutrons from the thermal column induced fissions in the U-235 source plate, and the shielding specimen was placed adjacent to the source plate where it was subjected to the fission neutrons and gamma radiations. The radiations were detected by sensors suspended from the instrument tower which is supported by a motorized bridge spanning the shielding tank. When background measurements were made, the thermal-neutron current was cut off from the fission plate by lowering a boral-cadmium curtain between the plate and thermal column. The facility is shown in Figure 11.1.

The fission plate was made of a highly enriched nickel-plated uranium foil jacketed in aluminum. The complete source plate assembly consists of an aluminum frame containing the fission plate, electrical-heater plate, resistance thermometers, and Lavite spacers. A diagram of the assembly is shown in Figure 11.2. The 2-1/2-inch lead plate is a gamma shield, and the boral curtain on the pool side of the assembly minimizes power changes in the plate due to neutron reflections from shielding specimens.

The instrumentation for the bridge measurement, fission plate control, and radiation-detecting instruments was assembled into one console located on a balcony overlooking the shield tank.

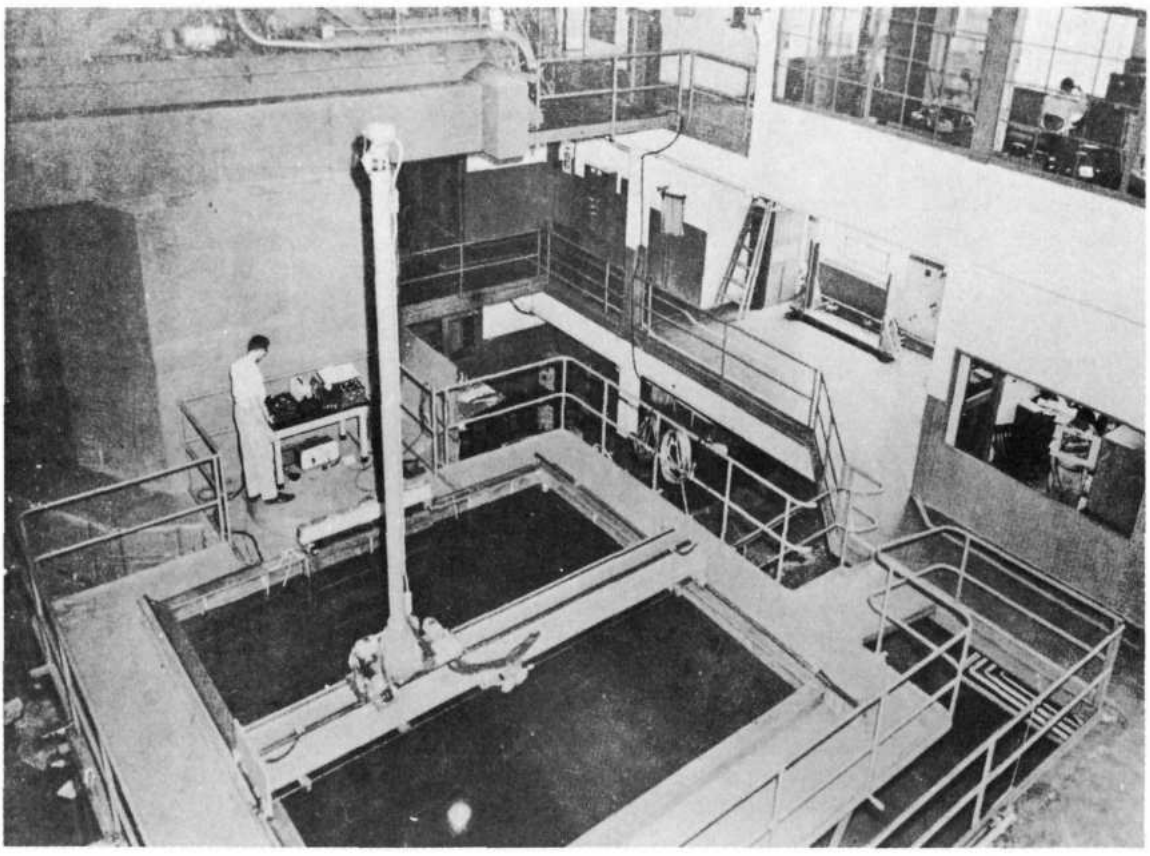

Fig. 11.1 – Shielding-research area

CONFIDENTIAL

DECLASSIFIED

DECLASSIFIED

CONFIDENTIAL

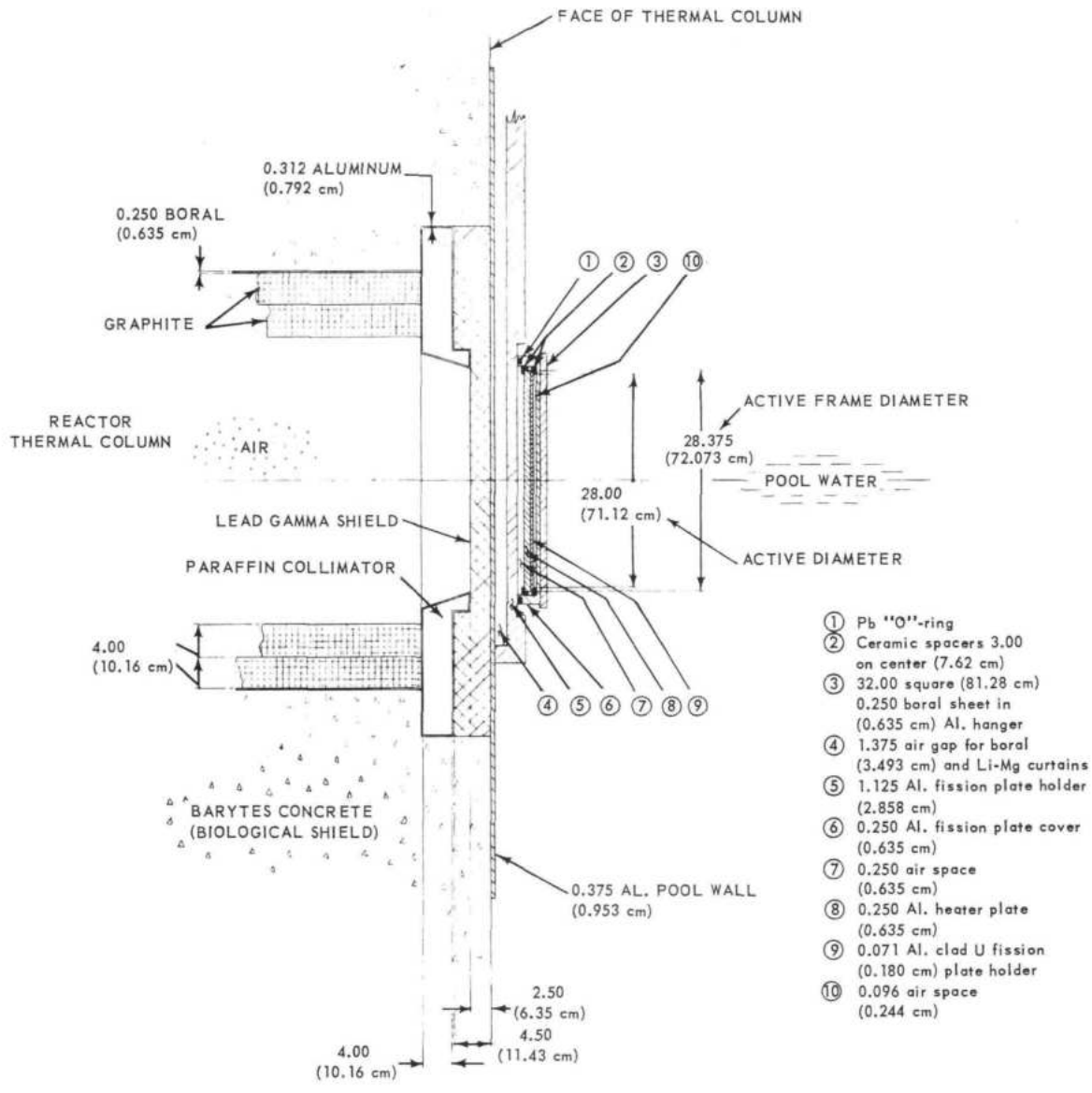

Fig. 11.2 – Vertical cross section of fission-plate environment (Dwg. 737D931)

CONFIDENTIAL

DECLASSIFIED

DECLASSIFIED

11.4 NEUTRON ACTIVATION - FOIL REDUCTION

In support of the experimental program relating to the shielding or reactor studies, a large number of foils are exposed to neutron fluxes. The feedback of this experimental data is needed as soon as possible so that the next experiment may be initiated. GE-ANPD Computer Program 185 was designed to provide a rapid and consistent method for reducing "raw" foil counting data into an immediately useful form.[47] The program features flexibility to provide for nearly all commonly encountered data-acquisition and data-reduction techniques. It is further designed to provide the maximum information obtainable from the input data.

NUCLEAR INSTRUMENTS AT BATTELLE MEMORIAL INSTITUTE

The shielding-research area at Battelle Memorial Institute was equipped to measure fast-neutron dose rate, gamma dose rate, thermal-neutron flux, gamma spectrum, and resonance and threshold foil activations.[35,36] A list of the instruments used to make the above measurements is given in the following paragraphs.

Fast-neutron dose rates were measured with Hurst-type dosimeters. In regions where the ratio of thermal flux to fast flux was high, measurements were made with a cadmium cover placed over the dosimeter. This cover was necessary to keep out impurities which caused the dosimeters to be sensitive to thermal neutrons.

Gamma dose rates were measured with three different ionization chambers: A CO_2-filled carbon-wall, 500-cm^3 chamber, a CO_2-filled carbon-wall, 10-cm^3 chamber, and a Westinghouse WX-343 50-cm^3 aluminum-wall chamber, filled with argon.

Thermal-neutron flux was measured with fission chambers and gold foils. The thermal fluxes reported were based on a Maxwellian average gold cross section.

Gamma spectra behind the various slab arrays was measured with an 8-inch-high by 8-inch-diameter collimated NaI(Tl) scintillation spectrometer.[37]

Various threshold and resonance foils were used. The activations were measured and the data were reduced to neutron spectra.

FISSION-PLATE CALIBRATION

The thermal neutron-flux distribution incident on the fission plate was measured by activating manganese-iron wires.[35] From these measurements the power distribution over the plate was approximated[38] by the equation

$$P(r) = 2.894 \times 10^{-4} \cos .0204\, r$$ when P(r) is the

number of watts per cm^2 at radius r, normalized to 1 watt.

The power of the fission plate was measured by the electro-substitution method. This method consists of matching the temperatures produced by the fission source to those produced by an equivalent electric source.

WATER MEASUREMENTS

Measurements in water were made at the GE-ANPD Source Plate Facility in order to compare the measurements with other shielding facilities, to provide standard measurements for checking the consistency of future calibrations, and to make comparisons between theory and experimental values for a single-region hydrogenous shield. A data report and analysis of the measurements was published.[39]

DECLASSIFIED

DECLASSIFIED

The measurements were:

1. Fast-neutron dose rate traverses on the centerline and in a symmetry plane 10, 20, 30, 40, and 50 centimeters off the centerline to a penetration of approximately 90 centimeters with a Hurst-type dosimeter.
2. Gamma dose rate traverses on the centerline and in a symmetry plane 10, 20, 30, 40, and 50 centimeters off the centerline to a penetration of approximately 180 centimeters with a 500-cubic centimeter carbon-wall ionization chamber.
3. Thermal flux traverses on the centerline and in a symmetry plane 10, 30, 40, and 50 centimeters off the centerline, to a penetration of approximately 40 centimeters with gold foils and from 40 to 110 centimeters with a fission chamber.

The water centerline data are shown in Figures 11.3, 11.4, and 11.5.

GADOLINIUM MEASUREMENTS

In mid-1958, a requirement developed within the Department for a knowledge of the fast-neutron removal cross section of gadolinium. Since only a limited quantity of gadolinium was available, a double-iris arrangement (each iris consisting of a sheet of boron-loaded material with a 6-centimeter diameter hole) was placed between the thermal column and the fission plate. This arrangement peaked the fission plate power behind the gadolinium. A shield fixture, composed of a 5-3/8-inch-thick rectangular slab or iron, 4-feet square with a 10-inch diameter hole at the center, was placed adjacent to the source plate. Plugs of gadolinium, iron, aluminum, lead, and titanium were used in the hole so that the fast-neutron attenuation properties could be compared. Fast-neutron dose rates were measured to a penetration of 80 centimeters of water behind each material. In addition the source distribution over the fission plate was measured. The data were published.[36,40]

From the measured values, it was determined that the removal cross section for gadolinium lies between the values for iron and aluminum with a value approximately the same as lead. A macroscopic removal cross section of 0.108 cm^{-1} gave the best fit to the experimental data.[40] The results indicated that gadolinium is not a highly desirable fast-neutron shield material.

LITHIUM HYDRIDE MEASUREMENTS

Measurements were made at the GE-ANPD Source Plate Facility in order to compare the shielding effectiveness of Li^6H with that of ordinary LiH. To accomplish this, various slab arrays were placed adjacent to the source plate, and measurements were made in the shield tank on the source plate centerline. In addition, using a slab with an instrument well, a solid centerline fast-neutron dose rate traverse was measured through approximately 30 inches of LiH. The purpose of this traverse was to determine the removal cross section of Li. A plot of the solid centerline traverse is shown in Figure 11.5. The complete data for the above measurements were published.[38,41]

From the measurements it was determined that both LiH and Li^6H are more effective fast-neutron shielding materials than water, but both LiH and Li^6H are less effective gamma shielding material than water. Li^6H was found to be as effective as LiH as a shielding material on a thickness basis. Hence, the substitution of Li^6H for ordinary LiH leads to a weight saving. The removal cross section for Li in LiH was found to be 0.070 cm^{-1}.

BERYLLIUM OXIDE MEASUREMENTS

A series of tests were run at the Source Plate Facility to determine the shielding properties of BeO. The material consisted of three 4-inch-thick slabs and one 9-inch-thick slab. All slabs were 35 inches square, and they were mounted in 6-inch-thick steel frames. One 4-inch-thick slab had a 7/8-inch diameter and a 27-inch-long instrument well. A complete description of the slabs and the measurements were published.[42,43]

DECLASSIFIED

DECLASSIFIED

CONFIDENTIAL

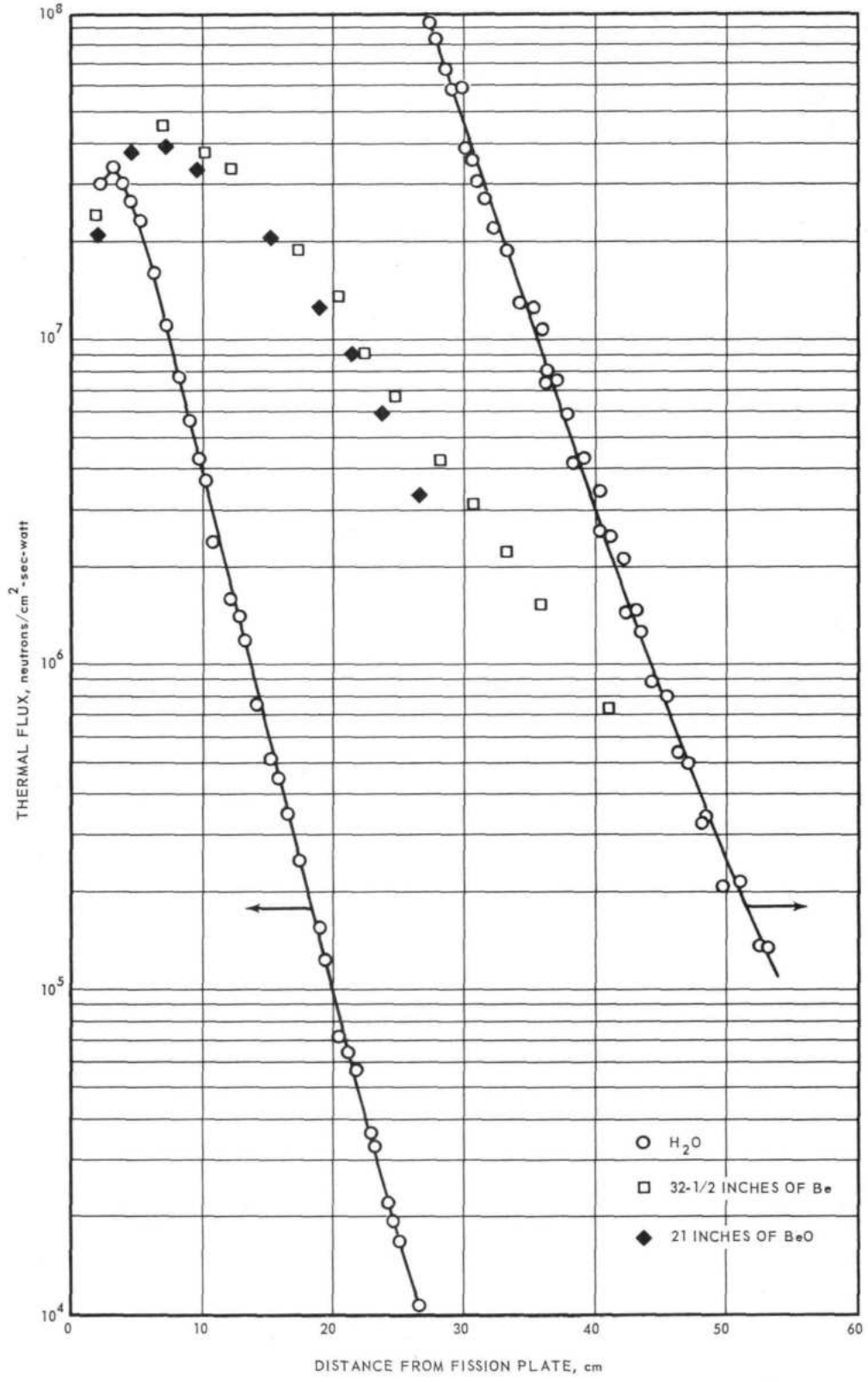

Fig. 11.3 – Measured centerline thermal flux within beryllium, beryllium oxide, and water

CONFIDENTIAL

DECLASSIFIED

DECLASSIFIED

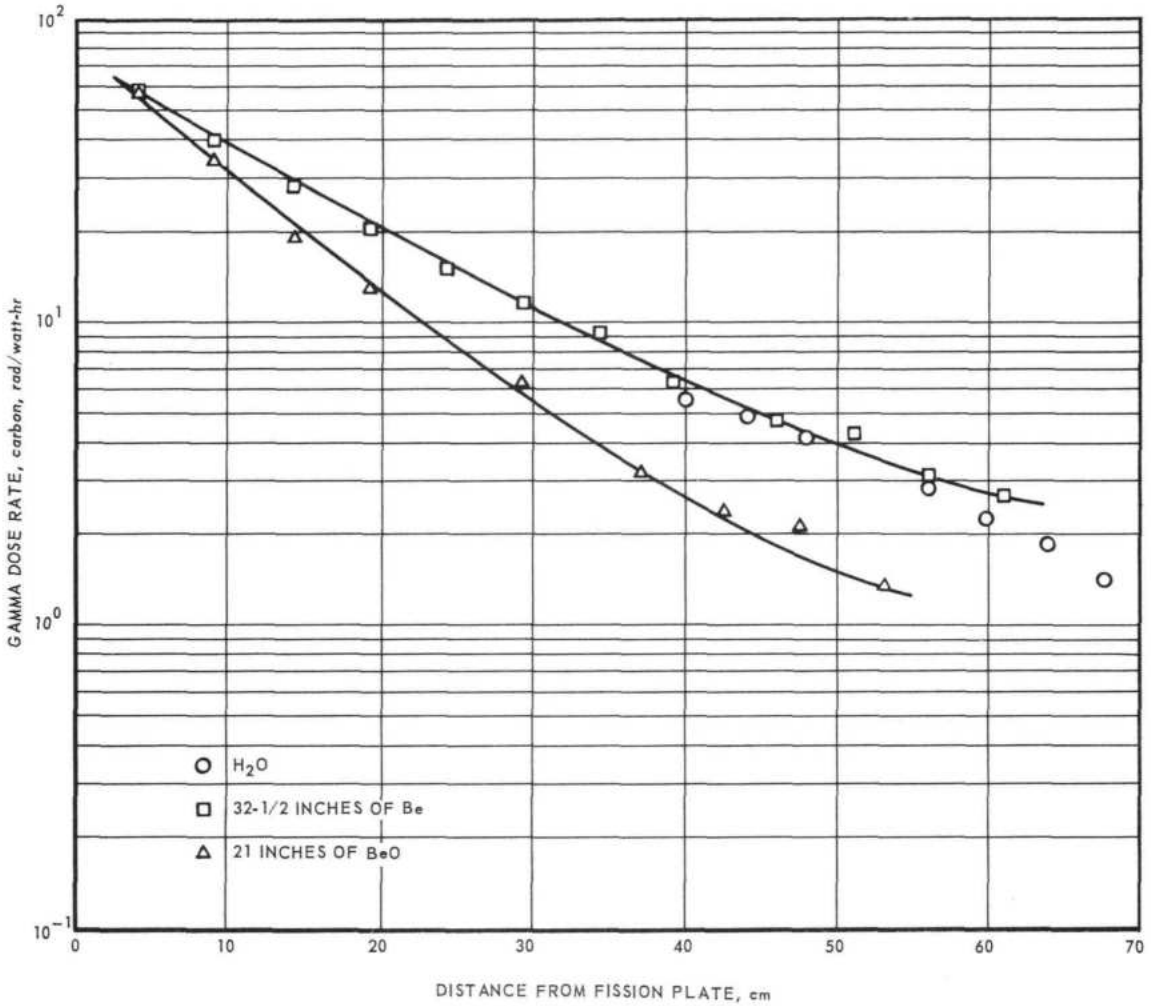

Fig. 11.4 – Measured centerline gamma dose rates within beryllium, beryllium oxide, and water

The fast-neutron dose rate and threshold foil activation traverses within BeO were compared with point kernel calculations based on NDA data for a point fission source in an infinite medium of BeO. The results indicated that the measured values are consistent with the NDA data. In addition, the other measurements listed above were compared with calculated values using point kernel computer programs and a multilevel diffusion program. The results were published.[44]

BERYLLIUM MEASUREMENTS

Extensive shielding measurements using slab arrays of beryllium in the shielding tank at the Source Plate Facility were completed. The beryllium consisted of seven 4-inch-thick slabs and one slab 4-1/2 inches thick. Each slab was composed of three beryllium logs (16 inches by 51 inches) held in place by an aluminum frame. One beryllium log had a 7/8-inch-diameter instrument well 27 inches long. The measurement data was published.[45,46]

An analysis of the above data was not completed. However, the measured data were consistent with the NDA data for beryllium.

DECLASSIFIED

DECLASSIFIED

CONFIDENTIAL

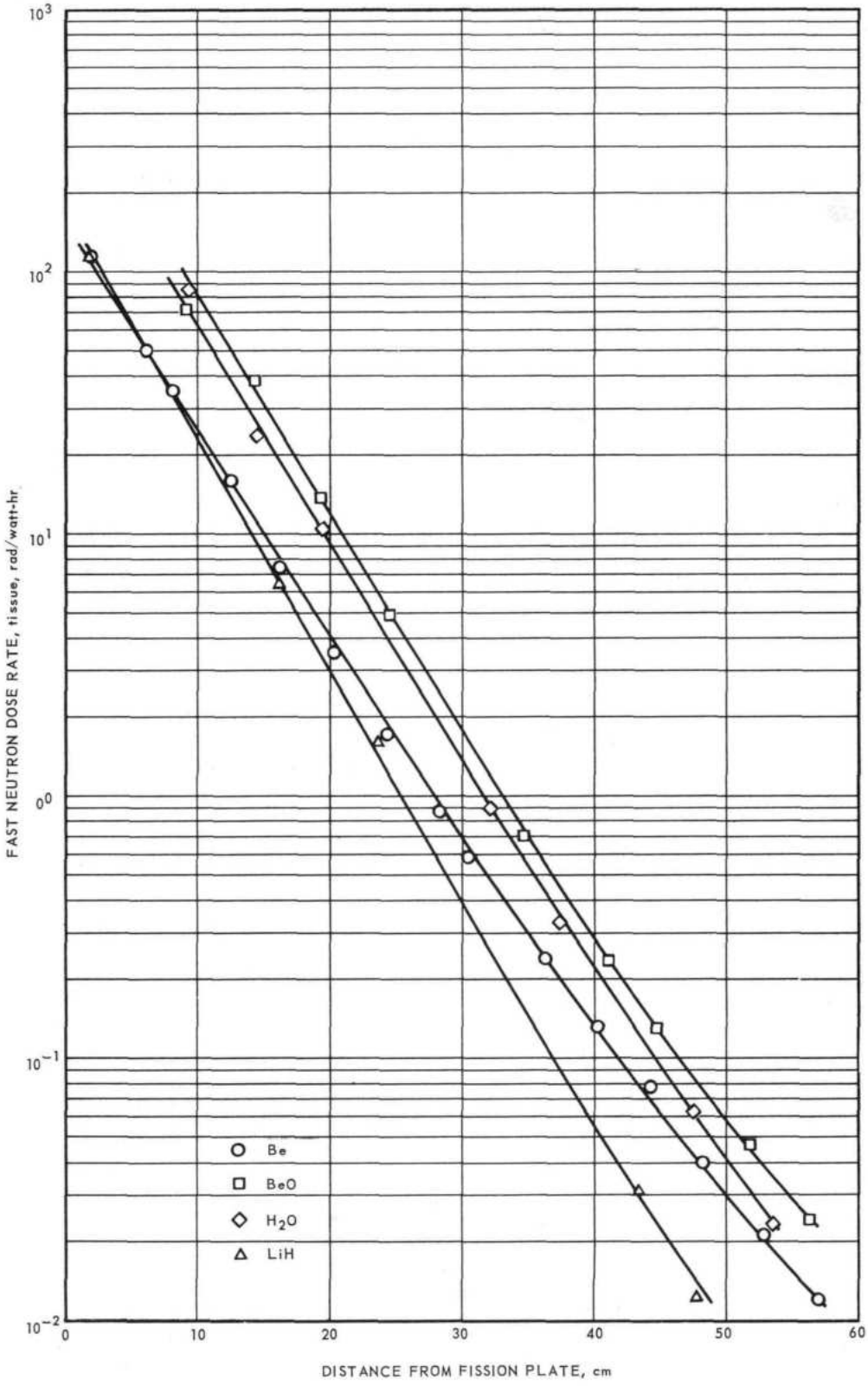

Fig. 11.5 – Measured centerline fast-neutron dose rates within beryllium, beryllium oxide, lithium hydride, and water

CONFIDENTIAL

DECLASSIFIED

DECLASSIFIED

11.5 REFERENCES

1. Goldstein, H., and Wilkins, J. E., "Calculations of the Penetration of Gamma Rays," Nuclear Development Corporation of America, NYO-3075, June 30, 1954.
2. Mitchell, V. J., "Planned Gamma Ray Point Source Experiments," GE-ANPD, DC 58-1-119, January 14, 1958.
3. Brenton, R. F., "Point Source Experiment Procedure," GE-ANPD, DC 58-1-708, January 2, 1958.
4. Carver, J. G., "Schedule for Point Source Experiments," GE-ANPD, DCL 58-7-69, July 14, 1958.
5. Feinauer, E., and Newton, G. W., "Preliminary Data from Point Source Experiment," GE-ANPD, DC 59-12-731, December 17, 1958.
6. Mitchell, V. J., and Smith, R. B., "Water-Air Boundary Dose Rate Measurements Using Cobalt 60 Source," GE-ANPD, DC 58-4-54, April 7, 1958.
7. Mitchell, V. J., "Summary Report of Gamma Ray Point Source Data from Single Material Measurements," GE-ANPD, DC 59-12-229, December 31, 1959.
8. Mitchell, V. J., "Summary Report of Gamma Ray Point Source Data from Multiple Material Measurements," GE-ANPD, DC 60-4-108, April 19, 1960.
9. Mitchell, V. J., "Analysis of Gamma Ray Point Source Data from Single Material Measurements," GE-ANPD, DC 60-2-215, February 23, 1960.
10. Mitchell, V. J., "Interim Report on the Analysis of Gamma Ray Point Source Data from Single Material Measurements," GE-ANPD, DC 61-1-101, January 27, 1961.
11. Mitchell, V. J., "Request for Additional Point Source Measurements," GE-ANPD, DCL 61-2-30, January 24, 1961.
12. Carver, J. G., "Description and Preanalysis of Proposed BSF Nuclear Heating Measurements," GE-ANPD, XDC 58-1-51, December 23, 1957.
13. Brenton, R. F., "Low Power Flux Map and Power Calibration of SUSIE Reactor," GE-ANPD, DC 60-6-722, June 13, 1960.
14. Maier, R. J., "Report of Data from First Nuclear Heating Measurements in Bulk Shielding Facility," GE-ANPD, XDC 58-8-61, July 28, 1958.
15. Maier, R. J., "Report of Data from Second Nuclear Heating Measurements in Bulk Shielding Facility," GE-ANPD, XDC 59-6-34, May 13, 1959.
16. Baumgardt, N. R., "Shielding Program 17-0, Analysis of Heating and Cooling Data," GE-ANPD, DC 58-7-157, May 1958.
17. Casper, A. W., "Point Kernel Calculations of Core Gamma Heating in the BSF Nuclear Heating Experiment," GE-ANPD, XDC 58-8-234, August 20, 1958.
18. Maier, R. J., "Comparison Between Calculated and Measured Nuclear Heating Rates in BSF Experiments," GE-ANPD, XDC 60-2-64, February 4, 1960.
19. Maier, R. J., "Test Request for SUSIE," GE-ANPD, DCL 58-10-213, October 31, 1958.
20. Maier, R. J., "Details of Test Request for Nuclear Heating Experiments," GE-ANPD, DCL 60-1-148, January 15, 1960.
21. Maier, R. J., "Preanalysis of SUSIE Reactor," GE-ANPD, DCL 59-5-115, May 11, 1959.
22. Maier, R. J., "Preanalysis of Nuclear Heating," GE-ANPD, DCL 60-2-72, February 8, 1960.
23. Rusch, G. K., "Heating Rate Sensors," GE-ANPD, DC 60-3-85, March 7, 1960.
24. Rusch, G. K., and Gralenski, N. M., "Heating Rate Sensors," GE-ANPD, DC 60-3-85, March 7, 1960.
25. Madison, J. H., Jr., "Calibration of Chromel-Constantan Thermocouple for Nuclear Heat Rate Sensors," GE-ANPD, XDC 61-2-41, February 10, 1961.

DECLASSIFIED

DECLASSIFIED

26. Aschenbrenner, F. A., "Description of Scheduled Lid Tank Experiments with Advanced Shield Materials," GE-ANPD, DC 55-8-2, July 1955.
27. Mitchell, V. J., "Data Report of Lid Tank Experiments with Advanced Shield Materials," GE-ANPD, DC 57-3-99, March 1957.
28. Weiss, W. L., and Belcher, J. A., "Data Report of Lid Tank Experiments for July 1957," GE-ANPD, DC 57-9-133, September 1957.
29. Hanchen, K. B., and Haffner, J. W., "Description and Analysis of the Lid Tank with Advanced Shielding Materials," GE-ANPD, DC 57-10-83, October 1957.
30. Aschenbrenner, F. A., "Description of Additional Measurements Requested at ORNL Lid Tank During October and November 1957," GE-ANPD, XDC 57-10-95, October 1957.
31. Belcher, J. A., "Lid Tank Data July 1957 to February 1958," GE-ANPD, XDC 60-2-166, February 1960.
32. Friedman, T. S., "Analysis of Late 1957 and Early 1958 Lid Tank Experiments Pertaining to Project 103 Shield Design," GE-ANPD, XDC 58-6-163, June 1958.
33. Friedman, T. S., "Analysis of Late 1957 and Early 1958 Lid Tank Experiments," GE-ANPD, APEX-524, June 1958.
34. Anno, J. N., Plummer, A. M., and Chastain, J. W., "Pool-Type Research Reactor," Battelle Memorial Institute, March 1958.
35. Morgan, W. R., Epstein, H. M., Anno, J. N., and Chastain, J. W., "Shielding Research Area at Battelle," Battelle Memorial Institute, BMI-1291, September 1958.
36. Klingensmith, R. W., Epstein, H. W., and Chastain, J. W., "Shielding Studies on Salt Slabs, Gadolinium, and Water," Battelle Memorial Institute, BMI-1384, October 1959.
37. Weiss, W. L., "Calibration of An 8" x 8" Sodium Iodide (T1) Crystal," GE-ANPD, XDC 60-3-212, March 1960.
38. West, D. L., "Data Report and Analysis of Fast-Neutron Attenuation Within LiH," GE-ANPD, XDC 60-1-17, December 1959.
39. Casper, A. W., "Data Report and Analysis of Battelle Pool Mapping," GE-ANPD, XDC 59-8-228, August 1959.
40. Casper, A. W., "Data Report and Postanalysis of Battelle Source Plate 'Plug' Tests," GE-ANPD, XDC 59-5-220, May 1960.
41. Casper, A. W., "Data Report and Analysis of Measurements Made in Water Behind Arrays of LiH and Li^6H," GE-ANPD, XDC 59-10-69, October 1956.
42. Vieli, N., and Kodras, F. D., "Chemical Inspection and Material Data - Test Slabs," GE-ANPD, Supplement to DC 58-5-26, February 1960.
43. Klingensmith, R. W., Jung, R. G., Lindgren, W. A., Epstein, H. M., and Chastain, J. A., "Fast-Neutron and Gamma Spectrum, and Dose in Beryllium Oxide," Battelle Memorial Institute, BMI-1493, January 1961.
44. Schreiber, P. W., and Kodras, F. D., "Measured and Calculated Radiation Levels Within and Behind Beryllium Oxide," GE-ANPD, XDC 61-1-14, February 1961.
45. Schreiber, P. W., and Kodras, F. D., "Measured and Calculated Radiation Levels Within and Behind Beryllium," GE-ANPD, APEX-701, July 1961.
46. Schreiber, P. W., "Data Report of Gamma Spectra Behind Various Thicknesses of Beryllium, Beryllium Oxide and Lithium Hydride," GE-ANPD, APEX-700, July 1961.
47. Zoller, L. K., "Neutron Activation - Foil Reduction (Program 185)," GE-NMPO, DC 61-11-13, January 1962.

DECLASSIFIED

DECLASSIFIED

CONFIDENTIAL

12. MOCKUP SHIELD EXPERIMENTS

Much of the early experimental shielding effort at ANPD was devoted to measurements of partial and complete shield mockups. These were frequently planned to check calculations for a specific power plant design and to provide experimental data which could be applied directly to the design. Other mockup experiments were planned to investigate duct leakage, secondary gamma rays, material attenuation without hydrogenous backing, attenuation through combinations of materials, nuclear heating, and many other special problems.

Unfortunately, many of the shield mockups were not as realistic as necessary because the reactor sources available for these tests were fairly small and were rectangular rather than cylindrical as in the design power plants. Also, the reactor compositions differed. As a result, the neutron and gamma ray leakage spectra differed. The Lid Tank Shielding Facility source plate provided an even poorer approximation of design reactors. Most of the mockups were necessarily scaled down in size to fit the dimensions of the available radiation sources and to minimize costs. Because of all these limitations, the effects of ducts, shadow shields, and secondary sources, could not always be accurately determined.

Nevertheless, many of the experiments did provide useful information. Because fundamental methods of analysis were not adequately developed, most of the experiments were essential at the time. Several serious nuclear problems were revealed that were previously overlooked or neglected. Also assurance was gained that design shields, with corrective perturbations, would perform satisfactorily.

Because much of the information acquired from mockup experiments could be applied appropriately only to the design for which the mockup was intended only limited basic shield physics information was obtained. Few of the data have lasting general applicability to a variety of shield design problems because of the complexity of the experiments.

After several successive ANP program changes, it became obvious that a more fundamental approach to shield nuclear analysis and design was necessary. Consequently, after cancellation of the XMA-1A power plant, the main emphasis in the supporting experimental program was diverted to basic shield penetration measurements (see section 11).

Some mockup tests were continued in support of the main power plant development. However, all of these were incorporated as additional measurements in the regular program of measurements, with critical assemblies simulating the design reactor. The desired experimental data[2] was thus acquired more economically and much quicker than would have been possible with specially constructed mockups.

12.1 PARTIAL DUCT AND SHIELD MOCKUPS

The Lid Tank Shielding Facility at Oak Ridge National Laboratory was used periodically over a span of several years for measurement of thermal neutron fluxes and fast neutron and gamma ray dose rates after penetration through various arrays of liquid and solid

CONFIDENTIAL

DECLASSIFIED

DECLASSIFIED

shield materials. Some of these arrays were designed as partial mockups of design shields, and others were designed to determine radiation attenuation properties of shield materials and to investigate the importance of secondary gamma ray sources. Also, several partial mockups of annular and helical ducting systems were tested to determine leakage properties. Details of some of the most important tests were published. (See references 3 through 9, inclusive.)

Several mockups were also tested in the Bulk Shielding Facility at the Oak Ridge National Laboratory. These included partial mockups of ducting systems and a unit shield.

An Outside Test Tank (OTT) was built for the Department for the purpose of making nuclear measurements in air at great distances from full-scale porous duct mockups. The OTT is a cylindrical steel tank, 13.5 feet in height, 15 feet in diameter, with a 0.188 inch wall. It is divided internally into a reactor-moderator compartment, a test specimen tank, and a bulk shield tank. The OTT was located at the Nuclear Aircraft Research Facility operated for the Air Force by Convair, Fort Worth. Their Ground Test Reactor (GTR) served as the radiation source in these measurements. A complete description of the OTT and associated test hardware was published.[10]

Numerous wavy-wall, strut, and rod-and-tube-sheet porous shield plugs were tested in the OTT. A Variable Geometry Shield Test System was built to facilitate testing of basic porous plug geometries (see references 11 through 15, inclusive).

In addition, the OTT was used for extensive in-air measurements of neutron and gamma ray penetration of several combinations of multiple material shields. Many of these measurements provided penetration data for shield materials without hydrogenous backing. Few similar measurements have been made elsewhere. A directory of the OTT slab configuration was published.[16] Descriptions and analyses of many of the tests are given in references 17 through 25, inclusive.

Most of the OTT tests were performed in support of the XMA-1A power plant development. A complete discussion of the tests and a list of references are included in a summary report[26] on the XMA-1A shielding effort. (See also APEX-907 of this summary report.)

Annular duct mockup tests were performed for the Department by Convair with the GTR. Measurements made in water around the mockups are presented in references 27 through 33, inclusive.

12.2 COMPLETE SHIELD MOCKUP

A complete mockup of the lead and water shield for the R-1 nuclear reactor was tested at the Bulk Shielding Facility and the Tower Shielding Facility at Oak Ridge National Laboratory. Measurements of thermal neutron flux and fast neutron and gamma ray dose rate were made in water surrounding the shield at the BSF. The TSF test included similar measurements in air in the vicinity of the shield, in a water-filled detector tank, and in a crew-shield mockup. Descriptions of these tests are available in references 34 through 42, inclusive.

In order to learn more about some of the physical phenomena associated with reactor shield assemblies composed of depleted uranium and lithium hydride and employing realistic shield design geometries, a mockup called the Solid Shield Mockup (SS-1) was constructed at Oak Ridge and tested at Convair, using the GTR. The SS-1 consisted essen-

DECLASSIFIED

DECLASSIFIED

tially of concentric cylinders of LiH and uranium-238, with end plugs composed of the same materials.

Four geometric arrangements of the concentric cylinders and end plugs were tested: (1) to obtain information of the shielding effectiveness of LiH and U, (2) to obtain some information on the optimum arrangement of fast neutron and gamma ray shielding, and (3) to obtain additional information on certain physical processes, such as duct leakage, and secondary gamma ray production.

The mockup was constructed to be highly flexible, with the various cylinders and discs being removable and, in some cases, interchangeable. For example, the discs of uranium-238 and LiH which composed the front plug could be removed, and the discs in the front plug could be interchanged. The four uranium-238 cylinders inside the LiH cylinder forming the main body of the SS-1 could also be removed.

The experiments consisted of measuring fast neutron dose rates, gamma ray dose rates, and thermal neutron fluxes at points outside the SS-1, under various conditions. For these measurements the SS-1 was positioned with its centerline 12.5 feet above the concrete pad. The instruments used to measure the dose rates and fluxes were:

1. Hurst dosimeter for fast neutron dose rates
2. 50 cc ion chamber - anthracene scintillation detector for gamma ray dose rates
3. BF_3 proportional counter for thermal neutron fluxes.

In order to separate out the effects of air and ground scattering, the measurements were made with and without a right circular cylinder of lead and rubber as a shadow cone. References 44, 45, and 46 give the results and analysis of these tests.

12.3 TWO-PI SHIELD EXPERIMENTS

One of the problems in the design of an aircraft nuclear shield system is to determine the origin and magnitude of the radiation entering the crew shield. Existing analytical methods are still not adequate to provide an exact reliable solution to the problem. Therefore, direct measurement of the radiation arriving at and penetrating the crew shield is needed to supplement the analytical methods and provide a basis for testing and improving analytical methods.

The problem of making such measurements is complicated by the fact that the largest thicknesses of shielding materials in a practical system are located directly between the reactor and the crew compartment. Radiation, which penetrates the thinner portions of the reactor shield, scatters in the surrounding air and enters through the thinner side walls of the crew shield to contribute a significant fraction of the total dose received by the crew. If measurements are made near the earth's surface, the quantity of scattered radiation at the crew's position is altered by the change in the scattering medium from air to ground.

One solution to this difficulty is provided by suspending the entire shield system at a sufficient altitude above the ground while measurements are taken. Another solution which might prove adequate is that of screening out the ground-scattered radiation to enable reliable measurements to be made at some lower altitude or even at ground level. To test this latter possibility, the 2-pi experiments were undertaken. The name was derived from the auxiliary shields covering 2-pi solid angles placed on the reactor and crew shields to screen out the radiation effect of the ground.

DECLASSIFIED

DECLASSIFIED

The primary purpose of these experiments was to determine the altitudes necessary to perform meaningful measurements of the radiation inside a crew shield both with and without the use of screening devices, to minimize the effects of radiation scatterings or interactions occurring in the ground.

During the design of the experiment, it became apparent that the shield structures required for the primary measurements could be arranged in different combinations to yield a substantial quantity of additional shielding information. This additional information formed several subordinate objectives for the experiments.[47]

1. Investigation of a sufficient number of shielding configurations to provide design criteria for shield test facilities required for the measurement of crew compartment dose rates.
2. Separation of the contributions to dose rates within the crew shield from fast neutrons and from gamma rays escaping from the reactor shield, thus obtaining information on the importance of secondary gamma ray radiation.
3. Separation, as far as possible, of the effects of processes occurring in air and ground at various altitudes for the improvement of basic technology.

TEST PROCEDURE

The experiment was conducted in two parts utilizing two basically different reactor shields.[48] The first part, using reactor shield assembly number 1, was designed to test neutron effects. This shield provided a large gamma ray attenuation and a relatively small neutron attenuation. The second part of the experiment, using reactor shield assembly number 2, was designed to test gamma ray effects. This shield provided a large neutron attenuation and a relatively small gamma ray attenuation. Both shield assemblies had neutron and gamma ray shadow shields in the direction of the crew shield, and detachable 2-pi solid-angle auxiliary shields that could be placed on the shield in the direction of the ground. These auxiliary shields, along with the auxiliary shield for the crew box, were designed to provide an additional attenuation of about a factor of 50 for both neutrons and gamma rays.

The crew shield for this experiment had a shadow shield in the direction of the reactor and was also fitted with an auxiliary 2-pi solid-angle shield.

The measurements were taken at the Oak Ridge Tower Shielding Facility. This facility has the unique capability of permitting a reactor shield system consisting of one or more shields to be operated out-of-doors, suspended by a system of towers and hoists. The facility is complete with reactor and instrumentation for shield measurements. The shield system may be located at any altitude up to 200 feet above the ground, or raised and lowered with the reactor in operation.

The principal measurements taken during this experiment were the fast neutron dose rates, gamma ray dose rates, and BF_3 ion chamber thermal fluxes, while the shield system was raised from ground level to a position 195 feet above the ground and then lowered. These measurements were termed altitude traverses. Four separate sets of altitude traverses were planned for each configuration:

Traverse A:

2-pi shielding omitted; all air and ground scattering effects present.

Traverse B:

2-pi shielding on the reactor shield only; this served to reduce the importance of all single or multiple scattering events in which the first scattering occurred in the ground and eliminated half the theoretical single air scattering contribution.

DECLASSIFIED

DECLASSIFIED

Traverse C:

2-pi shielding on the crew shield only; this served to reduce the importance of all single or multiple scattering events in which the last scattering occurred in the ground and again eliminated approximately half of the theoretical single air scattering.

Traverse D:

2-pi shielding on both the reactor shield and the crew shield. This arrangement should have yielded approximately half the theoretical single air scattering.

The interpretation of these altitude traverses were based on the variation of dose rate with altitude. In addition to the altitude traverses, many supporting measurements of the dose rates leaking from the reactor shield were taken. These measurements were used to make comparisons between calculations and absolute measurements of the flux leaking from the reactor shield or arriving at the crew shield.

CONCLUSIONS

For the shield system tested, all the altitude traverses without auxiliary 2-pi shields on either the reactor or crew shield were still showing a decrease in dose rate with altitude at 195 feet. The typical traverse at first rose sharply with altitude to some maximum at 40 to 60 feet and then decreased monotonically with altitude. Typically, the maximum would be something greater than twice the value at full altitude. In cases where gamma rays were being measured with the reactor shield emitting relatively more neutrons than gamma rays (secondary gammas) the ratio of maximum-to-minimum was the largest, while the same ratio for the neutron dose rate was the smallest.

By including a 2-pi shield on the reactor shield, the ratio of the measured dose rates at 10 feet to the measured dose rates at 195 feet without 2-pi shields was typically 1.09 for fast neutrons, and 1.13 for primary gamma rays when the reactor shield leaked more gamma rays than neutrons, and 1.60 for gamma rays when the reactor shield leaked more neutrons than gamma rays. Neutron interactions were responsible for most of gamma dose rate at the crew shield in the latter case.[49]

As a result of this experiment, it is estimated that ground-level measurements made with a 2-pi cover on the reactor shield may be safely corrected to an altitude of 195 feet by multiplying by the ground-to-full-altitude ratios measured in this experiment. The overall uncertainty of the correction should be about 21 percent when the altitude correction factor is less than 1.5, and about 16 percent when the factor is less than 1.2. These uncertainties represent, on a root-mean-square basis, the combined uncertainties associated with the altitude correction factor and with the estimate of the effectiveness of the 2-pi cover.

At the conclusion of the first set of measurements it was clear that a great deal had been learned concerning measurement techniques. However, the comparisons between dose rate calculations and absolute dose rate measurements raised many more questions than answers.[50] Generally, comparisons between calculated and measured fast neutron dose rates, and between calculated and measured dose rates due to primary gamma rays and gamma rays originating in the reactor shield, were satisfactory. The comparisons between calculated and measured dose rates for secondary gammas; that is, gamma ray measurements with the shield emitting more neutrons than gamma rays, was very poor. In this latter case, calculations yielded from one-third to one-tenth of the measured values. The purpose of the second set of measurements was to examine this problem with the following objectives:[51]

1. To remeasure the secondary gamma ray shield configuration for confirmation of the problem
2. To carefully map the flux leakage from the reactor shield to determine if a better spatial distribution of the leakage might provide a solution

DECLASSIFIED

DECLASSIFIED

3. To make energy spectrum measurements of the gamma ray flux arriving at the crew shield to check possible sources of secondary gammas.

TEST PROCEDURE

In the second series of measurements, the emphasis was on measurements taken at a fixed altitude.[52] As nearly as possible, the measurements to confirm the existence of a secondary problem were duplications of the measurements taken in the altitude traverses at maximum altitude. The mapping of the reactor shield was accomplished with an electrical rotator and an aluminum truss. The reactor was suspended in the air and rotated remotely while the detectors were positioned fixed distances from the center of the reactor on the truss.

The energy spectrum measurements were made with a 3- by 3-inch NaI(T1) crystal inside several crew shields. The crew shields used were the original crew shield, a crew shield with a variable water shielding thickness surrounding the detector, and a crew shield without any major metal parts.

At the end of this experiment, it was clear that the unidentified portion of the secondary gamma ray dose rate, which prevented accurate calculation of the dose rate inside the crew shield, resulted from thermalization and capture of the fast neutrons in the walls of the crew shield. Addition of this factor to the calculations of the total dose rate inside the crew shield caused satisfactory agreement between calculated and measured dose rates (reference 53 and 54).

DECLASSIFIED

UNCLASSIFIED DECLASSIFIED
CONFIDENTIAL

12.4 REFERENCES

1. Wayne, W. D., et al., "Shield Test Air Reactor (STAR) Program Summary Report," GE-ANPD, DC 60-2-230, February 19, 1960.
2. Vieli, N., "A Comparison of Calculated and Measured Fast Neutron and Gamma Dose Rates Outside the Shields of the ASM-III E and SSR-1 Critical Assemblies," GE-ANPD, DC 60-6-155, June 1960.
3. Aschenbrenner, F. A., "Preliminary Comparison of Lid Tank Data with Semi-Empirical Calculations," GE-ANPD, DC 55-5-20, May 1955.
4. Aschenbrenner, F. A., "Description of Schedules - Lid Tank Experiments With Advanced Shield Materials," GE-ANPD, DC 55-8-2, August 1955.
5. Clark, R. H., "XMA-1 Shielding Tests Using Slabs of Advanced Shielding Materials," GE-ANPD, XDC 58-8-54, August 1958.
6. Friedman, S. T., "An Analysis of Late 1957, Early 1958, Lid Tank Experiments Pertaining to Project 103 Shield Design," GE-ANPD, XDC 58-7-163, June 1958.
7. Haffner, J. W., and Hanchon, K. B., "Description and Analysis of the Lid Tank with Advanced Shielding Materials," GE-ANPD, DC-57-10-83, October 1957.
8. Mitchell, V. J., "Data Report of Lid Tank Experiments With Advanced Shield Materials," GE-ANPD, DC 57-3-99, March 1957.
9. Weiss, W. L., and Belcher, J. A., "Data Report of Lid Tank Experiments for July 1957," GE-ANPD, DC 57-9-133, September 1957.
10. Belcher, J. A., and Zoller, L. K., "The Outside Test Tank and Associated Hardware," GE-ANPD, XDC 59-11-154, November 6, 1959.
11. Johnson, F., Jr., "Variable Geometry Shield Test Systems A and B Test Configurations," GE-ANPD, XDCL 58-8-23, August 1958.
12. Johnson, F., Jr., "Variable Geometry Shield Test System C Test Configurations," GE-ANPD, XDCL 58-10-120, October 1958.
13. Johnson, F., Jr., "Variable Geometry Shield Test Systems Configurations AB 7 (CB 7), AB 8 (CB 8), AY 1 (CY 1)," GE-ANPD, XDCL 58-12-238, December 1958.
14. Johnson, F., Jr., "Porous Shield Tests in GE-OTT, Data Report I," GE-ANPD, XDC 59-5-17, May 1959.
15. Johnson, F., Jr., "OTT V Coffin Test Results as of May 28, 1959," GE-ANPD, DCL 59-6-273, June 1959.
16. Belcher, J. A., "Directory of OTT Slab Configurations," GE-ANPD, DC 59-7-132, July 1959.
17. Belcher, J. A., et al., "Preliminary Calculations of Dose Rates Behind Configurations Being Tested at the OTT," GE-ANPD, DC 58-1-115, January 1958.
18. Belcher, J. A., Clark, R. H., and Friedman, S. T., "Preliminary Calculations of Dose Rates Behind Configurations Being Tested at the OTT," GE-ANPD, DC 58-3-115, March 1958.
19. Belcher, J. A., "Preliminary Calculations of Dose Rates Behind Configurations Being Tested at OTT," GE-ANPD, DC 58-6-133, June 25, 1958.
20. Belcher, J. A., "Prediction of OTT IV Shielding Tests," GE-ANPD, DC 58-12-75, December 1958.
21. Friedman, S. T., "Shielding Tests Performed in the GE-OTT in the Period March-June 1958," GE-ANPD, XDC 59-1-130, January 1959.
22. Gerardo, H. A., "The Experimental Data of the Neutron Flux and Gamma Dose Rates Measured Within Slab Configurations of Shield Components," GE-ANPD, DC 58-5-129, May 1958.
23. Gerardo, H. A., and Belcher, J. A., "Preliminary Analysis of OTT Configurations Using Diffusion Theory," GE-ANPD, DC 58-11-147, November 1958.
24. Zoller, L. K., "Water Centerline Data Within the OTT," GE-ANPD, DC 59-8-174, August 1959.

CONFIDENTIAL
UNCLASSIFIED DECLASSIFIED

UNCLASSIFIED

CONFIDENTIAL

25. Zoller, L. K., "Fast Neutron Removal Cross Sections," GE-ANPD, DCL 59-11-32, November 1959.
26. Zoller, L. K., "Summary of Analytical and Experimental Shielding Unit Effort for the XMA-1A," GE-ANPD, DC 60-2-105, February 2, 1960.
27. Friedman, S. T., Clark, R. H., and Weiss, W. L., "Schedule and Preanalysis of In-Pool Measurements At Convair, Ft. Worth, During July and August 1957," GE-ANPD, DC 57-8-135, August 1957.
28. Haffner, J. W., "Analysis of the Mockup Experiments Conducted at Convair With the ETR During February and March 1955," GE-ANPD, DC 56-7-98, July 1956.
29. Haffner, J. W., and Mitchell, V. J., "Analysis of the Mockup Experiments Conducted at Convair with the GTR During April-June 1956," GE-ANPD, DC 56-11-94, November 1956.
30. Haffner, J. W., "Duct Mockup Experiments at the Convair Ground Test Reactor," GE-ANPD, APEX-364, June 21, 1958.
31. Klotz, R. J., and Aschenbrenner, F. A., "Description of Preanalysis of Mockup Experiments to be Performed in Convair NARF Swimming Pool," GE-ANPD, DC 55-10-114, October 1959.
32. Mitchell, V. J., "Data Report of Experiment 3.2 E With GTR," GE-ANPD, DC 56-11-62, November 1956.
33. Weiss, W. L., and Belcher, J. A., "Data Report of In-Pool Measurements at Convair, Ft. Worth, During July and August 1957," GE-ANPD, DC 58-2-179, February 1958.
34. Aschenbrenner, F. A., and Haffner, J. W., "Analysis of R-1 Mockup Experiments," GE-ANPD, APEX-242, February 10, 1956.
35. Aschenbrenner, F. A., "Analysis of R-1 Mockup Experiments," GE-ANPD, XDC 55-6-57, June 1955.
36. Aschenbrenner, F. A., "Analysis of R-1 Mockup Experiments, Report I," GE-ANPD, XDC 55-6-58, June 1955.
37. Aschenbrenner, F. A., "Analysis of R-1 Mockup Experiments, Report II," GE-ANPD, XDC 55-6-59, June 1955.
38. Aschenbrenner, F. A., "Analysis of R-1 Mockup Experiments, Report III," GE-ANPD, XDC 55-7-97, July 1955.
39. Aschenbrenner, F. A., and Haffner, J. W., "Analysis of R-1 Mockup Experiments, Report IV," GE-ANPD, XDC 55-9-149, September 1955.
40. Aschenbrenner, F. A., Haffner, J. W., and MacDonald, J. E., "Analysis of R-1 Mockup Experiments, Report VI," GE-ANPD, XDC 55-12-32, December 1955.
41. Haffner, J. W., "Analysis of R-1 Mockup Experiments Conducted at the BSF During February and March 1955," GE-ANPD, XDC 55-7-103, July 1955.
42. Haffner, J. W., and MacDonald, J. E., "Analysis of R-1 Mockup Experiments, Report V," GE-ANPD, XDC 55-10-45, October 1955.
43. Haffner, J. W., and VanValkenburg, H. M., "Analysis of R-1 Mockup Experiments, A Correction to Report III," GE-ANPD, XDC 55-11-131, November 1955.
44. Carver, J. G., and Mitchell, V. J., "Results of Solid Shield (SS-1) Mockup Experiments Performed With the ETR at Convair," GE-ANPD, DC 57-3-61, March 7, 1957.
45. Haffner, J. W., and Carver, J. G., "Preanalysis of SS-1 Experiments," GE-ANPD, DC 56-8-125, August 1956.
46. Haffner, J. W., and Friedman, S. T., "Description and Analysis of the Solid Shield (SS-1) Mockup Experiments Performed with the GTR at Convair," GE-ANPD, DC 57-4-119, April 16, 1956.
47. Carver, J. G., and Aschenbrenner, F. A., "Program of Measurements at Lower Shielding Facility," GE-ANPD, XDC 56-11-103.
48. Clark, R. A., Carver, J. G., Brenton, R. F., Weiss, W. L., and Rohrer, R. F., "Test Data from the 2 Pi Solid Angle Shield-Cover Experiment," GE-ANPD, APEX-439, December 19, 1958.

CONFIDENTIAL

UNCLASSIFIED

UNCLASSIFIED
CONFIDENTIAL
UNCLASSIFIED

49. Burns, L. S., "Analysis of 2 Pi Experiments," GE-ANPD, DC 57-10-46, September 30, 1957.
50. Aschenbrenner, F. A., "TSF Two Pi Recheck Measurements," GE-ANPD, XDCL 58-4-65, April 3, 1958.
51. Burns, L. S., "Schedules and Measurements for the Two Pi Rechecks," GE-ANPD, XDCL 58-9-36, September 2, 1958.
52. Burns, L. S., "Test Data from the 2 Pi Solid Angle Shield Cover Experiments, Part Two," GE-ANPD, XDC 59-5-78, April 24, 1959.
53. Burns, L. S., "A Comparison of Calculated and Measured Crew Shield Capture Gamma Rays," GE-ANPD, DC 60-4-172, April 27, 1960.
54. Burns, L. S., and Mann, R. A., "Comparison of a Calculated and Measured Direct-Beam Gamma Ray Energy Spectrum Through the Side of a Reactor Shield," GE-ANPD, XDC 60-5-99, May 4, 1960.

UNCLASSIFIED
CONFIDENTIAL
UNCLASSIFIED